TECHNICAL REPORT
January 1967

ARMY • NAVY • AIR FORCE • AEC • NASA

PROCEEDINGS OF THE FIFTH PHOTOVOLTAIC SPECIALISTS CONFERENCE

VOLUME II

THIN FILM SOLAR CELLS

AND

RADIATION DAMAGE

13 October 1966
held at the NASA-Goddard Space Flight Center
Greenbelt, Maryland

PIC-SOL 209/6.1
January 1966

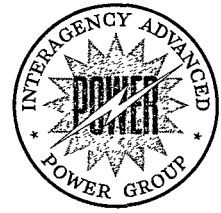

ARMY • NAVY • AIR FORCE • AEC • NASA

PROCEEDINGS OF THE FIFTH PHOTOVOLTAIC SPECIALISTS CONFERENCE

VOLUME II

(Of Three Volumes)

THIN FILM SOLAR CELLS

and

RADIATION DAMAGE

19 October 1965
Held at the NASA-Goddard Space Flight Center
Greenbelt, Maryland

This publication was prepared for the Interagency Advanced Power Group by the Power Information Center under Contract NASr-191. Questions concerning this publication should be directed to the following address:

Power Information Center
103 Moore School Building
200 South 33rd Street
Philadelphia, Pennsylvania 19104

Institute for Cooperative Research
University of Pennsylvania

FOREWORD

Continuing its interest in the photovoltaic area, the Interagency Advanced Power Group (IAPG) has published for the third time the proceedings of the Photovoltaic Specialists Conference. The content of these proceedings - a significant part of the information exchange activities of the IAPG - is of particular interest to members of its Solar Working Group.

This conference, the fifth of its kind, was cosponsored by IEEE, AIAA, and the NASA-Goddard Space Flight Center. Facilities for meetings and other arrangements were the responsibility of NASA-Goddard.

Presentations are included in the order in which delivered at the conference and were prepared from papers submitted to the Power Information Center (PIC) through the IEEE. Where papers have been authored by more than one person, cover sheets bear the name of the person who actually gave the presentation.

Presentations are arranged in three volumes and five sections reflecting the arrangement of the conference into three days and five sessions. Contents of the volumes are as follows:

Volume I - Advanced Solar Cells

Volume II - Thin Film Solar Cells and Radiation Damage

Volume III - Solar Power Systems Considerations

Transcriptions of the discussion periods following each presentation were prepared by Mrs. Marion Beckwith of Mr. Cherry's staff at NASA-Goddard. This effort is acknowledged as an important contribution to the proceedings.

Inclusion of a paper in these proceedings in no way precludes later publication in professional society journals.

PROCEEDINGS OF THE FIFTH PHOTOVOLTAIC SPECIALISTS CONFERENCE

Dates: 18, 19, and 20 October 1965

Place: NASA-Goddard Space Flight Center
Greenbelt, Maryland

Attendance

Based upon information available at the time of publication, the following list represents those who attended at least one of the conference sessions:

IAPG Members Present:

Brancato, E. L.	NRL
Cherry, W. R.	NASA-Goddard
Fischell, Robert	APL
Hamilton, R. C.	IDA
Kittl, Emil	USAECOM
Potter, Andrew	NASA-Lewis
Schwarz, F. C.	NASA-ERC
Shapiro, S. J.	USAECOM
Smith, A. H.	NASA-HQ
Uchiyama, A. A.	JPL
Wise, J. F.	AF-APL
Yannoni, N. F.	AFCRL

Government:

Anderson, Donald	NASA-Ames
Brandhorst, H. W., Jr.	NASA-Lewis
Bullis, W. M.	NBS
Campbell, Frank	NRL
Cunningham, B. T.	NASA-Goddard
Danchenko, Vitaly	NASA-Goddard
Dawson, J. R.	NASA-Langley
Duncan, C. H.	NASA-Goddard
Ellis, W. E.	NASA-Langley
Fang, P. H.	NASA-Goddard
Faraday, B. J.	NRL
Ferris-Prabhu, A. V. M.	NASA-Goddard
Finger, H. B.	NASA-HQ
Foster, J. V.	NASA-Ames
Gallagher, D. J.	NASA-Goddard
Gdula, William	NASA-Goddard
Geiger, F. E., Jr.	NASA-Goddard

Government: (continued)

Goldsmith, Paul	JPL
Gordon, Frederick	NASA-Goddard
Green, Milton	USNUSL
Haynes, G. A.	NASA-Langley
Haynos, J. G.	NASA-Goddard
Hirschfield, Jule	NASA-Goddard
Hobbs, A. J.	NASA-Goddard
Janda, R. J.	NASA-Goddard
Jones, W. P.	NASA-Goddard
Kautz, H. E.	NASA-Lewis
Lambert, R. J.	NRL
Lillywhite, Malcolm	NASA-Goddard
Litynski, Z.	Library of Congress
Liu, Y. M.	NASA-Goddard
MacKenzie, C. M.	NASA-Goddard
Massie, L. D.	AFAPL
McCarron, S. G.	NASA-Goddard
Meszaros, George	NASA-Goddard
Mejia, N. V.	NASA-Goddard
Moses, E. G.	NASA-Goddard
Reetz, Art	NASA-HQ
Ritchie, D. W.	JPL
Salay, J. B.	NASA-Goddard
Schach, Milton	NASA-Goddard
Shepherd, J. M., Jr.	NRL
Shumaker, H. A.	NASA-Lewis
Sizemore, K. O.	NASA-Goddard
Slifer, L. W., Jr.	NASA-Goddard
Sokoloski, M. M.	NASA-Goddard
Spakowski, A. E.	NASA-Lewis
Statler, R. C.	NRL
Sullivan, R. M.	NASA-Goddard
Swartz, C. K.	NASA-Lewis
Tauke, Regina	NRL
Tucker, W. M.	NASA-Goddard
Waddel, R. C.	NASA-Goddard
Wannemacher, H. E.	NASA-Goddard
Wappaus, W. A.	NASA-Goddard
Weitzel, R. L.	NASA-Goddard
Yasui, Robert K.	JPL
Yuen, Joseph	NRL

Nongovernment:

Abrahams, Samuel	Fairchild Hiller
Adams, J. R.	Ball Brothers
Albright, George	Grumman Aircraft Corp.

Nongovernment: (continued)

Aldrich, R. W.	G.E. - Syracuse
Alexander, S. M.	Texas Instruments
Asbed, Norig	Hittman Associates
Augustine, Frank	Clevite Corp.
Bachner, R. L.	Solar Systems, Inc.
Baicker, J. A.	Princeton R&D Co.
Baker, J. K.	G.E. - Philadelphia
Barkley, D. W.	Libby Owens Ford
Barnhart, P. W.	Booz, Allen Applied Research
Barrett, Matt	Exotech, Inc.
Berry, Edwin	Aerospace Corp.
Bickler, Don	Hoffman Electronics Corp.
Blair, John	MIT
Boer, K. W.	Univ. of Delaware
Borson, E. N.	Aerospace Corp.
Burrill, J. T.	Ion Physics Corp.
Cain, Orison	Dow Corning
Chamberlin, R. R.	National Cash Register Co.
Chidester, L. G.	Lockheed M&S Co.
Close, J. R.	Minnesota Mining & Manuf. Co.
Cole, R. L.	Texas Instruments
Colehower, E. W.	Martin Co. - Baltimore
Cooley, W. C.	Exotech, Inc.
Cusano, D. A.	G.E. - Schenectady
Davis, Robert	Fenwal, Inc.
Downing. R. G.	TRW Systems
Downs, W. R.	Ball Brothers
Ellis, S. G.	RCA - Princeton
Feagin, R. B.	Texas Instruments
Feitknecht, J.	Allen Bradley Co.
Ferguson, G. D., Jr.	G.E. - Lynchburg
Flicker, H.	TRW Systems
Goldstein, Bernard	RCA - Princeton
Gould, J. A.	Clevite Research Center
Griffin, T. A.	Harshaw Chemical Co.
Halstead, R. E.	G.E. - Schenectady
Hangen, N. R.	RCA - Princeton
Hawkins, K. D.	Ryan Aeronautical Co.
Hicks, J. M.	Westinghouse Research
Hietanen, J. R.	Clevite Corp.
Hill, E. R.	Harshaw Chemical Co.
Holmes-Siedle, A. G.	RCA Labs. - Princeton
Hui, W. L. C.	RCA - Princeton
Holloway, H.	Philco Research
Hood, John	Dow Corning Corp.
Huffman, F. N.	Martin Co. - Baltimore
Ichikawa, Y.	Westinghouse - Youngwood
Iles, P. A.	Hoffman Electronics Corp.

Nongovernment: (continued)

Jilg, E. T.	Communications Satellite Corp.
Johnson, C. E.	Bellcomm Inc.
Julius, R. F.	Keltec Industries, Inc.
Kaye, S.	EOS, Inc.
Keramidas, B. G.	Harshaw Chemical Co.
King, W. J.	Ion Physics Corp.
Kling, H. P.	Hittman Associates
Lamb, A. H.	Atlantic Instruments & Electronics, Inc.
Ling, K. S.	RCA - Mountaintop
Lisak, L. R.	General Dynamics/Convair
Loferski, J. J.	Brown University
Luft, Werner	TRW Systems
Mann, A. E.	Spectrolab
Marks, B. S.	Lockheed M&S Co.
Martin, J. H.	Johns Hopkins Univ. - APL
Maxwell, K. H.	Philco Corp.
Medved, D. B.	EOS, Inc.
Mihm, F. I.	Heliotek
Miller, W. J.	G.E. - Lynchburg
Mlavsky, A. I.	Tyco Labs., Inc.
Mott, J. L.	Fairchild Hiller Corp.
Nelms, G. E.	Honeywell, Inc.
Nichols, Donald	General Atomic
Noble, E. B.	Westinghouse - Washington
Noel, G.	RCA - Princeton
Oman, Henry	Boeing Co.
Pearson, G. L.	Stanford University
Perkins, D. M.	RCA - Princeton
Pollack, S. R.	Univ. of Pennsylvania
Prince, M. B.	EOS
Ralph, E. L.	Heliotek
Rappaport, Paul	RCA - Princeton
Ratcheson, W. I.	Boeing Co.
Ray, K. A.	Hughes Aircraft Co.
Rensin, Ernest	ITT Federal Labs.
Reynard, D. L.	Lockheed M&S Co.
Riel, R. K.	Westinghouse - Youngwood
Rubin, Irwin	Solar Systems, Inc.
Runyan, W. R.	Texas Instruments
Sachs, I. M.	Optical Coating Labs.
Schaefer, J. C.	Harshaw Chemical Co.
Schlotterbeck, R. S.	G.E. - Lynchburg
Schwarz, F. R.	RCA - Princeton
Sequeira, Edward	EOS
Shirland, F. A.	Clevite Corp.
Skarman, J. S.	National Cash Register
Stanley, A. G.	MIT Lincoln Lab.

Nongovernment: (continued)

Stein, Irving	RCA - Princeton
Stevenson, R. D.	Douglas Aircraft
Stewart, Elmer	Harshaw Chemical Co.
Stonebraker, E. R.	Westinghouse - Youngwood
Stroebel, J. D.	Dow Corning Corp.
Tada, H. Y.	TRW Systems
Tarneja, K. S.	Westinghouse - Youngwood
Teener, J. W.	Johns Hopkins Univ. APL
Thomareas, Steve	Ryan Aeronautical Co.
Timberlake, A. B.	Battelle Memorial Institute
Toole, J. M.	RCA - Mountaintop
Uhler, E. F.	RCA - Harrison
Vette, James	Aerospace Corp.
Vineyard, Ray	Texas Instruments
Vohn, Paul	RCA - Princeton
Vrablik, E. A.	MIT - Lincoln Lab.
Wiener, Paul	RCA - Princeton
Williamson, E. M., Jr.	Libby Owens Ford
Winkler, S. H.	RCA - Princeton
Wolf, Martin	RCA - Princeton
Wysocki, J. J.	RCA - Princeton
Zehner, D. W.	Westinghouse - Baltimore
Zimmerman, Elizabeth	Philco Research Labs.

IAPG Secretariat:

Ashleigh, R. F.	PIC
Williams, F. E.	PIC

Program Committee

Paul Rappaport - Chairman
Robert E. Fischell - Secretary
Arvin H. Smith - Treasurer
William R. Cherry - Arrangements
Joseph J. Loferski - Technical Papers Coordinator

Robert Hamilton
Andrew E. Potter
Bernd Ross
Fred A. Shirland
Joseph F. Wise
Martin Wolf

VOLUME II

TABLE OF CONTENTS

PART C. THIN FILM SOLAR CELLS

PART D. RADIATION DAMAGE

*Papers presented at the conference, but not made available for this volume

**Papers not presented at the conference, but included at the request of the sponsors.

PIC-SOL 209/6.1
Section C-1

PROGRESS ON CADMIUM TELLURIDE THIN FILM SOLAR CELLS

Presented by

Lowell D. Massie

Research and Technology Division

Air Force Aero Propulsion Laboratory

Wright-Patterson AFB, Ohio

19 October 1965

PROGRESS ON CADMIUM TELLURIDE THIN FILM SOLAR CELLS

Lowell D. Massie
Joseph F. Wise
Air Force Aero Propulsion Laboratory

Introduction

This paper describes work accomplished and results achieved on cadmium telluride thin film solar cells under Air Force contracts AF 33(657)-10601 and AF 33(615)-2695 with the General Electric Company. Work under contract AF 33(657)-10601 was completed in February 1965 with submission of AFAPL Technical Report 65-8, Research on Thin Film Polycrystalline Solar Cells. Much of the information presented in this paper is extracted from the report.

Research on cadmium telluride film cells is presently continuing under contract AF 33(615)-2695, which became effective 1 June 1965. The First Quarterly Technical Report prepared under this contract was distributed 15 September 1965.

The basic objective of thin film solar cell research is to develop the technology for economical fabrication of efficient, lightweight, radiation resistant solar cell arrays capable of reliable operation in space for extended periods of time.

More specifically, the program goals are (a) rapid, automated fabrication and assembly techniques to permit major photovoltaic array cost reductions to less than $10.00/watt; (b) thin film array power to weight ratio of 100/watts/lb including stowage and deployment weights at 10 percent efficiency; and (c) less than 10 percent degradation for 5 years operation in space.

The work is highly exploratory and is a long term approach, in contrast to single crystal silicon cell work, to meeting future power requirements of aerospace vehicles. Cadmium telluride with a bandgap of 1.45 electron volts is near the theoretical optimum for conversion of solar energy by the photovoltaic effect. Steady progress toward larger cell areas and improved efficiencies has been made with results of preliminary tests indicating superior radiation resistance in contrast to silicon solar cells. Consequently, cadmium telluride is considered a promising material potentially capable of meeting thin film cell program objectives.

Cadmium Telluride Film Cell Configuration

The cross section of a cadmium telluride thin film solar cell is shown in Figure 1. Molybdenum foil 0.001" to 0.002" in thickness is first heavily oxidized in nitric acid and then the oxide is removed with hydrochloric acid. This results in a slightly matte substrate surface for film growth. Film growth

proceeds in three stages. The molybdenum is first precoated with a low resistivity cadmium sulfide layer which subsequently orients the cadmium telluride layer, reduces the metal-semiconductor barrier height, and improves the adherence of the composite cadmium telluride-cadmium sulfide film. The main N-type cadmium telluride film heavily doped with gallium, is then deposited to a thickness of about 10 microns on the cadmium sulfide layer. During the final few minutes of film growth, a relatively high resistivity upper layer is grown by compensating gallium doping with copper acceptor atoms.

Junction formation is accomplished by immersing the sample in an 85°C copper ion solution for 10 seconds after having properly masked the back and edges of the substrate. This step forms the P-type copper telluride layer having a sheet resistivity of approximately 500 ohms/square. The high sheet resistivity of the P layer requires the application of a close spaced top contact. A metallic screen grid has been used to give good initial results but cells employing this type of contact have invariably deteriorated. A vacuum deposited gold grid is presently used as standard construction and has provided good efficiencies and greatly improved cell stability. Figure 2 shows a typical 56 cm^2 cadmium telluride film cell and a conventional 2 cm^2 silicon cell for comparison.

Electrical Performance of Large Area Cadmium Telluride Film Cells

In November 1964, several large area (56 cm^2) cadmium telluride film cells were submitted under contract AF 33(657)-10601 for evaluation by the AF Aero Propulsion Laboratory. The cells were tested under 85 mw/cm^2 natural sunlight and produced efficiencies of better than 4 percent.

The V-I characteristic curve of one cell (SP-34) is shown in Figure 3. The electrical performance of this cell is the best observed to date for any large area thin film solar cell at AFAPL. The calculated efficiency under the 85 mw/cm^2 intensity and 10°C ambient temperature conditions is approximately 5 percent. The power to weight ratio based upon the matched load power of 226 milliwatts and a cell weight of 1.44 grams is 71 watts/lb. Projecting cell performance to space sunlight conditions would result in a power to weight ratio approaching 100 watts/lb.

Cadmium Telluride Film Cell Temperature Dependence

The effects of temperature on cadmium telluride film cell open circuit voltage and efficiency has been determined over the range from -10°C to +90°C. These data are shown in Figure 4 for cadmium telluride cells SP-28 and SP-38. Both the voltage and efficiency dependences are linear functions of increasing temperature in the range from 0°C to +60°C with average negative slopes of -1.6 millivolts/°C and -0.008 percent/°C respectively. Based upon these data, very minor losses in output power would be expected in going from typical laboratory test temperatures of 30°C to space operating temperatures of 70 to 80°C.

Cadmium Telluride Film Cell Stability

As mentioned earlier, the change in cell P layer contact method from a mechanical screen grid to an evaporated gold, comb type grid with krylon protective overlay, greatly improved cell stability. The effects of storage on the short circuit current, open circuit voltage, and maximum power of two cadmium telluride film cells are shown in Figure 5. During the 3 month period of observation, there is some increase in cell voltage, some decrease in cell current with the maximum power remaining essentially unchanged. While this indicates relatively good stability, the fact remains that adjustments in current and voltage are occurring. The causes of these adjustments are under investigation but are not fully understood at this time.

Generally, special precautions have neither been taken by the contractor nor the AF Aero Propulsion Laboratory in protecting cadmium telluride film cells from laboratory ambients. It is unlikely that the system design engineer would seriously consider use of components highly sensitive to ordinary laboratory environment. Figure 6 shows results of stability observations at AFAPL on the V-I characteristics of cell SP-105 over a 4 month period. There is a 2 percent change in open circuit voltage, a 10 percent change in short circuit current, and a 28 percent change in efficiency. Thus, the problem of stability in cadmium compound film cells remains to be understood and remains to be solved. Transparent, inorganic coatings such as oxides of silicon and aluminum capable of serving as moisture barriers while enhancing the light absorption and proton radiation resistance characteristics are under investigation.

Radiation Resistance of Cadmium Telluride Film Cells

Cadmium telluride film cells have been exposed to cobalt 60 gamma radiation, 5 Mev electron radiation, and 2.4 Mev proton radiation. A dose of 1.6×10^{17} R of cobalt 60 gamma radiation and a dose of 2×10^{14} cm^{-2} 5 Mev electron radiation produced no effect on cell characteristics.

Mr. R. L. Statler of the Naval Research Laboratory has conducted 2.4 Mev proton radiation studies on cells supplied by AFAPL with results as shown in Figure 7. Cadmium sulfide cells were included in the same test. There is approximately 15 percent decrease in short circuit current for both film cell types after a 3×10^{13} cm^{-2} dose.

AFAPL is currently planning a space experiment to obtain additional radiation damage data on these cell types and advanced silicon types. Figure 8 shows space experiment modules mounted in a laboratory test fixture. The module types are from left to right, Ion Physics Corporation ion implanted silicon, Clevite Corporation cadmium sulfide thin film, General Electric Company cadmium telluride thin film, Westinghouse dendritic silicon 10 ohm cm, and Westinghouse dendritic silicon drift field.

Integrated Array Fabrication Techniques for Cadmium Telluride Cells

Approximately one-third of the present contract effort on cadmium telluride film cells is directed toward investigation of techniques for fabricating integrated array segments with areas of 5 to 10 ft^2. The objectives of this approach are to circumvent handling, mounting, and interconnection of individual cells thus reducing costs and increasing reliability. Also, as power requirements are extended into the multikilowatt range, the capability to utilize component large area array segments rather than individual cells becomes increasingly important to facilitate construction.

Figure 9 shows in schematic form the processing steps in fabricating an integrated film cell array segment. The segment width would be approximately 12 inches with a length of 5 to 10 feet. The first step would be to metallize 1 inch by 12 inch substrate islands on an insulating plastic substrate. Step II would be to deposit cadmium telluride over the entire insulating substrate. The photovoltaic junction would be formed in Step III over the entire film surface. Step IV would be to mask and remove the film from unwanted regions and finally in Step V the vacuum deposited grid and interconnection pattern would be formed.

Such an integrated segment would contain 60, 12 in^2 cells for a 5 ft^2 area and 120, 12 in^2 cells for a 10 ft^2 area. It is estimated that such segments can eventually be fabricated with weights as low as 0.10 lb/ft^2. Segment power to weight ratios of 115 watts/lb would be attainable at 10 percent efficiency. If more than half the theoretical efficiency of 21 percent for cadmium telluride material can be realized in a thin film cell configuration, even further improvements in performance would be possible.

Summary

Cadmium telluride thin film solar cells having areas of 56 cm^2 and gridded area (53 cm^2) efficiencies of 4 to 5 percent in sunlight have been fabricated in laboratory quantities. These cells provide typical power to weight ratios of 80 watts/lb under air mass 1 sunlight. Work is in progress to reproducibly achieve cell efficiencies at the 6 to 8 percent level during the next two years and to investigate techniques of fabricating 5 to 10 ft^2 integrated array segments. The segments would consist of a number of cells fabricated simultaneously in sequential steps on a flexible substrate. Results of this work will be applied to thin-film array concept designs in the 0.1 to 40 KW power range.

Thin film cadmium telluride solar cells stored under unprotected conditions in laboratory ambients have been found to exhibit stability comparable to cadmium sulfide film cells stored under desicated conditions. Detailed investigations of the stability problem in cadmium telluride film cells and means of circumventing these problems are being pursued. The effects of simulated space environment on electrical performance of cells is also under investigation and a space flight experiment to verify results is in the assembly stage.

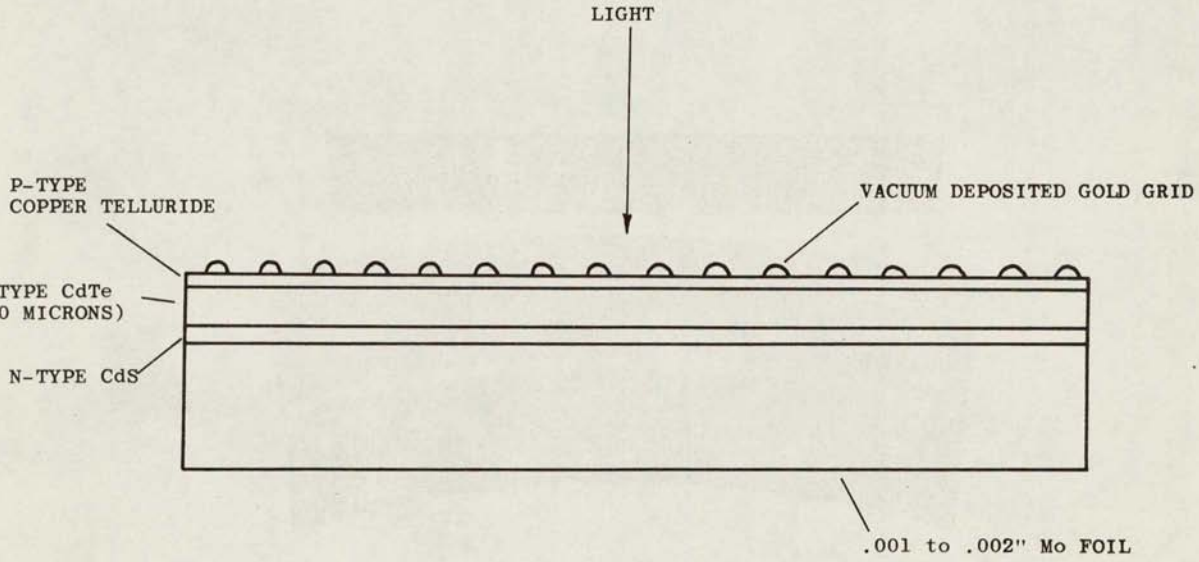

Figure 1 CROSS SECTION OF CADMIUM TELLURIDE FILM CELL

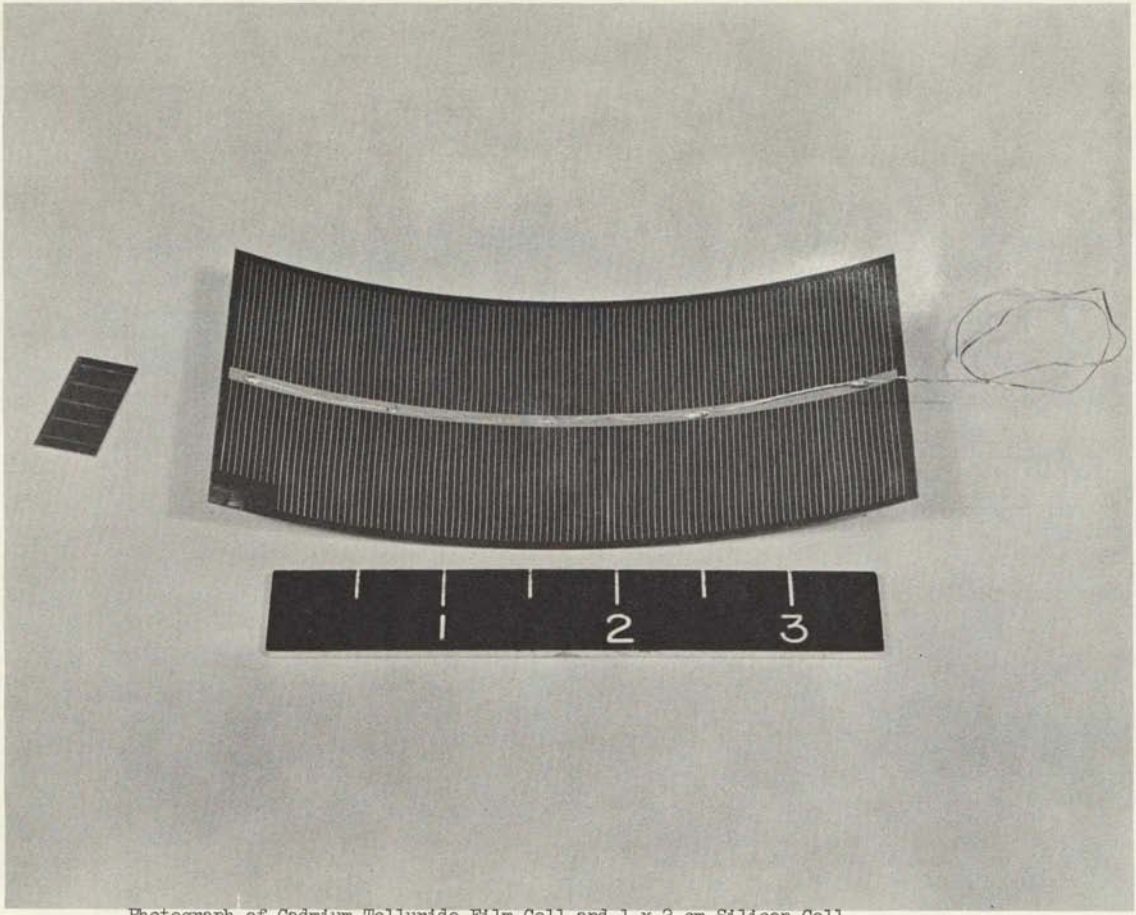

Photograph of Cadmium Telluride Film Cell and 1 x 2 cm Silicon Cell

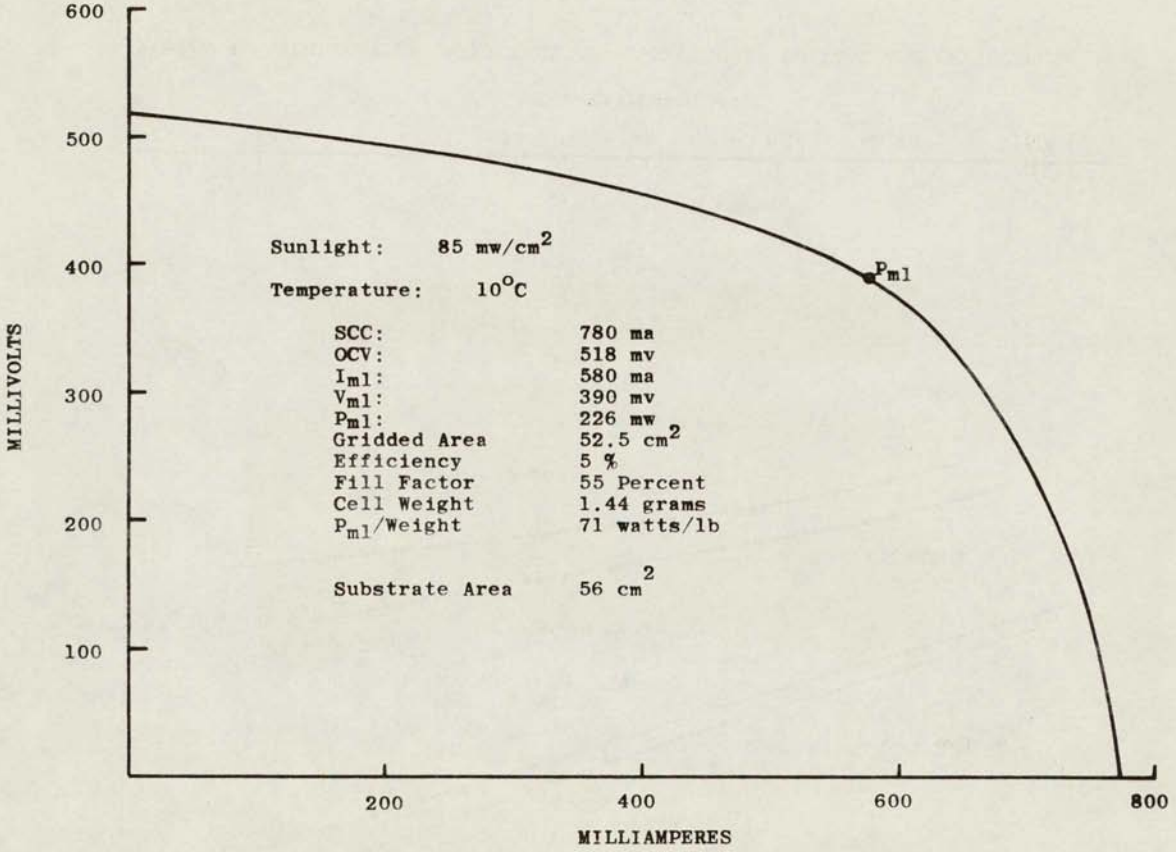

Figure 3 V-I CHARACTERISTIC CURVE - CdTe FILM CELL SP-34

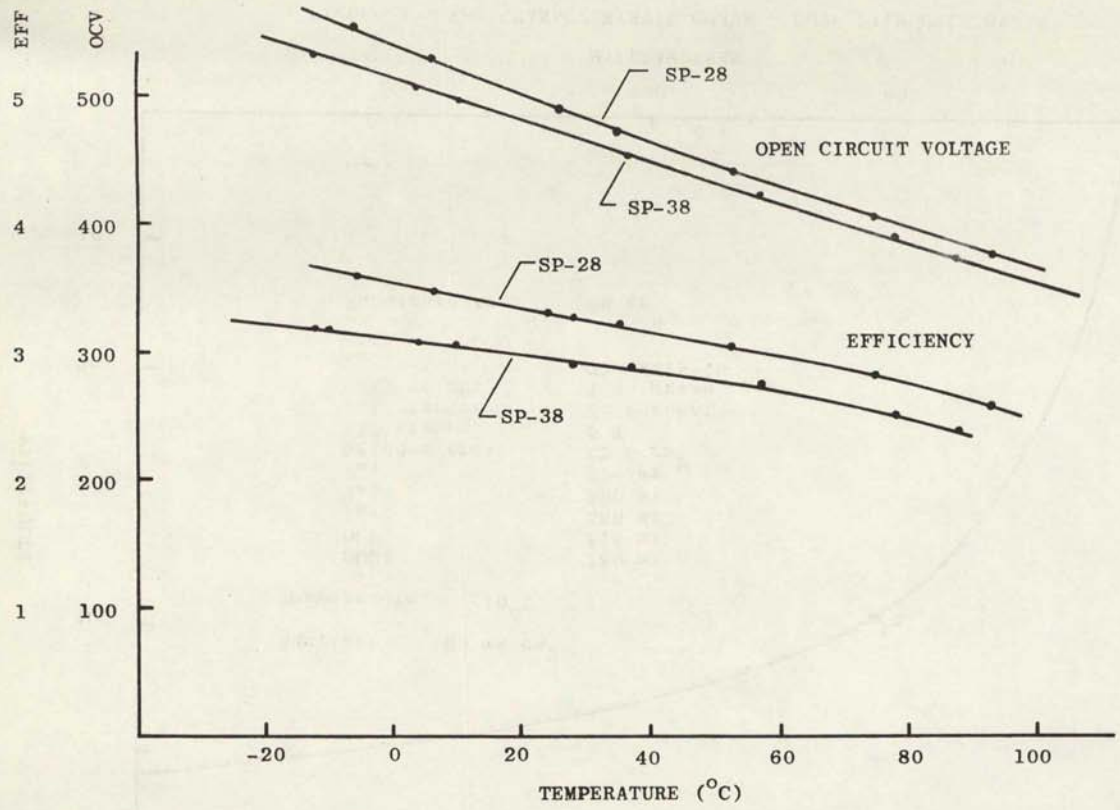

Figure 4 TEMPERATURE DEPENDENCE OF OPEN CIRCUIT VOLTAGE AND EFFICIENCY

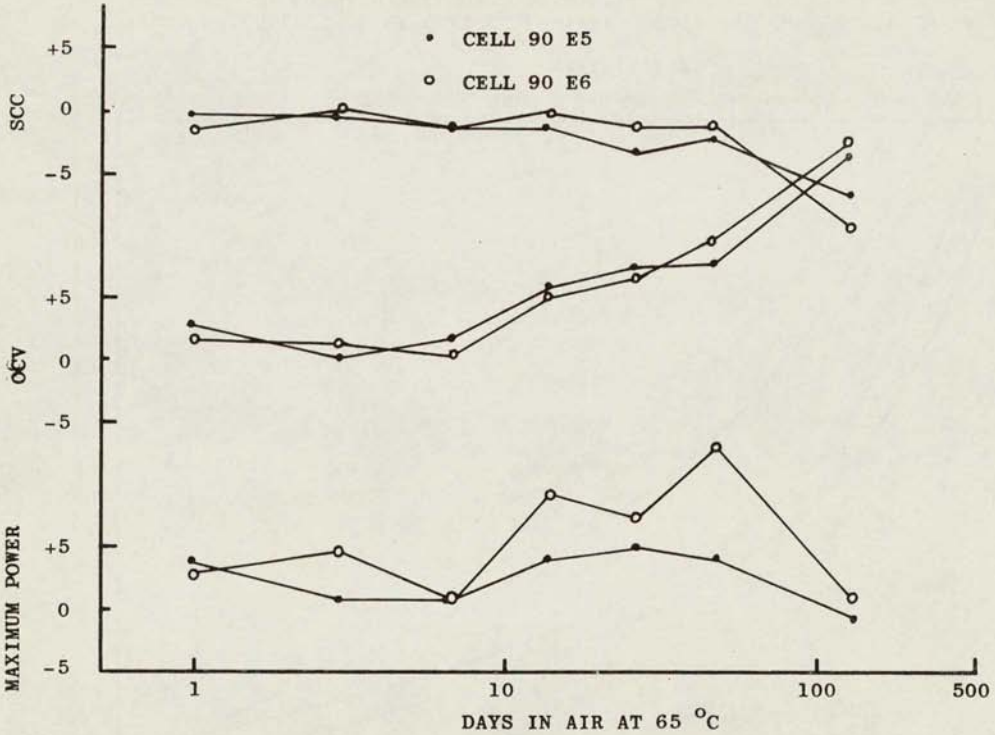

Figure 5 EFFECT OF STORAGE ON THE SHORT CIRCUIT CURRENT, OPEN CIRCUIT VOLTAGE, AND MAXIMUM POWER OF TWO CdTe FILM CELLS WITH VACUUM DEPOSITED GOLD GRIDS AND KRYLON PROTECTIVE OVERLAY

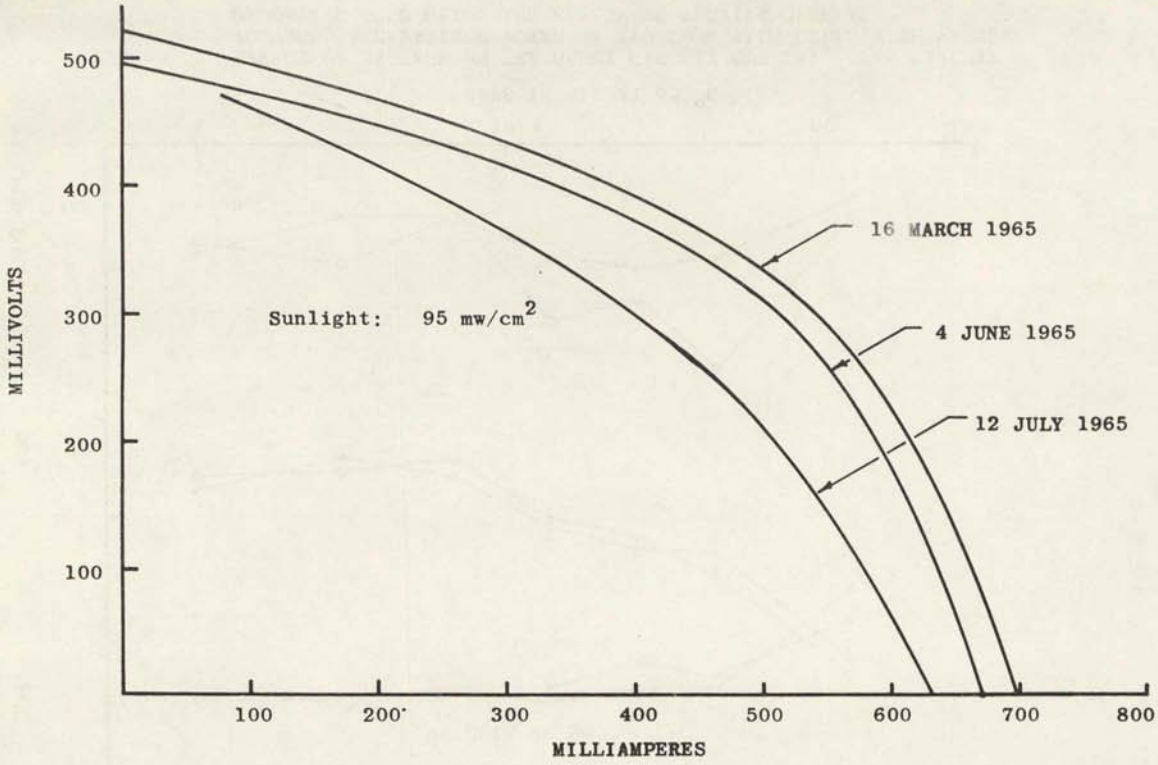

Figure 6 EFFECT OF LABORATORY AMBIENT CONDITIONS ON THE V-I CHARACTERISTICS OF CADMIUM TELLURIDE FILM CELL SP-105

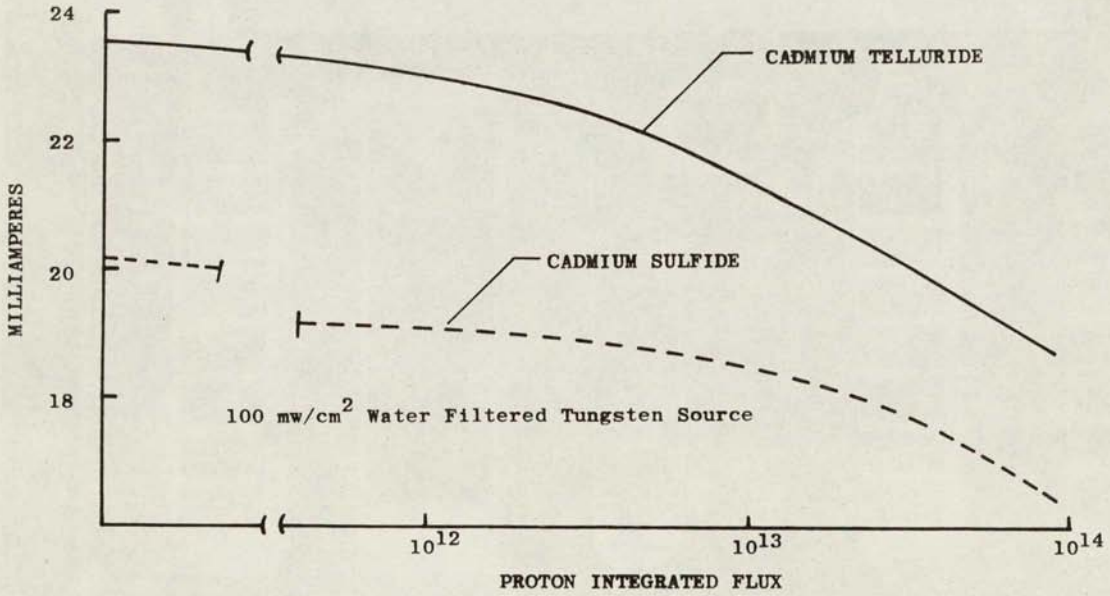

Figure 7 EFFECT OF 2.4 Mev PROTONS ON THE SHORT CIRCUIT CURRENT OF CADMIUM TELLURIDE THIN FILM SOLAR CELLS

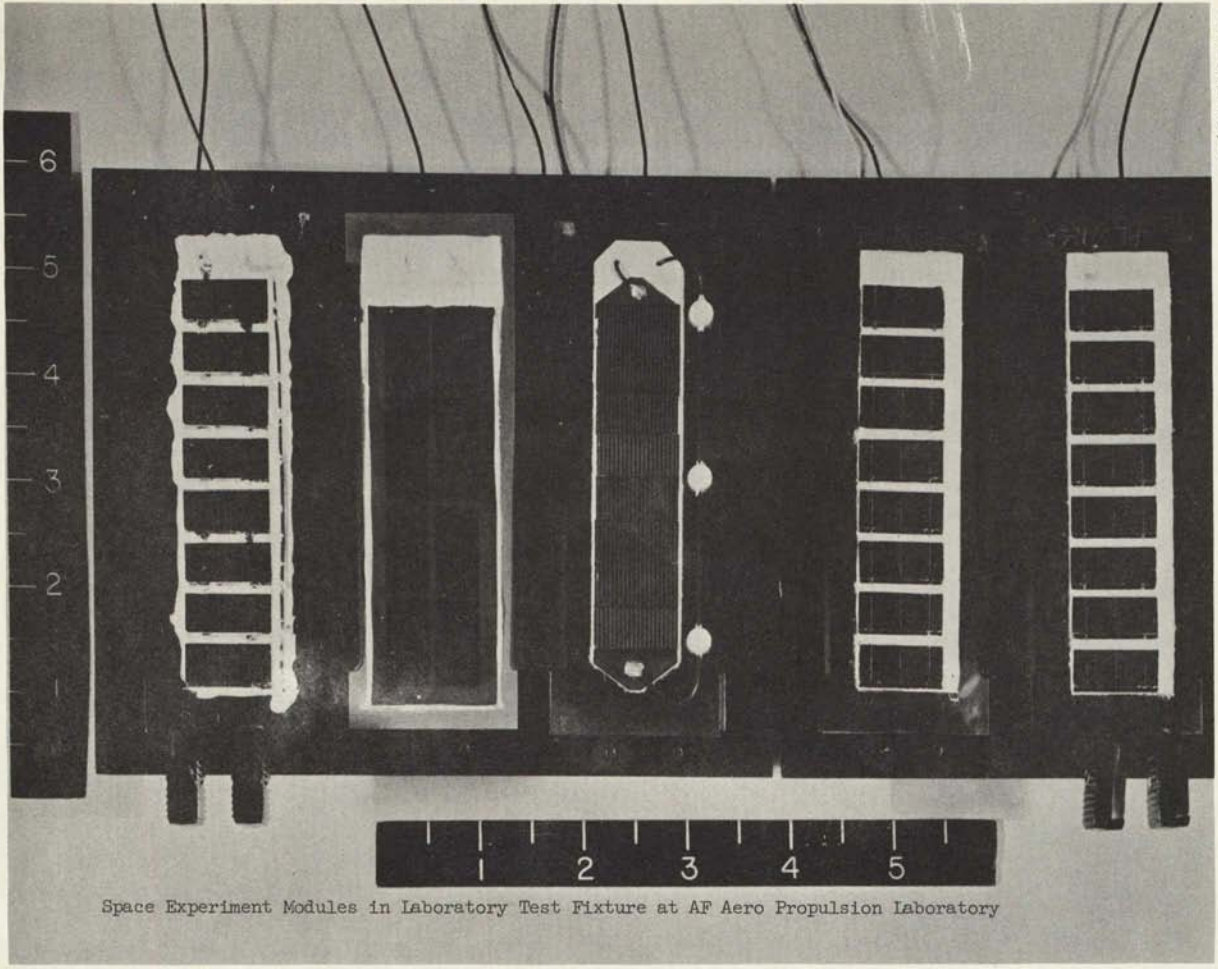

Space Experiment Modules in Laboratory Test Fixture at AF Aero Propulsion Laboratory

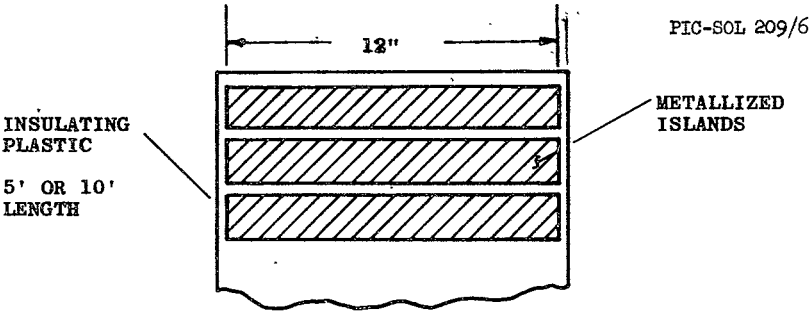

STEP I - METALLIZE SUBSTRATE ISLANDS ON INSULATING PLASTIC

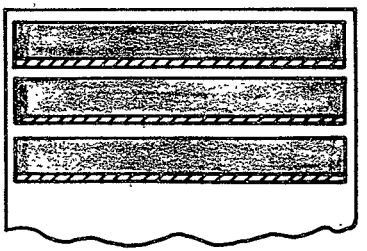

STEP II - DEPOSIT CdTe ON ENTIRE SUBSTRATE

STEP III - FORM JUNCTION OVER ENTIRE FILM SURFACE

STEP IV - MASK AND REMOVE FILM FROM UNWANTED REGIONS

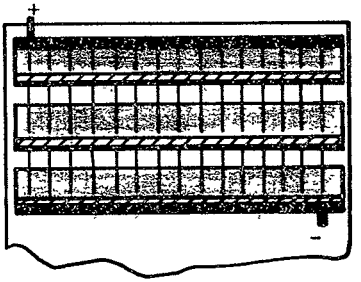

STEP V - EVAPORATE GRID AND INTERCONNECTION PATTERN

Figure 9 PROCESSING STEPS IN FABRICATING INTEGRATED THIN FILM SOLAR CELL ARRAY SEGMENT

PIC-SOL 209/6.1
Section C-2

GaAs THIN FILM SOLAR CELLS

Presented by

S. G. Ellis

RCA Laboratories

Princeton, New Jersey

19 October 1965

GaAs THIN FILM SOLAR CELLS+

P. Vohl
D. M. Perkins
S. G. Ellis
R. R. Addiss*
RCA Laboratories, Princeton, New Jersey
W. Hui
G. Noel
RCA Astro-Electronic Division, Princeton, New Jersey

Introduction

The properties of GaAs indicate that this material may be suitable for use in large area thin film solar cells. Because of the high absorption constant of GaAs, sunlight is absorbed within a few microns of the surface. Moreover, the bandgap is a good match to the solar spectrum. These characteristics alone, however, do not insure that GaAs will make a practical thin film solar cell; such properties as strength and stability cannot be predicted on a theoretical basis. Thus, the ultimate evaluation of the possibilities of GaAs for thin film solar cells must derive from the performance of fabricated cells.

This paper is a report on the development of thin film GaAs solar cells. The paper covers film formation on various substrates, junction formation, solar cell structures and results obtained.

Film Formation

Polycrystalline GaAs films have been deposited on various substrates by several methods. The most suitable films have been vapor grown in a hydrogen ambient containing water vapor, according to the gallium oxide reaction described by Thurmond and Frosch.(1) The GaAs source material (wafers or powder) is positioned between 20 and 30 mils from the source material and the substrate provides for efficient transport as described by Nicoll.(2)

---

* present address Itek Corporation, Lexington, Mass.

+ Research reported in this paper was sponsored by the Aero-Propulsion Laboratory, Research and Technology Division, Air Force Systems Command, Wright-Patterson Air Force Base, Ohio, under contract No. AF33(615)2259; the National Aeronautics and Space Administration, Lewis Research Center, Cleveland, Ohio under contract Nos. NAS3-2796 and NAS3-6466 and the NASA Western Operations Office, Santa Monica, California under contract No. NAS7-202 and RCA Laboratories, Princeton, N. J.

Ideally, a substrate should satisfy several criteria; it should be lightweight, flexible, and chemically nonreactive in the growth environment. In addition, its thermal expansion coefficient should match that of the GaAs film and its interface with the GaAs should be characterized by strong adherence and low electrical resistance. Mo is one of the few materials approaching the above requirements. Two mil Mo sheet was therefore used for most of this work. In a typical deposition process, the temperature of the Mo foil is approximately 750°C while that of the GaAs source is about 850°C. Under these conditions a growth rate of 5 microns per hour has been obtained.

One disadvantage of the Mo substrate is that the Mo-GaAs interface has a high resistance. This resistance has been reduced to a satisfactory level by precoating the substrate with a layer of tin-germanium alloy. The substrate coating also serves to control the doping of the deposited GaAs film. Free electron concentrations of 10^{15} to 10^{16} cm^{-3}, as determined by differential capacitance measurements, are usually obtained.

In an attempt to get a lighter more flexible cell, GaAs has also been grown on Al foil. Foils from 3 to 6 microns thick have been successfully used as substrates. Film growth on Al is a slower process than on Mo because of the lower growth temperatures imposed by the melting point of Al. Typically, the temperature of the Al foil is 600°C to 650°C with the source crystal about 100°C higher resulting in a growth rate of approximately 0.5 microns per hour. A layer of crystalline InAs deposited by the close spaced method onto the Al foil has been used to reduce the resistance of the Al-GaAs interface.

The properties of sputtered and flash evaporated GaAs films have been investigated to determine whether such films could be used in solar cell fabrication. In general, it was found that the optical and electrical properties of these films were quite different from those of either single crystal GaAs or vapor deposited films.

The adsorption coefficients of sputtered, flash evaporated, and vapor deposited films have been computed from measurements of the optical density. When it appears from the shape of the optical density curve that the films are not absorbing between 2.0 and 2.5 microns, the absolute value of reflectivity is calculated from the optical density. The absorption coefficients near the band edge are quite insensitive to errors in the reflectivity. Surfaces of films which appeared to scatter light were polished before obtaining the optical data. The results are shown in Figure 1. Sputtered or flash evaporated films deposited on substrates at room temperature were amorphous and crystalline films are anomolously high at bandgap energy. Also, the absorption edges of these films are very poorly defined. By contrast, the absorption coefficients of the vapor grown films more nearly approximate that of single crystal GaAs. The "tails" between 0.9 and 1.2 microns are probably connected with optical effects at the grain boundaries.

The conductivity type and resistivity of sputtered and flash evaporated films were difficult to control. These films were nearly always p-type; n-type conductivity was achieved in flash evaporated films only when doped with about 1% tin. The resistivities of all sputtered and flash evaporated films were too high for solar cell applications.

The more satisfactory electrical and optical properties of the vapor deposited films are probably due to the more nearly reversible and equilibrium nature of this deposition process.

Junction Formation

In general, solar energy conversion can be accomplished by three types of photovoltaic potential barriers: p-n homojunctions, p-n heterojunctions, and surface barriers. Each of these structures has been investigated on GaAs films.

Junctions of the p-n type have been formed by Zn diffusion and by vapor growth or flash evaporation of a p-type layer of GaAs onto an n-type film. The rectification characteristics, however, were poor. In the case of Zn, rapid diffusion along grain boundaries caused excessive junction leakage. When vapor growth, sputtering or flash evaporation was used to form a junction, the combination of sheet conductivity and optical transmission of the p-layer was far too low to be practical for use in solar cells.

Heterojunctions consisting of GaP vapor deposited onto the GaAs films were also briefly investigated. The electrical characteristics of this structure, however, were unsatisfactory due to the diffusion of impurities during the GaP transport process. In some cases the electrical junction did not coincide with the chemical interface.

The most satisfactory photovoltaic structure obtained to date on GaAs films consists of a surface barrier made with an evaporated metal or semiconductor layer. In contrast to p-n junction formation, surface barriers can be fabricated at comparatively low temperatures, thus avoiding grain boundary diffusion. In addition, most of the carriers are generated in the depletion region at the GaAs surface, thus minimizing recombination losses.

It should be noted that the material used to establish the surface barrier must satisfy several requirements. First, the resultant GaAs surface barrier must be comparatively high, ideally approaching the GaAs bandgap. Second, the barrier material must allow for a satisfactory compromise between its light transmission and sheet resistance. Finally, it must be stable in both the earth and space environments.

Of various rectifying metallic contacts investigated, Pt has been found to be best for GaAs solar cells, as discussed in a previous paper by Perkins and Pasierb.[4] Pt-GaAs solar cells have been made by sputtering, electroplating, and evaporating semitransparent Pt layers onto the GaAs

film. The first two techniques were unsatisfactory because sputtered Pt contacts had low open circuit voltages, while electroplated contacts were not uniform enough to be useful for large area cells. Uniform evaporated Pt films, on the other hand, can be reproducibly made by conventional vacuum evaporation techniques. These films have been found to satisfy the requirements stipulated above for the barrier forming material.

The Pt-GaAs contact barrier height has been measured by studying the spectral variation of the electron photoemission from the Pt into the GaAs[5]; the value obtained is approximately 1.2 eV, which compares favorably with the GaAs bandgap of 1.4 eV. Barrier height values obtained from studies of the (dark) I-V characteristics are, however, generally lower. Fig. 2 shows a plot of log I vs V for two typical cells. For most cells the characteristics can be approximately described by the equation: $I = I_o (\exp \frac{qV}{\alpha kT} - 1)$, where $2.0 \leq \alpha \leq 2.5$ and $I_o \sim 5 \times 10^{-8}$ amp/cm^2. The corresponding barrier height is ~ 0.75 eV. Approximately the same values are obtained using single crystal GaAs. The discrepancy in barrier height values determined from the photoemission measurements and the I-V characteristics is probably due to small patches of low barrier height on the contact surface.

The use of a degenerate p-type semiconductor for the barrier forming material may have advantages in optical transmission for a given sheet resistance as compared to metallic barriers. Several semiconducting compounds were tested as barrier materials to GaAs and the best results have been achieved with cuprous selenide. This compound is a degenerate p-type semiconductor in which copper vacancies act as acceptors. Differential capacitance studies of cuprous selenide-GaAs barriers indicate a barrier height of 1.2 eV. Because cuprous selenide disproportionates under conventional evaporation, flash evaporation is a better means of controlling the composition of the film.

The conductivity and optical properties of cuprous selenide depend on the departure from stoichiometry in the films which in turn relates to the composition of the cuprous selenide charge and the evaporation parameters. Having flash evaporated cuprous selenide charges of various composition, it was found that $Cu_{1.8}Se$ gave the most conductive and stable films. The cuprous selenide has been prepared by reacting weighed amounts of the elements in a sealed evacuated quartz tube. Figure 3 shows the optical transmission spectrum of a typical $Cu_{1.8}Se$ film. The absorption at the higher energies is indicative of a bandgap near 2 eV. The absorption in the infrared is believed to be due to free carriers.

Cell Structures

Fig. 4 indicates schematically two of the forms in which gallium arsenide thin film solar cells have been made. The cells on molybdenum have a gallium arsenide film which is typically 2-5 mils thick, so that the total thickness of the cell is approximately 4-7 mils.

When Pt is used as the barrier forming material, the GaAs film is etched with aqua regia. Pt is then evaporated onto the film to a thickness of approximately 40Å, resulting in a white light transmissivity of 70% and a sheet resistivity on the order of 500 ohms per square. In most cases, the cell is given a post-evaporation etch in HCl which has been found to increase the initial efficiency (stability effects associated with this etching process will be discussed later). A gold grid is then evaporated onto the Pt layer to reduce the resistance; in most cases a grid geometry consisting of lines 0.002 in. wide, separated by 0.020 in. has been used. Finally, an antireflection coating of Krylon or SiO is usually applied.

When $Cu_{1.8}Se$-GaAs solar cells are fabricated, the GaAs film is first etched with 1% bromine-alcohol prior to the flash evaporation of the barrier layer. The cuprous selenide film is typically 200Å thick and 70% transmitting at 1.5 eV. The specific resistivity in these films is of the order of 10^{-4} Ω-cm. A "comb" shaped gold grid is then evaporated in order to lower the sheet resistance. In some cases an antireflection coating of Krylon has been added.

Fig. 4b shows diagramatically a cell made on Al foil. The approximate thickness of the Al, InAs layer and GaAs film are 4, 10 and 15μ respectively. The completed cell is then about 1.5 mils thick.

Results

Fig. 5 shows the spectral response of platinum and cuprous selenide barrier cells. The responses have been arbitrarily normalized to one hundred at their maxima and do not, therefore, afford a comparison of the absolute responses of these two types of cells. These curves are notably different from the spectral response obtained with a p-n junction in gallium arsenide. As long as the optical transmission through the barrier remains constant, the relative response per photon is practically independent of energy when the optical absorption becomes high enough for all photons to be absorbed in the depletion region. The decrease in response at higher energies is attributed to increased absorption in the platinum and cuprous selenide layers.

The method used to measure cell efficiency in this work is as follows: The incident light intensity and short-circuit current are first measured in sunlight. The I_{sc} corresponding to 100 mw/cm^2 incident intensity is then calculated by assuming I_{sc} to be proportional to incident intensity. This current is then reproduced in the laboratory under tungsten illumination and the complete I-V curve is obtained. The assumption of linearity is more justifiable as the extrapolation becomes smaller. In addition, of course, this method assumes that the cell is not limited by series resistance.

Fig. 6 shows the I-V characteristic under illumination for a cuprous selenide-GaAs barrier on Al foil. The shape of the I-V curve makes evident

the present limitations imposed by series and sheet resistance. The efficiency of 4.26% is calculated without subtracting the gridded area. By weighing the cell, a power to weight ratio of 135 watts per lb. was measured. The current density obtained with this cell, 15 ma/cm^2, can be compared with 17 ma/cm^2 for 11% efficient GaAs single crystal p-n junction cells.(6)

Efficiency measurements for Pt-GaAs cells are shown in Fig. 7. These measurements are the best results obtained to date for cells of three different areas. It can be seen that, for small areas, efficiencies of 5% have been obtained, whereas for 2 cm^2 cell areas the best efficiency value was 4.5%, and for 4 cm^2 cells the highest efficiency obtained thus far is 3%. These efficiency values are based on total cell area. As the area becomes larger it is increasingly more difficult to prevent inhomogeneities in the film caused by nonuniform temperature distributions and thermal stress. As a result the shunt leakage increases with area which in turn lowers the cell efficiency.

A number of life test measurements have been made for Pt-GaAs cells stored at room ambient. These measurements have shown that most cells subjected to a post-evaporation etch in HCl or HF degrade. Although a degraded cell can usually be restored to its initial characteristics by re-etching, it will again deteriorate. Protective coatings, such as Krylon, can partially inhibit cell degradation. Cells which have not been etched show no significant deterioration.

Fig. 8 shows normalized power output as a function of storage time for unetched, unprotected cells, and cells that have been etched and covered with Krylon. Cell degradation is manifested by an increase in the apparent series resistance with a resultant decrease in short circuit current and fill factor. Although the initial efficiency of the etched cells is higher, after about three weeks the efficiency deteriorated to a value less than that of the unetched cells. Since the highest cell efficiencies measured to date have been obtained from etched and therefore unstable cells, a major problem is the elimination of degradation without decreasing cell efficiency.

The characteristics of solar cells made with cuprous selenide-GaAs barriers have been observed for several months. A cell made on a Mo substrate was stable under continuous load testing at room ambient for a period of 35 days with no protective coating. (See Fig. 9, bottom curve). In addition, this cell had been stable in vacuum for several days under load. Cells made on Al substrates degraded noticeably after several days. The degradation manifested itself mainly be an apparent increase in resistance resulting in a decrease of the short circuit current and the fill factor. A gradual discoloration of the cuprous-selenide film was also observed during this period. Degraded cells could be restored to their original characteristic by etching them in a solution of 1% HNO_3. Fig. 9 shows examples of the stability of etched cells using Al substrate under periodic and continuous load testing.

*It has recently been found that the optical transmission of some cuprous selenide films flash evaporated onto glass can slowly decrease when stored under room ambient conditions. This, too, may be a factor affecting cell degradation.

Conclusions

A comparison of the electrical and optical properties of sputtered, flash evaporated, and vapor grown GaAs films has shown that only the latter are suitable for solar cell applications.

Satisfactory junctions on GaAs films have been obtained only with Pt or $Cu_{1.8}Se$ surface barriers.

Efficiencies with Pt-GaAs barriers on Mo substrates of from 3% for 4 cm^2 areas to 5% for 0.2 cm^2 areas have been obtained. For $Cu_{1.8}Se$-GaAs barriers on Mo, an efficiency of 4.6% for 0.73 cm^2 area has been measured. With Al substrates this figure is 4.3% for the same area.

Aluminum foil has been shown to be a practical substrate for the fabrication of a flexible, lightweight cell. A power to weight ratio of 135 watts per pound was obtained in such a structure.

The use of post-evaporation etching for Pt-GaAs cells causes subsequent degradation in the photovoltaic response. Although unetched cells seem to be stable, their initial efficiencies have been lower than those obtained with etching. Cells made with cuprous selenide-GaAs barriers on Mo substrates have been stable under continuous load for at least 35 days with no protection. The degradation rate of such cells on Al substrates has been greatly reduced with a suitable etching treatment.

---

* We include here some observations made since 19 October 1965.

References

1. C. D. Thurmond and C. J. Frosch, J. Electrochem Soc. 111, 184 (1964)

2. F. H. Nicoll, J. Electrochem Soc. 110, 1165 (1963)

3. M. D. Sturge, Phys, Rev. 127, 768 (1962)

4. D. Perkins and E. F. Pasierb, Proc. Fourth Photovoltaic Specialists Conf. Vol II, A2 (1964)

5. W. G. Spitzer et al, Phys. Rev. Letters 8, 7 (1962)

6. A. R. Gobat, M. E. LaMorte and G. W. McIver, IRE Trans on Military Electronics Publication No. ST 2194. Jan. 1962

Acknowledgments

We wish to acknowledge the technical assistance of E. F. Pasierb, J. J. O'Neill, Jr., G. Mark and R. W. Pratt, and the help of Miss M. L. Kuettel, R. J. Paff, and W. C. Roth of our Materials Analysis Group.

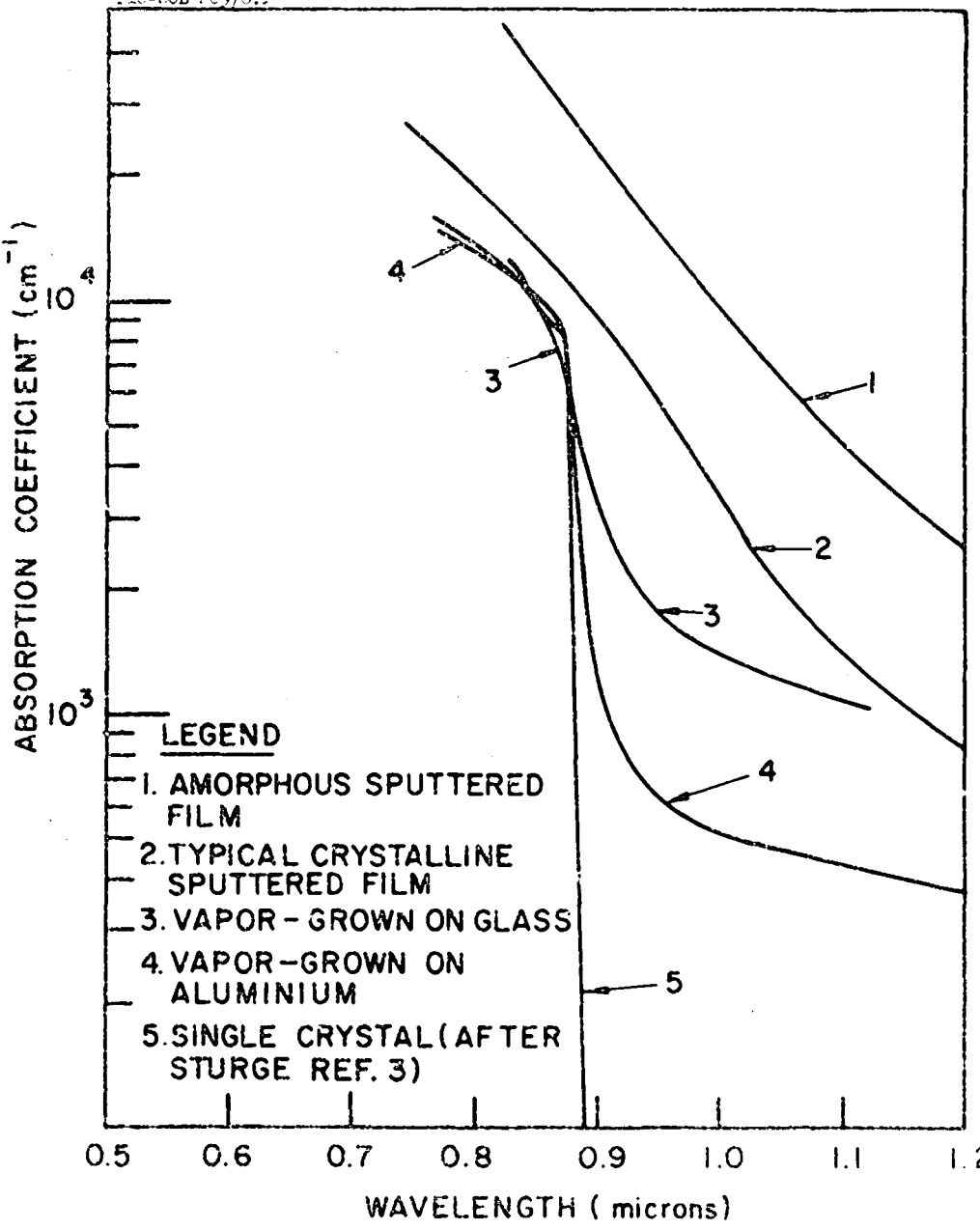

FIG.1 ABSORPTION COEFFICIENTS OF GaAs FILMS

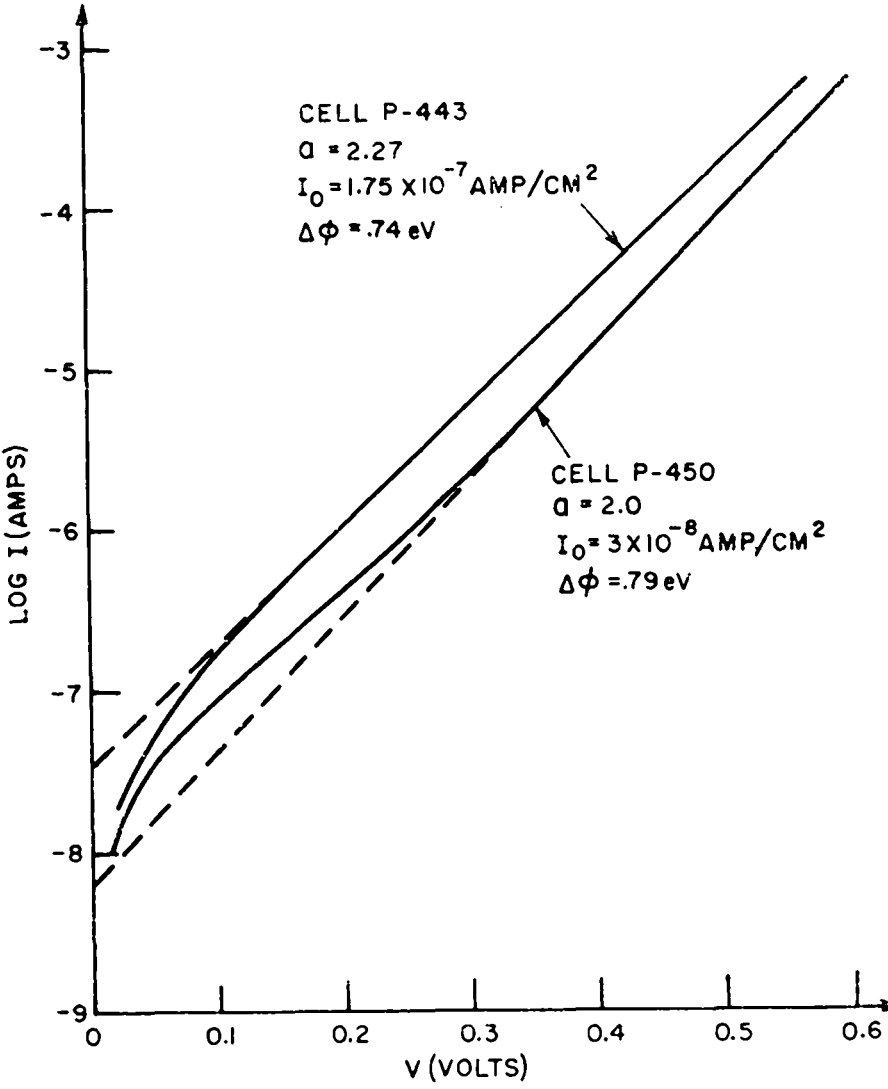

FIG. 2 FORWARD CURRENT VOLTAGE CHARACTERISTICS OF Pt – GaAs CELLS

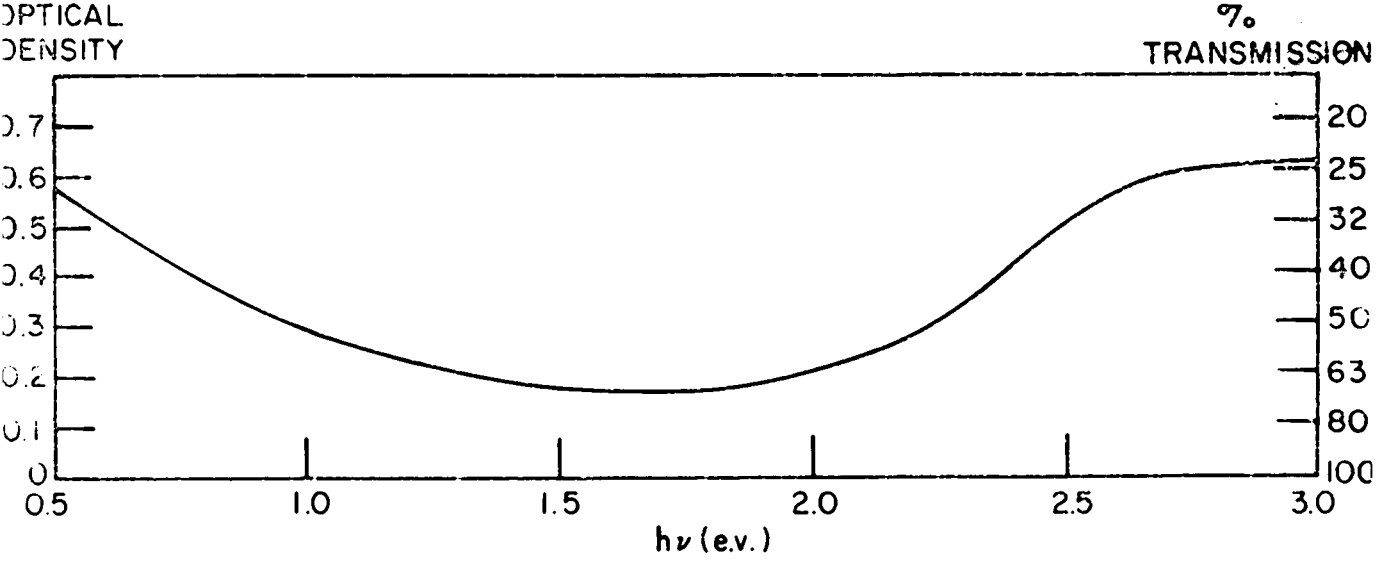

FIG. 3 OPTICAL ABSORPTION SPECTRA OF TYPICAL COPPER SELENIDE FILM FLASH EVAPORATED ON GLASS

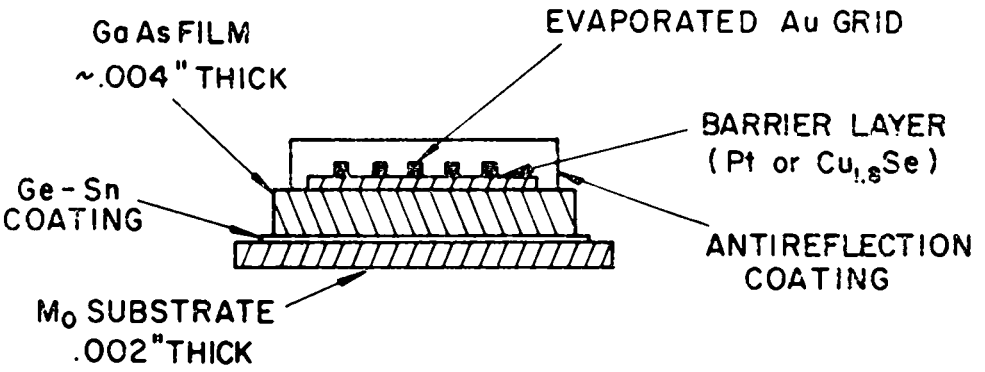

(A.) CELL WITH Mo SUBSTRATE

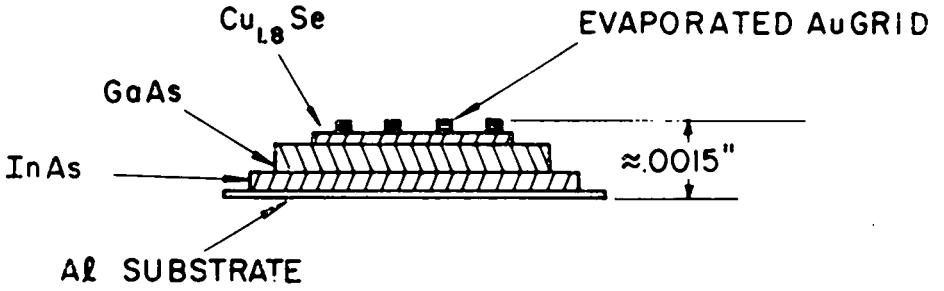

(B.) $Cu_{1.8}Se$-GaAs CELL WITH Al SUBSTRATE

FIG. 4 SURFACE BARRIER CELL STRUCTURES

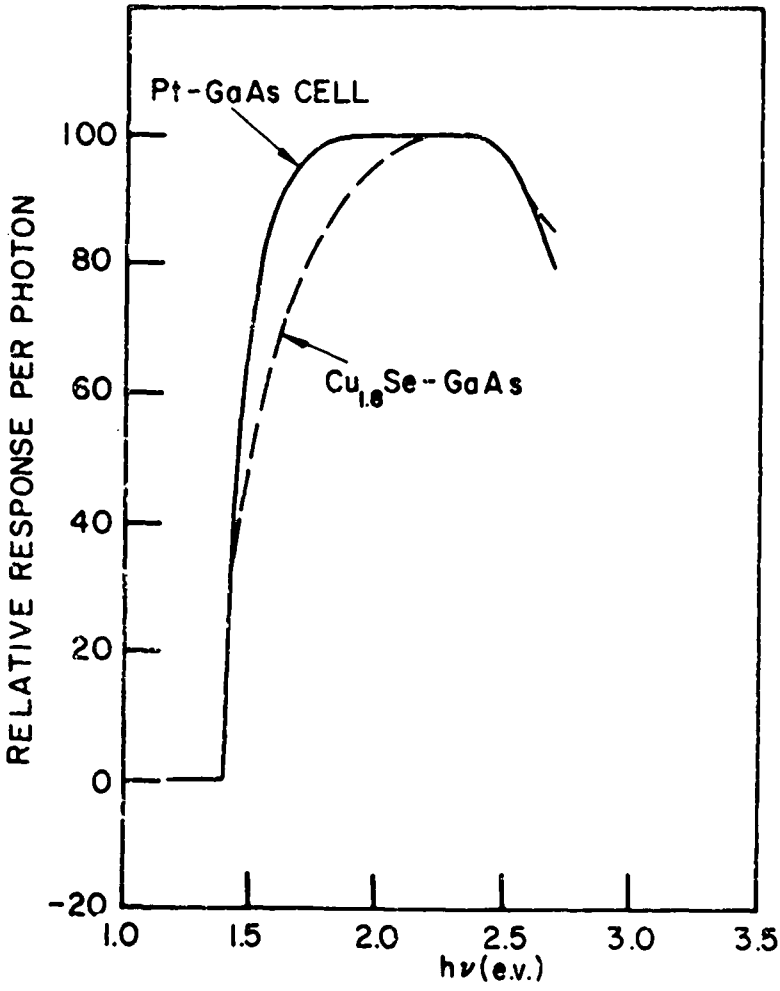

FIG. 5 SPECTRAL RESPONSE OF Pt AND $Cu_{1.8}Se$ BARRIER CELLS

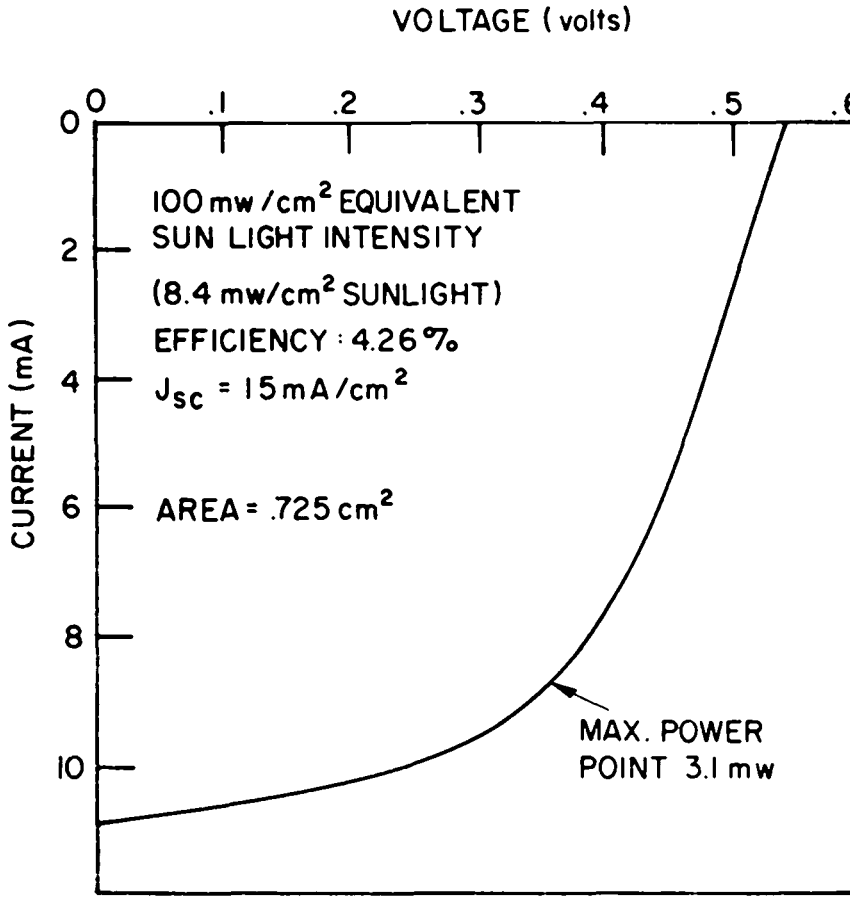

FIG. 6 EFFICIENCY MEASUREMENT OF
$Cu_{1.8}Se$-GaAs ON Aℓ FOIL

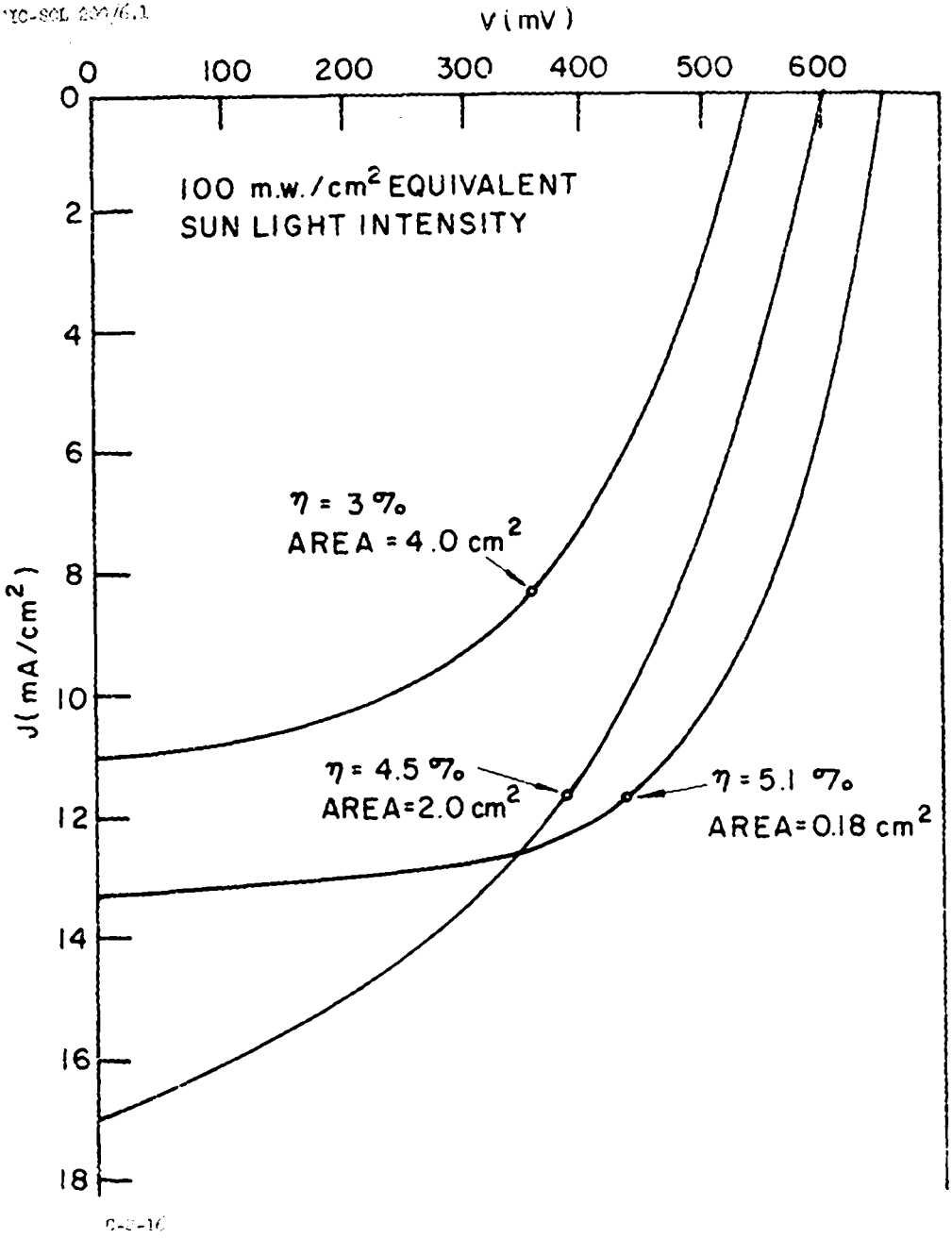

FIG. 7 EFFICIENCY MEASUREMENT OF Pt-GaAs CELLS.

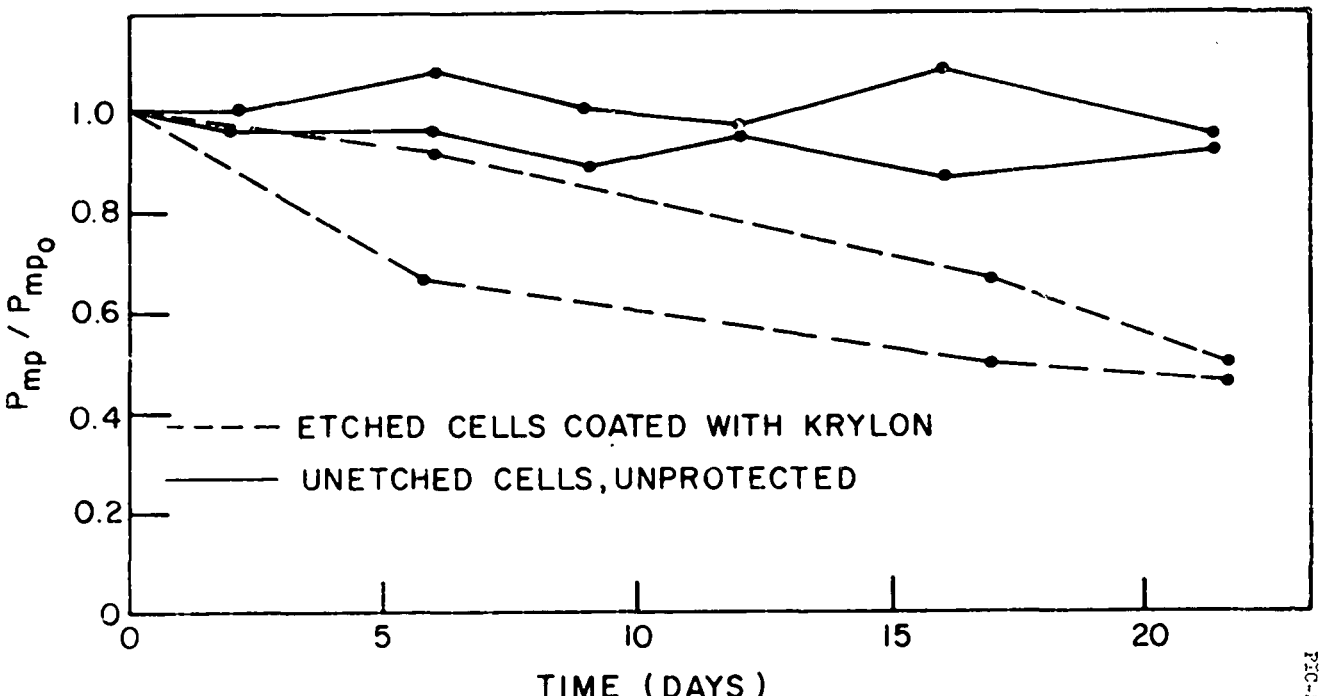

FIG. 8 POWER OUTPUT vs. TIME FOR Pi-GaAs CELLS (ROOM AMBIENT STORAGE)

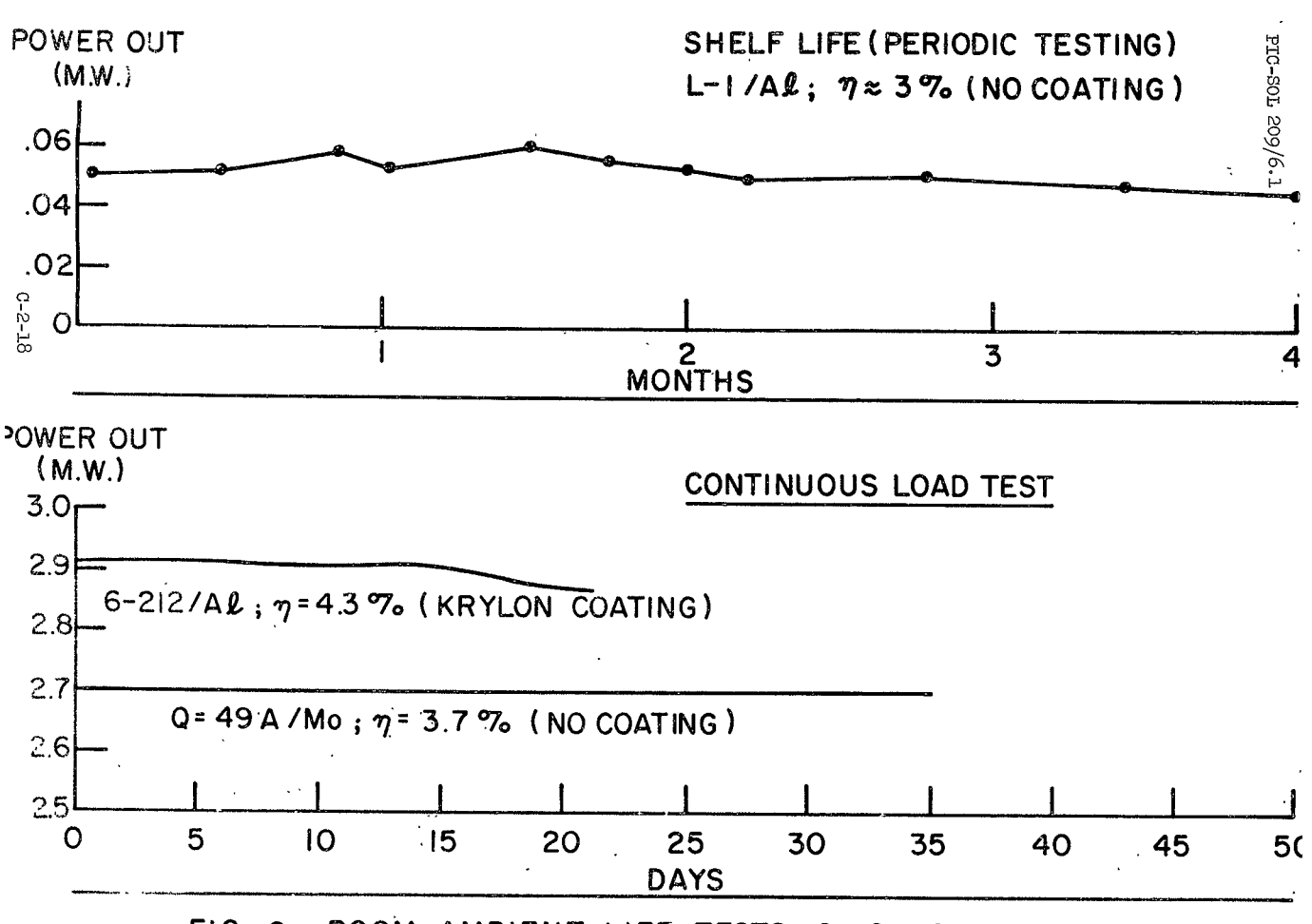

FIG. 9 ROOM AMBIENT LIFE TESTS, $Cu_{1.8}Se$-GaAs CELLS

Discussion

Massie: Thank you, Dr. Ellis. We'll now have a question and answer period.

Keramidas - Harshaw Chemical: I have two questions. One of them has to do with the thickness of your depletion layer. Could you please comment on how thick it is?

Ellis - RCA: You mean the thickness - the distance over which the band bending occurs in the gallium arsenide?

Keramidas: Yes.

Ellis: Dave, would you have any comment on that?

Perkins - RCA: What you really want to know is the junction depth in the gallium arsenide? For the best polycrystalline films, this is about 6 or 7 tenths of a micron.

Keramidas: OK. And the other one has to do with the material itself. You identify it as $Cu_{1.8}Se$?

Ellis: Yes.

Keramidas: Could you please tell me - how do you identify it as being that?

Ellis: We've analyzed both the starting material and we've analyzed films thicker films than this. We've analyzed films of about 2000 angstroms thick. As I recall it, both elements are determined, but I think the accuracy for copper is higher and the selenium is taken by difference.

Keramidas: OK. Thank you.

Pollack - University of Pennsylvania: Did you try doping the films by a flash evaporation technique? In the flash evaporation, did you try to flash-evaporate the stoichiometric gallium arsenide? Or did you try to actually dope - have you ever tried doping the film, using a flash evaporation technique?

Ellis: I think that is in Paul Vohl's area.

Perkins: I think the question is that whether in the flash-evaporating or sputtering, an attempt was made to dope at the time of film formation.

Vohl - RCA: We have used two methods to dope the films. One is to mix particles of dopent and pure GaAs and flash evaporate. The other is to flash evaporate doped GaAs. The latter method results in a more uniformly doped film. Undoped films are always high resistivity P-type. Films can

be doped to low resistivity P-type with Zn or Mn. We have not been able to deposit n-type films from a source of GaAs doped with the normal n-type dopents i.e. Se or Te. However, we have been able to deposit high resistance n-type films by mixing 0.1% Sn particles with the source GaAs.

Pollack: What was the substrate temperature during the flash evaporation?

Vohl: We varied the substrate temperature from room temperature up to about 600 degrees C.

Pollack: Thank you.

Ellis: I think one reason we included these results on flash evaporation and sputtering was to discourage other people from getting into this area.

Mlavsky - TYCO: Would you comment, please, on the crystallinity of this film. How big are the crystallites? How are they oriented? And just one further question in general: Three-five compounds usually, and in gallium arsenide certainly, are not characterized by their willingness to form crystalline films on amorphous substrates at low temperatures, and the big emphasis on two-six is surely - is the fact that they are so characterized. What's the prognosis in terms of your working with a material which has to be crystalline to give you some properties, but doesn't want to be crystalline in the first place?

Ellis: That's a good question. Let's answer the question first about crystal size. In a film, which is, say, 3 mils thick - and these have been sectioned, the crystal size - distance across typical crystals at the top of the film is of the order of 1 to 2 mils. The general structure of the film starts off with small crystals which compete, and then some take over and then grow. It looks very much, incidentally, like an electroplated film of copper. There's some evidence of stacking faults in the crystals - a slight tendency to <111> orientation as the film gets thicker.

Now, on the crystallinity, the reason why these films, I think, show a well-defined band gap by the oxide transport process is that this is a reversible process running near equilibrium, so that an atom which enters a crystal in a wrong place has an opportunity to come out and reenter in a right place. And I think that the reason why the sputtered and flash-evaporated film shows such poor properties is that there essentially an atom which enters in the wrong place is trapped. It's a nonreversible process. Does that answer the question?

Cusano - GE: Did you do elevated temperature measurements, and if you did, what turned out to be...

Ellis: None.

Cusano: How about the lower room temperature? Did you take...

Ellis: Unless Dave has some results which he wants to talk about...

Perkins: We've done a few measurements of the effects of temperature on the platinum-gallium arsenide cells. The temperature range, in which we measured chiefly the variation of the open circuit voltage with temperature, was from room temperature up to about 100 degrees C, and we got a slope of about minus 2-1/2 millivolts per degree C for the open circuit voltage. We have not done systematic measurements below room temperature, although we have made a few spot measurements of the open circuit voltage at liquid nitrogen temperature.

Question (inaudible)

Perkins: Yes, we've made stability measurements on - again, I can only speak of the platinum-gallium arsenide cells - at elevated temperatures in a hydrogen atmosphere, and we found essentially the same effects that we find at room temperature.

****

PIC-SOL 209/6.1
Section C-3

THE THIN FILM CdS SOLAR CELL

Presented by

F. A. Shirland

Electronic Research Division

Clevite Corporation

Cleveland, Ohio

19 October 1965

Abstract N66 17329

The present Clevite CdS thin film solar cell is inherently 6 to 8% efficient with short circuit current densities of 20 to 25 mA/cm^2 and fill factors of 60 to 70%. Lower outputs are ascribed to incomplete contacting of the barrier or to accidental causes.

Two factors, adsorption of moisture and loosening of the pressure grid contact, are believed to be responsible for most if not all of the degradation that has been experienced for some CdS cells. When these two factors are controlled the CdS solar cell appears to be stable. Large area cells stored in a dry atmosphere have been stable at the 4 to 5% level for as long as a year to date.

The design and fabrication of large area CdS film solar cells is described. Recent improvements in evaporated CdS films, metal substrates, collector grids, and cell packaging are discussed. Predictions are made for low cost large area light weight cells with conversion efficiencies greater than 10%. auths

THE THIN FILM CdS SOLAR CELL

by F. A. Shirland and J. R. Hietenan
Electronic Research Division, Clevite Corporation
Cleveland, Ohio 44108

Introduction

The photovoltaic effect in CdS was discovered by Donald C. Reynolds[1, 2] of the Air Force Aerospace Research Laboratory in 1954. The concept of a CdS thin film solar cell was advanced by Allan Carlson, whose group[3, 4] demonstrated its feasibility in 1955. It was 1960, however, before conversion efficiencies of as much as a few per cent were obtained from CdS films.[5, 6]

About a year ago the authors developed a process that increased the efficiency of large area CdS thin film solar cells to the 4-6% range on a reproducible basis. This was described[7] at the Power Sources Conference earlier this year.

The present paper summarizes the progress made since in understanding the functioning of the component parts of the CdS film solar cell in general. An attempt is made to interpret what this will mean to future device performance. The paper to follow describes progress on the plastic substrate CdS thin film solar cell.

Construction

The CdS thin film solar cell is a simple device consisting of a substrate, a polycrystalline CdS layer, a barrier layer, a top contact, leads, and some form of protection for the barrier. This is illustrated in Fig. 1 for the metal substrate frontwall cell construction.

There are a number of different configurations of CdS thin film solar cells that have been fabricated experimentally. However, the essential components which are common to all constructions are the CdS film and the barrier layer. These are the heart of the CdS cell. The remaining elements (the substrate, grids, leads, plastics, etc.) are really only packaging, but, as has been painfully learned, the packaging can be extremely important.

A description of the component parts of the frontwall metal substrate cell will help illustrate the problems which have been encountered and show how an understanding of these is expected to lead to further improvements.

Functioning of the Component Parts

The Substrate

The substrate forms the base for the CdS film during deposition and maintains its physical integrity thereafter. The substrate must be conductive, must withstand the temperatures necessary to deposit CdS, and be compatible mechanically and electrically with the CdS film. It is also desirable that it be strong in the form of thin light weight foils. Molybdenum has been widely used for thin film solar cell substrates and is still standard for our metal substrate cell.

In practice we have found that most difficulties with poor CdS films result from incomplete cleaning of the substrate. In order to secure well structured adherent films that are practical for solar cells, the substrate surface must be uniformly clean on a microscopic scale.

CdS Films

CdS films can be formed in a variety of ways. We have found the vacuum deposition of undoped or lightly doped sintered CdS powder to be effective and economic. The CdS film can be as thin as a few microns, but the very thin films require a higher degree of crystalline perfection than can presently be obtained reproducibly over large areas. Hence, we have settled, for now, on film thicknesses of about 15 to 20 microns which have been found to perform satisfactorily. The CdS film is n-type semiconducting with about 10^{17} to 10^{18} carriers per cm^3. Hall mobilities of these films have generally been just under 25 cm^2/ volt-sec.

The conditions for forming CdS films do not appear to be critical, but the substrate temperature should be hot enough to prevent condensation of the constituent elements. High deposition rates seem to yield better cells. We feel, but have not proved, that better cells result from films containing fine grain size and a high dislocation density.

The Barrier Layer

The barrier layer and the junction it forms with CdS are the part of the CdS solar cell that is least understood. The barrier layer appears to consist of copper deficient Cu_2S. It is formed by a chemical exchange of Cu^+ ions for cadmium at the surface of the crystal. The Cu_2S layer is evidently very thin, on the order of 1000 Å. It gives a strong indication of p-type semiconduction on thermoelectric probing, and has a sheet resistance on the order of 1000 ohms per square.

Various methods of forming barriers on CdS have been developed. Our method consists of dipping a freshly etched CdS film in a hot solution of CuCl for a few seconds, rinsing, drying, and heating at 250°C for a few minutes. It is our belief that during this process some copper ions, possibly in association with chlorine ions, diffuse a short distance into the CdS lattice at dislocations to yield photon absorbing-electron trapping centers. These centers are presumed to be within or very close to the depletion region. It is thought that the higher efficiency CdS cells obtained by the Clevite process are due to improvements in the number and physical location of these centers.

The Barrier Contact

The barrier contact is made with a fine electroformed metal mesh grid which is placed against the barrier layer and held there by a fused plastic film. The grid must be sufficiently conductive to carry the generated current with minimal voltage drop, yet block as little light as possible. The grid lines should be as close together as practical in order to minimize sheet resistance losses in the barrier layer itself. This is a case of optimization of conflicting requirements. A commercially available[8] 60 line per inch electroformed copper mesh, 0.0005 inch thick, having about 85% light transmission, has been used for the cells described here.

The Leads

The leads are thin metal foil strips attached to the grid and to the substrate which are positive and negative respectively. Silver foil, 0.001 inch thick, with a protective gold plating, has been used. Earlier the plastic encapsulation was depended on to hold the leads in pressure contact. Recently we have started attaching the leads with a conductive epoxy cement.

The Plastic Envelope

The plastic envelope is required to protect the cell barrier from moisture, though it is not really adequate for this purpose. It is probably required also as protection against low energy protons. It is a means of minimizing reflective losses at the barrier surface, and it can help to hold a number of cells together in larger arrays. Its main function to date has been to hold the collector grid in pressure contact to the barrier.

Mylar[9] plastic has been used most extensively though Kapton[9] plastic is much more resistant to UV and Van Allen radiation. Kapton is not transparent to shorter wavelengths of light and hence CdS film cells protected by Kapton yield about 20% less output initially than those protected by Mylar.

Kapton and Mylar both require the use of an adhesive in order to secure adherence to the CdS cell. Capran,[10] a nylon polymer, has been used chiefly for this purpose. It adheres well, is transparent, and has a favorable melting temperature.

Indicated Design Improvements

Except for the substitution of copper for the earlier gold grids and the use of conductive epoxy cement for lead attachment, the design of the present frontwall metal substrate cell is still the same as that of the cell characterized at the Power Sources Conference. There are a number of aspects of this design that have not been entirely satisfactory. In investigating these aspects a great deal has been learned about the thin film CdS solar cell which should shortly be translated into a markedly improved cell.

Stability studies have had the most attention in recent months and have pointed the way to major cell improvements. Some CdS thin film solar cells of the standard construction have been stable for peric of a year or more. This is shown in Table I which gives the original and present performance levels for several of the first 4 to 5% cells made a year ago. Cell 73C was the first to emerge from the improved Clevite process and has been kept on desiccated shelf storage except for occasional testing. Cells 205 and 213 were 3 inch by 3 inch cells sent to the Energy Conversion Laboratory of Lewis Research Center, NASA, in October, 1964, where they were exposed in vacuum to 2920 temperature cycles (between approximately +60°C and -60°C) and then returned to Clevite and kept on desiccated shelf storage.

Other newer cells of this general construction have also held their initial high efficiency levels for many months. For example the group of 13 plastic substrate cells listed in Table I of the following paper have held an average output of 5.1% for four months to date. These data reveal a degree of stability which suggest an intrinsically stable cell when kept away from moisture.

However, there have been other cells that have degraded at various rates from as little as 1 to 2% of the initial output each month to as much as 30 to 40% a month. Studies have led to the conclusion that most of this kind of degradation is caused by loosening of the pressure contact of the grid to the barrier. This loosening apparently results from incomplete lamination rather than from cold flow of the Capran adhesive. Cells that have degraded this way can be restored by a simple re-lamination.

In an attempt to correct this weakness, higher lamination temperatures were tried. These resulted in the Capran plastic flowing under the grid, probably by capillary action, to block most of the grid contact area, giving low generated currents and high series resistance. When lower lamination temperatures were tried, the degradation rate of the cells increased markedly. Significantly, the initial outputs of the cells also increased markedly. Table II shows how a decrease of just a few degrees in the lamination temperature increased the initial current, fill factor and efficiency of large area cells.

Some of these 7%+ initial efficiency cells were carefully dissected. It was discovered that even these cells had up to half of the collector grid-barrier layer contact blocked by a layer of Capran adhesive. The implication of these various observations is that the present Clevite barrier formation process yields large area cells of 6 to 8% conversion efficiency, and that these outputs are intrinsically stable. The present means of contacting the barrier and packaging the cells evidently prevents the attainment of the higher outputs on a stable basis.

Thus it is clear that the pressure grid contact needs replacing by a more positive and more permanent contact. We have experimented with electroplated grids, ruled grids, vacuum evaporated grids, and cemented grids and have found the latter most promising. This method of cell contacting is accomplished by coating one surface of commercial electroformed mesh grids with conductive epoxy cement which is then pressed against the barrier layer and cured in place. Difficulties with smearing and spreading of the cement can be minimized by careful handling techniques. Dozens of large area cells with efficiencies up to 6% have been made in this manner and these show every indication of being stable when kept dry. Even when these cells are deliberately degraded by moisture they can be restored by simply heating to drive off the moisture.

Figure 2 illustrates the deliberate degradation of one cell with a cemented grid, and its restoration. It had been stable at the 5.8% level for 3 weeks and was then exposed to 80% humidity at 30°C for a week. During that week it degraded steadily to less than 2% (for simplicity only selected curves from the complete sequence are shown here) until finally the leads came loose. It was then dried in a desiccator and relaminated. It came back to the 5.5% level and has remained there for the several weeks since.

The Metal Substrate

Molybdenum was selected for this substrate several years ago on the basis of the close match of its thermal expansion coefficient to CdS, and because it worked. The disadvantage of molybdenum is that the use of foils thinner than 0.002 inch have not been practical. In addition, molybdenum is a relatively poor conductor, is expensive, cannot be readily soldered or welded, and is fairly heavy.

We have obtained very satisfactory results with 0.001 inch thick zinc coated copper foil substrates. Copper promises to be superior in all respects except in the match of thermal expansion coefficients. Improved handling techniques however have made this factor less important. With the use of copper it is convenient to extend the substrate to form the negative lead of the cell. Larger scale trials of copper foil substrates are in progress and no difficulty in substituting copper for molybdenum is now foreseen.

The Collector Grid

The present electroformed copper mesh grid is expensive and is not really optimized for the CdS film cell contact. A grid with more wires in one direction and fewer in the perpendicular direction would be more efficient. Such a grid has been designed having an integral extension along one edge to form the positive lead of the cell. This design also provides for a tapering of the main current carrying wires so that they are wider at the base near the positive lead where the current density is greatest. This should minimize the voltage drop in the grid while increasing transmission of light through it.

The use of leads that are integral parts of the substrate and the collector grid will eliminate two separate components from each cell with a consequent decrease in cell cost and increase in reliability.

The Cover Plastic

Development work is underway at other laboratories to use vacuum deposited silica and alumina coatings to protect the barriers of thin film solar cells. These could have many advantages over the present plastic encapsulation, particularly for long lived space missions.

Present Problems and Future Possibilities

The design improvements discussed above should correct the major weaknesses of the present thin film CdS solar cell and permit a real appraisal of the suitability of the cell for space power systems. In light of the data presented, cell efficiencies of 6 to 8 per cent on a regular basis are expected. At present there is no indication of any costly parts or processes being needed.

Eliminating the pressure contact for the grid will help to pin point lesser causes of instability. Because some cells have shown no degradation on dry shelf storage for as long as a year, such lesser causes of instability can presumably also be eliminated.

There remain two major problem areas which must be removed before the CdS cell can be accepted for space power systems. Most important is the demonstration of a cell construction able to withstand the thermal cycling that would be encountered in the earth orbit. Of lesser importance is sufficient protection of the cells from moisture to permit the necessary test procedures to be run on the ground prior to lift-off into orbit.

Many cells with pressure contact grids have developed short circuits on extended temperature cycling. These shorts were localized and were always under a grid wire. They appeared to be due to the grid rubbing through the barrier, possibly due to relative movement under the stresses of sudden temperature gradients. Permanently bonded grids have not developed such shorts. Hence, if the cemented grid process mentioned earlier can be improved to provide a truly permanent bond the cells may then be able to withstand the rigors of extended thermal cycling.

Eliminating the hygroscopic nylon layer may well reduce the moisture problem sufficiently to carry the cells through the necessary periods of testing while in high humidity ambients on the ground. The CdTe cell, which appears to be analogous to the CdS cell, has no nylon plastic layer adjacent to the barrier and is evidently much less affected by humid ambients. Also, there are other possible means of protecting barriers from moisture pick-up, including formation of a thicker more continuous Cu_2S layer over the barrier, and the deposition of a glassy protective coating.

Assuming that these improvements can be effected, it is appropriate to ask what might be obtained in the way of output from the CdS cell in the future. The lack of a clear understanding of how the photovoltaic effect operates in CdS makes this difficult to answer. However, the outputs obtained recently are higher than were expected just a few years ago, and therefore a reappraisal of the potential of this cell is in order.

The I-V characteristic curve of the highest output obtained from a 3 inch by 3 inch sized CdS film solar cell is shown in Figure 3. This was a frontwall metal substrate cell which, when tested at 25°C in tungsten light equivalent to 100 mw/cm^2 sunlight, gave 0.4 watts at maximum power. The total gridded area was 52.1 cm^2 representing a conversion efficiency, as normally calculated, of 8.20%. If allowance is made for the 15% of incident light blocked by the grid, the illuminated barrier actually converted 9.5% of the intercepted light to useful power. On this basis its short circuit current density was over 30 ma/cm^2. Yet, this is not a particularly rectangular characteristic curve. The fill factor is 66.5%, and fill factors have run up to 74% for CdS film cells.

Another cell, 1 1/2 inch by 1 1/2 inch in size, gave an initial efficiency at maximum power of 8.35% as normally calculated, or 9.8% on the basis of active illuminated barrier area. Two additional cells of 50 cm^2 area have been at the 8.0% level as normally calculated. In view of the incidence of these higher output cells and the evidence that they are still not optimized, it seems likely to the authors that CdS cell efficiencies greater than 10% may be realized. Efforts along these lines are continuing.

Earlier, Wolf[11] calculated that a CdS solar cell with a two stage transition of carriers from valence to conduction bands should have theoretically a 38% ultimate ceiling of efficiency as compared with 25% for silicon solar cells with a single step transition. With the realization of efficiencies at the 8% level this calculation suggests exciting possibilities for further improvements.

Acknowledgement

The help of Frank Augustine, Warren Bower, James Gould, Donald Lehmann, Lawrence Sliker, and Lee Shiozawa in this work is gratefully acknowledged.

The cell stability and design improvement studies described in this paper were carried out with the support of NASA, under Contract NAS 3-6461. This support is also acknowledged.

References

1. D. C. Reynolds, et al., "Photovoltaic Effect in Cadmium Sulfide," Phy. Rev., 96, pp. 533-4 (1954).

2. D. C. Reynolds, "Cadmium Sulfide Barrier Layer Cell," U. S. Patent 2, 844, 640 (July 22, 1958).

3. A. E. Carlson, "Research on Semiconductor Films, "WADC Technical Report 56-52, (January, 1956).

4. A. E. Carlson, et al., "Photovoltaic Cells and Methods of Fabricating Same," U. S. Patent 2, 820, 841 (January 21, 1958).

5. F. A. Shirland and D. A. Gorski, "Research on a Composite Energy Gap Photovoltaic Cell," WADD Third Quarterly Progress Report on Contract AF 33(616)-6548, (March 7, 1960).

6. A. E. Middleton, et al., "Evaporated CdS Film Photovoltaic Cells for Solar Energy Conversion," ARS Space Power Systems Conference Paper 1291-60, Santa Monica, California, (September, 1960).

7. F. A. Shirland and J. R. Hietanen, "Improved CdS Thin Film Solar Cells," Nineteenth Annual Power Sources Conference, Atlantic City, New Jersey, (May, 1965).

8. Obtained from the Buckbee Mears Co., St. Paul, Minnesota.

9. Mylar and Kapton are trademarks of E. I. DuPont Co.

10. Capran polyamide film supplied by General Chemical Div., Allied Chemical Co.

11. M. Wolf, Proceedings of the IRE, pp. 1246-63, (July, 1960).

TABLE I

STABILITY OF SOME EARLY HIGH OUTPUT CdS FILM CELLS

Cell	Area	Initial Efficiency	Present Efficiency	Age
73C	4.3 cm^2	4.8%	4.8%	14-1/2 months
205	49.0	4.2	4.1	11-1/2
213	46.8	4.2	4.2	11-1/2

TABLE II

EFFECT OF LAMINATION TEMPERATURE ON CELL OUTPUT

(50 cm^2 Area Cells)

Lamination Temperature	OCV	J	R_S	Fill	Eff.
°C	V	mA/cm^2	ohms	%	%
235	0.48	18.8	0.10	57	5.4
	0.47	18.8	0.11	54	4.8
	0.48	20.6	0.10	55	5.5
	0.46	20.9	0.10	53	5.3
228	0.47	19.7	0.09	58	5.9
	0.47	19.3	0.08	64	5.8
224	0.47	22.4	0.05	70	7.2
	0.47	23.1	0.05	68	7.4
	0.47	24.0	0.05	70	7.8
	0.47	21.5	0.05	69	7.0

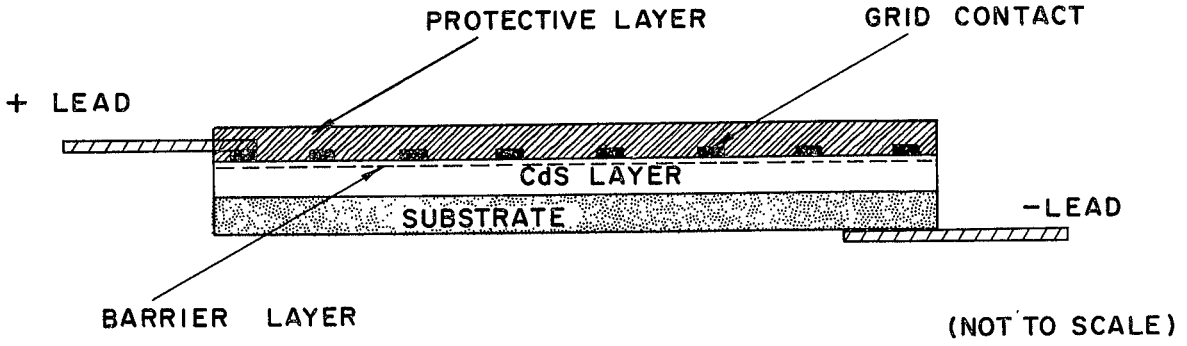

FIG. 1. CROSS SECTION OF CdS THIN FILM SOLAR CELL

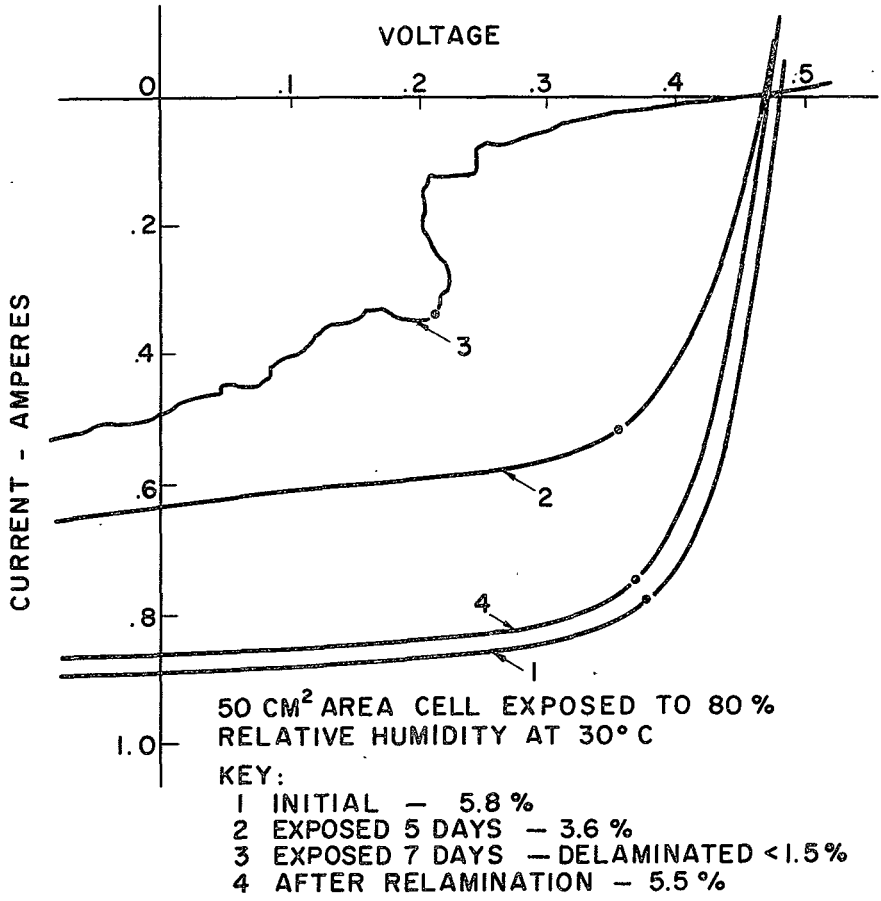

FIG. 2. MOISTURE DEGRADATION OF CdS FILM CELL WITH CEMENTED COLLECTOR GRID

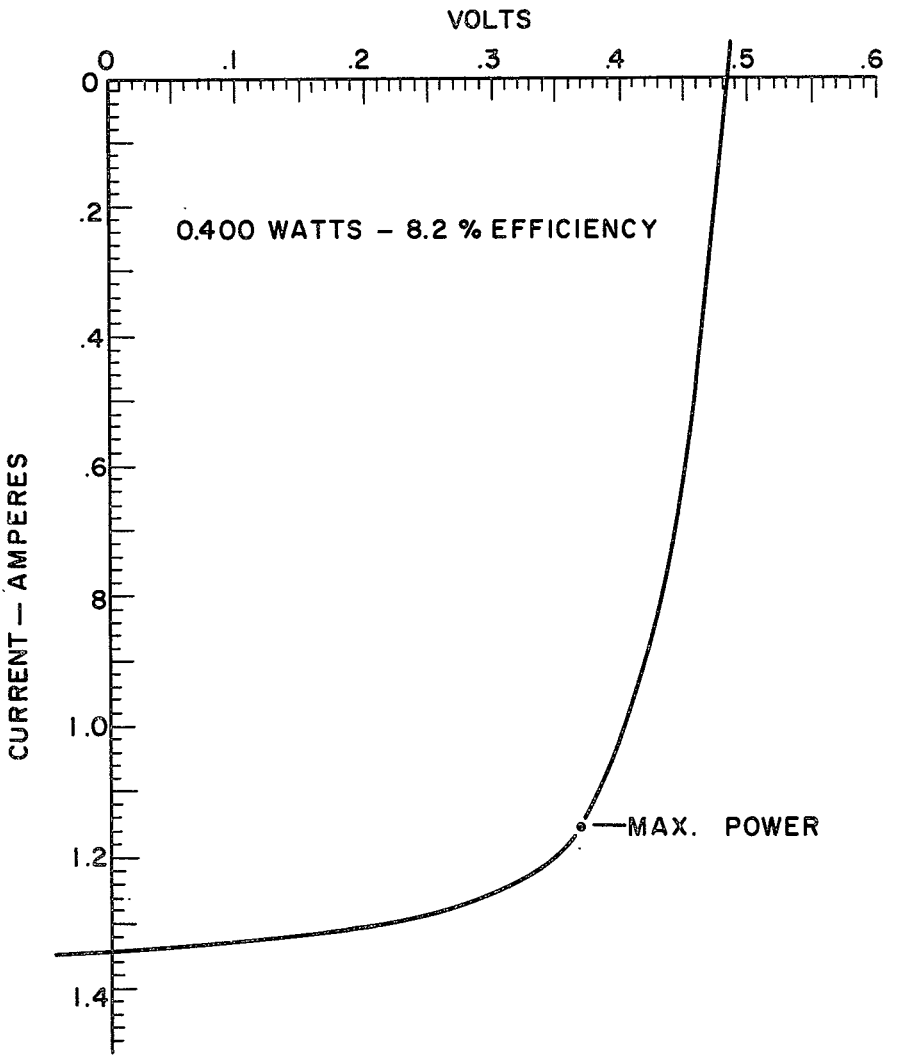

FIG. 3. I-V CHARACTERISTIC CURVE OF HIGHEST OUTPUT CdS FILM SOLAR CELL

Discussion

Massie: I think we all agree that that was a very interesting paper, and we'll now have a question and answer period.

Loferski - Brown: In what way does this process of barrier formation differ from the earlier processes? My memory may be faulty, but I thought that in Reynolds' original single crystal cells it involved the plating of copper and then subsequent heating, I guess below 400 or about 300°C. How does this differ from previous junction - barrier formation?

Shirland: Reynolds' original process was dipping the crystal into a copper sulphate solution, plating out copper, oxidizing the copper in place, and then heating. The present process, as was mentioned in the paper, consists of dipping the cell in a solution of cuprous chloride at about 85 degrees, for a few seconds, and then rinsing, drying, and heating for just a few minutes.

Perkins - RCA: Several questions, one relating to Joe's. Without the elevated temperature barrier forming process, do you get any response below band gap?

Shirland: We have done very few experiments forming these without using elevated temperatures, so I can't really answer that question. But I have yet to see a cadmium sulphide cell that has not given an extrinsic response.

Perkins: That would seem to be a critical experiment to your hypothesis of copper diffusion into the cadmium sulphide.

Shirland: A lot of work on those aspects is being planned at the present time. There's a considerable amount of controversy on this particular subject.

Perkins: Yes. How do you measure your efficiencies? Could you detail that a little bit?

Shirland: The outputs of a number of cells are measured in direct sunlight. They are then normalized to 100 milliwatts per sq. cm., and the conditions to produce that are reproduced in 3400 degree water-filtered tungsten light and then standaridized with a radiation detector and kept at that level for subsequent tests. They are cross-calibrated at regular intervals.

Perkins: They're normalized with the same cells used to measure the original sunlight efficiency?

Shirland: Yes. The cell efficiencies have generally been verified by independent measurements at both the Lewis Research Center and at the Aero Propulsion Laboratory.

Perkins: One final question. Could you comment on the shelf life of the cells when they are not desiccated?

Shirland: It all depends on the ambient humidity. In normal Cleveland weather, the cells will generally last a few months (laughter). In the summertime, they'll last a lot shorter period than they will in the winter months. In general, these cells can be brought back by simple drying or heating action, as long as the mechanical contact has not been interrupted. On some of these cells, however, the mechanical contact is loosened by moisture swelling the plastic layer and lifting the grid; these cells cannot be brought back.

Perkins: When they last a few months, what is the extent of the degradation in that time?

Shirland: Well, it is extremely variable. It may be as much as 10 or 20%, it may be 50%, it may be 80%, depending on really how severe the exposure has been.

Perkins: OK. Thank you.

Ritchie - JPL: In figuring your efficiency, do you take the total active area with the grid lines, or do your subtract the area from the grid lines in these efficiency measurements? In applying these into a system, what would be the maximum packing factor that you might achiev on such a system - taking the sealed edge into account?

Shirland: To answer the first question, the efficiencies are for the total gridded area without making allowance for the area blocked by the grids. If we did take the exposed area only, that would give about a 15% higher value than we quoted. As regards the packing factors, we have done very little work in actually mounting cells into larger arrays. Most of our work has been involved with the cell itself, but packing factors on the order of 90% should not be too difficult to obtain.

Ratcheson - Boeing: Have you calculated the watts per pound of a, say 50 sq. cm. cell?

Shirland: Yes, we have. There will be more on this subject in the next paper which will be given after the coffee break.

Loferski, Brown: Are there marked changes in the spectral response of these high-efficiency cells compared to the , say, 3% cell such as a broadening of the spectrum?

Shirland: We have not taken extensive spectral response measurements on these higher-efficiency cells. We did present some of these spectral response measurements at the Power Sources Symposium in May, and they are in the Transactions which came out last week.

Boer - Univ. of Delaware: What is the influence of the ambient atmosphere during heat treatment? Did you investigate this?

Shirland: We have a series of investigations of this under way at the present time. We are not ready to report on this work.

Boer: Did you increase your temperature... to something on the order of 500 degrees, during heat treatment?

Shirland: No, our heat treatment is normally at 250 degrees centigrade for just a few minutes. There have been occasions when other cells have been exposed to temperatures as high as 300 degrees centigrade for periods of a week, and if those cells were protected from ambient atmosphere - they didn't show any degradation.

Boer: Yes, did we understand each other correctly? After the deposition of copper chloride, you made a heat treatment only at 250 degrees?

Shirland: Right.

Boer - U of Dela: I see.

Ralph, Heliotek: What is the relationship between the air mass one or the 100 mw/cm^2 efficiency to the air mass zero or 140 mw/cm^2 efficiency?

Shirland: That's an interesting question. Of course, there has been very little direct data on this subject. This has been one of the thorns in our sides - not being able to get these cells up into space. Brandhorst and his group at NASA-Lewis have conducted airplane flights of the cadmium sulphide cells, and we have it from them that the cells should give about 1.20 times the output at air mass zero that they give at air mass one.

PIC-SOL 209/6.1
Section C-4

THIN FILM PLASTIC SUBSTRATE CdS SOLAR CELLS

Presented by

F. Augustine

Electronic Research Division

Clevite Corporation

Cleveland, Ohio

19 October 1965

Abstract

N66 17330

Major advances have been effected in the state of the art of fabricating CdS thin film solar cells on an organic plastic substrate. Cells of 50 cm^2 area with initial efficiencies of 5 to 6% are being made regularly on a laboratory scale. These cells show a slight drop in output in the first week after fabrication but then hold stable at about the 5% level.

Large area cell efficiencies greater than 7% have been obtained, and power to weight ratios in excess of 100 watts per pound have been achieved for these large area cells.

The design of these plastic substrate cells and the methods of processing are described along with indications of present problem areas and anticipated improvements.

THIN FILM PLASTIC SUBSTRATE CdS SOLAR CELLS

F. A. Shirland and F. Augustine
Electronic Research Division, Clevite Corporation
Cleveland, Ohio 44108

Introduction

In this paper a major advance in the art of making thin film CdS solar cells on plastic substrates is reported. This advance has been made possible through the development of a highly conducting strongly bonded coating on a plastic substrate. This coating is compatible with the CdS film. Large area cells of 50 cm^2 area are being made regularly with efficiencies of 4 to 6%, and efficiencies greater than 7% have been obtained.

These cells are thin and light in weight, complete with leads and a transparent plastic covering. The best cell has had a power to weight ratio of 106 watts per pound, calculated for air mass 0 sunlight conditions.

Fabrication

The substrate material is a heat stable polyimide organic polymer[1] available commercially as a high strength semi-transparent film. Films as thin as 0.0005 in. are available though most of our cells have been made on 0.002 in. and 0.001 in. thick films. One surface of the plastic film is made electrically conducting by applying a 0.0001 to 0.0003 in. thick sprayed layer of silver filled varnish.[2] This coating is then cured and given a very thin zinc overcoating by electroplating or vacuum evaporation in order to ensure an ohmic contact to the CdS. A well prepared substrate coating presents a uniform fine grained surface for the subsequent deposition of CdS, and has a sheet resistance less than 0.01 ohms per square.

Presintered commercially available CdS powder[3] is vacuum deposited onto the substrate using substrate temperatures in the range of 200-250°C, and deposition rates of 200-300 Å per second, to secure 0.0006-0.0008 in. thick polycrystalline films. These films are very adherent and will withstand repeated flexing with bends as sharp as 1/8 in. radius. However, particular care is needed to ensure that the substrate used is clean and uniform in texture, and that spattering of CdS particles from open evaporation sources is avoided.

As in the case of the metal substrate cell, barriers are formed on these plastic substrate CdS films by dipping for a few seconds in hot CuCl solution, followed by rinsing and heating for a few minutes at 250°C.

The cell is contacted with an electroformed metal mesh grid which is laminated in place with heat and pressure. The materials and processes are the same as described in the previous paper for the metal substrate cell, except that only a top cover plastic layer is utilized. The plastic substrate itself acts as the lower plastic layer. In this manner the forces due to the different thermal expansion coefficients of the CdS and the plastic are approximately equal and opposite on the two sides of the CdS film so that no curling is experienced.

The construction of the plastic substrate cell is illustrated in Fig. 1. The substrate with its conductive coating extends about 3/8 in. beyond the active portion of the cell along one edge to form the negative lead. The positive lead is a gold plated silver foil tab, 0.001 in. thick, attached to the collector grid and extending about 3/8 in. beyond the active portion of the cell along the edge opposite to the negative lead. This arrangement is advantageous when interconnecting cells into arrays.

Performance

More than a hundred plastic substrate cells of the general construction outlined above have been made in our laboratory this year using a steadily evolving fabrication process. The yield, uniformity and level of power output have shown a steady improvement throughout the period. Figure 2 is a histogram showing the frequency distribution of efficiency for 54 large area cells fabricated during a recent three month period. In addition, there was one cell scrapped due to internal shorting.

The average conversion efficiency for these 54 cells, as measured in equivalent air mass 1 sunlight, was 5.1% with a minimum of 3.2% and a maximum of 7.1%. The average open circuit voltage was 0.48 volts (0.44 to 0.51), the average current density was 16.0 mA/cm^2 (12.6 to 21.7), and the average fill factor was 64% (50 to 71).

The I-V characteristic curve of a typical plastic substrate large area CdS film solar cell is illustrated in Fig. 3, and that of a high performance cell is shown in Fig. 4. These curves were taken with the cells held at 25°C and illuminated with tungsten light equivalent to 100 mW/cm^2 sunlight. The area used for the efficiency calculation was in each case the total gridded area of the cell without making allowance for the portion of the cell blocked by the grid.

The high performance cell of Fig. 4 was made on an 0.001 in. thick plastic substrate with an 0.001 in. thick Mylar cover plastic. It weighed 1.78 grams. High altitude airplane flight tests[4] indicate that in near earth space CdS film solar cells should yield 1.20 times their air mass 1 sunlight output value. On this basis, this plastic substrate CdS thin film solar cell had an initial power to weight ratio of 106 watts per pound. Some 44 days later the efficiency had dropped and levelled off at 6.2% representing a power to weight ratio of 95 watts per pound.

The effect of temperature on the open circuit voltage, short circuit current and conversion efficiency of a large area frontwall plastic substrate CdS thin film solar cell was measured in tungsten light equivalent to air mass 1 sunlight at 10°C intervals from 10° to 100°C, as shown in Fig. 5. Over this range, the variation of each of these parameters was essentially linear. This is different from earlier indications[5,6] on lower efficiency CdS thin film solar cells. More extensive measurements on more cells over a wider temperature range are needed to adequately characterize the temperature performance of these cells.

Stability

As in the case of the metal substrate cell, the plastic substrate CdS film cell seems to be stable if protected from moisture. The plastic substrate cells have in fact seemed less susceptible to mechanical degradation, i.e., loss in output due to loosening of the grid contact. The causes for this are not positively known. Thermal stress factors, better bonded laminations, etc. may be possible causes.

The experience to date on dry shelf storage of this construction film cell is summarized in Table I. Some cells appear to have degraded slightly over the 5 month period while other cells actually improved. On the average the cells dropped about 8% in the first few weeks and then rose gradually to their original value in about 3 to 4 months. Some of the individual cell variances are probably due to the accuracy of the test, but it is believed that the average trend is reasonably accurate and that a true drop is experienced in the first week or two followed by a gradual rise in output. This rise in output, which is also observed on occasion on metal substrate cells, is not presently explainable. It may be associated with a drying action from the desiccated storage ambient.

It does appear that the plastic substrate CdS cell is inherently stable, after an initial adjustment. Some instabilities that have been observed have been attributable to accidental or to mechanical causes and these can be eliminated by better cell design and improved control of the fabrication process.

Improvements

The plastic substrate CdS cell will benefit from those design improvements being developed for the metal substrate cell, including the cemented grid contact, an integral positive lead, better encapsulating materials, and increased cell efficiency. In addition to these improvements, decreases in the thickness and weight of the plastic substrate cell are anticipated which will lead to increased cell flexibility and to further increases in the power to weight ratio.

Within the next year the plastic substrate in the cover plastic are expected to be reduced in thickness to about 0.0005 in. The conductive coating on the plastic substrate should be reduced to about 0.0001 in.

The CdS polycrystalline film should be reduced to 0.0005 in. maximum and may even be as thin as 0.0002 in. These reductions can lead to 50 cm^2 area cells weighing less than 1 gram and overall cell thicknesses on the order of 0.002 in. Average stable cell conversion efficiencies of 7% are anticipated in this period also. These improvements should make feasible very thin light weight arrays for space power systems.

Figure 6 is our conception of a possible design for an array of 72 thin film plastic substrate CdS solar cells. Each cell is 50 cm^2 in area, and is connected in series and laminated into a 28 volt module with a bus bar at opposite ends. This module would be approximately 1 foot wide by 5 feet long. It could readily be connected with other similar modules to build up larger arrays to meet specific power requirements.

A module of this design constructed from present state of the art 5% CdS cells would yield 21.6 watts in air mass zero sunlight and would weigh 136 grams representing a power to weight ratio of 72 watts per pound for the array.

Table II gives a detailed breakdown of the weight of each of the components of such a 72 cell module. Also included are the weights of the components after the improvements expected in the next year. With the thickness reductions in the plastic and CdS films, the overall weight would be reduced to about 79 grams. This would give a power to weight ratio of 126 watts per pound for 5% cells and 175 watts per pound when the average cell efficiency is raised to 7%.

Acknowledgment

The work described above was supported by the National Aeronautics and Space Administration, Lewis Research Center, under Contract NAS3-6461.

References

1. "Kapton" - a polyimide film supplied by DuPont Co.

2. "Pyre M. L. " - a polyimide varnish supplied by DuPont Co.

3. Luminescent Grade CdS Powder - supplied by G. E. Co.

4. H. W. Brandhorst, "Airplane Testing of Solar Cells," in Proc. of Fourth Photovoltaic Specialists Conference, Vol. II, PIC-SOL 209/5.1 (August, 1964).

5. A. E. Middleton, et al, "Evaporated CdS Film Photovoltaic Cells" in Vol. 3 of "Progress in Astronautics and Rocketry," pp. 275-298, Academic Press (1961).

6. F. A. Shirland, et al, "Thin Film CdS Frontwall Solar Cells," in Vol .II of "Progress in Astronautics and Aeronautics," pp. 335-349, Academic Press (1963).

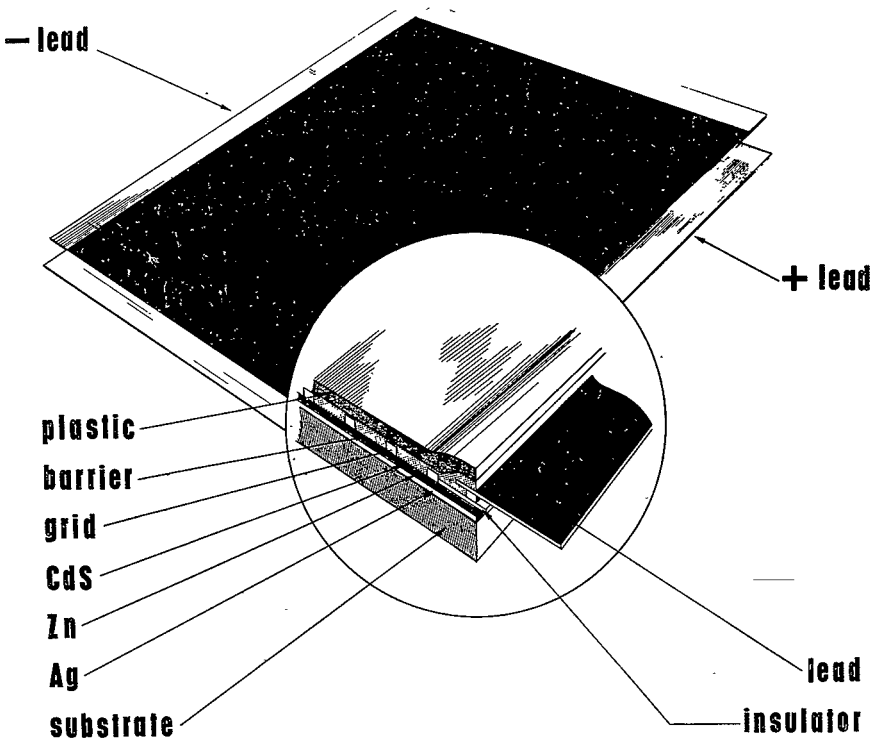

FIGURE 1

CdS THIN FILM SOLAR CELL ON PLASTIC SUBSTRATE

TABLE I

EFFICIENCY OF 3"x 3" PLASTIC SUBSTRATE CELLS ON DESICCATED STORAGE

No.	INITIAL	$\frac{1}{2}$ MONTH	1 MONTH	2 MONTHS	3 MONTHS	4 MONTHS
A490	5.3 %	3.6 %	3.7%	3.6 %	4.3 %	4.3 %
A491	4.0	3.1	3.5	3.5	3.8	3.7
A497	5.0	4.2	5.0	4.8	5.5	5.5
A500	5.7	5.0	5.3	5.0	5.7	5.7
A513	4.6	4.7	4.8	5.2	5.2	5.0
A531	5.2	4.7	5.0	5.3	5.2	5.2
A538	5.8	5.4	5.4	5.6	5.6	5.7
A550	5.4	5.6	6.2	6.2	6.2	6.2
A552	5.0	4.6	4.4	4.9	4.9	4.9
A554	5.2	4.7	4.5	5.3	5.3	5.2
A565	4.7	4.6	4.6	5.0	5.0	5.0
A568	5.4	4.5	4.5	4.8	4.6	4.0
D43E	4.8	5.4	5.0	4.7	4.7	—
AVG.	5.1	4.7	4.8	4.9	5.0	5.2

TABLE II

28 VOLT MODULE. PRESENT AND FUTURE DESIGN

CELL COMPONENTS	PRESENT DESIGN	IMPROVED DESIGN
72 PCS KAPTON-H (3"x 3⅜ x .001")	15.3 gm	7.7 gm
72 EA. Aq PYRE-M.L COAT, (.0003")	28.5	9.3
72 EA. CdS FILMS, (.0008")	40.8	20.4
1 SHEET MYLAR COVER PLASTIC, (.001")	15.7	7.9
1 SHEET CAPRAN ADHESIVE PLASTIC, (.0005")	5.4	5.4
SEPARATORS AND INSULATORS	8.0	5.0
2 EA. SILVER BUS BARS, (¼ x 13"x.005")	6.0	6.0
72 PCS Cu MESH (2.9"x 3.1")	11.0	11.0
EPOXY CEMENT	5.2	5.2
TOTAL WEIGHT	135.9	77.9
WATTS/lb AT 5%	21.6W/.30 = 72	21.6W/.17 = 127
WATTS/lb AT 7%	30.2W/.30 = 101	30.2W/.17 = 179

Page intentionally left blank

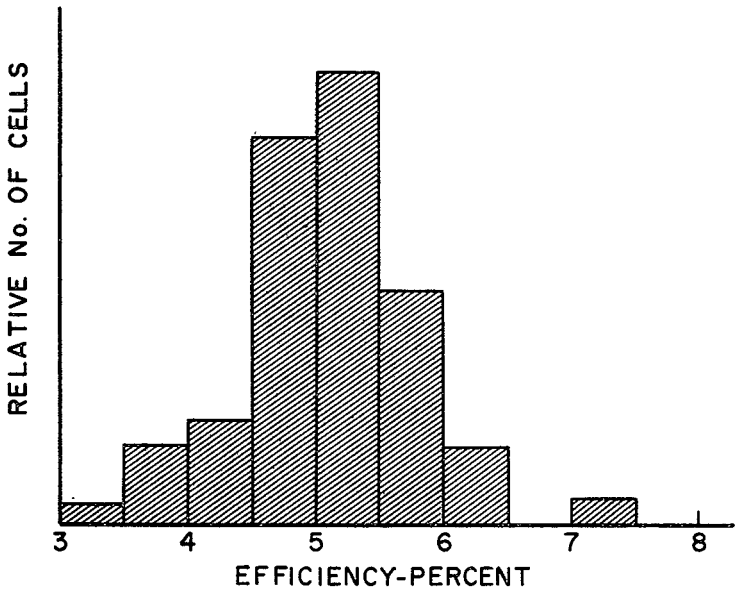

FIG. 2. DISTRIBUTION OF EFFICIENCIES OF PLASTIC SUBSTRATE CELLS

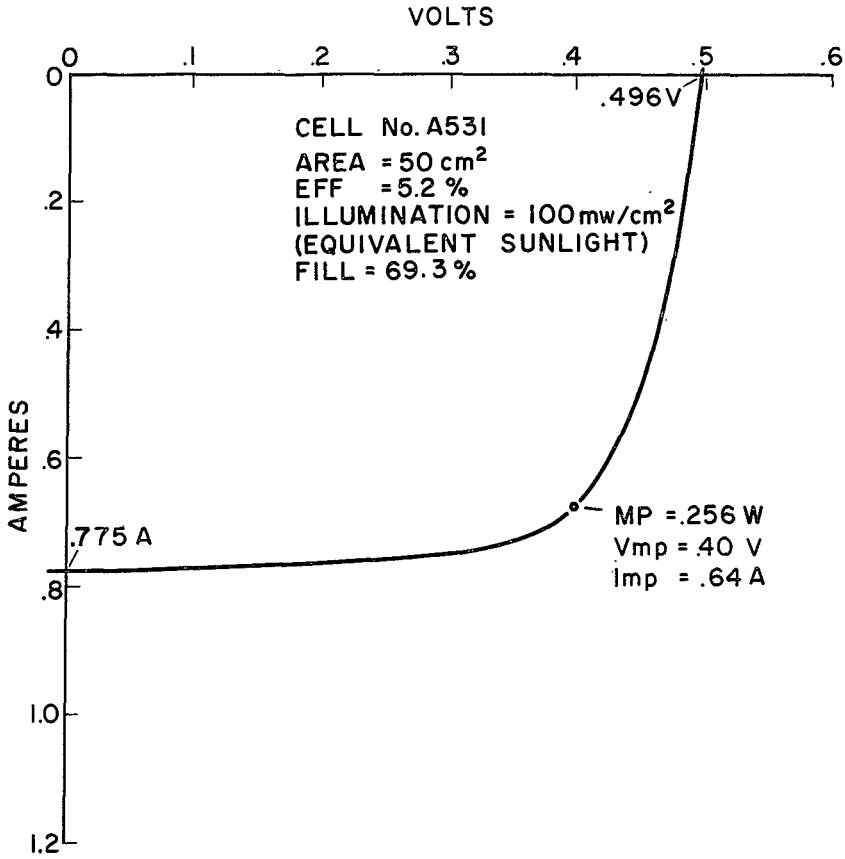

FIG. 3. I-V CURVE OF AVERAGE PLASTIC SUBSTRATE CELL

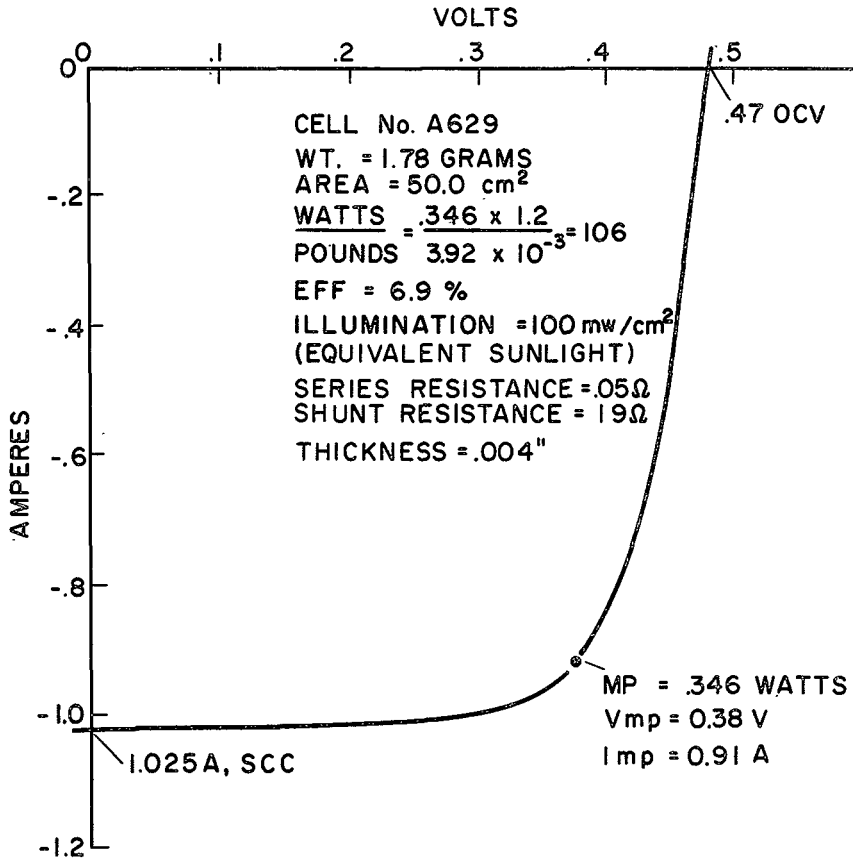

FIG. 4. I-V CURVE OF A HIGH PERFORMANCE PLASTIC SUBSTRATE CELL

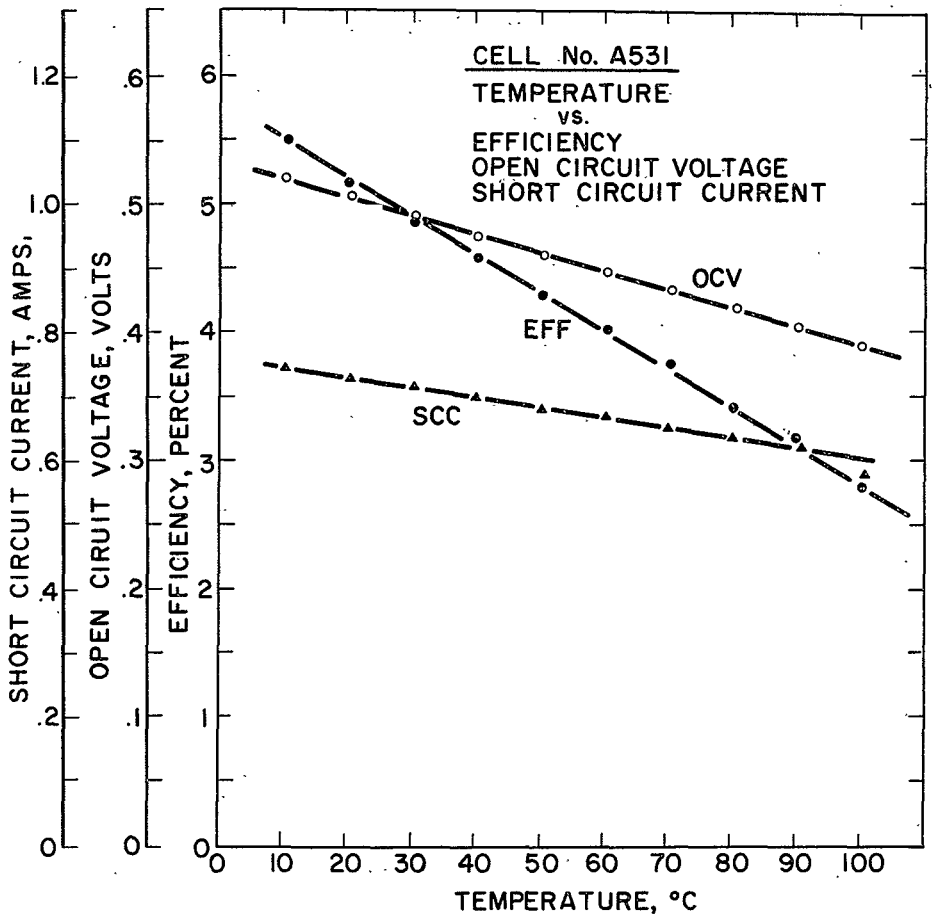

FIG. 5. TEMPERATURE PERFORMANCE OF 5% PLASTIC SUBSTRATE CELL.

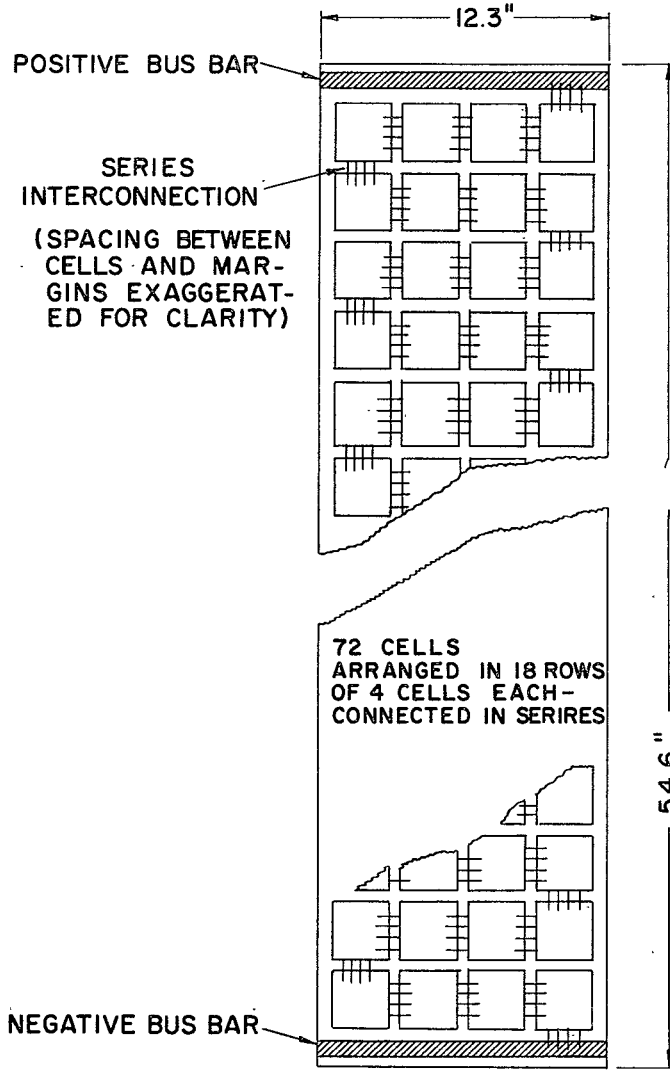

FIG. 6. TENTATIVE PROPOSED DESIGN OF 28 VOLT MODULE

Discussion

Massie: Are there any questions for Mr. Augustine, then, on the thin film plastic substrate cell?

Wise - Aero Propulsion Lab: Can you tell me how you measured your short circuit current versus temperature? You don't normally expect to see it drop.

Augustine: That is true. We simply took the cell up in steps of 10 degrees and then plotted curves on an automatic plotter and determined the short circuit current, the open circuit voltage, and the other parameters.

Wise: Did you have a feedback loop so that you get exactly zero voltage when you measured short circuit current?

Augustine: Fred, would you like to answer that?

Shirland: Yes. It's the same method that was used on the tests we ran at APL, except that the cells were held firmly against a cooled block, and then the temperature was raised.

Wise: Thank you.

Perkins - RCA: A question relating to Mr. Wise's - Why does the short circuit current degrade with increasing temperature?

Augustine: I don't know.

Perkins: One further question. I may have missed it from your slide. What is the coefficient for the decrease in cell efficiency with increasing temperature - per degree? Do you have this number?

Augustine: We dont't have that number.

Perkins: Thank you.

Ritchie - JPL: Was that test run in tungsten or in sunlight?

Augustine: That was run in tungsten.

Ritchie: Thank you.

Halstead - GE: What would you expect in terms of efficiencies, if you go to thinner CdS films - since you are dealing apparently with a significant amount of extrinsic response, I mean, beyond the band edge?

Augustine: The absorption is in a very thin section. What we would expect in efficiency if we went to thinner films, I couldn't say. Fred, would you like to comment?

Shirland: I'd like to comment just briefly on that point. We have run films as thin as 3 and 4 microns and we have had efficiencies of 4 and 5% from the cells. The problem facing us is a practical problem of collecting the current without a lot of series resistance, and it's a problem of getting large-area films laid down perfect enough to keep them from shorting out.

Dr. Wolf - RCA: I would like to make a comment to this point. I think that in these polycrystalline films with a surface barrier type junction, as the collection mechanism is determined by the width of the space-charge region, we cannot expect to collect many carriers out of the polycrystalline region below the space-charge region by diffusion, so the limitation will be - the width of the space-charge region rather than the thickness of the layer in which absorption takes place. So that if you have a low absorption coefficient, the light penetrates deeper, and I don't think you will collect the minority carriers from them. Does that answer your question?

Halstead: Yes and no. I think it still raises an interesting problem because the depth of the depletion region is on the order of half a micron, according to these estimates. If you're dealing with that, then you have extremely strong absorption due to the extrinsic process accounting for essentially half of the response.

Wolf: Yes, this is correct. You must have, due to the extrinsic process, a rather heavy absorption, but you cannot expect to collect any carriers which generate further down in the polycrystalline layer.

Uchiyama - JPL: On cell efficiency versus desiccated storage time, would you care to comment on the desiccator you used for this particular data gathering?

Augustine: Desiccated what, sir?

Uchiyama: Desiccated storage time. You had a table there, in your talk.

Augustine: Yes.

Uchiyama: Would you care to comment on the desiccator that you used - to obtain these results?

Augustine: It was an ordinary laboratory-type desiccant.

Uchiyama: What specifically was it?

Augustine: "Drierite"

Uchiyama: Thank you.

Skarman - National Cash Register: I was interested in your technique for metallizing the plastic. It's my understanding that this is something like a silver paint that you apply and cure and then put a zinc coating on top. Is this an electroplated zinc?

Augustine: That is correct.

Skarman: And is it just a rather commercially available silver paint, or is this a special paint that you're using of your own type?

Augustine: It's a paint that we mix in our laboratory.

Skarman: I see. Thank you.

PIC-SOL 209/6.1
Section C-5

THIN-FILM CADMIUM SULFIDE SOLAR ARRAY ON PLASTIC SUBSTRATE

Presented by

W. L. C. Hui

Radio Corporation of America

Astro-Electronics Division

Princeton, New Jersey

19 October 1965

Abstract N66 17331

Arrays of multiple CdS solar cells on an insulating plastic substrate, with improved efficiency and specific power to weight ratio, have been developed. These arrays consist of two cells, or four cells, with a total area of about 11 cm^2 and are prepared simultaneously and interconnected in series. Conversion efficiency of 5.1% under equivalent sunlight and specific-power-to-weight ratio of 80 watts per pound have been obtained. The thickness of the array, including the encapsulation and the continuous cell-support array member, ranges between 0.002 and 0.004 inches. There has been no change in four years in the electrical and physical properties of a cell of this general type when sealed in a rough vacuum container. There is also practically no change in the properties for cells on plastic substrate after 500 cycles in a vacuum of 10^{-7} torr and between cycling temperatures of -85° to 70°C. Irradiation with 0.4 MeV protons shows that, for a cell of this type, with a thin silicone coating, there is no change in V_{oc} and only 8% decrease in I_{sc} at a flux of 1×10^{14} protons/cm^2. For N-on-P silicon cells, the V_{oc} decreased by 20% and the I_{sc} decreased by 10% at a flux of 2×10^{11} protons per cm^2 and proton energy of 0.4 MeV. With this basic process, techniques can be developed for the continuous fabrication of a large number of interconnected cells on long strips of the substrate. The cost and wieght of such an array should be significantly lower than other type cells and assemblies.

author

THIN-FILM CADMIUM SULFIDE SOLAR CELL ARRAY ON PLASTIC SUBSTRATE

William L. C. Hui and John P. Corra
David Sarnoff Research Center
Astro-Electronics Division
Radio Corporation of America
Princeton, New Jersey

Introduction

In recent years, polycrystalline thin-film solar cells have been of much interest because of their potential in the reduction of weight and cost[1,2]. This is even more so when solar cells are to be considered for multi-kilowatt power systems.[3] However, most of the work has been concentrated on individual cells. The conventional assembly of these cells into large arrays would be, to a certain degree, similiar to that for single-crystal cells. In these assembly techniques lies the major portion of the cost and weight for the final power system. To realize more fully the potentials of thin-film cells, techniques should be developed whereby large arrays containing numerous interconnected cells can be produced automatically, thus eliminating the separate, manual operations of cell mounting and interconnection - also eliminating the need for a separate cell-support array member. This is quite analogous to the increasing application of integrated microelectronic circuits today.

With this goal in mind, the Astro-Electronics Division of RCA has been conducting a program with thin-film cadmium sulfide as the active material, and DuPont Kapton plastic film as the substrate. As compared to molybdenum, this material offers significant advantages as shown in Table I.

Developmental Arrays

The structures of the developmental arrays are shown in Figure 1. Figure 1(a) shows two cells connected in series, 1(b) the cross-section of the array, the 1(c) the four-cell module. The actual arrays are shown in Figure 2.

These arrays are prepared by first depositing the bottom electrodes and interconnection tabs and then cadmium sulfide (CdS) onto the plastic substrate by evaporation in vacuum. The barrier layers are then fabricated over the CdS layers and annealed. Metal grid-top electrodes are placed, and the cells are encapsulated. As seen, the entire CdS and the barrier-layer areas are utilized as deposited. Trimming around the edges of the cell is not required, nor is there a requirement for selection of the best film areas. Etching of the substrate is not necessary to reduce its weight after the cell is made. These are important economic factors.

TABLE I

COMPARISON OF SUBSTRATE MATERIALS

	Materials	
	Molybdenum	Kapton
Density (gm/cc)	10.2	1.4
Thickness (mils)	1 to 2(before etching)	0.5 to 2.
Thermal expansion coef (in./in./°C)	4×10^{-6}	5×10^{-5}
Electrical connection for multiple cells on same substrate	Parallel only	Parallel or series
Weight of necessary bus bar for array	Heavy	Light
Cost ($/ft^2/mil starting material, before etching)	6.650	0.045

The thickness of the array ranges between 0.002 and 0.004 inches, and the external contacts to the array are made outside of the active cell areas. This enables the use of soldering or welding contacts without danger of shorting.

Array Performance

Conversion efficiency of 5.1% has been obtained for a two-cell array. These measurements were made under equivalent sunlight intensity of 86 mw/cm^2, one week after fabrication. The current-voltage characteristics of the two-cell series array and of each individual cell are shown in Figure 3. It is seen that the two cells are well matched electrically. The open-circuit voltage of the array is 0.89v, short-circuit current is 83.5 ma, maximum power is 48 mw, and fill factor is 1.55. The total area for the two cells is 10.8 cm^2. The characteristics for a four-cell array with efficiency of 4.7% are shown in Figure 4. The V_{oc} is 1.8 volts, and I_{sc} density is 14 ma/cm^2. The dependence of efficiency of the array on light intensity is shown in Figure 5. The equivalent shunt resistance of the cells is about 300 ohms, and series resistance is 2 ohms or greater. Through a reduction of the series resistance of the array to 0.1 ohm, it is expected that array efficiency near 6 or 7% can be achieved, based on data obtained from other arrays.

The specific-power-to-weight ratio of several arrays was determined, by actual weighing, to be 80 w/lb, including the encapsulation and the external contact tabs. This ratio can be increased by 2 to 3 times with improved array geometry and efficiency.

The spectral response of a typical array is shown in Figure 6. As seen, the cells have a considerable response in the UV region and peak in almost the same wavelength region as the Sun.

The resistivity, as determined from Hall measurements, of the barrier-layer ranges between 10^{-2} to 10^{-3} ohm-cm, corresponding to a sheet resistance of 10^{2} to 10^{3} ohm/square. The carrier concentration of this layer is greater than 10^{21} carriers/cm^3.

Calculations based on diode measurements, in darkness, showed the barrier height of the CdS cells to be greater than 0.6 volts. High series resistance has prevented a better determination of the barrier height by this method.

Array Stability

Under conditions of low humidity, the arrays appear quite stable. A number of the arrays have been exposed to room air during the daytime and stored in a container at a pressure of 10^{-1} torr at night; the efficiency of these arrays was measured periodically as shown in Figure 7. Some arrays appear to be stable or show a slight increase in efficiency for periods up to 160 days. It should be noted that CdS cells of this type seemed stable in a partial-vacuum condition. One CdS cell was sealed in a glass tube evacuated to 10^{-2} torr pressure; its output has not changed in 4 years. Five CdS cells of the type used in the arrays were given a 500-cycle thermal-vacuum test between -85°C and +70°C in a vacuum of 10^{-7} torr. After the test, there was no observable physical change and only slight changes in the short-circuit current.

Susceptibility to Low-Energy Proton Radiation

It was felt that radiation experiments with low-energy rather than high-energy protons should reveal more significant information both on the extent of the damage and the junction depth of thin-film cells, because (1) solar cells with shallow junctions are most susceptible to radiation damage by low-energy protons, as evidenced by earlier investigations on single-crystal GaAs cells, and (2) the incidence of a large flux of such particles in the orbits of the Relay and Telstar satellites. Several CdS cells of the type used in the array - some bare cells, one with Mylar encapsulation, and one with silicone coating - were subjected to radiation of 50,100, and 400 KeV protons at flux levels of 10^{12} to 10^{15} protons/cm^2 at Brown University under the guidance of Professor J. Loferski. The short-circuit currents of CdS cells without any encapsulation or coating are shown in Figure 8, and the corresponding open-circuit voltages are shown in Figure 9. The radiation effect on a CdS

cell encapsulated with Mylar is shown in Figure 10, and the effect on a cell with a silicone coating is shown in Figure 11. This experiment indicates that:

1. For the bare cells, the greatest decrease of the open circuit voltage occurs at the 100 KeV proton energy. Open-circuit voltage decrease is indicative of the amount of damage in the junction region. Based on data on aluminum, the corresponding penetration depth for cuprous sulfide is 0.35 microns and for cadmium sulfide 0.41 microns. The depletion region of the CdS cells is believed to lie in this range from the surface.

2. The Mylar encapsulation appears unsuitable from the proton irradiation point of view.

3. The silicone coating affords radiation protection up to 1×10^{14} protons/cm^2 of 400 KeV energy, where there is no change in V_{oc} and only an 8% drop in I_{sc}. This compares very favorably with the 20% drop in V_{oc} and 10% drop in I_{sc} for N-on-P single-crystal silicon cells[4] at 400 KeV and 10^{11} protons/cm^2.

Conclusion

Arrays of multiple CdS cells interconnected in series have been made on plastic substrate with efficiencies over 5% and a specific-power-to-weight ratio of 80 watts/lb. It has been shown that further improvement in these areas can be made. Thermal-vacuum cycling tests on similar cells between -85° to +70°C showed no physical change and only slight change in short-circuit current. It appears that CdS cells with a thin silicone or other equivalent coating has at least three orders of magnitude more resistance to low-energy proton damage than N-on-P silicon cells. With this basic process, techniques can be developed for the continuous fabrication of large arrays containing numerous interconnected cells. The cost and weight of such arrays should be significantly lower than other type cells and assemblies.

Acknowledgement

The author acknowledges Dr. E. C. Hutter for his guidance of this program; G. R. Auth who prepared and tested the arrays; G. Noel who contributed to the early work of the program; A. G. Holmes-Siedle who made suggestions on the proton radiation experiment and G. Brucker and H. Flicker who assisted in performing it, and G. L. Raffaelli for assistance in the thermal-vacuum-cycling test.

References

1. ASD Technical Report 611-11, Solar Cell Array Optimization, prepared by the RCA Astro-Electronics Division for the Aeronautical Systems Division of USAF, Contract No. AF33(716)7415 (Aug 1961)

2. Rappaport, P. and Moss, H., "Low Cost Photovoltaic Conversion of Solar Energy, " United Nations Conference on New Sources of Energy, Reprint No. E - CONF. 35-S-106 (May 20, 1961)

3. Gordén, G. D. "Thirty Kilowatt Power Supply from Thin-Film Solar Cells," 3rd Biennial Aerospace Power Systems Conference, AIAA Reprint No. 64-740 (Sep 1-4, 1964)

4. Wysocki, J. J., Transcript of the Photovoltaic Specialist Conference, Vol.1, Section B-1 (July 1963).

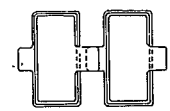

(a) TWO CELLS IN SERIES

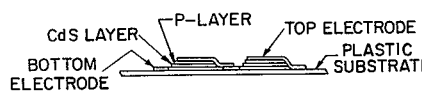

(b) SIDE VIEW OF ARRAY

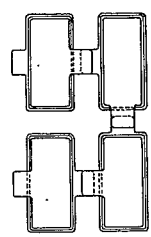

(c) FOUR CELLS IN SERIES

FIG.1 STRUCTURE OF CdS CELL-ARRAYS

(a) TWO-CELL IN SERIES

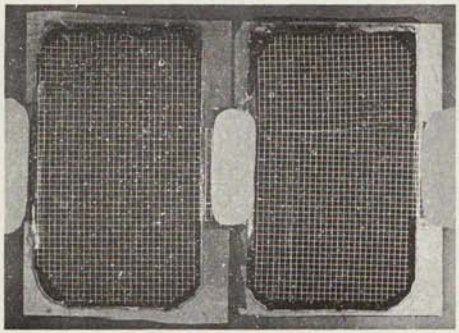

(b) FOUR-CELL IN SERIES

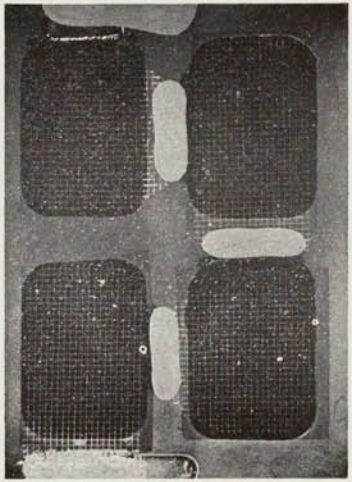

FIG. 2 ARRAYS OF INTERCONNECTED CdS CELLS

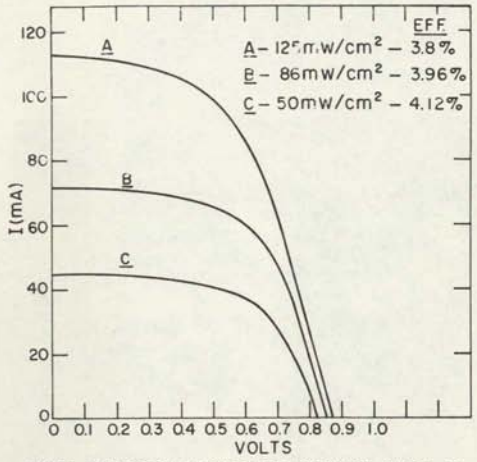

FIG.5 EFFECT OF LIGHT INTENSITY ON THE I-V CHARACTERISTIC OF CdS THIN FILM SOLAR CELL ARRAY

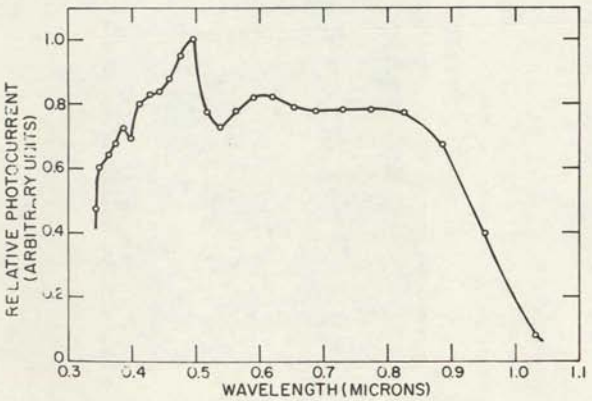

FIG.6 SPECTRAL RESPONSE OF CdS CELL ARRAY

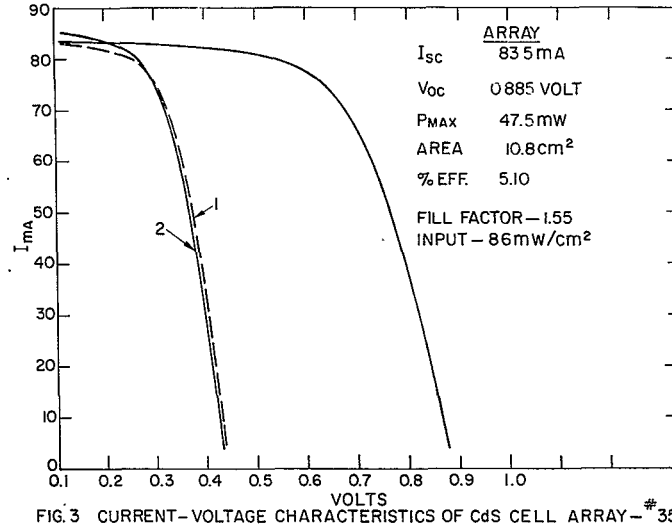

FIG. 3 CURRENT–VOLTAGE CHARACTERISTICS OF CdS CELL ARRAY – #352

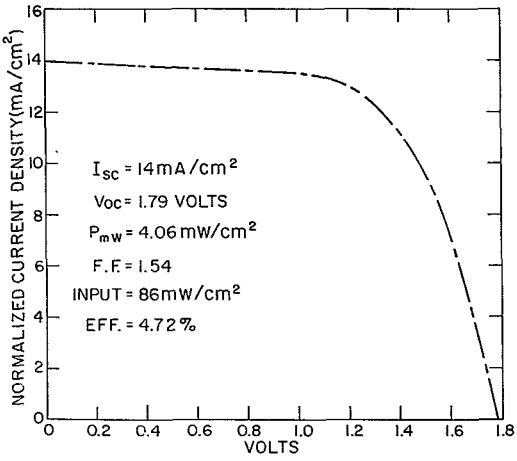

FIG. 4 CURRENT–VOLTAGE CHARACTERISTIC OF CdS THIN FILM 4 CELL ARRAY

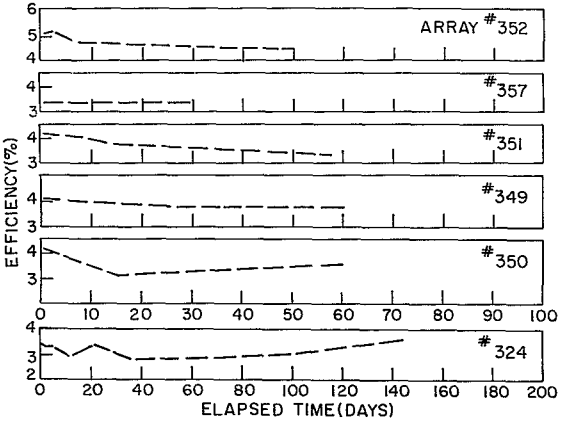

FIG. 7 STABILITY OF THIN FILM CdS CELL ARRAYS

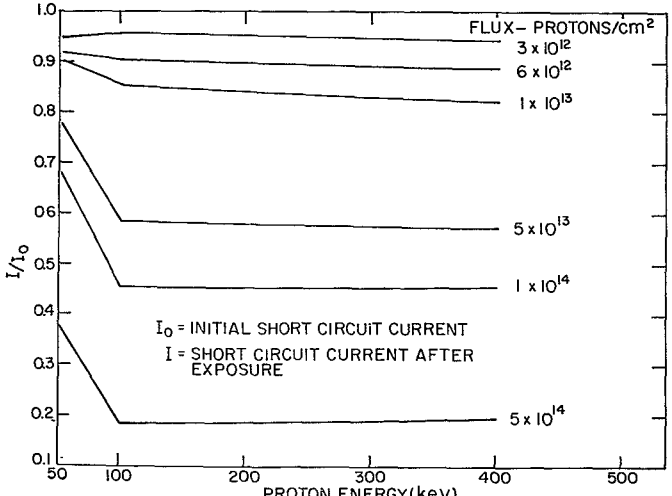

FIG.8 EFFECT OF LOW ENERGY PROTON IRRADIATION ON SHORT CIRCUIT

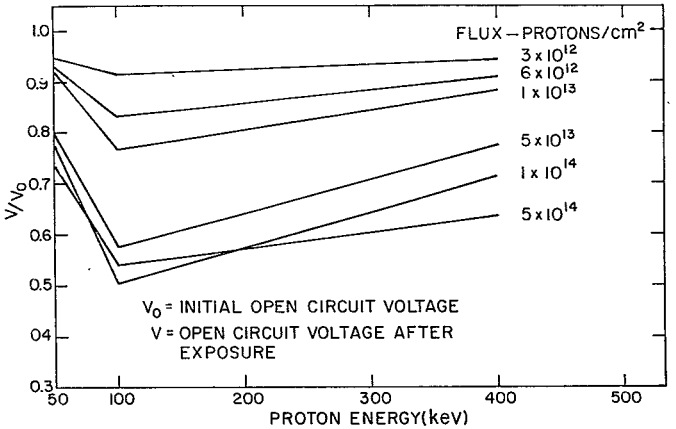

FIG. 9 EFFECT OF LOW ENERGY PROTON IRRADIATION ON OPEN CIRCUIT VOLTAGE OF BARE CdS CELLS

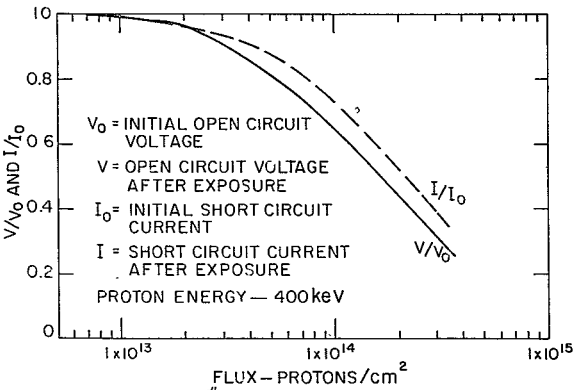

FIG. 10 CdS CELL #287-3 COVERED WITH 0.001" THICK MYLAR

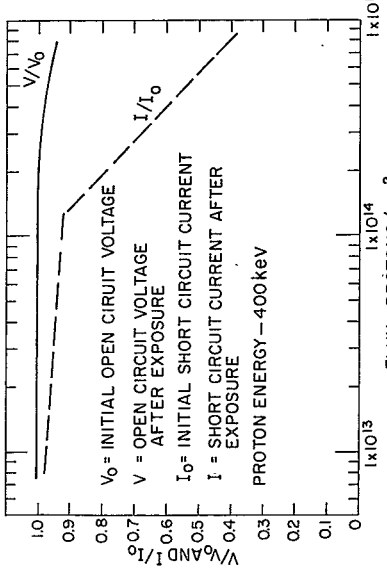

FIG. 11 CdS CELL #292-1 COVERED WITH SILICONE COATING

Discussion

Massie: We will now open for discussion the last two papers. While Mr. Hui is here, do you have any questions for him?

Borson - Aerospace Corporation: What was the silicone coating that was used on that last slide?

Hui: One of the commercial silicone coatings.

Borson: You don't know the name?

Hui: Yes, it is one of the Dow Corning Silicones.

Waddel - GSFC: Was this coating a grease or a plastic film?

Hui: It comes in liquid form - you can spray it on.

Wise - Aero Propulsion Lab: Would you care to speculate on the intrinsic cost of these cells?

Hui: If I can recall yesterday's discussion on production cost of silicone cells, it depends on the quantity of production. I would guess ultimately they may come to a dollar a watt or something in that order after development of automatic production techniques and machines.

Wise: Thank You.

Ratcheson - Boeing: Did that 80 watts per pound ratio include the weight of the silicone coating?

Hui: Yes.

Voice: Thank you.

New Voice (unidentified): Your spectral response curve indicated a strong response in the entire solar range. I believe, out to 9000, 10,000 angstroms, or something like this. I wondered if you or the previous speaker would care to comment. I think in Mr. Shirland's case, he was estimating that cell thicknesses down to something like 5 microns might be projected in the interest of getting thinner cells; two-tenths mil, I think, was quoted. Do you feel that there would be serious loss in efficiency as you go to thinner cells in view of the fact that you're dealing with impurity absorption rather than intrinsic?

Hui: We have made thin cells with thickness anywhere between 1 and 10 microns, but we have encountered a number of problems. The primary problem is associated with the high resistivity experienced in the thinner films. So we don't really know how thin we can practically go on this type of cells. The cells we reported on here range in thickness between 15 to 20 microns.

Hamilton - IDA: Have you run tests to determine the ability of the silicone coating or the mylar to keep moisture from getting to the cells and degrading their efficiency?

Hui: We have some preliminary indications that silicone will afford some moisture protection.

PIC-SOL 209/6.1
Section C-6

A MODEL FOR THE CdS SOLAR CELL*

Presented by

E. R. Hill

Harshaw Chemical Co.

Cleveland, Ohio

19 October 1965

*Research supported by grant from the Harshaw Chemical Company and contracts from NASA, Lewis Laboratory and Wright-Patterson AFB.

A MODEL FOR THE CdS SOLAR CELL

E. R. Hill & B. G. Keramidas
Harshaw Chemical Co.
Cleveland, Ohio

The CdS solar cell in its present form consists of a film or sheet of CdS which has had one face chemically treated to form a rectifying function. The treatment consists of an immersion of the CdS in an acidified hot water solution of Cu_2Cl_2. The chemical reaction is described by the upper equation in Fig. 1. Thermodynamically, the reaction proceeds to the right, since that side of the reaction has a lower free energy. Kinetically, the reaction is aided by $CdCl_2$ dissolving in the water solution. The equilibrium concentrations of the four reaction components are governed by the lower equation (the Nernst relation), where the right hand member is a function of temperature only. Since CdS and Cu_2S are somewhat ionic, Cu_2^{+2} can replace the Cu_2Cl_2 and $CdCl_2$ in both equations and retain approximately the same thermodynamic properties.

Cu_2S as made in above manner is a p-type semiconductor with a band gap near 1 eV and a hole concentration of about 10^{20} per cm^3. The CdS is n-type with a band gap of 2.4 eV, and generally has an electron concentration of about 10^{18} per cm^3. Consequently, if these two materials can be joined with the proper physical arrangement, a rectifying junction should result. This does take place since an evaporated CdS film which is treated chemically and electrically contacted has the electrical character of a diode. This diode is usually rather leaky and has a high saturation current on the order of microamperes per cm^2. When illuminated, it generates current, the spectral response of which is shown in Fig. 2. Nothing unusual is present in this response except at about 1 eV, and it is concluded that the active material has a 1 eV optical bandgap. We can also conclude that CdS is not optically active, since no change in response occurs at 2.4 eV. This has described the overall nature of the materials, processing and end product.

To understand the more detailed nature of the cell, it is necessary to examine the process on a microscopic level. The chemical reaction is a double displacement type which requires that each time two Cu^+ ions enter the CdS film, one Cd^{2+} ion must leave. If the CdS is highly ordered as in the case of a single crystalline face, only a few monolayers of Cu_2S are formed. This is to be expected since few sites of high chemical activity such as dislocations and grain boundaries are present. Also, the reaction takes place at a temperature around 100°C, and the diffusion coefficients of the components in CdS will be low. However, if the CdS is highly disordered, as in the case of a polycrystalline film or a lapped single crystal, regions of high chemical activity are plentiful and diffusion is enhanced by the presence of grain boundaries and dislocations. In fact, chemical action is seen to penetrate to depths of several microns in evaporated films.

In order for the chemical reaction to occur past the solid surface, diffusion of the reactants must take place, which implies concentration gradients. Fig. 3 shows a schematic picture of the CdS cell cross section representing the cell at any time after immersion in the solution. As can be seen, a gradient of Cu^+ ions and Cu_2S extends into the CdS and a gradient of CdS and Cd^{2+} ions extends out to the surface. These gradients must exist for the reaction to proceed at all, and consequently must exist in the cell when it is removed from the solution. When it reaches thermal equilibrium after the chemical treatment, it will still be in a state of chemical nonequilibrium, since the concentration gradients are still present. This can be called a state of quasi-chemical equilibrium, i.e. over a small region, the Nernst relation governing the component concentrations will be only slightly perturbed. Ultimately, in deference to the second law of thermodynamics, a state of equilibrium will be reached where all four reaction components are uniformly distributed throughout the solid and are in equilibrium with their vapor state. The rate at which this condition is approached is determined by the mobilities and concentration gradients of the species and the temperature. At room temperature, this occurs very slowly, but over a period of weeks, it can be detected.

When the cell is heated, however, this tendency is accelerated and five minutes at 300°C produces a marked change. It is unlikely that the Cu_2S and CdS molecules will be particularly mobile, but Cd^{2+} and Cu^+ ions can move. They will slide down their gradients, increasing the Cu^+ concentration inside and increasing the Cd^{2+} concentration near the surface. The Nernst relation says there will also be an increasing CdS concentration near the surface and increasing Cu_2S concentration deeper in the cell. Fig.4 shows the spectral response of the cell in this condition. The most significant feature is the step at 2.4 eV which says that carriers are produced in CdS within a diffusion length of the electrical junction. The I-V curve shown in Fig. 5 indicates a reasonably good diode and a true generated short circuit current. From this, we conclude that all the light which is being absorbed is absorbed within a diffusion length of the junction.

If this cell is further heated for 1 hour at 300°C, the gradients of concentration will become even flatter. The electrical junction should correspond to the region of chemical transition and will then become broader. It will also move further into the bulk CdS. Fig. 6 shows the spectral response of a cell subjected to such a treatment. Again, the most striking feature is the behavior at 2.4 eV where there is now almost a complete loss of response. Evidently a great deal of CdS has formed near the surface and the junction is deep inside the cell. The I-V curve, shown in Fig. 7, indicates a relatively low collected short-circuit current, and even begins to look like two junctions may be present. Thus, photons with energy above 2.4 eV are absorbed near the surface with a low resulting quantum yield. This low yield can be due simply to having the junction far inside the cell or to the presence of a second junction in the opposite direction.

Further heating causes additional change and after 15 minutes at 600°C the cell is useless as a power converter, but has developed a very interesting

behavior. Fig. 8 shows the spectral response of the generated current which can be seen to reverse direction with color of illumination. For red and infrared light, the current is of the sign produced by the cell initially. That is, the treated surface is positive and the bulk CdS negative. For green and blue light, the polarity reverses. For tungsten illumination, the net current is generally reversed from that of the normal cell. Red light is weakly absorbed and generates carriers deep in the cell near the normal Cu_2S-CdS junction. These carriers are separated and produce normally directed current. Green light is more strongly absorbed near the surface and produces oppositely directed current. This can be due to either non-uniform absorption as in the Dember effect, or due to the presence of a second junction with the opposite sense. Further heating merely results in material homogenization and loss due to evaporation.

This has been a sketchy discussion of the CdS cell fabrication in that only a few salient points have been examined and many microscopic details have been glossed over. For instance, Cu_2S and CdS are only weakly soluble in each other and undoubtedly the chemical transition region is composed of aggregates of clusters. On the atomic scale, this is a discontinuous structure, but on the scale of the Debye length for carriers, this is small. Likewise the transport equation for the heterojunction has been neglected, and the assumption made that a junction exists in a chemical transition region.

The important point is that the device is the result of a double displacement chemical reaction which stops before equilibrium is reached. Thus, concentration gradients of the reactants exist in the region of chemical change. Since the initial reaction occurs near room temperature, even moderate heating can be expected to alter the distribution of the reactants. From the Nernst relation and a knowledge of the gradients, the direction of material redistribution can be predicted. The behavior of the cell after various heating cycles can be correlated with the qualitative picture of the material distribution and their electrical and optical properties.

Finally, it is reasonable to expect this type of analysis to be suitable for application to many of the semiconductor devices where a low temperature chemical reaction takes place.

$$Cu_2Cl_2 + CdS = Cu_2S + CdCl_2$$

$$\Delta F^\circ \ (298^\circ K) = 12 \ \frac{kcal}{mole}$$

$$\ln \frac{[Cu_2Cl_2]\ [CdS]}{[CdCl_2]\ [Cu_2S]} = - \frac{\Delta F^\circ}{RT}$$

Figure 1

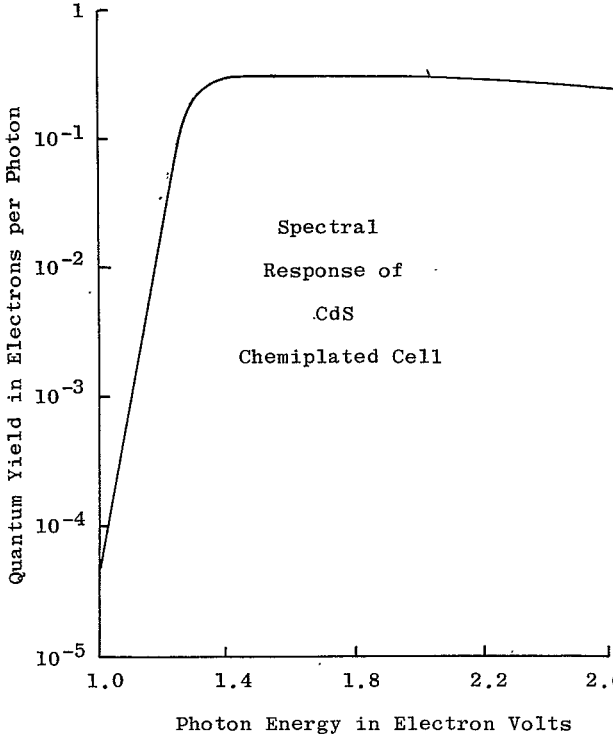
1
10^{-1}
10^{-2}
10^{-3}
10^{-4}
10^{-5}
Quantum Yield in Electrons per Photon
Spectral
Response of
CdS
Chemiplated Cell
1.0
1.4
1.8
2.2
2.6
Photon Energy in Electron Volts

Figure 2

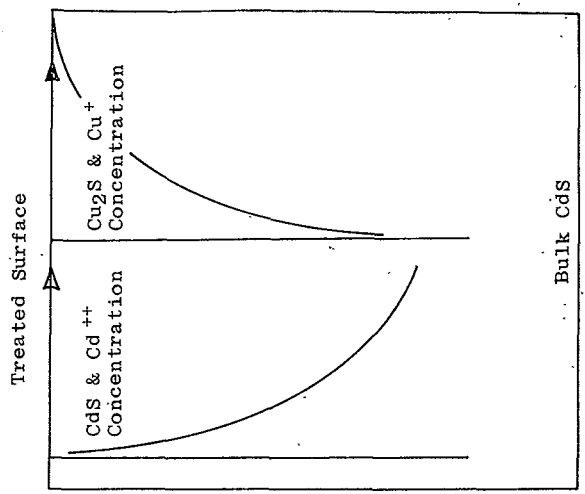

Schematic Cross Section

of Cell Junction

Figure 3

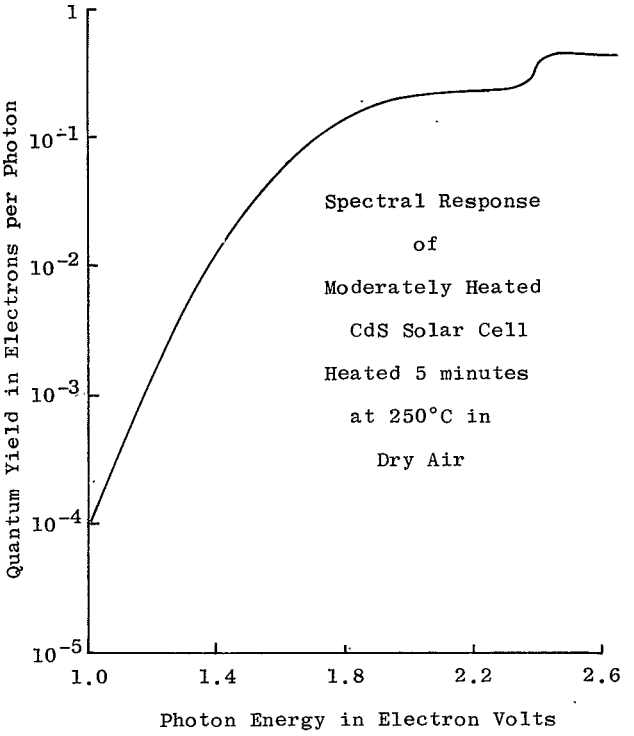
Quantum Yield in Electrons per Photon
1
10^{-1}
10^{-2}
10^{-3}
10^{-4}
10^{-5}
1.0
1.4
1.8
2.2
2.6
Photon Energy in Electron Volts
Spectral Response
of
Moderately Heated
CdS Solar Cell
Heated 5 minutes
at 250°C in
Dry Air

Figure 4

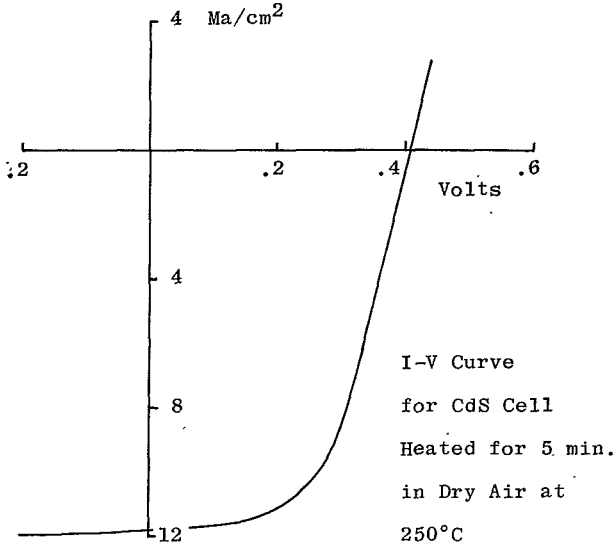
4 Ma/cm2
.2
.4
.6
Volts
4
8
12
I-V Curve
for CdS Cell
Heated for 5 min.
in Dry Air at
250°C

Figure 5

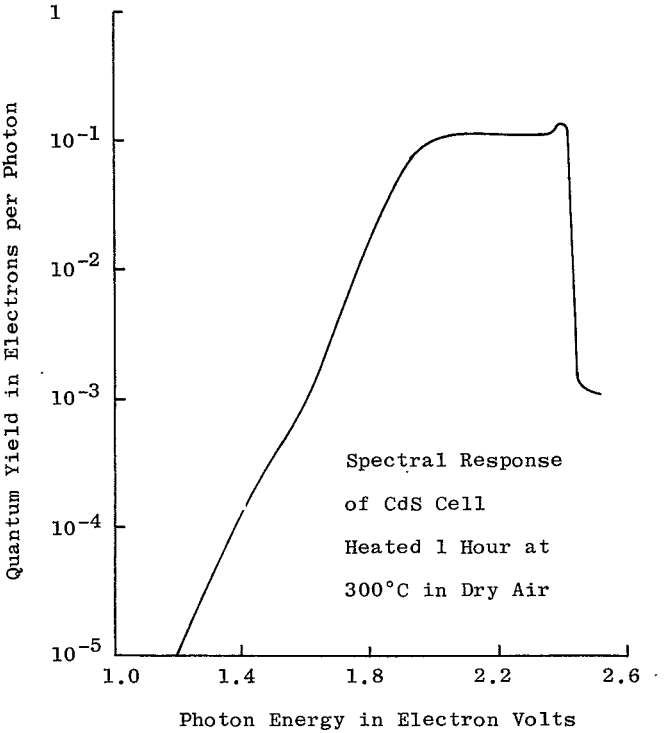
1
10^{-1}
10^{-2}
10^{-3}
10^{-4}
10^{-5}
Quantum Yield in Electrons per Photon
Spectral Response
of CdS Cell
Heated 1 Hour at
300°C in Dry Air
1.0
1.4
1.8
2.2
2.6
Photon Energy in Electron Volts

Figure 6

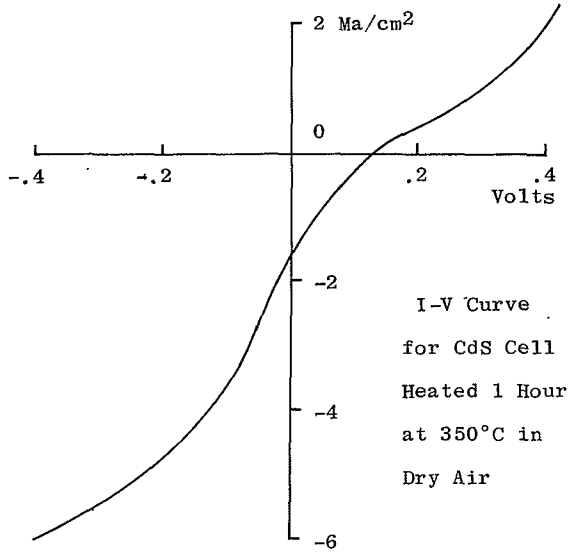
2 Ma/cm2
0
-.4
-.2
.2
.4
Volts
-2
-4
-6
I-V Curve
for CdS Cell
Heated 1 Hour
at 350°C in
Dry Air

Figure 7

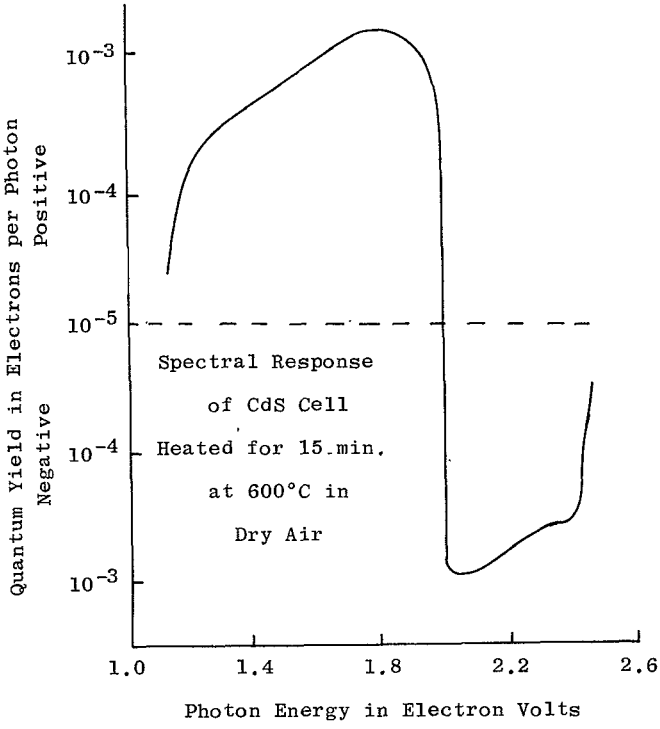
Quantum Yield in Electrons per Photon
Positive
Negative
10^{-3}
10^{-4}
10^{-5}
10^{-4}
10^{-3}
Spectral Response
of CdS Cell
Heated for 15 min.
at 600°C in
Dry Air
1.0
1.4
1.8
2.2
2.6
Photon Energy in Electron Volts

Figure 8

Discussion

Massie: Are there any questions?

Loferski - Brown: Is there any room in this model for explaining the degradation of the solar cells which occurs from exposure to moisture presumably?

Hill: Yes. There are two possibilities. One of these is the oxidation of cuprous sulfide to cupric sulfide, which is reported in the copper literature. This is a quantitative reaction in which the amount of water vapor involved can be measured by the amount of the cuprous sulfide changed. If the cuprous sulfide goes to a higher conductivity state, then obviously the junction is going to be all in cadmium sulfide. And when this happens, all we see is green response; the red response is absolutely lost. The other thing is that cadmium sulfide does decompose photochemically in the presence of water vapor. And cadmium sulfide which is near the surface of the cell after the heat treatment - can photochemically decompose, liberating sulphur. This then combines with the cuprous sulfide to make cupric sulfide, which is high in conductivity, practically metallic.

Cusano - GE: Have you done experiments like taking the cuprous sulfide off the surface with potassium cyanide and then redepositing the cuprous sulfide at room temperature to see whether you have retained photovoltaic response?

Hill: We've done two things with potassium cyanide. If we take the chemically made cell as it comes right out of the bath and etch it in cyanide, we apparently remove everything but cadmium sulfide. This blackish layer disappears.

Cusano: You mean this mixed layer where the aggregates are, all comes off.

Hill: If the cell is taken out of the bath and given no further heating, the black layer disappears in cyanide. If the cell is then contacted with a metal grid, we see only the cadmium sulfide intrinsic response. If we take a cell - which has been heat-treated, etch it in cyanide, we don't remove everything. We can still see black specks, inside the film. We remove a great deal off the surface, but we can't remove it all. There is still some red response left.

Cusano: So you still have a fairly active cell if you will then remake cuprous sulfide...

Hill: If it is put back into the dip, yes.

Cusano: But don't heat it again - just put it back in the dip?

Hill: Yes. We make more cuprous sulfide on the surface, sure.

Cusano: Sure. But now this cell is comparable to a heat-treated cell?

Hill: No, it's comparable to the cell that was made just by dipping.

Cusano: So, whether it's been heated after the first dipping or not, once you dip it in cyanide and reapply the copper sulfide without any further heat treatment, you've lost everything - in either type - in either the baked cell or the unbaked cell?

Hill: The cyanide dip removes all red response from an unheated cell, but some remains in a heated cell.

Skarman - National Cash Register: Asking a question about your negative current you saw for the green light absorption and positive current for the far infrared, you say that this can possibly - the negative current - can be accounted for by Dember effect or another junction. Now, I think because of current levels involved from your quantity, it is probably then not likely that it is a Dember effect. But do you have any sort of model that would maybe justify another junction, or where could another junction occur here?

Hill: Well, the justification for the second junction is that if powdered cadmium sulfide and powdered copper sulfide are mixed together and put into a test tube with a relatively small exposed area at the top, and heated to 500 or 600 degrees centigrade in air, we form cadmium sulfide on the top surface.

PIC-SOL 209/6.1
Section C-7

SOME PROBLEMS OF THE THIN FILM CADMIUM SULFIDE SOLAR CELL

Presented by

A. E. Spakowski

NASA-Lewis Research Center

Cleveland, Ohio

19 October 1965

SOME PROBLEMS OF THE THIN FILM CADMIUM SULFIDE SOLAR CELL

A. E. Spakowski, A. E. Potter, and R. L. Schalla
National Aeronautics and Space Administration
Lewis Research Center
Cleveland, Ohio 44135

Cadmium sulfide (CdS) thin film solar cells have come a long way in the past several years and now look promising. Currently being made are 4 to 7 percent efficient 3 by 3 inch cells with 8 to 10 percent cells not an unrealistic goal in the future. When one begins to consider arrays for space power systems, the necessity of assigning performance parameters to the cells becomes apparent. As a result, the stability of the thin film cells has come under closer scrutiny in recent months.

First, we will consider our experience at NASA Lewis Research Center on the storage stability, moisture degradation, and thermal cycling durability. Secondly, we will deal with some aspects of the mechanism for the CdS-Cu_2S solar cell.

The cells that we are concerned with have a thin metal or plastic substrate (1 or 2 mils thick) on which is deposited a mil of CdS, then a barrier of Cu_2S, a gold (Au) or copper (Cu) current collecting grid, and finally the adhesive and encapsulating plastic of either Mylar or H-film. The solar cell is 3 by 3 inches and about 5 mils thick. It is very flexible, light, and shows no sign of wear or damage as a result of normal handling. However, the cells do appear to degrade during storage in a double desiccator under ambient conditions or in a vacuum desiccator. Figure 1 shows the efficiency of several types of CdS cells as a function of the time in storage. The data presented are averages from more than 120 cells. The gold-gridded cells (solid lines) that depend on the pressure of the encapsulating plastic to hold the grid in contact with the barrier are quite stable, degrading about 0.1 percent every two months. The cells having the Au grids electroplating process reduces the power output of the cell. The copper-gridded cells (dotted lines) that depend on the pressure of the encapsulating Mylar to hold them in place degrade very rapidly but do reach a stable condition in 3 to 7 weeks. The Cu-gridded cells (dashed lines) that depend on the pressure of the H-film to hold them in place degrade slower and reach a stable condition in 2 to 6 weeks. The Au-gridded cells are quite satisfactory except for the cost of the grid, which is approximately $8 per cell. To lower this cost, one manufacturer has switched to Cu grids. The drop in efficiency for these cells is because of an increase of the series resistance due to the grid lifting from the barrier of the cell. Some of this current loss can be recovered by the application of pressure to the cell package while relamination usually results in a completely recovered cell. The voltage remains virtually unchanged.

It thus appears that the storage-stability problems occur because the grids do not maintain good contact with the barriers. The movement of the grid can result from the release of stresses built up in the cell during lamination. Since the grid becomes an integral part of the adhesive and plastic, it must either move or be deformed as the stresses are relieved. The more ductile Au grid can deform more easily than can the Cu, which would transfer the stress directly to the grid-barrier interface. Approaches to the problem now being evaluated include improved lamination conditions and epoxy cements to hold the grids in place. Proper annealing of the laminated cell may be another approach to the problem.

Moisture degradation of CdS cells has been a long-standing problem. The extent of the problem is shown in Figure 2 where the percent degradation of the maximum power per day is plotted as a function of the relative humidity. Both 1- and 2-mil Mylar and H-film encapsulated cells are plotted. Although at 100-percent relative humidity the cell's life is very short, the rate of degradation could be tolerated at low humidities. More will be said on this later.

A detailed study was made at 65-percent relative humidity. In Figure 3 the decrease of both the short-circuit current and the open-circuit voltage is shown as a function of time. The tests were made in humid air at ambient temperature and pressure. It is of interest to note that during the first month or so the current decreased rapidly before leveling off while the voltage decreased only slowly. In Figure 4 the series resistance R_s and the saturation current I_o are plotted as a function of time. Both the R_s and I_o increase very slowly for the first month then rapidly increase. The shunt resistance decreased during the first month, then tended to level off. The spectral response of the cells from 0.4 to 1.1 decreased uniformly during the first month. Later the intensities were too low for accurate measurements, although there was an indication that the red response was affected.

From these data we concluded that water penetrates the cell's plastic cover and is adsorbed in the junction thus increasing the number of recombination centers so that the current is reduced. No permanent damage is done to the junction, at least initially. It was also found that if the degraded cells were heated in a vacuum, a portion of the lost current could be restored, whereas pressure alone had no effect. (This is in contrast with the storage degradation where pressure alone did restore some of the current.) Thus, as mentioned earlier, low rates of degradation might be tolerated, since once in space the cells can be expected to recover at least a part of their lost power as they are heated by the sun.

The most stringent tests and probably the most important for space applications are the thermal cycling tests being run at Lewis. In Table I the main features of the two thermal cycling facilities now in use are listed. Currently, solar cells are subjected to a series of thermal cycles consisting of 15 minutes of light and 15 minutes of darkness. The data, consisting of temperature, open circuit voltage V_{oc}, and four load currents,

are automatically recorded when the cells approach equilibrium temperature. During the dark portion of the cycle, the cells are cooled to the temperature range of -90° to -120° C depending on the intensity of the light. Light intensities of 100 to 200 mw/cm^2 have been used for these tests. When this program began almost 2 years ago cells barely lasted 10 cycles, but progress has been steady and today we have cells that have not lost any of their original performance after 2,000,. 4,000 and even 10,000 thermal cycles.

In Figure 5 typical thermal cycling data are shown where the relative power output is plotted against the number of thermal cycles. All cells that depended on pressure alone to hold the grids in place (Au or Cu) failed in the manner shown. Some failed very soon and others after thousands of cycles but all failed in the same way. They developed short circuits as a result of the movement of the grid across the barrier during the thermal cycle. The shorts can be removed in most cases by buring them out, by relamination, or simply by annealing them. Epoxy-cemented grids failed because the epoxy did not bond to the grids. The best metal substrate cells are those where the Au grids are electroplated directly onto the barrier. They have stood up very well in thermal cycling. The front-wall plastic-substrate cells have also successfully withstood thermal cycling. One of these cells has shown almost no drop in power output after 10,000 cycles. The thermal cycling tests have uncovered many defects in thin-film cell construction. However, subsequent cells have proved to be much more reliable and, as improved film cells are developed, we shall continue to evaluate them in these simulated space chambers.

Another of the problems of this cell is that we do not understand very well how it works. Improvements in the cell have been made empirically for the most part. If we can make some progress in understanding the cell, this may help to improve the present cell and may possibly point the way to new types of cells.

To begin with, it is necessary to characterize the copper sulfide layer as completely as possible. Table II shows the results of our study of the crystal structure of the chemically formed copper sulfide layer. First of all electron diffraction was used to examine thin layers of the sulfide formed on single crystal CdS. It was found that the copper-sulfide film had a hexagonal structure with lattice spacings only a few percent different from CdS. This corresponds to a high T modification of Cu_2S, which is normally stable only down to 105° C. Thicker films of the copper sulfide, when examined by X-ray diffraction, show the film to be orthorhombic Cu_2S or chalcocite. Thus, the film is composed of Cu_2S with a crystal structure that closely matches the CdS structure at the interface. Further from the interface, the stable chalcocite form of Cu_2S is predominant. Since the crystal structures of the Cu_2S and CdS are similar at the junction, we expect a minimum number of imperfections at the interface. This may explain the high light-generated current in this cell.

We have learned three basic electrical properties of the copper sulfide layer. It is p-type. From Hall-coefficient measurements on the film we

have found that the carrier concentrations are in the range of 10^{21} carriers/cm^3. Hence, the material is degenerate. We have measured the optical absorption coefficient of the film as a function of the wavelength and, after correcting for the free carrier absorption, we find that the optical band edge is clearly defined and corresponds to a band gap of 0.9 eV.

Since we know something about the properties of the copper sulfide, it is possible to sketch the band structure for the cell. This is done in Figure 6. The barrier height of 0.8 eV shown in the figure was determined by capacity-voltage measurements. Nearly all of the band-bending occurs in the CdS, due to the high carrier concentration in the Cu_2S.

Now we would like to consider what might be expected for the spectral response of this heterojunction as a photovoltaic device. We should expect that the cell would begin to yield current from red light at an energy near 0.9 eV, the Cu_2S band gap. We should also expect to see an increase in the photocurrent when the photon energy reaches the band gap of CdS at 2.4 eV. Figure 7 shows the spectral response of a CdS film cell. The spectral responses shown here are all relative to the maximum response at around 2.6 eV. No bias or green light was used. The expected increase in photocurrent at 2.4 eV occurs, but the threshold energy for the cell is about 1.2 eV rather than the expected 0.9 eV. It should be mentioned that the magnitude of the red response of the cells (the response from 1.2 to 2.4 eV) is quite variable, depending on how the cell is made. More will be said about this later. However, for a typical CdS film, the threshold remains at about 1.2 eV. This result suggests that the red response in the cell does not originate in the Cu_2S layer. The other possibility is that it arises from deep impurity levels in the CdS located at an energy depth of about 1.2 eV.

We next tried to identify the impurity. After considering several possibilities, we have come to the tentative conclusion that the impurity responsible for the red response in the cell is excess cadmium. Evaporated CdS films are known to be nonstoichiometric and recent work has shown that they contain excess Cd. It has also been shown that some of the excess Cd can be evaporated out of the film by heat treatment. Hence, we expect that heat treatment of a film should lower the red response if Cd is responsible. We took two nominally identical CdS films, both from the same evaporation, and heated one in argon for 1/2 hour at 575° C. We then made cells from both films. The results are shown in Figure 8. The red response of the heated film is lowered considerably. This experiment was repeated several times with identical results. In a second experiment, we investigated the effect of putting Cd into the films. Two identical films were heat-treated to remove some of the excess Cd. One of the two was coated with a thin film of Cd metal and again heated briefly. The red response of the cell made from the Cd-treated film was higher than the untreated cell. This is again evidence that excess Cd is in some way responsible for the red response.

A third experiment was performed by exposing the cell to hydrogen sulfide. We expect H_2S to react chemically with the excess Cd thereby removing it. Cell performance degrades rapidly on exposure to H_2S. Spectral-response measurements of slightly degraded cells showed a considerable loss of red response, which can be explained by the removal of free Cd. We conclude from these three experiments that the red response of the cell is largely due to excess Cd in the lattice.

We then became interested in the possibility that other metals besides Cd might be used to produce deep donor impurities. Silver (Ag) and indium (In) are adjacent to Cd in the periodic table and have similar sizes. Therefore, we expect that they might enter the CdS lattice in a way similar to Cd. Figure 9 shows the effect of introducing these metals into CdS films. Both In and Ag increased the red response of the cells.

In summary, the major problem areas associated with the CdS film cells are storage, humidity, thermal cycling, and mechanism. The storage stability problem can be eliminated by the use of grids that are firmly attached to the cell. For humidity damage, we find that the cells can be exposed to 20-percent relative humidity for long periods of time (i.e., long enough to assemble an array with little or no damage). By proper construction methods, film cells that are very resistant to thermal cycling can be made. Plastic substrate and electroplated-grid cells have been made that can withstand 10,000 cycles, which is equivalent to two years in Earth orbit. As to the mechanism of the cells, they appear to be heterojunctions of CdS and Cu_2S, with the red response of the cell due to excess cadmium in the film. Possibly, better control of the Cd content or the use of other metals may improve the cell.

Table I. - THERMAL CYCLING FACILITIES

	NO. 1	NO. 2
Tank size	10-in. diam. by 26-in.	30-in. diam. by 4-ft.
Pumping system	8 in. D.P.	10 in. D.P.
Min. Pressure, Torr	10^{-5}	10^{-7}
Cooling medium	LN_2	LN_2
No. of solar cells (3 in. by 3 in.)	4	25
Solar simulation, watts	7 - 600 sun guns	5 KW Xenon 900 tungsten

Table II. - CRYSTAL STRUCTURE OF COPPER SULFIDE BARRIER LAYER

Technique	Result
Electron Diffraction (Thin Layer)	Cu_2S, Hexagonal, High Temp Modification, Close Match to CdS Lattice
X-ray Transmission	Cu_2S, Orthorhombic (Chalcocite)

STORAGE STABILITY OF CdS SOLAR CELLS

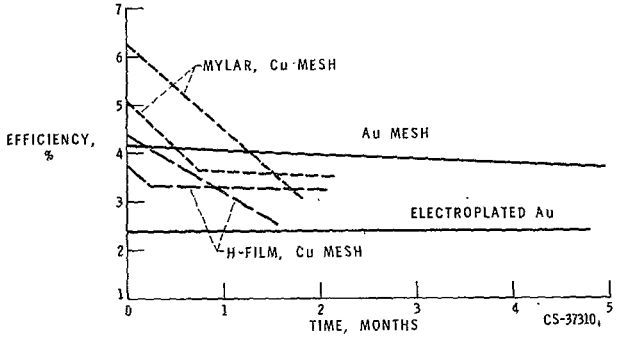

Figure 1.

DEGRADATION RATE OF MAXIMUM POWER

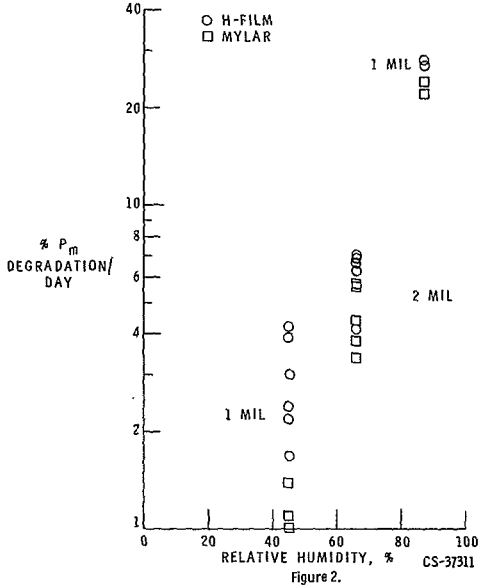

Figure 2.

DEGRADATION OF V_{oc} AND I_{sc} BY MOISTURE

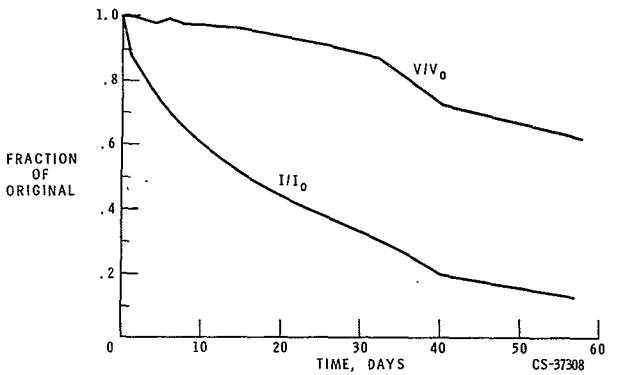

Figure 3.

EFFECT OF MOISTURE ON R_S AND I_0

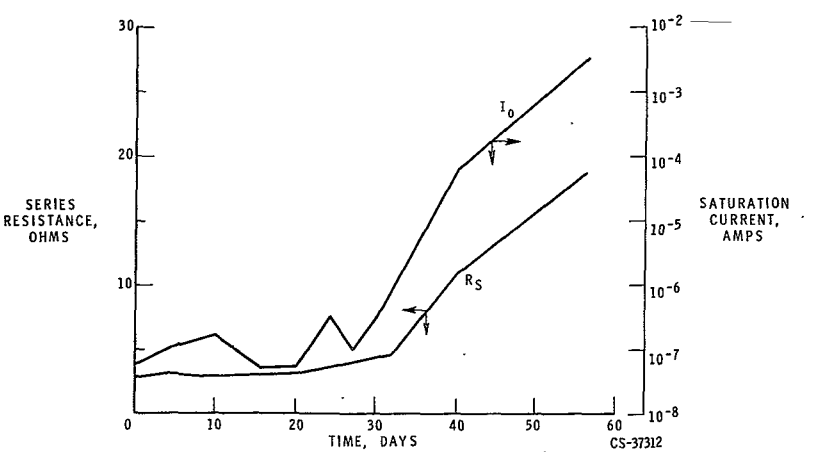

Figure 4.

THERMAL CYCLING OF CdS SOLAR CELLS

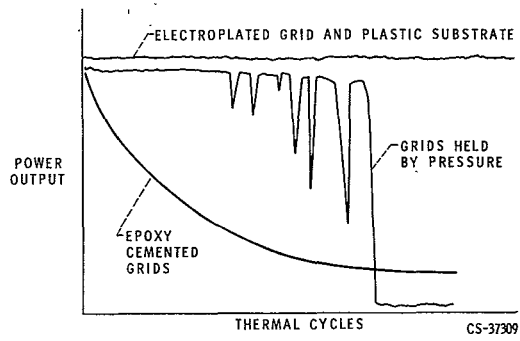

Figure 5.

ENERGY BAND STRUCTURE FOR CdS FILM CELL

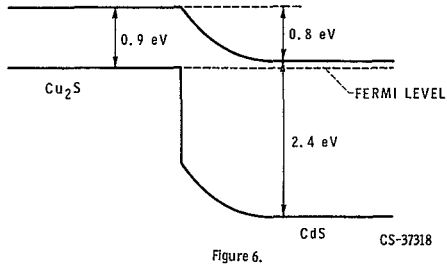

Figure 6.

SPECTRAL RESPONSE OF TYPICAL CdS FILM CELL

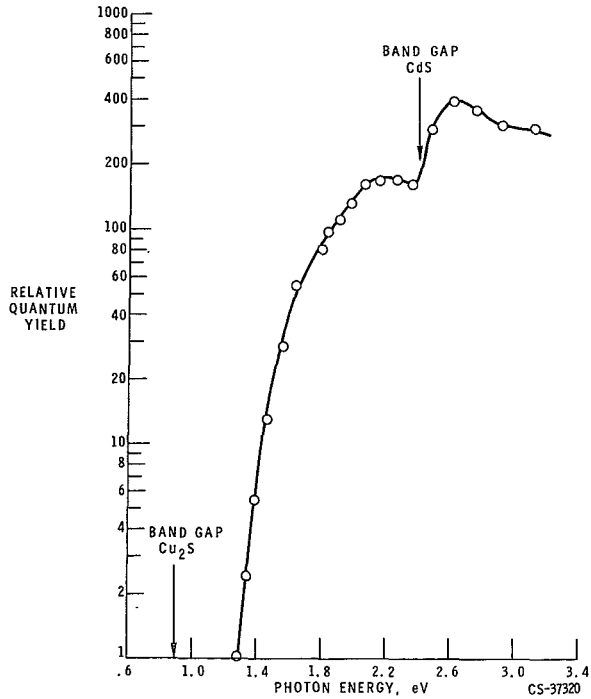

Figure 7.

REMOVAL OF EXCESS CADMIUM REDUCES RED RESPONSE OF CdS CELLS

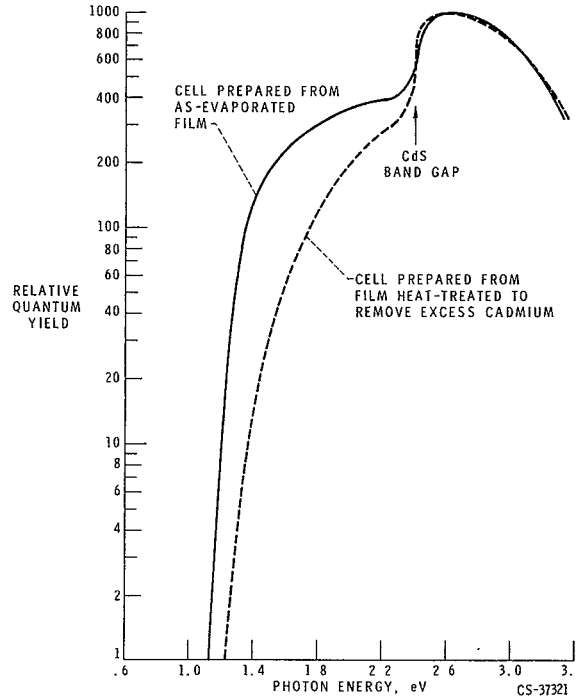

Figure 8.

METALS DIFFUSED INTO CdS FILM INCREASE RED RESPONSE OF CdS CELLS

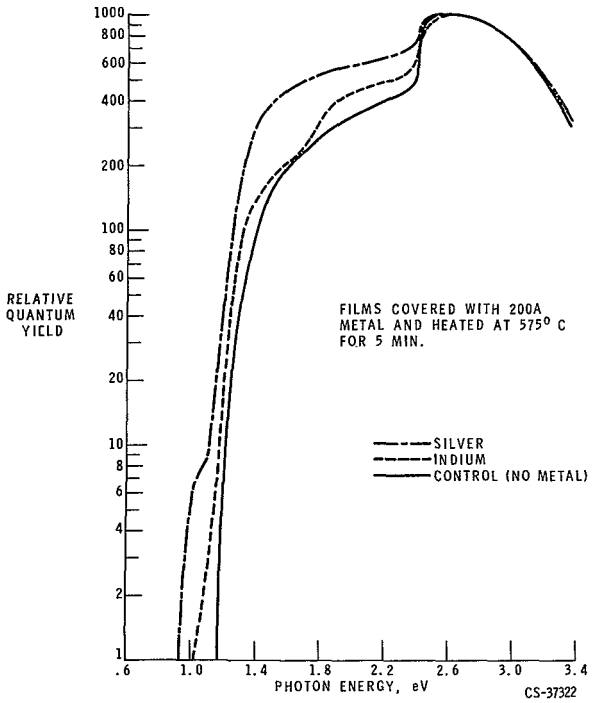

Figure 9.

Discussion

Massie: Can we have questions, please?

Chamberlin - National Cash Register: In these experiments where you were making various cells and treating the surfaces, how were the barriers made?

Spakowski: The copper sulfide barriers were formed by the chemical dip method.

Chamberlin: So, then, the reaction possibly would be expected to be different since you had a different surface prior to the dip. So you did not have complete control from one cell to another. Right?

Spakowski: This may be true.

Chamberlin: Did you run temperature dependency of your spectral response?

Spakowski: We have, but the results have not been published.

Rappaport: I would first like to congratulate you and your co-authors on a very excellent paper and presentation. I have two questions. One, did you measure the carrier mobility in the copper sulfide layers? And the other question is, would you care to speculate as to whether a cell, which had some degradation in standard air conditions and which could be completely recovered in outer space vacuum conditions, would be practical for space, or how much degradation one would expect to recover in outer space? I know that's a difficult one, but it would be interesting.

Spakowski: I might attempt the second part of the question before the real Drew Potter stands (laughter). As far as how low a cell can be degraded beyond which it cannot be recovered, we feel that it's around 70%, which is quite low. Beyond this point, it appears that the junction has been affected. We have recovered cells that have degraded 50% but how fast they recover depends on the temperature and time spent in the vacuum furnace.

Rappaport: Part of that question was, how much of this can be tolerated? Do you think this has to be completely eliminated or some amount of it...

Spakowski: I think a very small amount - say, 10% or so - could easily be tolerated. Drew, do you want to answer the first question?

Potter - NASA-Lewis: The mobility is low, about 1 cm^2/volt sec.

Rappaport: This might explain the lack of response from the Cu_2S.

Potter: Yes

Yannoni - AF Cambridge Research Lab.: I was interested in the length of your thermal cycles and the change in temperature at which you ran the tests.

Spakowski: We chose 15 minutes of light and 15 minutes of darkness for the thermal cycle to get a lot of thermal cycles in since the cells were very near their equilibrium light-on temperature after 8 minutes. The temperature depends on the intensity of light falling on the cell. We've cycled cells from 0^{o} to $100^{o}C$ with the light on to dark temperatures of $-100^{o}C$ to $-120^{o}C$. If we used a half-hour dark cycle, the temperature would get down to about $-140^{o}C$.

Yannoni: Do you have an idea of the energy per unit area for the test with the sun gun?

Spakowski: The sun gun test in the small tank has an intensity around 110 milliwatts/cm^2. The other tank has been operated from 100 up to 200 milliwatts/cm^2.

Yannoni: Thank you.

Cusano - GE: I'll go back to a question I asked the previous speaker. This has to do with cadmium - the impurity absorption - if you remove the copper sulfide by potassium cyanide treatment, then you should be able to reapply it and get a good cell. Have you done anything with removal of copper sulfide to find whether you have response left?

Potter: No, we haven't done that. The thing that may be pertinent is the one experiment that we did, which was to measure the spectral response of a cell immediately after it's been made. This cell has been made in a chemical dip, dipping in the hot solution, 90^{o} centigrade for 5 seconds, and brought out, cooled, and dried at room temperature. This is a bad cell. It's leaky, but it works, and you can measure the spectral response. You then heat this cell at the recommended heat treatment, which is 250 centigrade for a minute or two, and the cell improves dramatically. The current increases considerably, but there is no very large change in the spectral response. It's much the same. So this implies to me either one of two things. Either the impurity centers which are responsible for the red response exist in the film as it is made, and that's the explanation we followed, which of course may not be correct. Or, it implies that copper from the copper sulfide diffuses into the lattice with astonishing speed. It can't be bulk diffusion. It gets in there awfully fast and awfully easy, if copper is entering the lattice and is responsible for the impurity response.

Cusano - GE: Someone - I think it was the RCA people - removed the copper sulfide and got only intrinsic response back, which would indicate that somehow copper must get into this cadmium sulfide layer and account for it. The cadmium interpretation is a new one.

Shirland - Clevite: I'd like to comment on the change in spectral response that the people at NASA observed, particularly with degradation. We have, on at least one occasion, observed the moisture degradation all the way down to nothing, of a high-efficiency Clevite cell and taken the spectral response all the way down and found no change in it whatsoever.

Halstead - GE: I wondered a little about clarification on the last slide. You had spectral response here. This was normalized to a maximum response?

Spakowski: Yes, at 2.6 electron volts.

Halstead: Your results could then be interpreted as a difference in the intrinsic part of the response, rather than a change in impurity response. Consequently, your results are not quite as significant as they might be if they were on an absolute basis. This raises at least some question requiring further clarification in terms of the responsible impurity mechanism, doesn't it?

Potter: This is correct. Of course, we can see no change in shape or form of the intrinsic response curve, while we definitely see changes in the shape of the extrinsic response curve.

Halstead: I think this is very interesting data because there is literature indicating differences between the impurity levels that indium and silver introduce in cadmium sulfide.

Loferski - Brown: One thing that disturbed me about these degradation curves that you showed is that the cells that were stable started out rather poor; they're like 4% or 3% cells. Those that started out at 7% degraded until they got down to the 4 - between 4 and 3%-level, and then presumably stabilized. Does that mean that all cadmium sulfide cells are going to end up at this 4% level independent of how good they are to begin with?

Spakowski: No. I think that might have been a bit misleading. The cells, whether they are 6-1/2% cells or 4-1/2% cells seem to degrade about 1-1/2% before they stabilize. Fred wants to make a rebuttal.

Shirland: I still insist we have seen some cells that have not degraded at all, and therefore intrinsically the barrier is stable.

Spakowski: I must rebut that too, in that the data shown here are median values for groups of 20 to 30 cells. There are cells that degrade perhaps only a half percent and there are occasionally cells that are stable after the first day or so. But these data represent the majority of the cells.

Ritchie - JPL: This is a question directed to you or Dave Massie. Do you feel that cad sulfides are ready for flight applications at this date?

Shirland: I don't feel that they're quite ready at this time.

Spakowski: We have a thin film cell experiment ready now if someone will give us some space on a satellite.

Shirland: So do we. (laughter)

Skarman - National Cash Register: There seems to be some discrepancy in the measured band gap for what we're calling the junction material. In some of my measurements on the digenite form of copper sulfide, we came out with a band gap of something like 2.1, 2.2. This morning we heard a paper on gallium arsenide where they used a copper selenide junction and the band gap there was something quite a bit greater than what you measured - yet as you tend from the selenides to the sulfides, you would expect the band gap to become larger. Now, in spectral response work done several years ago at National Cash Register, we found that in some cases with a carrier concentration of 10^{21} to 10^{22} we did see a spectral response due to the digenite film. We could identify this in a couple of ways, one, we could apply the same digenite film to other n-type semiconductors such as silicon, look at the photovoltaic characteristics, and find a definite peak in the curve due to copper sulfide junction. We could also take the cadmium sulfide cell that we had and reverse it, turn it over to the other side, and get a response that was not due to the copper sulfide, because of the strong absorption of the CdS. So we had a front cell and back-wall cell. Now, I'm not trying to say that the long response is due to copper sulfide entirely. This is obviously not true, but I don't completely agree with your measurements of 0.9 ev, and I would question maybe whether the material you measured this on was with the exact same material as used in making the junction, or was this a bulk-type copper sulfide that you obtained some other way?

Potter: This is the exact same material that we used for making the junction. All we do is dip a thin film of evaporated cadmium sulfide for a long, long period of time, in the copper chloride solution, to replace all the cadmium. We find that this gives us a film of chalcocite Cu_2S rather than the digenite $Cu_{1.8}S$ that you had.

Skarman: That could possibly be it, because the color of the digenite film is just a little deeper yellow than CdS by itself, and therefore you would expect its band gap to be something like 2.2, which it actually comes out to be when done by absorption measurements.

PIC-SOL 209/6.1
Section D-1

SPACE RADIATION ENVIRONMENT*

Presented by

J. I. Vette

Aerospace Corporation

Los Angeles, California

19 October 1965

*This paper was presented at the IEEE Annual Conference on Nuclear and Space Radiation Effects at Ann Arbor, Michigan 12 July 1965 and is to appear in proceedings of that conference, consequently was not available for these proceedings.

PIC-SOL 209/6.1
Section D-2

STATUS OF SILICON SOLAR CELL RADIATION DAMAGE

Presented by

R. L. Statler

U. S. Naval Research Laboratory

Washington, D. C.

19 October 1965

STATUS OF SILICON SOLAR CELL RADIATION DAMAGE

R. L. Statler
U. S. Naval Research Laboratory
Washington, D. C.

Introduction

Radiation damage in solar cells has been extensively studied in the past five years by many investigators who have described radiation induced effects in a host of parameters, such as, for example, efficiency of energy conversion, maximum power point, short-circuit current, open-circuit voltage, minority-carrier-diffusion length, spectral response, junction capacitance, dark current, and curve power factor. To give an added dimension to these many results, many varied light sources have been used (on nonsatellite experiments), including carbon arcs, xenon arcs, and tungsten bulbs, often in combination with water or optical filters. Of course, sunlight at ground level, aircraft, and balloon altitudes has received a share of attention. In addition, solar cells have been fabricated from silicon of a wide range of resistivities, controlled dopants and uncontrolled impurities, with impurity-gradients producing internal electric fields, and with different types of surface coatings.

It has been stated [1,2] that there is no ideal way to present the data of radiation damage to solar cells, partly because there are so many measurable parameters which are sensitive to radiation, and, furthermore, because these parameters cannot always be precisely related to each other. Also the different specialists have interest in various aspects of radiation damage. However, from an engineering standpoint, certain parameters are more important than others in defining solar cell performance. Thus, the purpose of this paper is to present radiation damage results in a manner which is judged to be most useful to the majority of solar power system designers and users. A comparison will be made between different kinds of cells on this basis, using data from existing publications insofar as possible.

The most useful information to the systems designer is: how much power will the solar cell array continue to produce after a time in orbit which will correspond to a known amount of radiation exposure. The rate of radiation exposure will be fairly well determined before launching. As a specific point for the comparisons in this paper, a radiation dose of 10^{16} e/cm^2 - 1 MeV electrons was chosen, and cell temperatures of 28°C -30°C were considered since the maximum amount of literature exists for these conditions. Furthermore, all data used in this paper are those results obtained from measurements under air mass zero (AMO) conditions. No use has been made of any tungsten

light data and consequently the need for using conversion factors has not arisen. The various solar simulators which were used in the reported experiments have been identified.

Silicon Resistivity Effects

One of the most significant questions to be answered is: how does the output power of irradiated solar cells depend on the bulk resistivity of the silicon? Several laboratories have studied this dependence during the last few years. The cells of greatest interest are the one and ten ohm-cm boron doped n-on-p cells. Figure 1 shows the maximum obtainable power output of various brands of one and ten ohm-cm cells, as reported by several investigators. One notices good agreement between measurements under different simulators, and comparable efficiencies between one and ten ohm-cm cells. Figure 2 compares the relative power output* at maximum power point after 1 MeV electron bombardment to the indicated dose. At 10^{16} e/cm^2, there is little observed difference between relative power output of 1 ohm-cm cells and 10 ohm-cm cells: in the ratio of 0.53 to 0.57, approximately. There is considerable variation in the relative power of 10 ohm-cm cells at this dose as shown in this table. Figure 3 illustrates the greater difference existing in relative power for the two kinds of cells as measured under tungsten light. The red-rich tungsten light enhances the differences in radiation damage. For this reason, only AMO condition results are considered in this paper.

A more valid criterion than the relative power degradation is that of comparing actual power output. To do this in a way which attempts to simulate operating conditions, the cell voltage must be chosen and fixed a priori, as is done in practice for the majority of operating satellite power systems. If a power system is designed which allows changing voltage during flight, then maximum power point could be tracked for the type of cell under consideration.

Figure 4 (3) illustrates the way in which V_M, the voltage at maximum power point, shifts as a function of radiation dose, cell resistivity, and temperature. These data show that for the HOF 10 cell, V_M decreases from 0.420 to 0.345 volts while for the HOF 1 cell V_M goes from 0.440 to 0.385 volts after a dose of 5×10^{15} e/cm^2.

Figure 5 lists the output power at constant voltage, V_M, for each cell type, while Figure 6 indicates the relative power at constant voltage, V_M, referred to the initial power before irradiation. The above data are plotted in Figures 7 where it is seen that 1 ohm-cm cells are superior in power output to some 10 ohm-cm cells up to an integrated flux of $.2 \times 10^{15}$ 1 MeV e/cm^2. However the TI 10 cells at all levels of dose have a greater power output at their V_M than the other types.

*Relative power output at maximum power point is defined as the ratio of the maximum power after irradiation to the maximum power before the irradiation.

Temperature Effects

Many researchers have noted the effect of temperature on solar cell performance. Cherry [4] has shown that the 1962 1 ohm-cm n-on-p cells should be operated at 0.35 volts to obtain maximum power at 55°C, as on Nimbus, even before radiation damage. Figure 8, [5] depicts graphically how V_M changes with increasing temperature and bombardment level for 1 ohm-cm n-on-p cells measured at AM 1 (on Table Mountain). Broder [6] has disclosed in Figure 9 the rapid fall-off of power with increasing temperatures of heavily-bombarded solar cells. Here it is seen that cell voltages as low as 0.15 volts provide for more efficient operation at temperature of 100°C. Finally Reynard's results (Figure 10) furnish a convenient method for displaying temperature dependence of solar cell power versus voltage for a HOF 10 cell under electron bombardment. Such a plot provides a readily usable means for selecting proper cell operating voltages. It is evident from these preceding figures that the temperature coefficient for maximum power has different values for 10 ohm-cm and 1 ohm-cm cells. It is of greatest importance therefore, to have a prior knowledge of the temperature and radiation environment in which the solar power supply will operate.

Drift-Field Cells and Aluminum Doped Cells

Other approaches to the problem of increasing the radiation resistance of cells have turned to (1) drift-field cells or (2) additive-impurity doping. However, very little published data exists on radiation effects to the power output of drift field cells. The only available results are those on Westinghouse dendritic drift-field cells, manufactured in 1964, which were studied at NRL by means of a Spectrolab X25L simulator. At the same time, a group of Heliotek 5 ohm-cm aluminum doped cells was evaluated. These data, together with Cunningham's work [7] on Texas Instrument 10 ohm-cm cells, boron and aluminum doped, are shown in Figure 11. This particular group of TI 10 cells, (boron doped) exhibited much better radiation characteristics than the HEL 10 and HOF 10 in the same study. However, the experiment by Reynard did not show this same superiority. The output power is compared on a basis of a nominal 1 by 2 cm cell area, where the effective area is 1.8 cm^2.

Effect of Electron Energy

Previous work by Denny and Downing of TRW and Rosenzweig of BTL has reported damage constant values for solar cells as a function of electron energy. For comparable data on power damage rate under solar simulation, Figure 12, after Reynard [3], reveals the change in relative maximum power point of 10 and 1 ohm-cm n-on-p cells as the bombarding electron energy ranges from 0.5 MeV to 2.0 MeV. These data are in agreement with the earlier work on damage constant values, which increase in magnitude with increasing energy of the incident particle. The difference between cells with different resistivities becomes quite small at the largest dose of 10^{16} e/cm^2. At smaller integrated fluxes, the 10 ohm-cm cell has a few percent superiority.

Proton Bombardment

Existing data on proton bombardment of solar cells with solar simulator evaluation is also scarce. Figure 13 from Reynard[3] is a plot of relative maximum power of 10 and 1 ohm-cm cells with proton energies ranging from 0.5 MeV to 2.7 MeV. The general shape of the curve, with a maximum of damage rate occurring about 1 MeV is in accord with damage constant studies made by others. The HOF 10 cell appears to be about 4% better than the HOF 1 cell at the smaller doses. At the maximum dose used, the two types of cells are quite close in relative power output. The HOF 10 cell data which are plotted as solid square points are obtained from a TRW report.(8)

Conclusions

The following conclusions have been engendered by this review paper:

1. The superiority in radiation resistance for 10 ohm-cm cells over 1 ohm-cm has been exaggerated by comparing maximum power point degradation under tungsten light. When the cells are compared under the typical conditions as stated previously, where (1) the cell voltage is constant and equal to that of maximum power point after a dose of 10^{16} - 1 MeV e/cm^2, and (2) the cell temperature is between 28° and 30°C, then the average 1 ohm-cm cells have greater power output up to 10^{15} e/cm^2, where a crossover occurs, and the 10 ohm-cm cells then have greater power output out to the terminal dose of 10^{16}.

2. Reports of radiation damage studies have been generally lacking in sufficient detail to allow the power system designer to make a complete analysis of the predicted radiation damage history for his array. Temperature dependency and I-V curves under AMO conditions at all flux levels are the more important parameters to be reported.

3. Drift-field cells show definite indications of high resistance to radiation damage and should continue to be studied.

4. The case for aluminum-doped cells is not as definite as for drift-field cells, but the indication is that work should be continued, along with other group III dopants, and perhaps in combination with drift-field doping.

5. The wide variation in radiation damage behavior in some types of 10 ohm-cm boron doped cells as seen in different batches studied at different laboratories emphasizes a need for either greater stability in the manufacture of the cell or for cross-checking samples from a particular batch by different laboratories.

Acknowledgements

This work was sponsored by the Spacecraft Technology Division, Goddard Space Flight Center, NASA.

The author expresses his appreciation to Mr. E. Brancato for helpful discussions and advice, and to numerous individuals who kindly provided the use of reports and experimental data.

References

1. Statler, R. L., "Electron Bombardment Damage in Silicon Solar Cells", NRL Report 6091, October 7, 1964.

2. Rappaport, P., "Photovoltaics", Background Material for the Study of the National Space Power Program, PIC 120/5, Interagency Advanced Power Group, November 1964.

3. Reynard, D. L., "Proton and Electron Irradiation of N/P Silicon Solar Cells", LMSC 3-56-65-4, Lockheed Missile and Space Co., 12 April 1965.

4. Cherry, W. R., "Photovoltaic Solar Energy Converters", Background Material for the Study of the National Space Power Program, PIC 120/5, Interagency Advanced Power Group, November 1964.

5. Martin, J. H. "Solar Cell Characteristics, Determined as Function of Electron Irradiation and Temperature on Table Mountain", Proceedings of the Fourth Photovoltaic Specialists Conference, Cleveland, Ohio, PIC-SOL 209/5, August 1964.

6. Broder, J. D. et.al, "Solar Cell Performance at High Temperatures" Proceedings of the Fourth Photovoltaic Specialists Conference, Cleveland, Ohio, PIC-SOL 209/5, August 1964.

7. Cunningham, B. T. and Moss, E., "Post Irradiation Room Temperature Electrical Characteristics of N/P Silicon Solar Cells", X-636-64-253, Goddard Space Flight Center, August 1964.

8. Carter, J. R. and Downing, R. G., "Charged Particle Radiation Damage in Semiconductors, XI: Effects of Low Energy Protons and High Energy Electrons on Silicon", 4161-6012-RU-000, TRW Space Technology Laboratories, 4 May 1965.

MAXIMUM POWER OUTPUT OF SILICON SOLAR CELLS UNDER AMO SOLAR SIMULATORS

DATA SOURCE	LIGHT SOURCE	10 OHM-CM N ON P			1 OHM-CM N ON P		
		CELL TYPE	AVERAGE MAXIMUM POWER (MW)	AMO EFFICIENCY (%)*	CELL TYPE	AVERAGE MAXIMUM POWER (MW)	AMO EFFICIENCY (%)*
CUNNINGHAM (1964)	SPECTROSUN D1203	HEL HOF TI	24.9 25.3 25.7	9.9 10.0 10.2	RCA	26.7	10.6
REYNARD (1965)	OCLI MODEL 31	HEL HOF TI RCA	27.0 28.1 26.6 26.6	10.7 11.2 10.6 10.6	HEL HOF	26.5 27.0	10.5 10.7
STATLER (1965)	SPECTROSUN X25L	HEL	25.7	10.2	HEL	25.0	10.0
(1963)	SPECTROSUN (SIMULATOR 1)	HEL HOF	25.6 25.2	10.2 10.0	BTL	21.4	8.5
	HOFFMAN (SIMULATOR 2)	HEL HOF	24.8 24.8	9.9 9.9	BTL RCA	21.7 21.0	8.6 8.3
ROSENZWEIG	BTL FILTER WHEEL				BTL	22.0	8.7
MANDELKORN (1964)	LEWIS FILTER WHEEL	LEWIS	28.0	11.1	LEWIS	25.2	10.0
LUFT (1964)	OCLI			9.5 - 10.0			9.5 - 10.0

Fig. 1

RELATIVE MAXIMUM POWER OUTPUT OF SILICON SOLAR CELLS AFTER 1 MEV ELECTRON BOMBARDMENT

DATA SOURCE	LIGHT SOURCE	10 OHM-CM N ON P			1 OHM-CM N ON P		
		CELL TYPE	10^{15} E/CM^2 (P/P_o)	10^{16} E/CM^2 (P/P_o)	CELL TYPE	10^{15} E/CM^2 (P/P_o)	10^{16} E/CM^2 (P/P_o)
CUNNINGHAM (1964)	SPECTROSUN D1203	HEL HOF TI	0.73 0.74 0.79	0.58 0.60 0.60	RCA	0.67	0.50
REYNARD (1965)	OCLI MODEL 31	HEL HOF TI RCA	0.73 0.74 0.71 0.72	0.56 0.57 0.52 0.53	HOF	0.75	0.55
STATLER (1965)	SPECTROSUN X25L	HEL	0.70	0.54	HEL	0.73	0.53
MARTIN (1964)	SPECTROSUN D1203	HEL	0.74				
ROSENZWEIG (1962)	BTL FILTER WHEEL				BTL	0.77	0.55

Fig. 2

RELATIVE MAXIMUM POWER UNDER
FILTERED TUNGSTEN LIGHT
(1 MEV ELECTRON BOMBARDMENT)

DATA SOURCE	N on P SILICON SOLAR CELL RESISTIVITY (OHM-CM)	AFTER 10^{16} E/CM^2 P_{MAX}/P_{MAX_o}
NRL (1963)	10	0.48
	1	0.41
LSMC (1962)	10	0.48
	1	0.38

Fig. 3

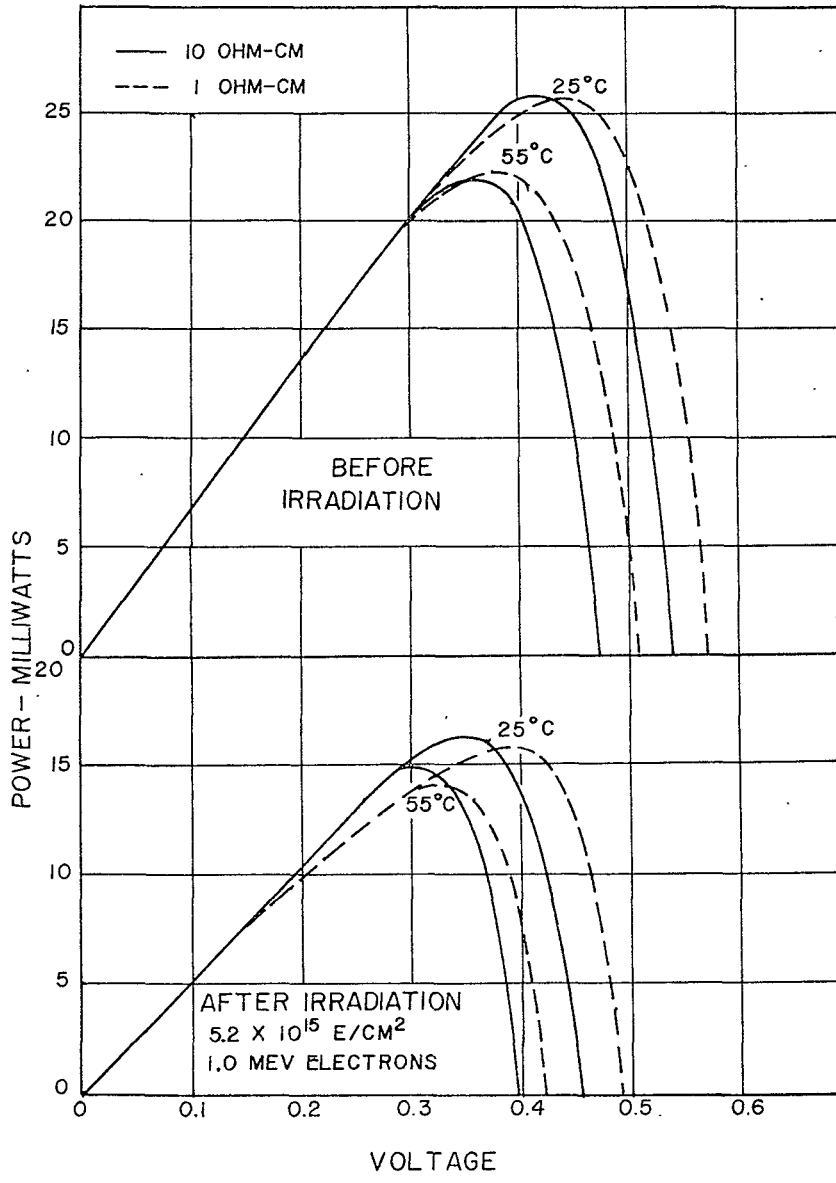

Fig. 4 (After Reynard[3])

OUTPUT POWER AT VOLTAGE V_M OF SILICON SOLAR CELLS
AFTER 1 MEV ELECTRON BOMBARDMENT

DATA SOURCE	LIGHT SOURCE	CELL TYPE	V_M*	INITIAL POWER (MW)	5×10^{13} E/CM^2 (MW)	5×10^{14} E/CM^2 (MW)	5×10^{15} E/CM^2 (MW)	10^{16} E/CM^2 (MW)
CUNNINGHAM (1964)	SPECTROSUN D1203	HEL 10	0.320	21.4	20.2	17.8	15.1	13.9
		HOF 10	0.325	22.5	21.4	18.9	16.0	14.8
		TI 10	0.350	24.0	23.4	20.9	17.4	15.4
		TI 10A	0.340	23.1	22.3	19.6	16.5	15.1
		RCA 1	0.380	24.8	23.2	19.7	15.3	13.3
REYNARD (1965)	OCLI MODEL 31	HOF 10	0.325	22.0			16.0	
		HOF 1	0.380	24.2			15.9	
					4×10^{13} E/CM^2 (MW)	2×10^{14} E/CM^2 (MW)	10^{15} E/CM^2 (MW)	10^{16} E/CM^2 (MW)
STATLER (1965)	SPECTROSUN X25L	HEL 10	0.330	22.4	21.0	18.5	17.5	13.8
		HEL 1	0.375	23.8	22.0	20.2	17.9	13.3
		HEL 5A	0.365	23.4	22.0	20.7	18.1	14.6
		WES DF†	0.375	22.3	21.5	21.1	19.8	15.3

* V_M is the voltage at the maximum power point after a bombardment of 10^{16} E/CM^2.

†The output power of the WES DF cell was computed for a nominal size of 1 x 2 cm.

Fig. 5

RELATIVE POWER OUTPUT AT VOLTAGE V_M OF SILICON SOLAR CELLS
AFTER 1 MEV ELECTRON BOMBARDMENT

DATA SOURCE	LIGHT SOURCE	CELL TYPE	V_M*	INITIAL POWER P_o (MW)	5×10^{13} E/CM^2 (P/P_o)	5×10^{14} E/CM^2 (P/P_o)	5×10^{15} E/CM^2 (P/P_o)	10^{16} E/CM^2 (P/P_o)
CUNNINGHAM (1964)	SPECTROSUN D1203	HEL 10	0.320	21.4	0.94	0.83	0.71	0.65
		HOF 10	0.325	22.5	0.95	0.84	0.71	0.66
		TI 10	0.350	24.0	0.97	0.87	0.72	0.64
		TI 10 A	0.340	23.1	0.97	0.85	0.72	0.65
		RCA 1	0.380	24.8	0.94	0.80	0.62	0.54
REYNARD (1965)	OCLI MODEL 31	HOF 10	0.325	22.0			0.73	
		HOF 1	0.380	24.2			0.66	
					4×10^{13} E/CM^2 (P/P_o)	2×10^{14} E/CM^2 (P/P_o)	10^{15} E/CM^2 (P/P_o)	10^{16} E/CM^2 (P/P_o)
STATLER (1965)	SPECTROSUN X25L	HEL 10	0.330	22.4	0.94	0.83	0.78	0.62
		HEL 1	0.375	23.8	0.93	0.85	0.75	0.56
		HEL 5 A	0.365	23.4	0.94	0.89	0.78	0.63
		WES DF	0.375	22.3	0.97	0.95	0.89	0.69

*V_M is the voltage at the maximum power point after a bombardment of 10^{16} E/CM^2.

Fig. 6

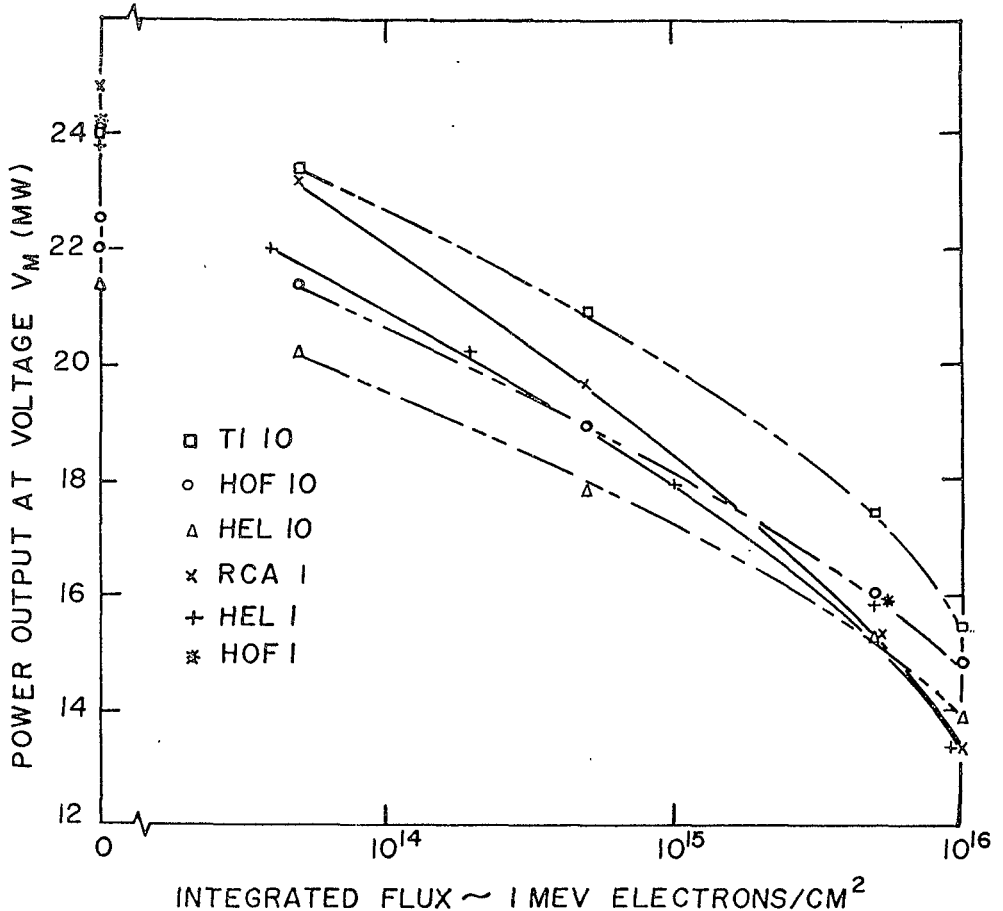
POWER OUTPUT AT VOLTAGE V_M (MW)
24
22
20
18
16
14
12
0
10^{14}
10^{15}
10^{16}
INTEGRATED FLUX ~ 1 MEV ELECTRONS/CM^2
TI 10
HOF 10
HEL 10
RCA 1
HEL 1
HOF 1

Fig. 7

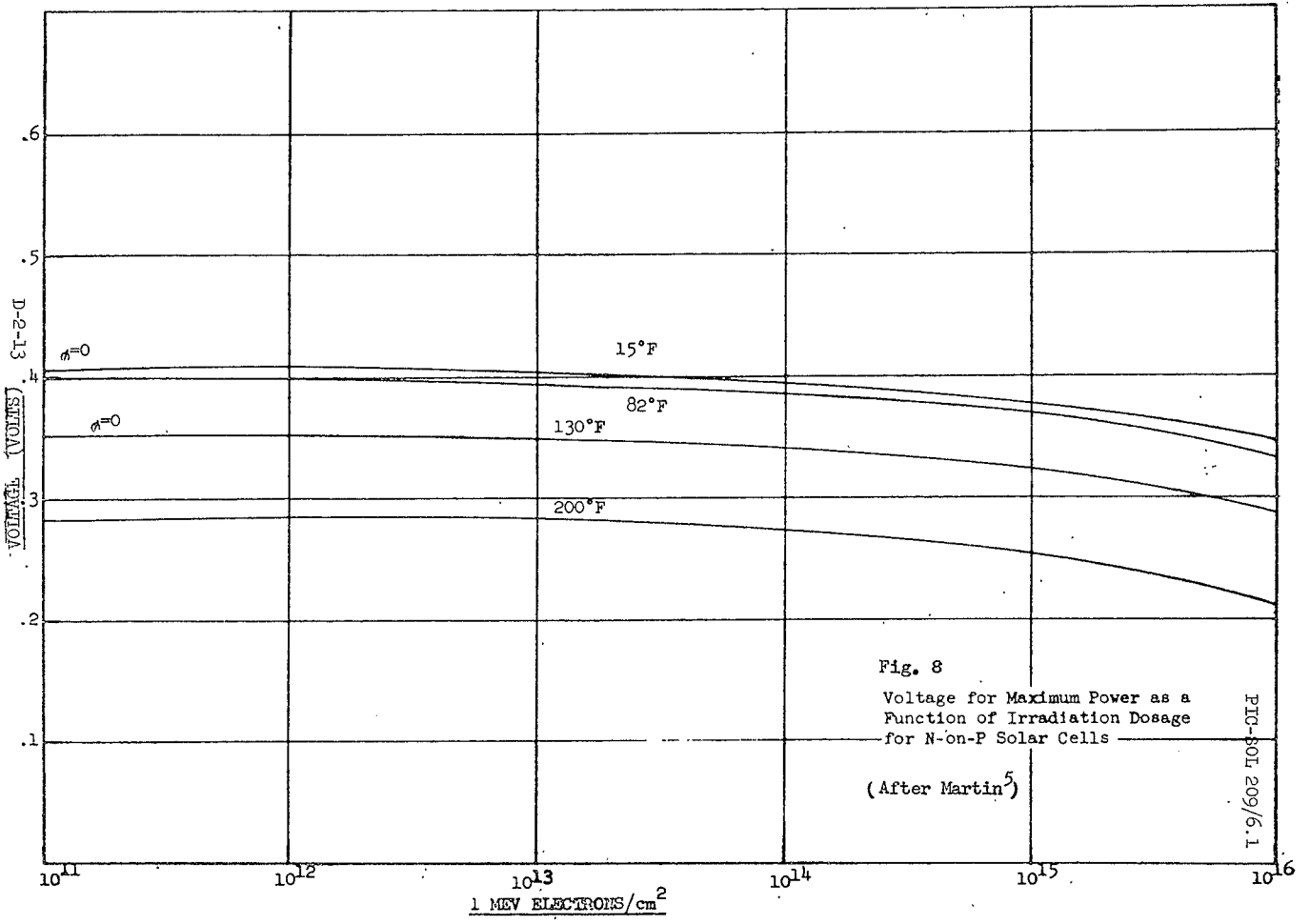

Fig. 8

Voltage for Maximum Power as a Function of Irradiation Dosage for N-on-P Solar Cells

(After Martin[5])

PIC-BOL 209/6.1

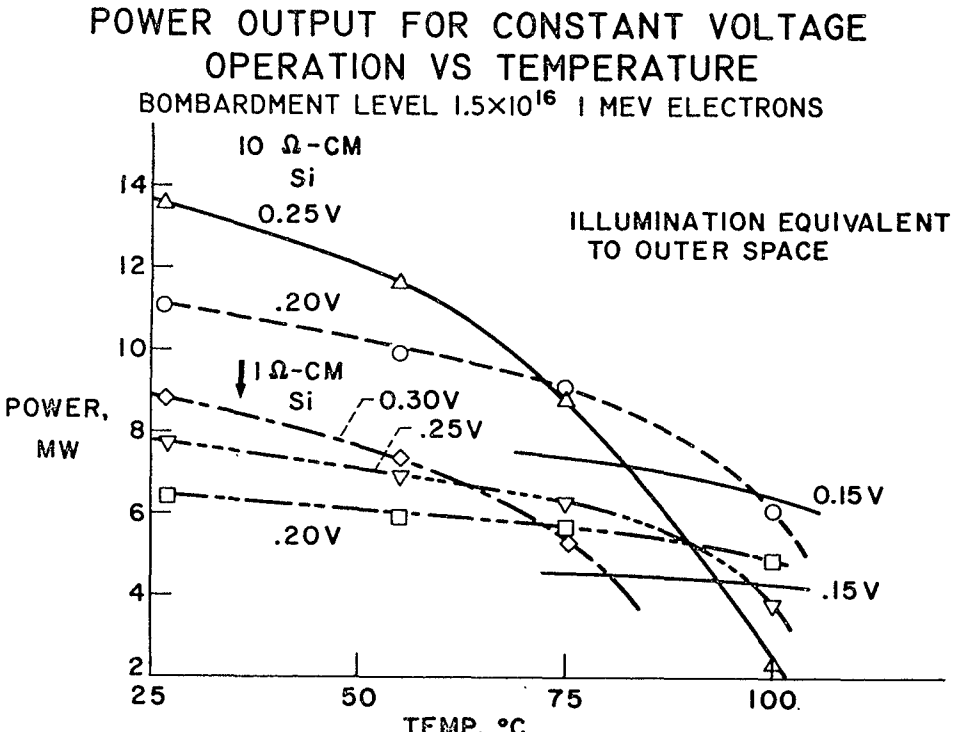

Fig. 9 (After Broder[6])

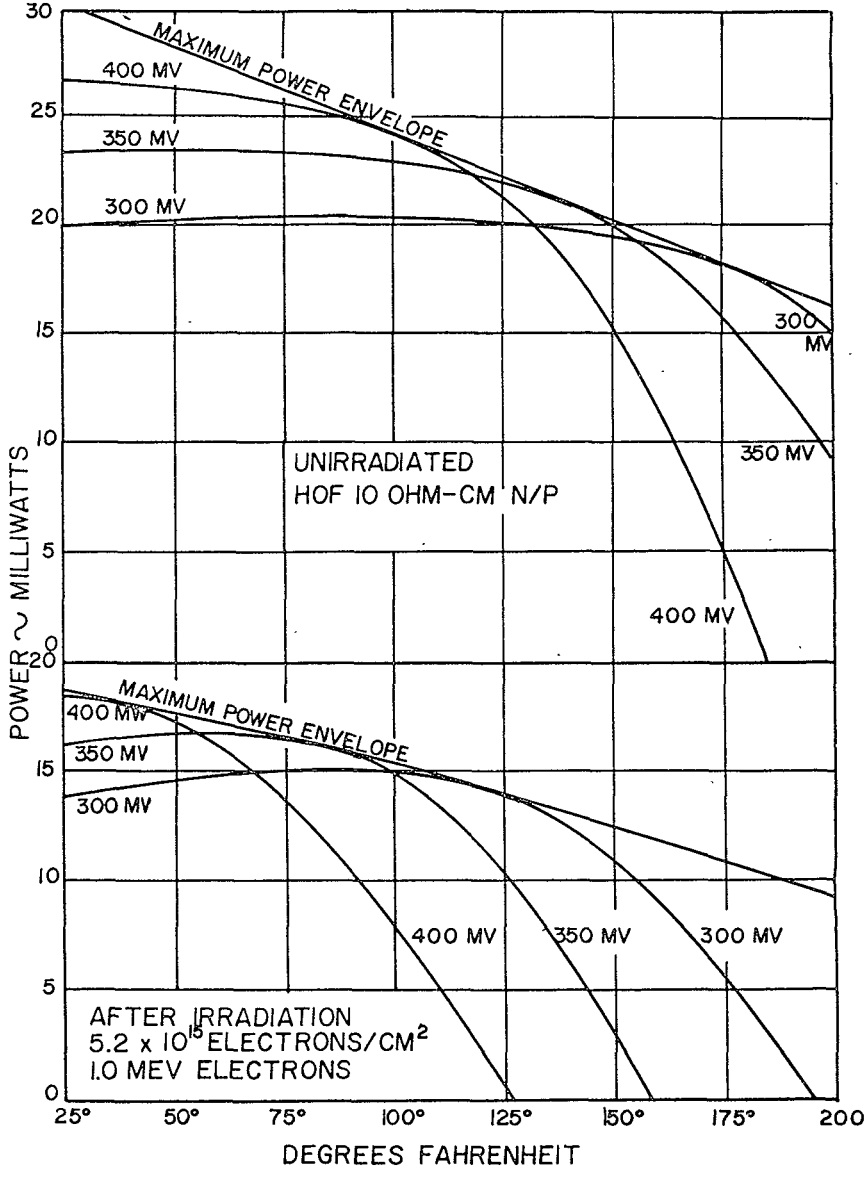

Fig. 10 (After Reynard[3])

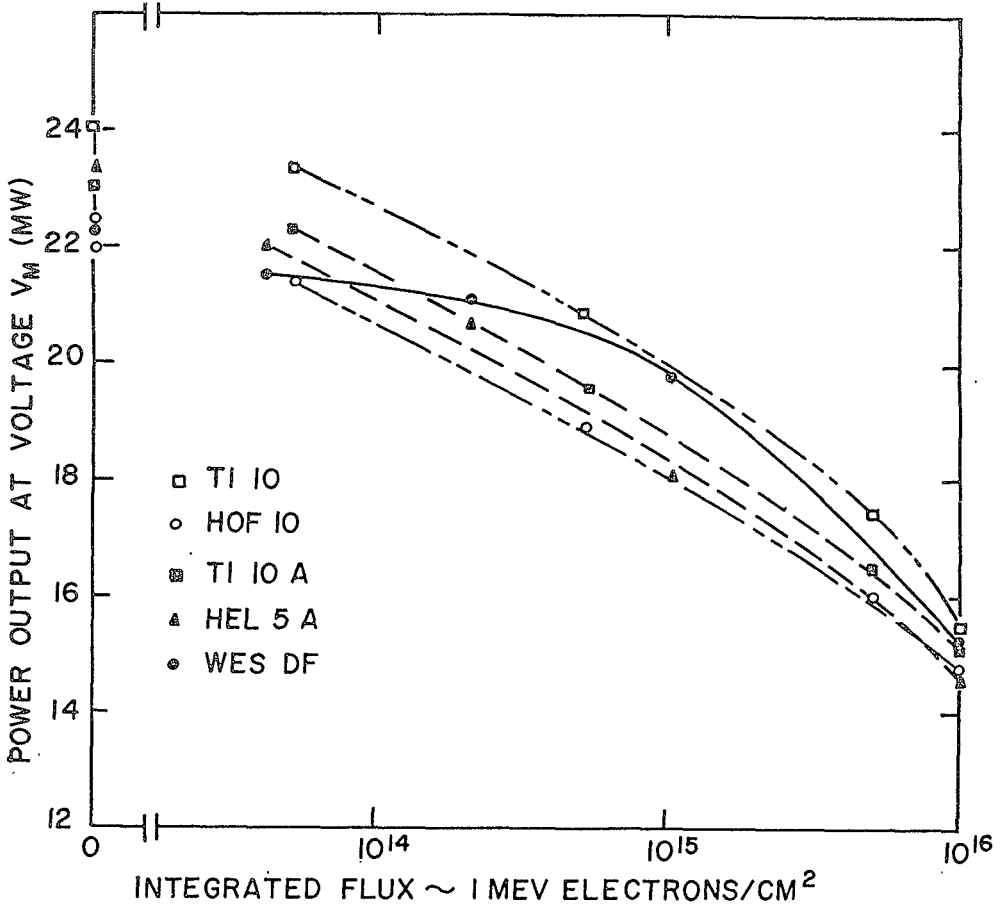
POWER OUTPUT AT VOLTAGE V_M (MW)
24
22
20
18
16
14
12
0
10^{14}
10^{15}
10^{16}
INTEGRATED FLUX ~ 1 MEV ELECTRONS/CM^2
TI 10
HOF 10
TI 10 A
HEL 5 A
WES DF

Fig. 11

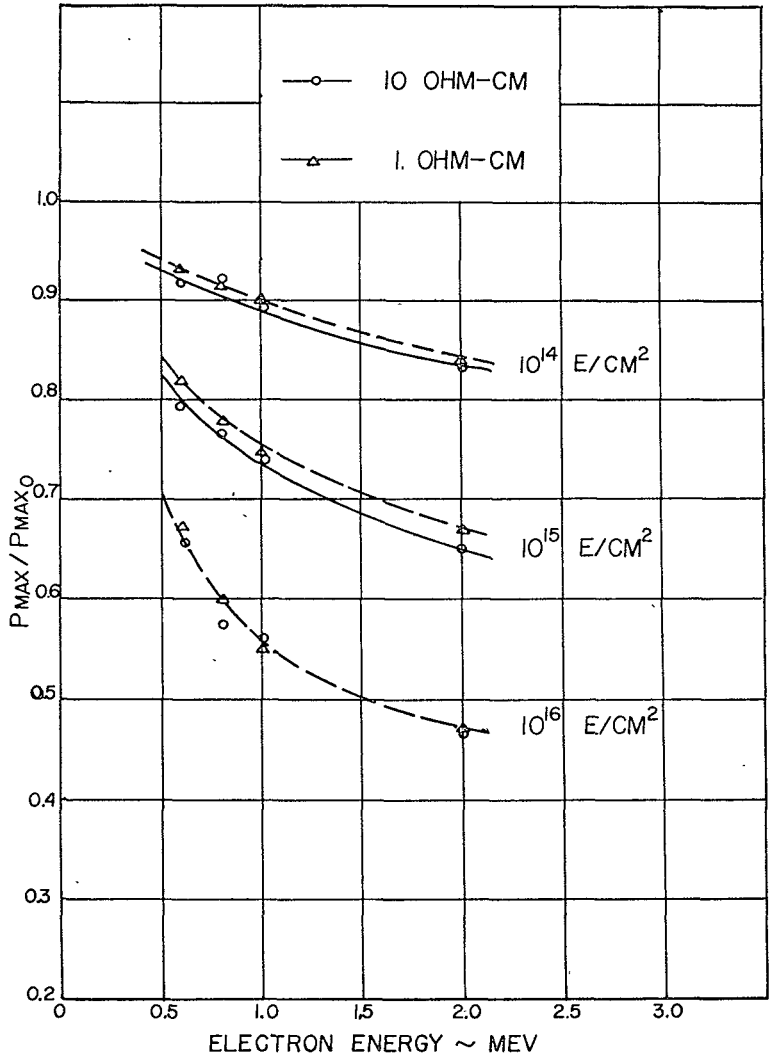

Fig. 12(After Reynard[3])

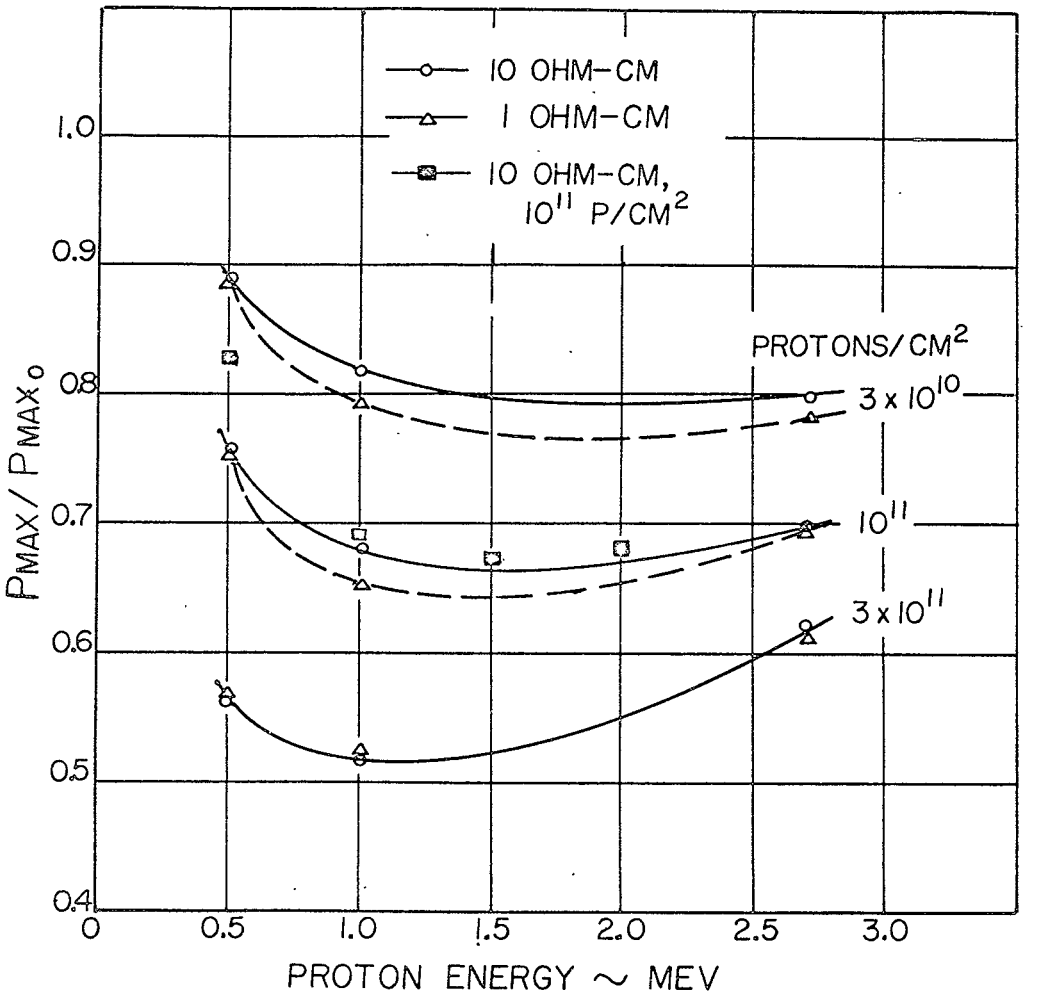

Fig. 13 (After Reynard[3])

Discussion

Schach: Thank you very kindly, Dick. We'll have time for a few questions.

Mann, Spectrolab: First, I'd like to say that you've compiled a great deal of information which will be very useful. I'd like to comment on one point. In choosing the voltages that you selected for 10 ohm-cm and 1 ohm-cm cells, I think you should perhaps have taken two different voltages since the characteristics might be weighted otherwise. Looking at the curves that you showed for beginning and end of life, I think the choice was not as good for the 10 ohm-cm as it was for the 1 ohm-cm.

Statler: This is a good point. We will try to take it into account when preparing this paper for the Proceedings.

Baker, GE: I'd like to take issue with one of your basic assumptions, and that is - that in designing a power subsystem, the important parameter is the degradation of power output at any voltage, and not at fixed voltage. The usefulness of the data of your degradation in a fixed voltage is really limited to the history - a predicted history - of a solar array output, of a power subsystem whose design is already frozen. If one is going to design a power subsystem using a solar array, one of the items of concern, of course, is the radiation environment - and one should know the voltage degradation occurring on the solar cells that he picks - but whether the degradation is in voltage or in current, the parameter of interest in picking your right area is the power degradation, not a fixed voltage, but power degradation, at the maximum point. Once this is picked, the degradation at constant voltage gives you a power history which may or may not have some interest for the subsystem designer. It is true, under certain circumstances, that even though there is a voltage degradation of the array, the spacecraft can get to use the power available at the maximum power point even though this maximum power point is changing in voltage, depending on the type of power-conditioning equipment that is used on a spacecraft. If you are using a switching-type voltage converter, you essentially have a DC-DC transformer, and if you're concerned with the limiting case where you're running at the maximum power point, the voltage ratio in the DC-DC converter will adjust, so that in a limiting case you are riding on the maximum power point, regardless of what the array maximum power point voltage is, within a certain range. So this is a - I'll take very strong issue with your basic premise on this fixed voltage of 0.35. I think you should pick the maximum power voltage, because this is what gives you the initial useful engineering data for subsystem design.

Fischell: I would have to agree with the way Dick Statler presented the data, in that most of the satellites in which I've been concerned, and most of them that I've seen, do operate at a fixed voltage. And therefore, although I know there are some systems which seek the peak power point - seek the peak power voltage and transform it to that voltage - the improvement of using that system, for example, compared to selecting a voltage life, how much you want - the best voltage at the end of life, - you see, because that device has to have some losses in it - it seems to us that it's important to work at a fixed voltage, and to know the degradation at that voltage, so that we can - and a voltage of about 23.5 is about what we'll be using. I think that most of the other spacecraft system people are using voltages about that level And in the design of a satellite, you cannot normally - on the satellite designs - you don't normally change the voltage in order.

Baker, GE: No, you missed the point - you misunderstand my point. My point was that in selecting a design, you adjust the number of cells that you hook in series. In making - in selecting a design - based on what the voltage degradation is. So that you don't - I mean - within limits, depending on whether or not you have body-mounted cells or panels, where you can adjust your panel dimensions, you don't really care whether degradation to the solar cells is in voltage or in current as long as you know what the power degradation is, because you can within limits adjust the number of cells you have connected in series and parallel. But the degradation at constant voltage is of interest only in tracing a history of the power subsystem after it has completed design. But in selecting the design in the first place, what you're interested in is the degradation in maximum power. And you can normally make whatever adjustments are necessary in the number of the cells that you select in series and parallel, to accommodate this degradation. I mean - this to me is a fundamental difference.

(Author' comment: This paper is a revision of the one presented at the Conference, taking account of the above discussion. The author is indebted to A. Mann, J. E. Baker, and R. E. Fischell for their suggestions).

STATUS OF SOLAR CELL COVER MATERIAL RADIATION DAMAGE*

Presented by

F. J. Campbell

U. S. Naval Research Laboratory

Washington, D. C.

19 October 1965

*This paper was not presented at the conference, however, was prepared at the request of the sponsors for inclusion in these proceedings.

STATUS OF SOLAR CELL COVER MATERIAL RADIATION DAMAGE

F. J. Campbell
U. S. Naval Research Laboratory
Washington, D. C.

Radiation damage is not just a function of the solar cell degradation - the entire assembly must be considered in an analysis of the power supply. In Figure 1 is shown the commonly used composite of materials in a solar cell assembly. The solar cell is covered with a transparent high density shield which will attenuate the incident particle radiation encountered in the Van Allen belts. This shield is coated on the outer surface with an anti-reflection coating which serves to increase the amount of light transmitted. On the inner surface a selectively reflecting filter is applied which rejects the ultraviolet energies which do not photo-activate the solar cell. This reduces internal heating and provides some protection against UV degradation of the adhesive used to bond the shield to the solar cell.

Studies have been carried out, both by laboratory radiation exposures and by satellite mounted experiments, to determine the nature of the degradation and the effects on the power efficiency of the solar cell composite assembly. This paper has been prepared at the request of the Conference chairman to provide a summary of the most important results achieved by the prominent researchers in this field within the past few years. Presentation of these studies will be most effective if they are discussed first with respect to studies of the individual components and then to the composite assemblies - showing how the two approaches have been related.

Shielding

A requirement of the shielding material is that it should not be degraded by radiation, either particle or electromagnetic, that would add to the decrease of efficiency of the solar cell assembly for utilization of the sun's available radiant energy.

The most immediate effect on these materials has been observed as the production of color-absorbing defects in the molecular structure. The resulting decrease in transmittance is greatest in the ultra violet region of the affected materials. An example of this degradation is shown in Figure 2 for a specimen of microsheet glass (Corning 0211) which was irradiated with 1×10^{16} electrons (1 MeV)/cm^2. Decreases in percent transmittance at specific wavelengths in the visible region are reported for microsheet, fused silica and several radiation shielding glasses after exposures to 1×10^{16} electrons (1 MeV)/cm^2 and 4×10^{11} protons (4.6 MeV)/cm^2 were reported at a previous conference.[1]

The most complete study of transparent materials that might be used for shielding has been reported by Haynes and Miller.[2] They observed the effects of electron irradiations at 1.2 and 0.3 MeV on samples of 22 different materials, observing for changes in spectral transmittance, "wide-band transmission", fluorescence, and post-irradiation bleaching by heat and ultraviolet light. For maximum damage densities they chose sample thicknesses, when available, to correspond to the energy range of the electrons. These materials represent the glass categories of synthetic fused sapphire, synthetic fused silica, fused quartz, natural quartz, radiation shielding grade glasses, microsheet, and common plate glass. Those which showed little or no decrease in "wide-band transmission" at doses of 2.7×10^{15} electrons (1.2 MeV)/cm^2 were sapphire, fused silica and some of the high density radiation shielding glasses. A summary of the effects of this dose on representative samples of materials in the various categories is presented in Table 1. "Wide-band transmission" measurements were with a silicon solar cell at room temperature illuminated with a tungsten light at 2800°K and at an intensity of 100 mw/cm^2. "Wide-band transmission" was calculated as the ratio of short-circuit current of the cell when covered with the sample glass to that of the bare cell. Fluorescence tests showed none existed in sapphire either before or after irradiation; while fused silica which did not fluoresce before, showed red fluorescence following irradiation.

Filters

The "blue" and "blue-red" reflecting filters consist of multi-layer vapor deposited metallic oxides and salts on the glass surface placed nearest the solar cell. Results of several studies have been reported recently which describe the effects of radiation on spectral transmittance and the effectiveness of these coatings as reflectors of ultraviolet energy in protecting adhesives from radiation damage. In one study Mauri found that ultraviolet exposures will produce a slight decrease in the "broad-band" transmittance (500-1100 mμ) of "blue" reflective filters and a greater decrease in that of "blue-red" filters. The percent changes from equivalent exposures are listed in Table 2.[3] In several other experiments in which ultraviolet exposures (600 ESH) were followed by 1.5 MeV electron irradiations (10^{16} e/cm^2) Reynard reported that Corning 7940 fused silica shields with "blue" filters showed a 2 to 3% loss in transmission after the ultraviolet exposure and a 3 to 4% loss after the electron exposure; whereas, samples of the uncoated Corning 7940 showed no change after either of these exposures. To determine the protection value of a "blue" filter he exposed a sandwich-type sample of an epoxy adhesive between two sheets of Corning 7940 to ultraviolet irradiation (600 ESH). The one with a "blue" filter suffered about a 10% loss.[5]

Examples of the changes in spectral transmittance of microsheet shields with "blue" and "blue-red" filters irradiated with 1 MeV electrons (10^{16} e/cm^2) are shown in Figures 3 and 4. By comparing these curves with Figure 1 it appears that some of the transmission loss is due to degradation in the filters.

In a proprietary cooperative study of the radiation stability of multilayer interference filters, ultraviolet irradiation experiments were conducted at Lockheed on evaporated films of some of the individual components of commercially produced filters as well as some other experimental film materials. Results showed that some films of these individual components degraded more than those in vacuum. Results will be utilized to improve the stability of filter coatings.[5]

Adhesives

Several radiation experiments on adhesive materials have led to the selection of silicone types over epoxy for greater stability to light transmittance degradation by either ultraviolet or electron irradiation. Two transparent silicone adhesives that have been investigated in several laboratories are Sylgard 182 (Dow Corning) and LTV-602 (General Electric). Another, (XR-63488) which is a purified version of 182 is slightly more stable[4]. Although bond strengths of these materials are much lower than that of epoxy resins, it has been reported sufficient to hold the shields, and they have successfully met environmental stability requirements of humidity exposures, temperature soaks, and temperature cycling. The experimental results listed in Table 3 show that primers which are available to increase the bond strength are degraded by ultraviolet so it would be better to leave them off. These specimens consisted of approximately one mil of adhesive with a "blue" filter on Corning 7940 as the front cover and uncoated Corning 7940 as the back cover.[3] That the silicones are inherently stable to ultraviolet irradiation effects on transmittance was demonstrated by Reynard in experiments without filter coatings on the fused silica cover slides.[4] Conclusions on the need for the filter coating are not in agreement since some believe the additional warming of the solar cell would render it less efficient than would filter degradation. More experiments are needed in this area.

Laboratory Radiation Experiments on Composites

Demonstrations of the effects of electron irradiations on the degradation of composite assemblies of solar cell-adhesive-shield, have been reported on in independent experiments in two laboratories. The results show that the contributions of the various components are additive and therefore degradation in a known space flux can be predicted.

Reynard irradiated samples of 10 ohm-cm n/p solar cells covered with various shields as follows: 20-mils Corning 7940 fused silica with no filter coatings, the same with a blue-reflective coating, and 26-mils Corning 0211 microsheet glass with no coating. All employed LTV-601 silicone adhesive. Irradiations with 2 MeV electrons to an integrated flux of 10^{16} e/cm^2 produced differential losses above that of the unfiltered specimen in maximum power and short-circuit current which were 3% greater in the sample with a blue filter and 15% to 20% greater in the sample with the microsheet cover. Changes in relative maximum power versus integrated electron flux are plotted for these specimens in Figure 5.[6]

Another study on composite assemblies duplicating the Syncom II power

supply design of p/n cells covered with 6-mils microsheet with a "blue" reflective filter and Furane 15E adhesive. By measuring spectral response of bare and covered cells with an integrating solar simulator it was demonstrated that light transmittance degradation in the individual materials could be translated to the short-circuit current degradation of the assembly when irradiated with 1 MeV electrons. The degradation of glass and adhesive transmittance at the "blue" end of the spectra produces a loss in "blue" response of the assembly while degradation of the solar cell is in "red" response. Thus, the combination of the two degradations produces a resulting decrease in spectral response as illustrated in Figure 6.7

Conclusions

Results of the studies reported here have led to a selection of more radiation resistant cover glass and adhesive materials for solar cell assemblies. To recapitulate, from this survey one may specifically conclude the following:

1. Synthetic sapphire and fused silicon are the most resistant glasses to ultraviolet and electron degradation.

2. Even when both are protected by "blue" filters, the silicone adhesives are about five times more stable than epoxies to radiation degradation of light transmittance.

3. The broad-band transmittance of reflective filters is decreased slightly by ultraviolet and electron radiation exposures.

Questions that require more research to provide the answers are as follows:

1. Can the reflective filters be eliminated on assemblies utilizing silicone adhesives?

2. Are reflectance and emissivity of cover glasses with reflective filters damaged by ultraviolet or particle irradiations?

3. Do low energy protons in the 1 to 100 KeV range damage the anti-reflective coating on the front surface of the glass shields?

Acknowledgements

Appreciation is gratefully expressed to Mr. E. L. Brancato for his encouragement during the preparation of this paper, and to all those who responded to his requests for material for this survey.

The research program of radiation effects on satellite surface materials at the Naval Research Laboratory is supported by the Spacecraft Technology Division of the Goddard Space Flight Center.

References

1. Campbell, F. J., "Effects of Radiation on Transmittance of Glasses and Adhesives", Proceedings of the 17th Annual Power Sources Conference, May 21, 1963.

2. Haynes, Gilbert A. and Miller, Wm. E., "Effects of 1.2 and 0.30 MeV Electrons on the Optical Transmission Properties of Several Transparent Materials", NASA Technical Note D-2620, Langley Research Center, Langley, Virginia, March 1965.

3. Mauri, R. E., "Evaluation of Optical Properties and Environmental Stability of Solar Cell Adhesives", LMSC AO 34229, Lockheed Missile and Space Co., Palo Alto, California, April 1964.

4. Reynard, D. L., "Irradiation of Solar Cell Cover Slides and Adhesives with 1.5 MeV Electrons", LMSC 3-56-64-5, Lockheed Missile and Space Co., Palo Alto, California, August 1964.

5. Reynard, D. L., Lockheed Missile and Space Co., private communication.

6. Reynard, D. L., "Proton and Electron Irradiations of n/p Silicon Solar Cells", LMSC 3-56-65-4, Lockheed Missile and Space Co., 12 April 1965.

7. Campbell, F. J., and Lambert, R. J., "Effects of Shielding on Electron Damages to Solar Cells", Proceedings of 4th Photovoltaic Specialists Conference, Cleveland, Ohio, PIC-SOL 209/5, August 1964.

Table 1
Effects of Electron Irradiation on "Wide-Band" Transmittance of Various Transparent Materials[2]

Electron Energy = 1.2 Mev
Integrated Flux = $2.7 \times 10^{15} e/cm^2$

Material	Manufacturer	% loss in "wide-band" transmittance
Linde sapphire	Linde Co., Division of Union Carbide Corp.	0
Corning 7940 (fused silica)	Corning Glass Works	0
Fused Quartz (optical grade)	Engelhard Ind. (Amersil Quartz Div.)	1.8
GE 104 (fused quartz)	General Electric Co.	0.8
Natural crystal quartz	–	26.8
Corning 8362 (non-browning lead glass)	Corning Glass Works	2.4
Corning 8363 (High-density lead glass)		0
Corning 8365 (non-browning lead glass)		0
Corning 0211 (micro-sheet)		7.6
Solex	Pittsburgh Plate Glass Co.	2.7
Soda-lime plate glass	–	26.0
Feurex (heat-resistant borosilicate glass)	Blue Ridge Glass Corp.	25.2

Table 2
Effects of Ultraviolet Radiation on Transmittance of
Reflective Filters Deposited on Corning 7940 Fused Silica[3]

Filter	Ultraviolet Exposure, sun-hours	Ave. Initial Transmittance %(500-1100 mμ)	Ave. Final Transmittance %(500-1100 mμ)	Ave. Change in Transmittance %(500-1100 mμ)
none	703	93.3	92.0	-1.4
"blue-red"	590	93.3	87.3	-6.4
"blue"	735	93.0	91.0	-2.2

Table 3
Effects of Ultraviolet Radiation on Silicone Adhesives
With and Without the use of Primers[3]

Adhesive	Primer	Ave. % change in Transmittance (500-900 mμ) after indicated sun-hours of exposure	
		500	2000
XR63488	no	0	0
XR63488	yes	1.1	1.2
LTV-602	no	1.1	0.6
LTV-602	yes	0.6	2.9

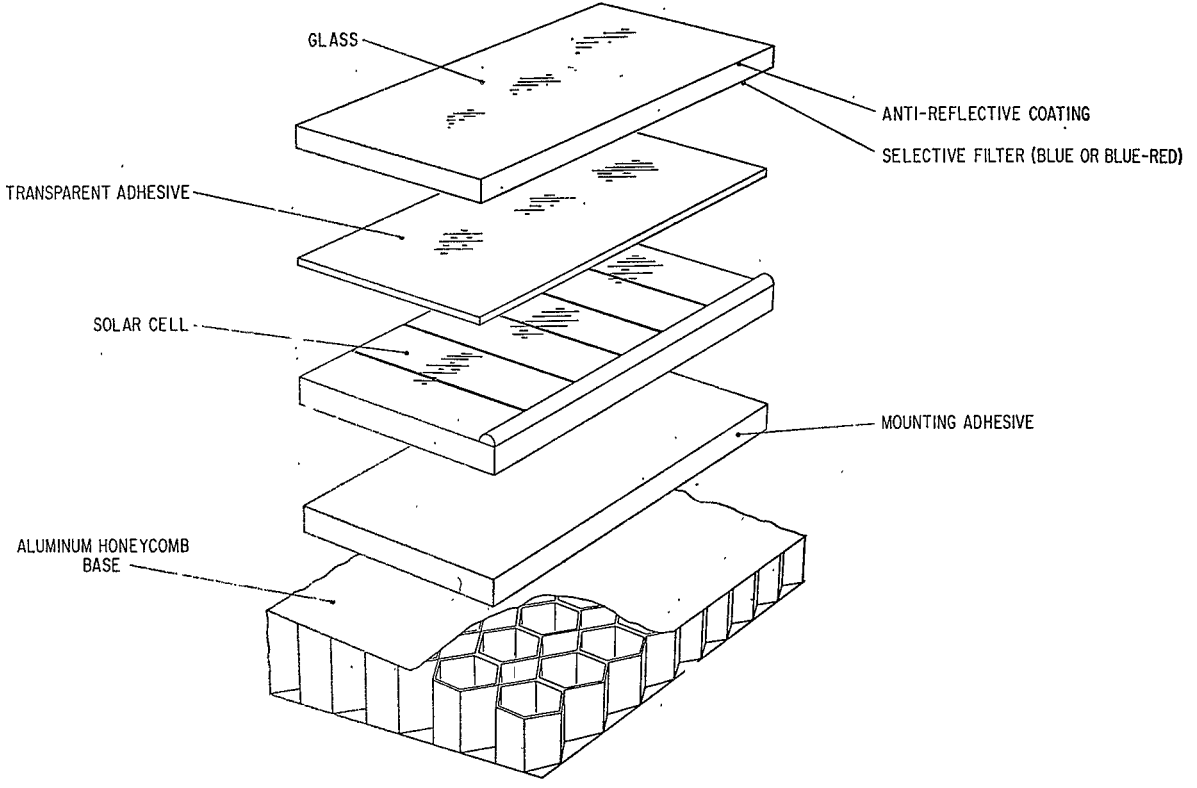

SOLAR PANEL CONSTRUCTION

Figure 1

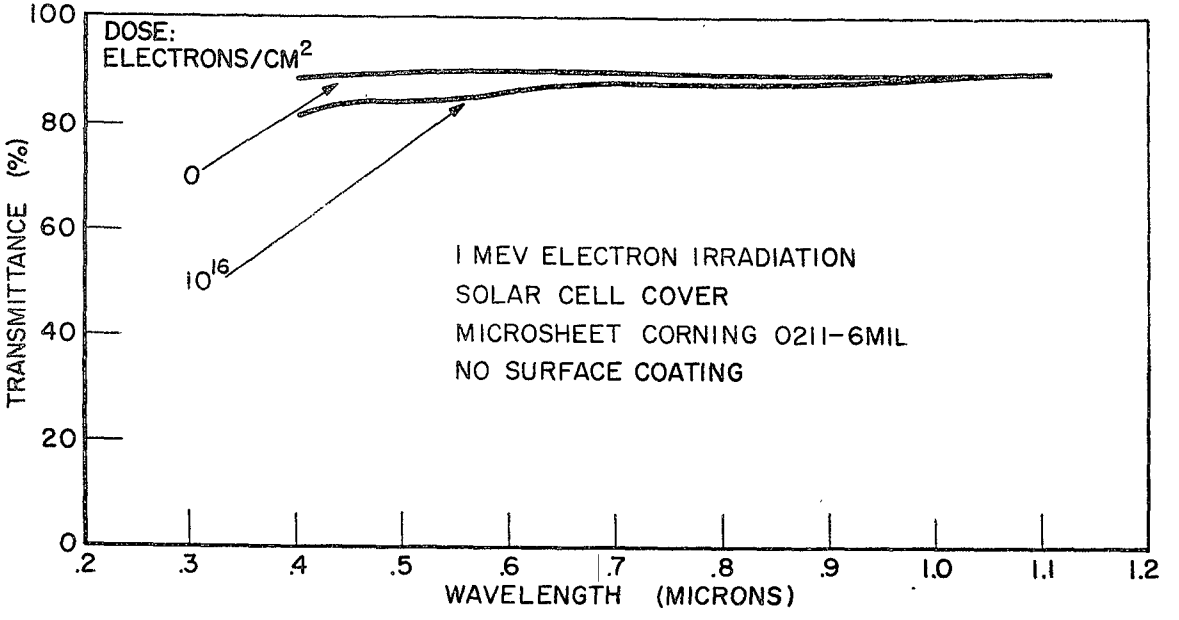
DOSE:
ELECTRONS/CM2
0
10^16
1 MEV ELECTRON IRRADIATION
SOLAR CELL COVER
MICROSHEET CORNING 0211-6MIL
NO SURFACE COATING
TRANSMITTANCE (%)
100
80
60
40
20
0
.2
.3
.4
.5
.6
.7
.8
.9
1.0
1.1
1.2
WAVELENGTH (MICRONS)

Figure 2

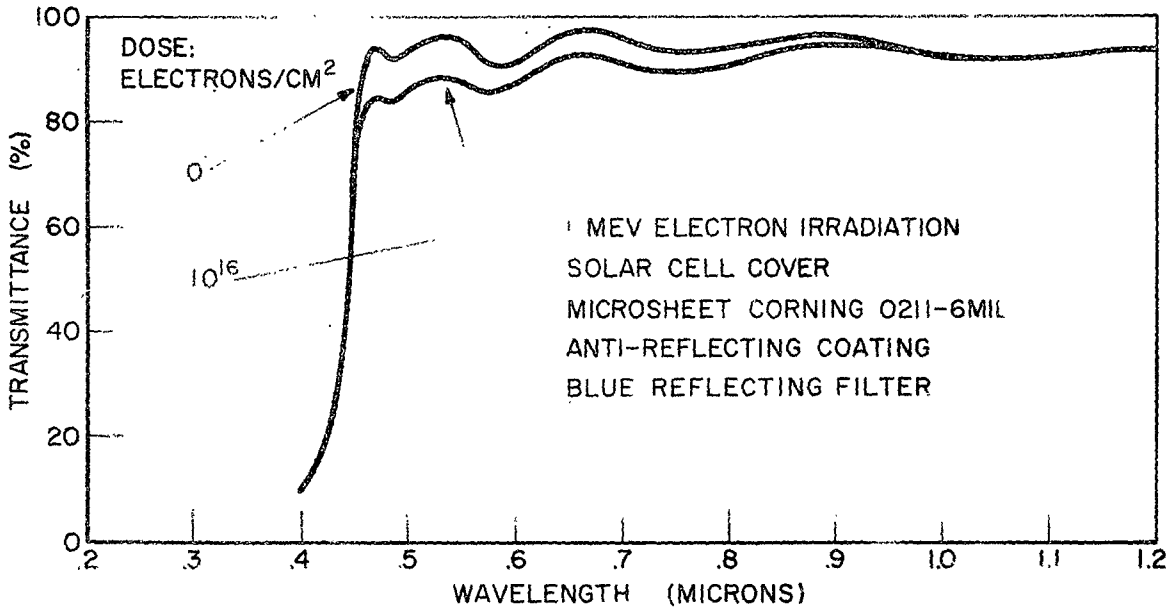

Figure

D-2.1-11

PIC-SOL 209/6.1

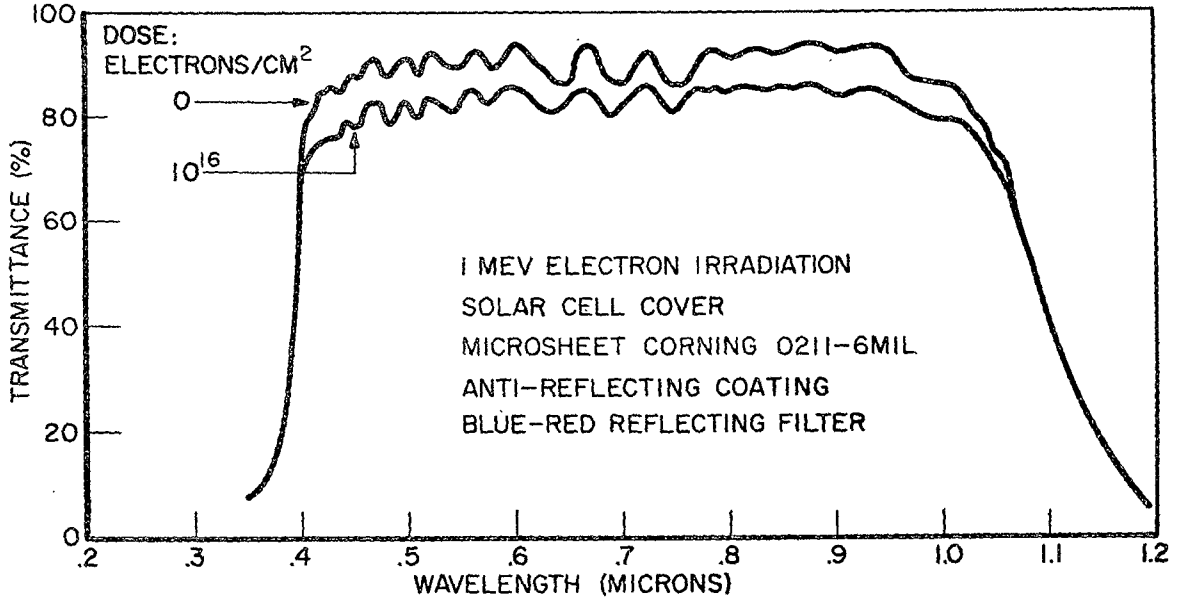
DOSE:
ELECTRONS/CM2
0
10^16
1 MEV ELECTRON IRRADIATION
SOLAR CELL COVER
MICROSHEET CORNING 0211-6MIL
ANTI-REFLECTING COATING
BLUE-RED REFLECTING FILTER
TRANSMITTANCE (%)
100
80
60
40
20
0
.2
.3
.4
.5
.6
.7
.8
.9
1.0
1.1
1.2
WAVELENGTH (MICRONS)

Figure 4

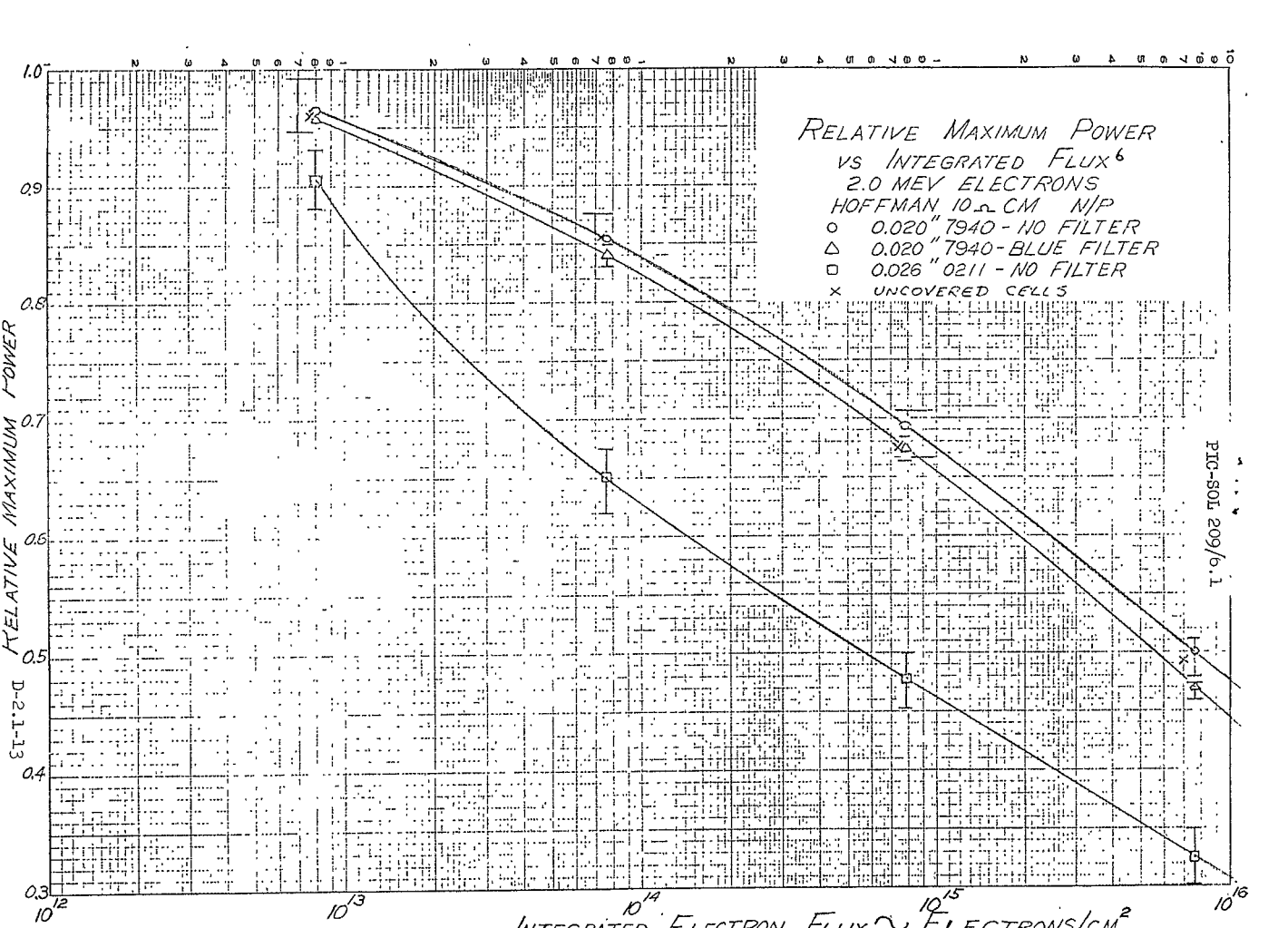
RELATIVE MAXIMUM POWER
VS INTEGRATED FLUX 6
2.0 MEV ELECTRONS
HOFFMAN 10Ω CM N/P
○ 0.020" 7940 - NO FILTER
△ 0.020" 7940 - BLUE FILTER
□ 0.026" 0211 - NO FILTER
× UNCOVERED CELLS
RELATIVE MAXIMUM POWER
INTEGRATED ELECTRON FLUX ~ ELECTRONS/CM²
1.0
0.9
0.8
0.7
0.6
0.5
0.4
0.3
10¹²
10¹³
10¹⁴
10¹⁵
10¹⁶
D-2-1-13
PIM-9801 209/6.1

Figure 5

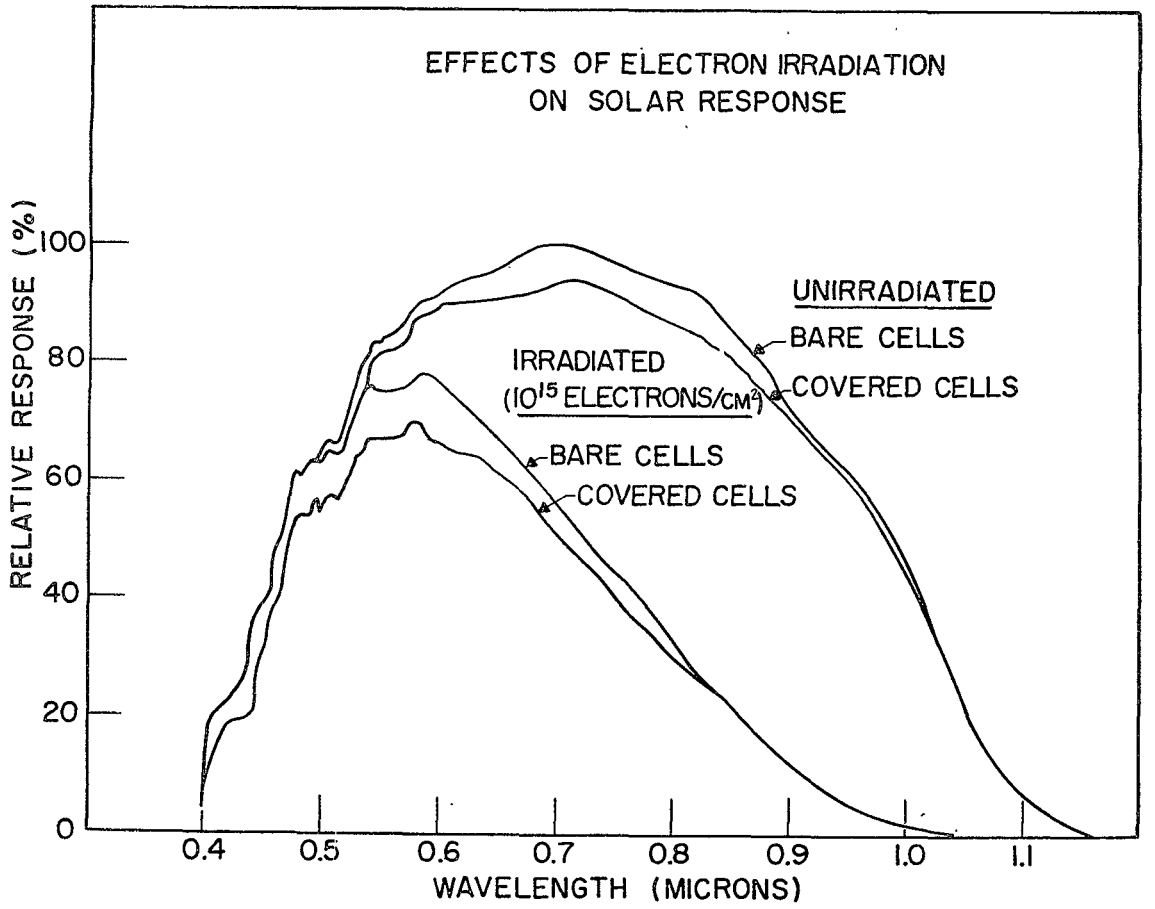
EFFECTS OF ELECTRON IRRADIATION
ON SOLAR RESPONSE
RELATIVE RESPONSE (%)
100
80
60
40
20
0
0.4
0.5
0.6
0.7
0.8
0.9
1.0
1.1
WAVELENGTH (MICRONS)
UNIRRADIATED
BARE CELLS
COVERED CELLS
IRRADIATED
(10^15 ELECTRONS/CM^2)
BARE CELLS
COVERED CELLS

Figure 6

PIC-SOL 209/6.1
Section D-3

PRELIMINARY RESULTS OF THE EXPLORER XXVI SOLAR CELL EXPERIMENT

Presented by

Luther W. Slifer, Jr.

NASA Goddard Space Flight Center

Greenbelt, Maryland

19 October 1965

Abstract N66 17336

To determine the integrated radiation effects on solar cells in an intense radiation orbit, an experiment consisting of four, 10-cell, series strings of N/P solar cells was mounted on one of the body facets of the Explorer XXVI spacecraft. Two strings were composed of 1 ohm-cm cells and two of 10 ohm-cm cells. One string of each base resistivity had a 6-mil glass shield and the other of each base resistivity had a 60-mil glass shield. A precision resistor across each string loaded it near the peak power point. The voltage drop across this load was measured and converted to current. The current was normalized on the basis of pre-launch calibrations for angle of incidence and comparisons were made. Preliminary results of this engineering experiment are presented. They show that, in this orbit, the 10 ohm-cm cells with a 6-mil shield provided significantly better radiation resistance than 1 ohm-cm cells with the same glass. When the heavy shield (60-mil glass) is used, the increased resistance is equally significant. The results also show that the use of the higher base resistivity cell provides a significant fraction of the radiation protection afforded by the heavy 60-mil cover glasses but at no cost in weight.

author

PRELIMINARY RESULTS OF THE EXPLORER XXVI SOLAR CELL EXPERIMENT

Luther W. Slifer, Jr.
and
Stephen G. McCarron
NASA-Goddard Space Flight Center
Greenbelt, Maryland

Introduction

In 1962, after the effects of the Starfish high-altitude nuclear explosion resulted in a review of the radiation resistance of solar cells, it was determined that conversion from P/N solar cells to N/P solar cells was required. Extensive radiation damage comparison tests were performed at the Naval Research Laboratory on N/P cells from various American manufacturers to determine the status and relative merits of their production capabilities[1,2]. In addition, these same cells were tested to obtain detailed information on their performance characteristics[3]. In May 1963 preparation of a follow-on to the SERB satellite was begun, presenting the opportunity to obtain flight information on cells from these same production lots. Authorization to fly such a solar cell experiment on a noninterference basis was requested and received.

The Experiment

Purpose

Results of prior testing of N/P solar cells had shown that, in laboratory experiments, cells with higher base resistivity exhibited a better radiation resistance than cells with lower base resistivity[1,2,4]. On the basis of these results most cell manufacturers were developing a capability for producing cells with higher base resistivities. The primary purpose of the solar cell experiment was to substantiate (or refute) the validity of the generalization of the results of monoenergetic electron and proton tests to the space radiation environment where an inhomogeneous flux is experienced. (A secondary purpose of the experiment was to provide a comparison of the performance of N/P solar cells to the P/N cells in the spacecraft power supply but will not be discussed here.)

Approach

In order to accomplish these objectives the experiment was designed as shown in Table I. Two rows of cells were provided for each of the two base resistivities - 1 ohm-cm and 10 ohm-cm. One row of each base resistivity type had a 6 mil coverglass and the other of each type had a 60 mil coverglass. In the space environment the 6 mil glasses would stop only the low energy protons (below 4.5 Mev) subjecting the cells to all

other radiation while the 60 mil glasses would stop protons with energies below 17 Mev and attenuate electron energies thus limiting damage to that produced by high energy particles. In this way it was intended that comparisons could be made of differences in radiation resistance to the two general categories of irradiation. (The use of the 60 mil shields also provided for comparisons with the spacecraft power supply which used 60 mil shields.)

Previously fixed mechanical and electrical interface requirements precluded optimization of the experiment. The number of cells used in series was limited (by the panel area) to ten, the choice of load resistors was restricted by the desire for a sizable signal in a 0-5 volt telemetry output range, and location of the experiment on one of the body facets made it sensitive to variations in both the aspect and the rotation of the satellite. The spinning satellite is shown in Figure 1.

As a result of the above restrictions, the precision load resistors, used across each cell string, were chosen so as to load the cells in the vicinity of the peak power point. In addition, some degree of matching of the initial space outputs for the various rows of cells was accomplished. A 100 ohm resistor was used for the 1 ohm-cm cells and a 90 ohm resistor was used for the 10 ohm-cm cells.

The temperature was monitored by the use of a calibrated thermistor imbedded in the panel. It was located near the geometrical center of the panel just below the aluminum skin on which the cells were mounted.

In order to assure a stable assembly of the solar cell experiment, radiation effects on various adhesives were studied and two pre-prototype panels were subjected to environmental tests(5). Results of these tests led to the choice of a flat-mounted cell assembly with silver expanded-metal interconnectors. RTV-40 (General Electric) was chosen to bond the cells to an aluminum skinned honeycomb substrate and Sylgard 182 (Dow Corning) was chosen as a coverglass adhesive. The completed solar cell experiment panel is shown in Figure 2.

Calibration and Data Reduction

Since the illumination of the solar cells is dependent upon both the angle of incidence and the solar constant, correction for these effects is necessary in the process of data reduction.

Satellite Rotation Effects

The effect of satellite rotation was eliminated with the aid of a computer program which sorted and reduced the data. By correlating data from the optical aspect sensor with telemetry rates and times it was possible to determine angle of rotation of the satellite for each solar cell experiment data point. Data considered here are for satellite rotation angles of $180^{\circ} \pm 20$ measured from the aspect sensor. This is

the rotational position at which the experiment panel faces the sun with variations from normal incidence being strictly sunline-spin axis angle variations.

Sunline-Spin Axis Angle Effects

The corrections for sunline-spin axis angle were accomplished using a pre-launch calibration of the experiment. This calibration was performed in sunlight on a clear (cloudless and haze-free to the naked eye) day using a collimator with a 10:1 length to aperture width ratio. The current variation with aspect angle was determined at a voltage of 50 mv/cell (or 500 mv for the 10-cell string) giving essentially the short circuit current variation. Deviations of the results from the cosine law are plotted in Figure 3 using the equation:

$$F(\psi) = \frac{I/I_{90}}{\text{Sin } \psi} \qquad (1)$$

where,

ψ is the sunline to spin axis (aspect) angle,
$F(\psi)$ is the aspect correction factor for this angle,
I is the current measured at this angle,

and

I_{90} is the current at normal incidence.

Note that, in this equation, sin ψ is used in applying the cosine law because the spin axis is perpendicular to the normal to the experiment. That is, the angle of incidence is $90^{o}-\psi$.

It can be seen in Figure 3 that deviations from the cosine law were significant, going as high as 7%, for the 60 mil shields but relatively insignificant, generally less than 1%, for the 6 mil shields in the aspect range from 45^{o} to 120^{o} which proved to be the range of interest. Comparison of these curves also shows quite clearly that the deviations are primarily dependent on the coverglasses.

Solar Constant Effects

The variation of the solar constant is a result of the ellipticity of the earth's orbit and therefore a function of the day of the year. The correction factor, f(D), for this variation is plotted in Figure 4(6).

Normalization of Current and Power

The above calibration and correction factors provided for normalization of the data to 140 mw/cm^2 insolance at normal incidence according to the equations:

$$I_N = \frac{I}{f(D)F(\psi)\sin\psi} \qquad (2)$$

and,

$$P_N = I_N V \qquad (3)$$

where,

I_N is the normalized current
P_N is the normalized power

and,

V is the voltage reading on the cell string.

I, V, and the precision load resistance, R, are interrelated by Ohm's Law.

Results

Spacecraft

Launch and orbit data for the Explorer XXVI spacecraft are listed in Table II. The results considered here are for the first 540 orbits covering a time period of 171 days - the conversion factor being 3.16 orbits/day.

Variation of the sunline-spin axis angle for this time period is shown in Figure 5(7). Both at the beginning and at the end of this time period there is some question as to the exact aspect angle. This results from the fact that the aspect sensor reads in discrete steps and the only accurately known points are those where the readout changes from one step to the next. Thus, when there is no change, the angle can be determined only to an accuracy within the width of the step. This is indicated by the blocks in the figure. The extrapolation for the early portion of the curve was inferred from the panel temperature and the solar array current profile measurements and that for the later portion is a best estimate including the consideration that the aspect angle is reversing direction.

This figure indicates that the aspect angle started at about 47° and held fairly constant for a period of roughly 16 days or 50 orbits at which time it began to change, increasing to 90° (normal incidence) at 98 days or 310 orbits. It continued to an extreme of approximately 117° at about 171 days or 540 orbits.

Solar Panel

The experiment panel temperatures are plotted in Figure 6. These are temperatures averaged on an orbit basis but excluding the eclipsed portion of the orbit. Several features in the temperature-time history require discussion. First, it can be seen in the figure that two orbits were

required for the panel to reach an equilibrium temperature after launch. This initial equilibrium temperature was then maintained essentially constant for the first 40 or 50 orbits indicating that the aspect angle was essentially constant. Secondly, because of the aspect variation, symmetry would ordinarily be expected about the 310 orbit (90° aspect) point. However, paddle shadowing during portions of the satellite rotation plus other more complex contributing factors destroy this symmetry. Finally, the total variation in panel temperature was from -9°C to 20°C indicating that effects of temperature variations on the solar cells would be secondary in nature.

Voltage readings for the various cell rows on the solar panel are shown in Figure 7. These data points each represent average voltage values for an orbit excluding the portion when the satellite was eclipsed. Because the solar cells were loaded in the vicinity of the peak power point, these voltages are important as indicators of cell operating conditions and must be considered in the analysis and interpretation of the final results.

The voltage data were reduced as previously described and the resulting normalized current and power data are plotted in Figures 8 and 9 respectively in terms of percent of initial normalized values. Apparent anomalies in the data result from the "wandering" operating voltage and will be discussed later. A degradation grid for 1 Mev electron bombardment of bare 1 ohm-cm cells[8] is also plotted in these figures for reference. It should be noted that the grids are not necessarily accurate at low flux or degradation levels because of general measurement difficulties.

Analysis and Discussion

The results depicted in Figures 8 and 9 appear confusing at first glance. Nevertheless, it is immediately clear that the 10 ohm-cm cells are significantly more radiation resistant than the 1 ohm-cm cells over the wide range of operating conditions experienced. Thus, the major objective of the experiment, that of determining whether laboratory test results showing 10 ohm-cm cells to be more radiation resistant than 1 ohm-cm cells could be generalized to space flight, was satisfied.

Closer analysis of the results (Figure 5 through 9) with reference to current-voltage curves as a function of radiation degradation[1] provides clarifying information. Operation for each of the cell strings is discussed qualitatively below in order to afford an understanding of the meaning and validity of the results shown in Figures 8 and 9. This is done in conjunction with the sketch in Figure 10 which depicts I-V curves for various cell conditions along with resistive load lines with differing relationships to the curves. This figure clearly illustrates that the current degradation ΔI is highly dependent on the operating point - the significant factor in the following discussion.

1 Ohm-cm Cells, 6 Mil Shields

Since the initial operating voltage for these cells was 399 mv/cell, a load similar to R_1 as related to curve (a) is indicated. During the first 40 orbits the voltage dropped to 345 mv/cell. Since the angle of incidence and the temperature both remained constant during this time, the voltage variation can be considered almost entirely the result of radiation degradation. That is, the I-V curve was shifting toward curve (b) and the voltage was decreasing along the R_1 load line. This voltage change is seen to be caused primarily by current degradation. It can thus be inferred that this degradation was less than, but not significantly different from, short circuit current degradation.

Following this the voltage continued to drop to 338 mv/cell at orbit 60 even though the aspect angle was beginning to improve. It then increased to 389 mv/cell at orbit 260. During this time the angle of incidence was decreasing at a rate such that variations with the cosine law were sufficient to overcome the effects of continued current degradation. Since the operation of the cells did not quite return to curve (a), it can still be inferred that operation is similar to the R_1 load - curve (a) relationship and that readings are still fairly representative of short circuit current readings. However, because of the increase in temperature (10°C for orbits between 160 and 260) as compared to the initial temperature and because of radiation degradation, both of which decrease the I-V curve voltages, operation was, in all probability, closer to the peak power point than it was initially. The degradation would thus be a little less representative of short circuit current degradation than it was initially.

After orbit 260 and until orbit 300, the voltage readings drop slightly in spite of the fact that the angle of incidence is approaching zero. This results from the fact that radiation degradation now exceeds, though very slightly, the small enhancements due to cosine law effects plus those due to the reduction in temperature. Operation is thus inferred to be practically unchanged relative to the I-V curve and therefore readings are still fairly representative of short circuit current readings.

In the final phase (beyond 300 orbits) the angle of incidence increases and the temperature decreases thus returning the I-V curve toward curve (b). With operation now in the R_1 load-curve (b) relationship, the readings again become more accurately representative of true short circuit current readings.

The results in Figures 8 and 9 are consistent with the above discussion. The degradation is relatively smooth and differs little from a nominal equivalent damage curve when plotted as short circuit current degradation but it varies considerably when plotted as a peak power degradation. The former is true because power readings on the short circuit current side of the peak power point vary linearly with voltage.

10 Ohm-cm Cells, 6 Mil Shields

The initial operating voltage for these cells was 392 mv/cell - just slightly lower than that for the 1 ohm-cm cells. However, because of the higher base resistivity, operation is shifted a little toward the peak power point as compared to the 1 ohm-cm cells. As a result the load is similar to R_4 as related to curve (a) and readings portray the initial short circuit current degradation a little less accurately as the I-V curve degrades toward curve (b) during the first 60 orbits.

Because of decreased radiation damage (compared to the 1 ohm-cm cells), the increase in operating voltage after orbit 60 continued until orbit 300 where nearly normal incidence was attained. At this time the voltage was 396 mv/cell which approaches the peak power point for the degraded cells. As a result operation is similar to R_4 as compared to curve (d). The current degradation is excessive compared to short circuit current degradation because of the drop-off in going from the short circuit current side of the knee of the I-V curve toward the peak power point.

After 300 orbits the operating point slides back up the knee as the angle of incidence increases and as degradation continues because both of these effects cause the I-V curve to collapse with the current changing much more rapidly than the voltage.

The above considerations indicate that the current degradation in the early portions (for the first 60 or more orbits) and for the later portions (around 500 orbits) of the time period studied is fairly representative of short circuit current degradation but in the proximity of 300 orbits the degradation is more representative of peak power degradation. In Figure 8 it is seen that degradations early and late in the time period studied are mutually consistent but between orbits 100 and 500 the degradation is excessive, reaching a maximum at 300 orbits. Simultaneously, Figure 9 shows the power degradation rate between 200 and 400 orbits to be fairly steady. The degradation is thus consistent with the analysis.

1 Ohm-cm Cells, 60 Mil Shields

Since these cells were initially at a voltage of 428 mv/cell, operation is typified by R_2 and curve (a). That is, the load is quite close to the peak power point. Because of the slow degradation the voltage only dropped to 411 mv/cell before increasing with decreased angle of incidence to 447 mv/cell at normal incidence. The final voltage, at orbit 540, was again reduced to 413 mv/cell. Thus operation throughout the time period was in the vicinity of the peak power point and current variations are generally significantly different from short circuit current variations which are approached only at the lowest voltages - around orbits 60 and 540. On the other hand, with operation near the peak power point where power does not change significantly with voltage, the readings are fairly valid when used in terms of power. This is readily observed in Figures 8 and 9.

10 Ohm-cm Cells, 60 Mil Shields

Operation of this cell string was very similar to the 1 ohm-cm cell string with 60 mil shields and the above discussion applies here also.

Constant Voltage Operation

In addition to the study of the results in terms of short circuit current and peak power degradation, it is possible, because of the variations encountered, to study the current degradation at constant voltage. This parameter is important whenever a shunt regulated solar array is employed.

The 1 ohm-cm cells with 6 mil shields started operating at a voltage of 399 mv/cell. Operation never returned to this voltage but the nearest approach occurred at the 260th orbit when the voltage was 389 mv/cell. At this time the current, and hence the power (to within 3%), had degraded 28%. The 10 ohm-cm cells with the same glass returned to their initial voltage of 392 mv/cell at orbit 219 when the degradation was 23% and again at orbit 340 when the degradation was 26%. Thus, at a constant voltage of approximately 400 mv/cell, the 10 ohm-cm cells degraded less in 340 orbits than the 1 ohm-cm cells in 260 orbits - a time factor of more than 1.3.

Similarly, the 1 ohm-cm cells with 60 mil shields started at 428 mv/cell and returned to this voltage at orbit 140 and orbit 440 with degradations of 11% and 16% respectively. The 10 ohm-cm cells with the same glass started at 419 mv/cell and returned to this voltage at orbit 100 and orbit 500 with degradations of 4% and 11% respectively. Thus, for operation near 425 mv/cell, the 1 ohm-cm cells degraded 11% in 140 orbits and the 10 ohm-cm cells degraded this same amount in 540 orbits - a time factor of 3.86.

Selected Orbits

Degradation results for selected orbits are given in Table III for general comparison purposes. The orbits were selected as follows:

a. Orbits 1-40 because aspect angle and temperature are constant.

b. Orbit 100 because voltages for the 6 mil glass strings had returned approximately to the 40 orbit value and those for the 60 mil strings had returned approximately to the initial value.

c. Orbit 300 because normal incidence is approached and the voltages are near the maximum experienced.

d. Orbit 500 because voltages had returned to a low value and were similar to those experienced in one or another of the previously selected orbits.

e. Orbit 180 because the angle of incidence was the same as in orbit 500.

In addition to providing a ready comparison of degradation data, this Table also points up the significant factors in the preceding discussion.

Correlation With Laboratory Measurements

Correlation of the flight data with laboratory measurements is incomplete at this time. The primary reason for this is that space radiation spectra obtained for this orbit consisted of a detailed breakdown of the electron spectrum and a two-part breakdown of the proton spectrum. This turned out to be inadequate when it was found that as much as 99% of the damage to the cells with 6 mil shields and as much as 60% of the damage to cells with 60 mil shields was the result of proton bombardment. It appears possible to obtain the proton spectrum in sufficient detail to afford a correlation of the data, however, it is not readily available because of complications arising from the ellipticity of the orbit. It is hoped that these data will be available for inclusion in a final report at a later date. The above information is presented to indicate the importance of proton damage and the need for emphasis by design engineers for proton spectrum considerations equal to those given (because of Starfish) to the electron spectrum.

Equivalent Flux

Nominal 1 ohm-cm, bare cell equivalent flux values obtained from Figures 8 and 9 are given in Table IV. In determining these values a nominal flux was obtained for those data in Figure 8 where the current was considered representative of short circuit current and another nominal flux was obtained for those data in Figure 9 which are considered most representative of peak power data. These are presented in separate columns and differences in the equivalent flux, ranging from a factor of 1.3 for the 10 ohm-cm cells with 6 mil shields to 2.5 for the 10 ohm-cm cells with 60 mil shields, are readily apparent. This appears excessive at first. After considering the fact that a factor of 2 in flux represents a difference of only 5% in degradation at the end of the time period studied and after considering the generalities required in arriving at a nominal equivalent flux, the disparity loses significance. It is believed that the primary reason for the values based on power being consistently 1 less than the values based on current is that the orbit 1 power value was low because initial operation was at a voltage below the peak power voltage in every case. Thus, the initial power was lower than the peak value and degradation when peak power is read will also be low.

In spite of the problems in the analysis of the data, the relative effectiveness of base resistivity and coverglass thickness remains clear. That is, the change in base resistivity from 1 ohm-cm to 10 ohm-cm provided a factor of 2 to 3 in radiation resistance whether 6 mil or 60 mil coverglasses were used and the change from 6 mil to 60 mil coverglass thickness provided a factor of 8 to 15 in radiation resistance whether

1 ohm-cm or 10 ohm-cm cells were used. It is evident that the use of higher base resistivity affords a significant fraction of the protection obtained with the heavy coverglass.

Conclusions and Recommendations

The preliminary results of the Explorer XXVI solar cell experiment led to the following conclusions and recommendations:

1. In orbital flight and under a wide variety of operating conditions, 10 ohm-cm N/P solar cells show significantly better radiation resistance than 1 ohm-cm N/P solar cells. The generalization of laboratory results which showed the same relationships for monoenergetic radiation was confirmed.

2. In this orbit the relative merits of the 10 ohm-cm cells and the 1 ohm-cm cells remained the same whether 6 mil or 60 mil shields were used. That is, energy dependent differences in relative radiation damage were not distinguishable.

3. The use of 10 ohm-cm cells compared to 1 ohm-cm cells provides an improvement in radiation resistance which is a significant fraction of the improvement obtained by using a 60 mil shield as compared to a 6 mil shield. It is therefore recommended that the use of higher base resistivity cells be given increased consideration by solar power system design engineers.

4. Attempts to quantitatively correlate orbital and laboratory measurements were unsuccessful because insufficient emphasis had been placed on the proton spectrum. The spectrum can be obtained and is mandatory for this orbit. Because of its significance in this orbit it is recommended that solar power systems design engineers give the proton spectrum emphasis equal to that given the electron spectrum for all orbits.

Acknowledgments

The authors wish to acknowledge the fact that this work was the result of a cooperative effort by the entire Solar Power Sources Section at GSFC. Specifically the work of B. T. Barbour in fabricating the panels, Nicolas Mejia in the calibration, test, and evaluation of the panels, Joseph Haynos in the study of materials, Ralph Sullivan in the solution of interface problems and the procurement of parts, and Brian Cunningham in providing helpful consultation is acknowledged. In addition, extensive assistance in the reduction of data provided by many persons under the direction of the Data Systems Division, GSFC is most gratefully acknowledged.

References

1. R. L. Statler, "Electron-Bombardment Damage in Silicon Solar Cells", NRL Report 6091, October 1964.

2. W. R. Cherry and L. W. Slifer, "Solar Cell Radiation Damage Studies with 1 Mev Electrons and 4.6 Mev Protons", NASA TN D-2098, February 1964.

3. B. T. Cunningham, R. L. Sharp, and L. W. Slifer, "The Electrical Characteristics of Irradiated Silicon Solar Cells as a Function of Temperature", Proceedings of the Fourth Photovoltaic Specialists Conference, June 1964.

4. J. Mandelkorn et al., "Behavior of Modified Radiation-Resistant Solar Cells", Proceedings of the 15th Annual Power Sources Conference, May 1961.

5. J. G. Haynos, "Investigation of Resinous Materials for Use as Solar Cell Cover Glass Adhesives", GSFC Report X-716-65-369, September 1965.

6. R. E. Fischell, "Solar Cell Experiments on the Transit and TRAAC Satellites", Proceedings of the Solar Working Group Conference, February 1962.

7. H. Meyerson, "Some Preliminary Engineering Data From the Explorer XXVI (EPE-D) Satellite", Project Office Memorandum to Experimenters, 30 July 1965.

8. F. M. Smits, W. Rosenzweig, and W. L. Brown, "Report of Solar Cell Work at Bell Telephone Laboratories", Proceedings of the Solar Working Group Conference, February 1962.

Table I

SOLAR CELL EXPERIMENT

Cell Strings		Solar Cells				Cover Glasses		
Row No.	Symbol (See Fig.)	No. in Series	Type	Mfg (Ref 1,2)	Nom Base Resistivity (ohm-cm)	Type (Corning)	Thick-ness (mil)	Load Resistor (ohms)
1	⊙	10	N/P	C	1	0211	6	100
2	●	10	N/P	C	1	7940	60	100
3	■	10	N/P	F	10	7940	60	90
4	⊡	10	N/P	F	10	0211	6	90

Table II

LAUNCH AND ORBIT PARAMETERS

FOR

EXPLORER XXVI

Launch Date	12/21/64
Perigee	309 km
Apogee	26,200 km
Inclination	20 degrees
Period	7.6 hours

Table III

DEGRADATION RESULTS FOR SELECTED ORBITS

Orbit No.	Aspect Angle (deg)	Temperature (°C)	Base Resistivity (ohm-cm)	6 Mil Glass			60 Mil Glass		
				Cell Voltage (mv)	Current Degradation (%)	Power Degradation (%)	Cell Voltage (mv)	Current Degradation (%)	Power Degradation (%)
1-40	46.7 (const)	9.8 (const)	1	399-345	13.6	25.3	428-413	3.6	7.0
			10	392-354	10.1	18.6	419-408	2.9	5.4
100	50.1	12.5	1	348	17.6	28.1	419	6.6	8.6
			10	359	13.7	20.8	419	4.1	4.1
180	63.2	19.2	1	377	23.5	27.7	437	13.7	11.9
			10	385	20.1	21.3	439	10.7	6.4
300	88.2	17.0	1	387	29.2	31.3	446	18.1	14.7
			10	396	25.6	24.6	449	14.1	8.0
500	116.8	13.5	1	321	32.9	46.0	418	14.4	16.4
			10	356	22.9	29.8	423	9.6	8.8

Table IV

NOMINAL EQUIVALENT FLUX VALUES FOR THE VARIOUS CELL CONDITIONS

Nominal Base Resistivity (ohm-cm)	Shield Thickness (mils)	Equivalent Flux ($e/cm^2/orbit$)		Flux Ratio	
		Based on Current	Based on Power	Based on Current	Based on Power
1	6	1×10^{13}	6×10^{12}	2.5	2
10	6	4×10^{12}	3×10^{12}		
1	60	1×10^{12}	6×10^{11}	4	5
10	60	5×10^{11}	2×10^{11}	2	3

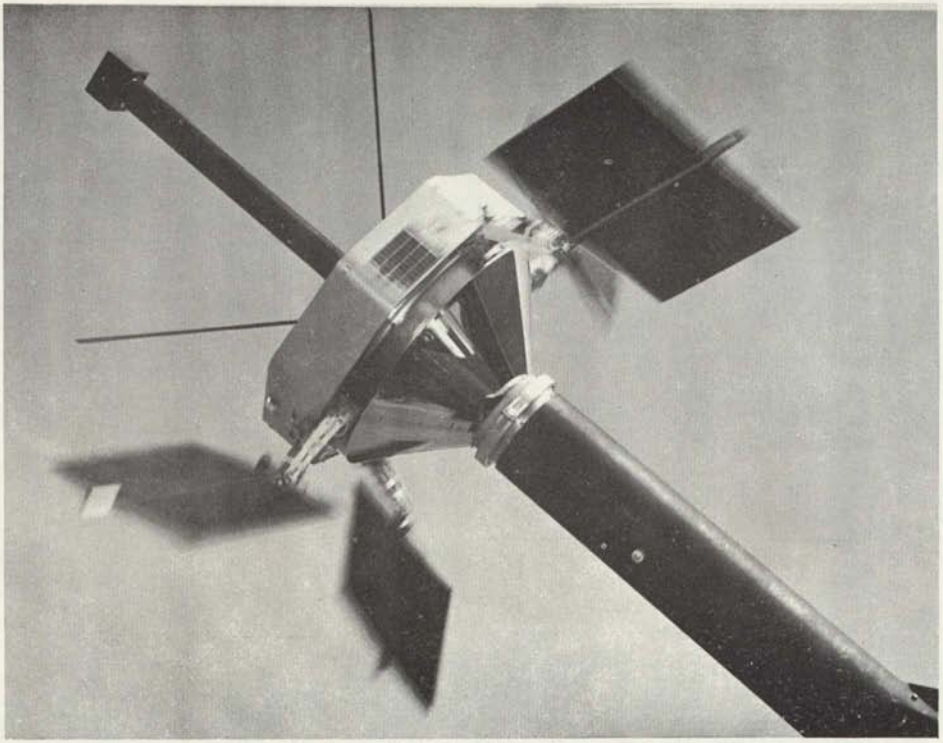

Figure 1 - The Explorer XXVI Satellite During Spin Tests

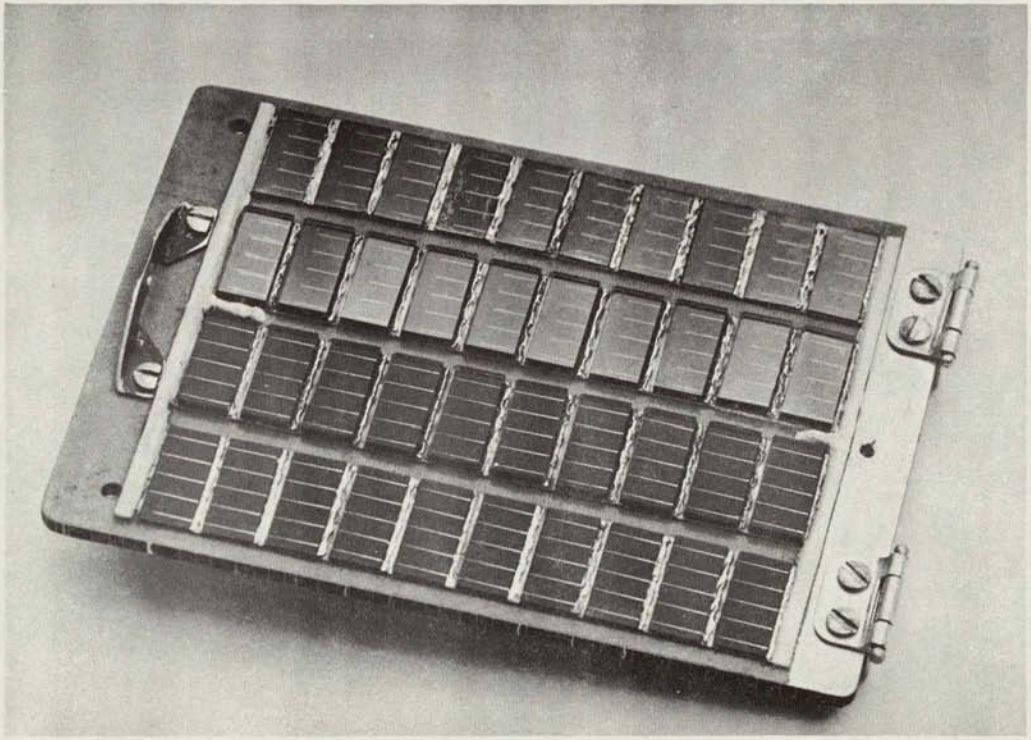

Figure 2 - The Explorer XXVI Solar Cell Experiment Panel

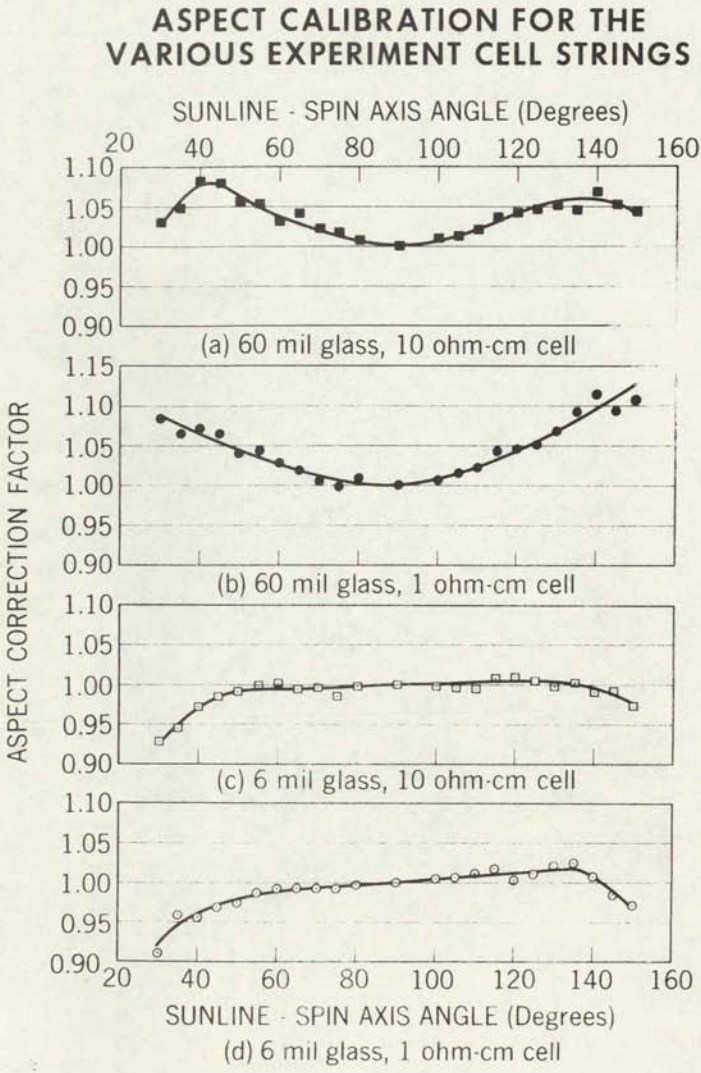

Figure 3-Aspect Calibration for the Various Experiment Cell Strings

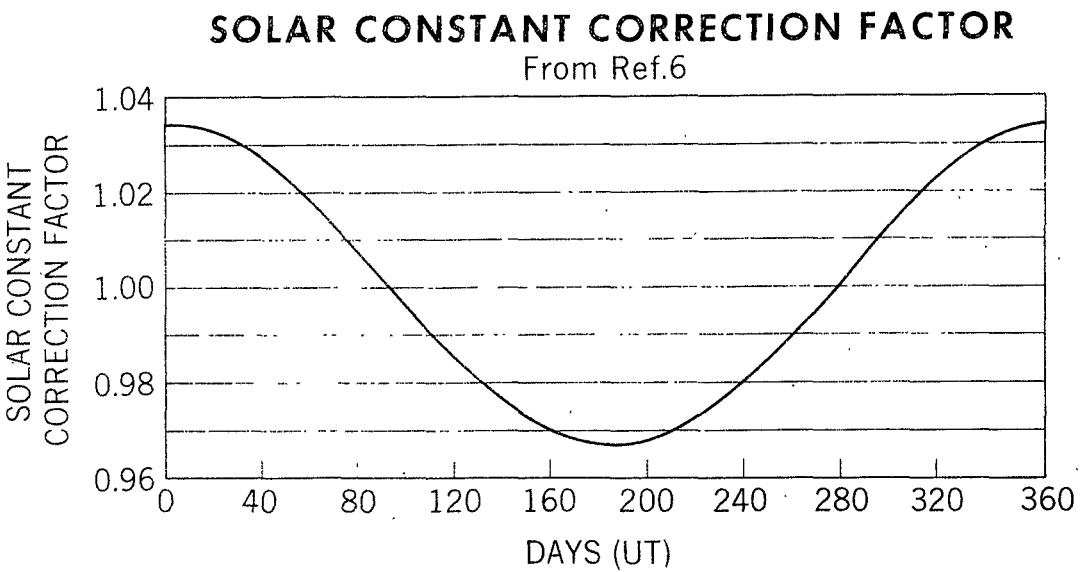

Figure 4–Solar Constant Correction Factor

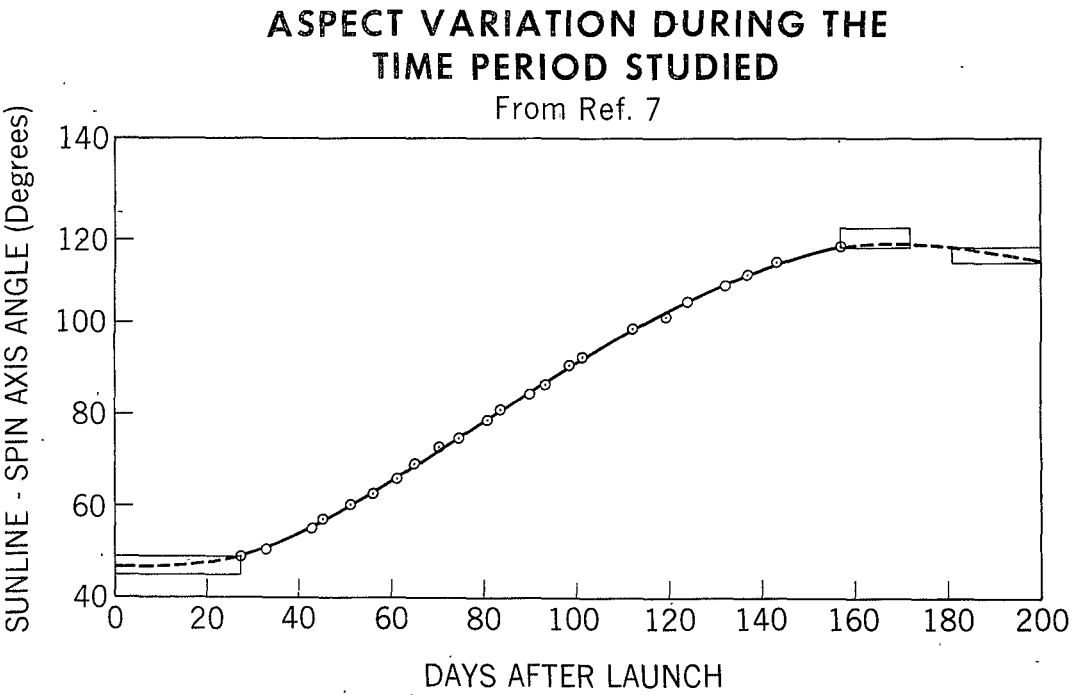

Figure 5–Aspect Variation During the Time Period Studied

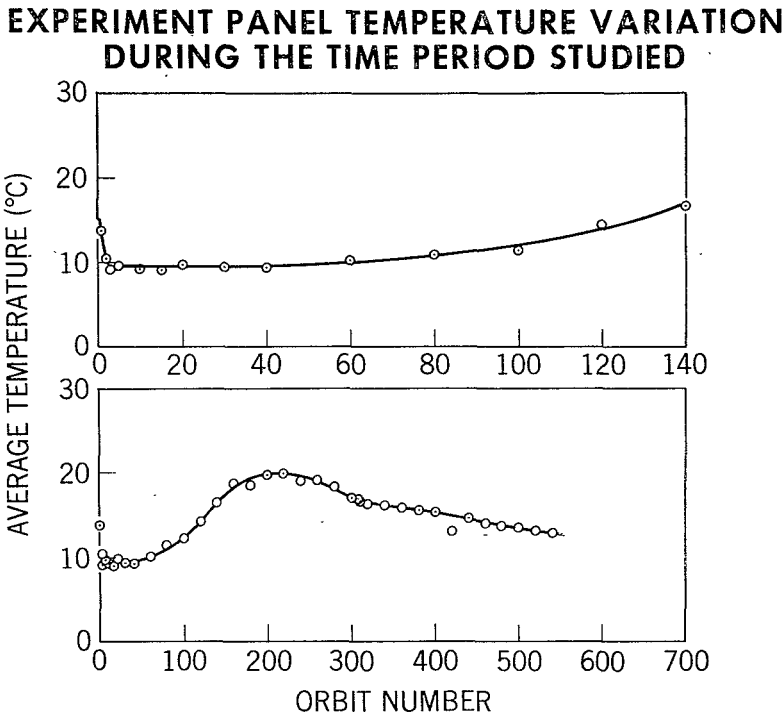

Figure 6–Experiment Panel Temperature Variation During the Time Period Studied

SOLAR CELL VOLTAGE VARIATION DURING THE TIME PERIOD STUDIED

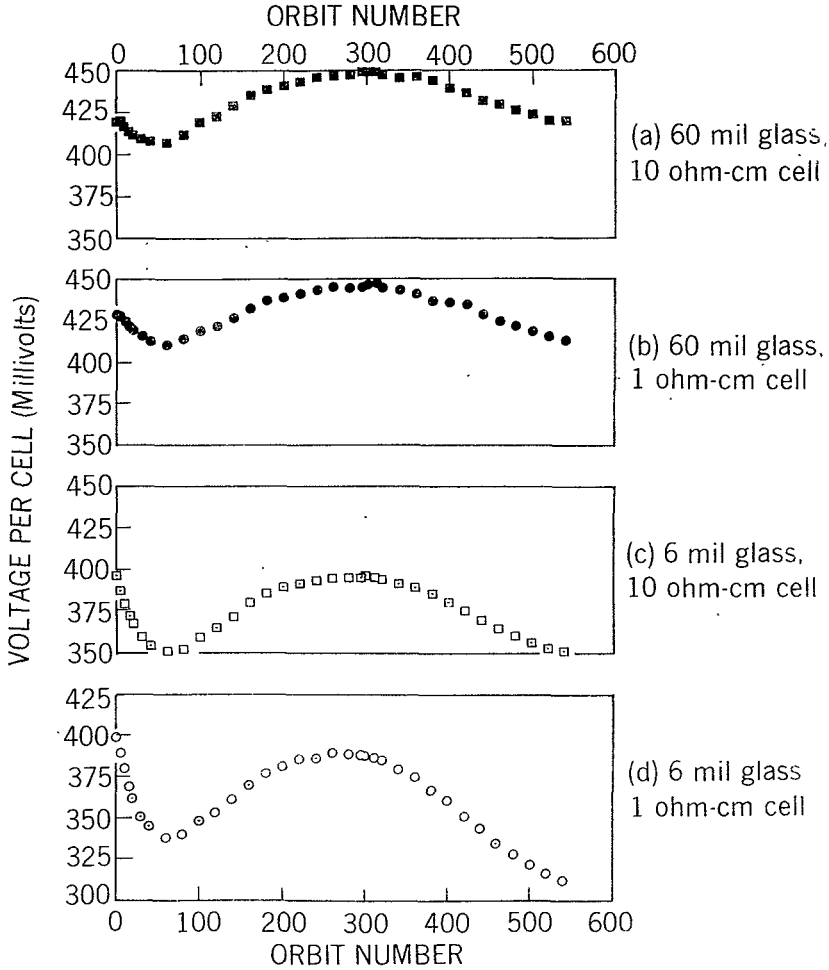

Figure 7–Solar Cell Voltage Variation During the Time Period Studied

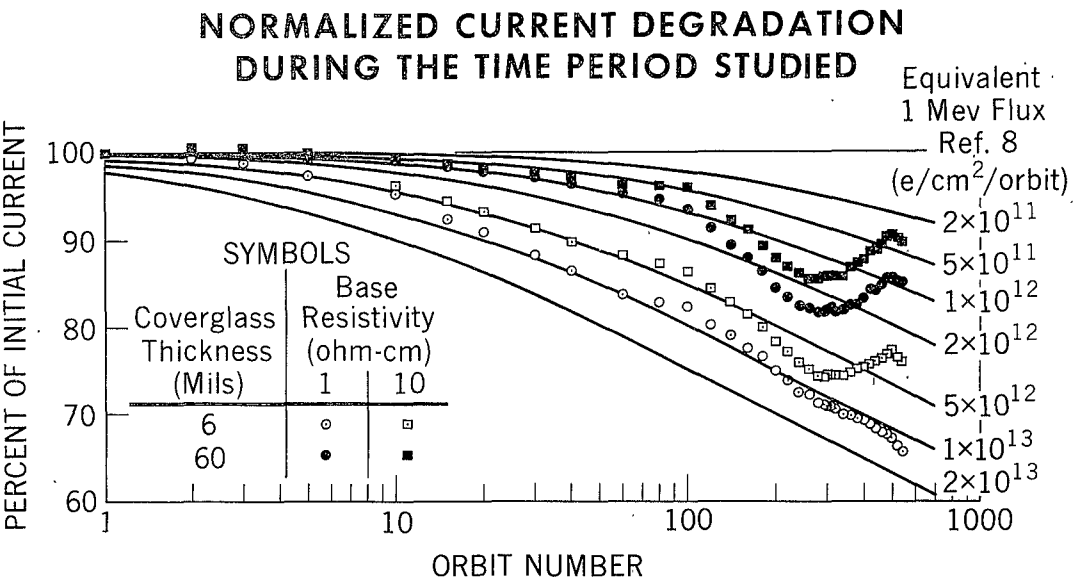

Figure 8–Normalized Current Degradation During the Time Period Studied

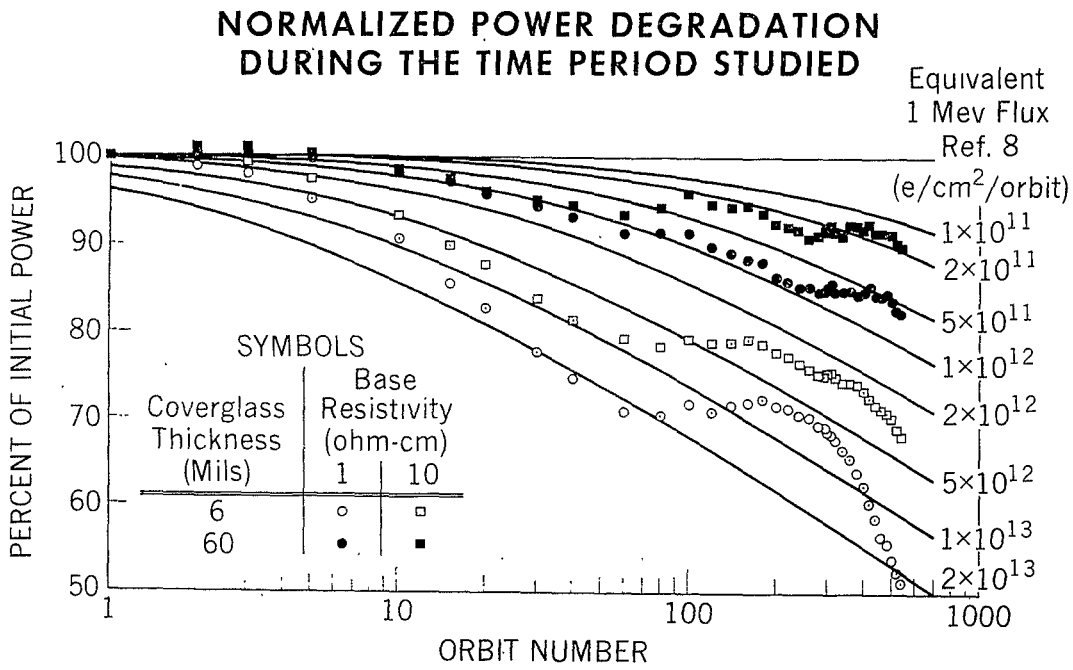

Figure 9–Normalized Power Degradation During the Time Period Studied

SKETCH DEPICTING THE EFFECT OF THE LOAD POINT ON THE DEGRADATION READINGS

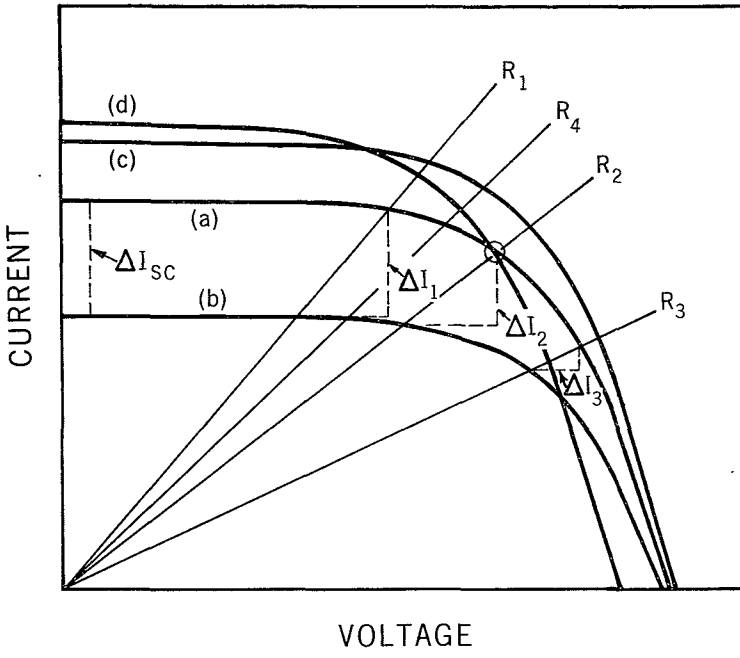

Figure 10–Sketch Depicting the Effect of the Load Point on the Degradation Readings

PIC-SOL 209/6.1
Section D-4

IN-ORBIT RESULTS ON RADIATION DAMAGE TO SOLAR CELLS*

Presented by

R. E. Fischell

Johns Hopkins University - Applied Physics Laboratory

Silver Spring, Md.

19 October 1965

*This paper was not available at the date of publication of these proceedings

PIC-SOL 209/6.1
Section D-5

BEHAVIOR OF BOMBARDED SOLAR CELLS MADE FROM VARIOUS SILICON MATERIALS

Presented by

A. E. Potter

NASA-Lewis Research Center

Cleveland, Ohio

19 October 1965

BEHAVIOR OF BOMBARDED SOLAR CELLS MADE FROM VARIOUS SILICON MATERIALS

by J. Mandelkorn, J. H. Lamneck, and R. P. Ulman
Lewis Research Center
National Aeronautics and Space Administration
Cleveland, Ohio 44135

At the Fourth Photovoltaic Specialists Conference, June 1964, it was reported that aluminum-doped silicon solar cells had superior characteristics and radiation damage resistance.

Since then, two laboratories engaged in solar cell radiation damage studies have concluded that there are no differences between aluminum-doped and boron-doped cells.[2,3] Their conclusion was based primarily upon the radiation damage behavior of aluminum-doped cells manufactured by Texas Instruments.

Figure 1 shows data obtained at the NASA Lewis Research Center on Texas Instruments 10 ohm-cm boron-doped and aluminum-doped cells. The cells were made from Lopex silicon which is high-purity, low-oxygen-content, extremely low dislocation density silicon. Resistivity of cell materials and fabrication processes were identical for all cells. The cells were bombarded in groups of 16 cells, each group being bombarded to one specific dose at room temperature. As shown in Figure 1, there are no differences in values of postbombardment diffusion lengths for these aluminum-doped and boron-doped cells.

Figure 2 shows the values of diffusion length for the cells previously described after annealing. Annealing was carried out by placing the cells in a constant temperature oven at a temperature of 200°C. The cells were removed from the oven periodically to make diffusion length measurements. The values of diffusion length shown for each group on the slide are the stabilized values which occur after 1 or 2 weeks of annealing. The stabilized values of diffusion length for the boron-doped cells are well below those of the aluminum-doped cells. This occurred as follows:

1. The values of diffusion length of the bombarded aluminum cells increased slightly upon annealing.

2. The values of diffusion length of the boron cells decreased drastically upon similar annealing.

The degradation of the annealed boron-doped cells is presented quantitatively in Figure 3. The upper points show the diffusion lengths preserved in the bombarded boron cells prior to annealing. The lower points show the diffusion lengths of the same cells after annealing. As can be seen the decrease in diffusion length resulting from annealing is equivalent to the decrease which would have occurred if each group had been bombarded to approximately three times its actual dose.

The recombination centers formed by annealing the boron cells are therefore much more damaging than the original centers introduced by the bombardment. The type of behavior manifested by the boron cells is called reverse annealing. Reverse annealing is behavior in which damage increases as a result of annealing.

Figure 4 shows reverse annealing of various resistivity boron-doped cells as a function of time at 200°C. The rate of reverse annealing is slowest in the cells with lowest boron concentration, 50 ohm-cm cells, and most rapid in the cells with highest boron concentration, 1 ohm-cm cells. The flat portions of the curves yield the stabilized or saturated values of diffusion length.

Appreciable reverse annealing can occur in boron cells at temperatures as low as 100°C. As shown in Figure 5, reverse annealing occurs rapidly at 100°C for 0.5 and 1.0 ohm-cm cells made from Lopex material. These cells reverse anneal at 50°C at a slower rate. This result conforms with the concepts that radiation-introduced defects are mobile at low temperatures and that boron atoms form stable recombination centers with such defects. The presence of dislocations and other impurities, such as oxygen, influences the movement of defects and their association with boron. Reverse annealing is therefore most obvious in Lopex silicon.

In our experiments cells were made from the best quality boron-doped silicon as well as from mediocre quality material. Cells were made from the highest quality silicon to which only the highest purity boron was added. Cells were made from thick epitaxially deposited boron-doped silicon. High dislocation density float-zone silicon as well as low dislocation density Lopex silicon were used to make cells. The concentration of boron in the cell materials was varied over an order of magnitude. Cells made from any of the boron-doped materials cited showed reverse annealing after bombardment; however, cells made from aluminum-doped silicon, grown in any manner and of any resistivity, have not manifested reverse annealing. The reverse annealing of boron-doped high-purity silicon cells is attributed to extremely damaging recombination centers formed by boron atoms interacting with defects in silicon. Boron is therefore an undesirable dopant for silicon.

The substitution of aluminum as a dopant in silicon has been investigated in detail during the past year. The use of aluminum presents several technological problems. Foremost is the problem of undesirable concentrations of iron and copper in the highest purity aluminum available today. Iron and copper, being "killer" impurities in silicon can degrade the minority carrier lifetime of silicon ingots to the point that the material is useless for devices.

Figure 6 compares the iron and copper contents of the highest available purity boron and aluminum. To the chemist, the iron and copper content of either dopant appears negligible; however, high quality silicon ingots are badly degraded by the addition of small amounts of boron or aluminum in their most pure elemental form. It is industrial practice to use a zone-refined boron-silicon alloy as a means of doping silicon. Aluminum cannot be adapted to such practice because of its low segregation coefficient in silicon. At present the best aluminum-doped silicon is made by Texas Instruments using their Lopex growth method; however, even Lopex aluminum-doped silicon contains undesirable amounts of copper and iron.

Figure 7 presents bombardment data for 0.5 and 1.0 ohm-cm aluminum-doped and boron-doped Lopex cells. The figure shows that the boron cells preserve appreciably longer diffusion lengths than those preserved by the aluminum cells at any bombardment dose. In fact, the diffusion length of the boron 1 ohm-cm cells at a dose of $5X10^{15}$ e/cm^2 is nearly the same as that for the aluminum 1.0 ohm-cm cells at a dose of only $1.5X10^{15}$ e/cm^2. It would be naive, however, to conclude from data of the type shown that boron-doped silicon is superior to aluminum-doped silicon. The lower diffusion lengths of the aluminum-doped cells result from iron and copper in the silicon.

Figure 8 shows the effects of iron and copper in the silicon of solar cells. The top curve shows postbombardment and postannealing diffusion lengths for cells doped with high-purity aluminum. The lower curve shows equivalent data for cells doped with comparatively impure aluminum. The impure aluminum cells obviously contain excessive quantities of iron and copper. It is noteworthy that the impure aluminum cells have appreciably lower diffusion lengths after bombardment. They also undergo a very large increase in diffusion length upon annealing at temperatures below 200°C.

The reactions shown in Figure 9 explain the behavior of the impure-aluminum-doped cells. The fact is emphasized once more that bombardment-introduced defects are mobile in silicon at low temperatures. Reactions 1 and 2 show such defects interacting with copper and iron to create recombination centers. The excessive copper and iron in the impure-aluminum-doped cells thus cause the lower values of postbombardment diffusion length of such cells. As reactions 1 and 2 indicate, copper and iron centers are not stable at temperatures above 25°C. The large degree of annealing which occurred below 200°C in the impure-aluminum-doped cells resulted from disintegration of the copper and iron centers at the annealing temperatures. The effects of excessive iron and copper are therefore lower diffusion lengths after bombardment and large increases in diffusion length upon annealing at temperatures below 200°C.

If we examine the bombardment and annealing behavior of low resistivity 1.0 ohm-cm Lopex aluminum cells, the effects described above are found. Figure 10 shows that the postbombardment diffusion lengths of the aluminum cells are lower than those of boron cells and that appreciable increases occur in aluminum cell diffusion lengths for 100°C annealing. The diffusion lengths increase further at 200°C. This contrasts with the behavior of boron-doped cells which show decreases after annealing at either 100° or 200°C. The annealing behavior of the 0.5 ohm Lopex aluminum cells follows the pattern of the 1 ohm cells (Fig.11).

The behavior of the low resistivity Lopex aluminum cells has been shown to be similar to that of the impure aluminum 10 ohm-cm cells. It is reasonable to conclude that such behavior results from the presence of copper and iron and is not caused by the presence of aluminum. Although pure aluminum was used to dope the silicon used in the low resistivity cells, the greater quantity of aluminum required to make low resistivity silicon introduces excessive amounts of iron and copper. The iron and copper then determine the radiation damage and annealing behavior of the cells.

In conclusion, boron is an undesirable dopant for silicon from the point of view of radiation damage and lattice interactions.[4] At present 10 ohm-cm Lopex aluminum-doped silicon, made by using high-purity aluminum, is a recommended alternative to 10 ohm-cm boron-doped silicon.

The extensive use of lower resistivity aluminum-doped silicon must, however, await preparation of higher purity aluminum than that presently available.

References

1. Mandelkorn, Joseph; Schwartz, Lawrence; Ulman, Robert; Broder, Jacob; Kautz, Harold; and Statler, R.: Effects of Impurities on Radiation Damage of Silicon Solar Cells. Proc. of 4th Photovoltaic Specialists Conference, June 1964.

2. Alemeleh, N.; Goldstein, B.; Szsochi, J. J.: Radiation Damage in Silicon. Final Rept., Dec. 1964, Contract NAS 5-3788, RCA Labs., Princeton, N. J.

3. Carter, J. R.; and Downing, R. G.: Charged Particle Radiation Damage in Semiconductors XI. Effects of Low Energy Protons and High Energy Electrons on Silicon. Final Rept. May 5, 1964-May 4, 1965, Contract NAS 5-3805, TRW Space Tech. Labs.

4. Mandelkorn, Joseph; Schwartz, Lawrence; Broder, Jacob; Kautz, Harold; and Ulman, Robert: Effects of Impurities on Radiation Damage of Silicon Solar Cells. J. Appl. Phys., 35, July 1964, 2258-2260.

COMPARISON OF T.I. LOPEX 10 OHM-CM CELLS

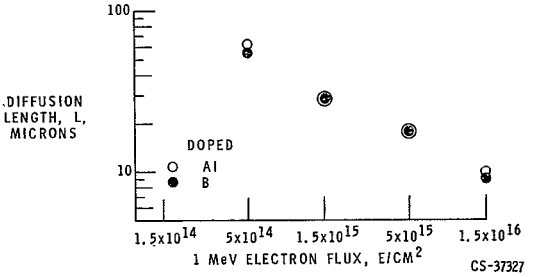

Figure 1.

T.I. LOPEX 10 OHM-CM CELLS POST ANNEALING

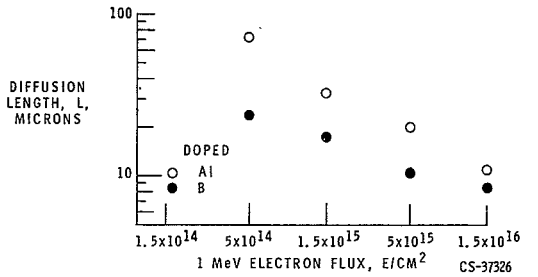

Figure 2.

EFFECT OF ANNEALING

BORON DOPED HIGH PURITY SILICON CELLS

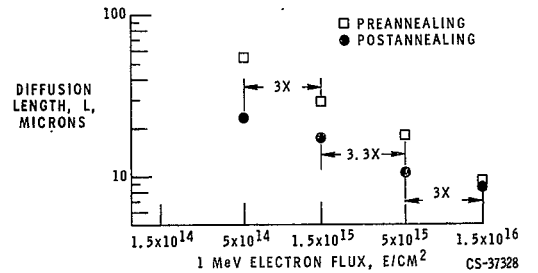

Figure 3.

200° C ANNEALING

HIGH PURITY SILICON BORON DOPED CELLS DOSE 1.5×10^{15} E/CM^2

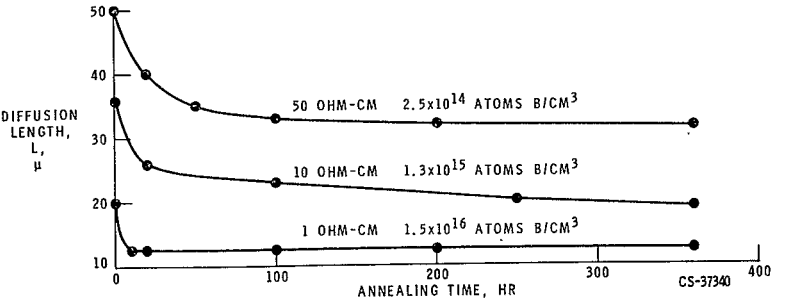

Figure 4.

100° C ANNEALING

LOPEX BORON CELLS DOSE 5×10^{15} E/CM^2

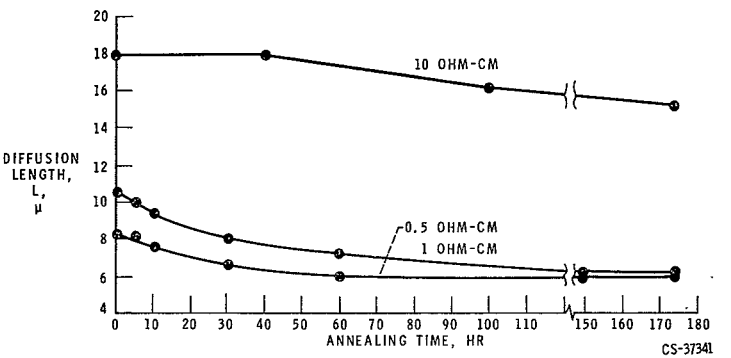

Figure 5.

COMPARISON OF DOPANT IMPURITIES

HIGHEST AVAILABLE PURITY

	IMPURITY ELEMENT			
DOPANT	Fe	Cu	Si	Mn
BORON	<1	<1	4-5	1-2
ALUMINUM	*1	1	<1	<1

*IMPURITY CONTENT IN PARTS PER MILLION

BORON DOPED SILICON CAN BE FLOAT-ZONE REFINED.

CS-37323

Figure 6.

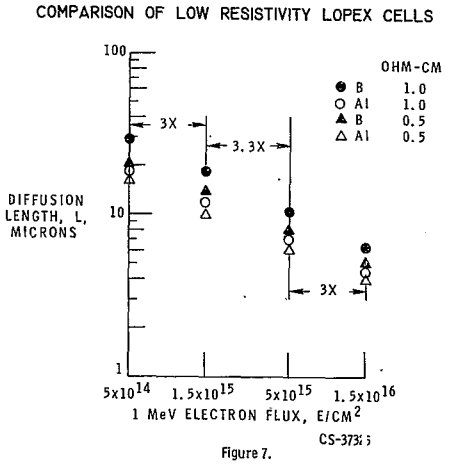

Figure 7.

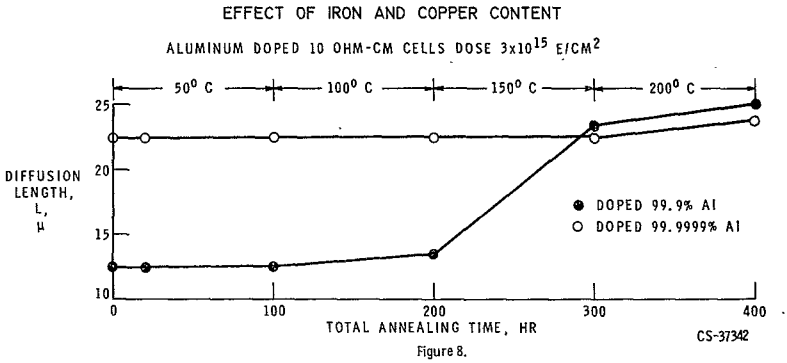

Figure 8.

RADIATION DAMAGE REACTIONS

REACTION	DAMAGE CENTER
$1\ Cu + D \underset{25^0\ C}{\rightleftharpoons} (Cu \cdot D)$	COPPER, RECOMBINATION
$2\ Fe + D \underset{25^0\ C}{\rightleftharpoons} (Fe \cdot D)$	IRON, RECOMBINATION
$(Cu \cdot D) \xrightarrow{200^0\ C} Cu + D$	ANNEALED
$(Fe \cdot D) \xrightarrow{200^0\ C} Fe + D$	ANNEALED

CS-37324

D, RADIATION INTRODUCED DEFECT IN SILICON.

Figure 9.

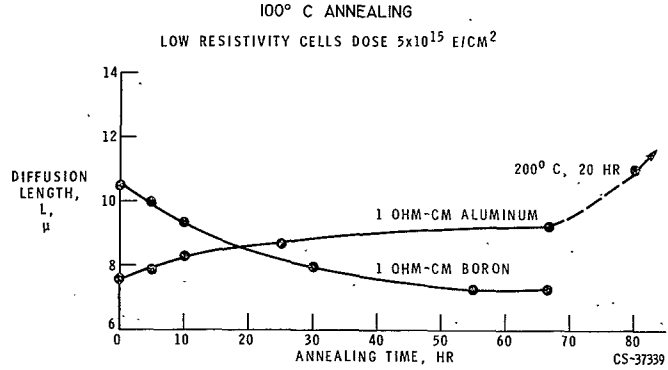

Figure 10.

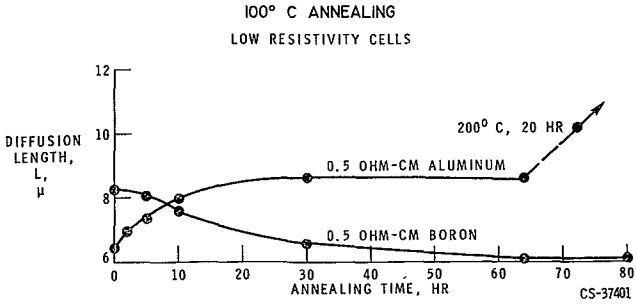

Figure 11.

Discussion

Schach: We will now entertain a few questions on the last two papers.

Kaye - EOS: Do you have any idea what sort of spread actually occurred in the data on the measurements of diffusion length?

Potter: Not exactly, but it was quite small.

Loferski - Brown: Would Dr. Potter like to comment on the fact that the annealing was stopped at 200° - it would seem to be the maximum temperature that it was shown in the slide. Obviously, if you had just increased the temperature somewhat, the reverse annealing would have been erased, and there would be no difference between aluminum and boron.

Potter: Well, this is true. If you go to sufficiently high temperatures you will see positive annealing and the damage will anneal out. We have data on this. It simply didn't seem important at this time to present it since it is exactly what you would expect. I think the interesting thing is the fact that reverse annealing does occur and it occurs at a low temperature.

Flicker - TRW: If I'm not mistaken, I saw a conflict between the data of Mandelkorn and the data of Fang, in that one saw that boron-doped electron-irradiated material suffered upon heat treating and the other found that it improved. Now, I think that there is really a basic comparison between the two because the Mandelkorn experiment was performed upon a very esoteric type of silicon; it's low-oxygen silicon, and we know very well that at least in n-type silicon, oxygen plays a very important role in the recombination process - that is, when you introduce vacancies, they interact with the oxygen present; whereas Dr. Fang's experiment was in a commercial solar cell that was made probably from milk quartz crucible-grown silicon. I think that the results of Mandelkorn are very interesting, but unless it can be shown that something equivalent takes place in ordinary quartz crucible-grown silicon, it can't be extended to any commercial product.

Potter: This reverse annealing occurs no matter how the boron is introduced, and into what type of crystal.

Flicker: I specifically heard you say that this was boron-doped material that was made on Lopex silicon.

Potter: Much of the data that I presented was. I did say - and this is a fact - that we didn't present all the data. The identical behavior the reverse annealing - is exhibited for boron-doped material, no matter how we make it. But we wished to make an exactly parallel comparison between aluminum-doped and boron-doped cells. We can only do this fairly if we use Lopex material, because that's our best aluminum material.

Schach: Actually, there may not be a conflict here. Reverse annealing was observed by Dr. Fang in his work.

PIC-SOL 209/6.1
Section D-6

THE EFFECT OF LITHIUM ON RADIATION DAMAGE IN SILICON SOLAR CELL DEVICES*

Presented by

J. J. Wysocki

RCA Laboratories

Princeton, New Jersey

19 October 1965

*The research reported here was sponsored by the National Aeronautical and Space Administration, Goddard Space Flight Center, Greenbelt, Maryland, under Contract No. NAS 5-9131 and RCA Laboratories, Princeton, N. J.

THE EFFECT OF LITHIUM ON RADIATION DAMAGE IN SILICON SOLAR CELL DEVICES

J.J. Wysocki
B. Goldstein
P. Rappaport
RCA Laboratories
Princeton, N. J.

Introduction

The experiments reported here are part of an effort to find an impurity which will interact with radiation-induced damage centers in silicon in such a manner that the degradation of lifetime by energetic particles is reduced. That impurity damage-center interactions do occur has been amply demonstrated by the well-known vacancy-oxygen ("A") and vacancy-phosphorus ("E") combinations which are observed in n-type silicon.[1] In this paper, we will consider how lithium affects the degradation of diffusion length in n-type silicon.

The use of lithium, and not some other impurity, was suggested by its remarkable properties in silicon. Lithium is an interstitial donor, and one of the fastest known diffusants in silicon.[2] Its motion is strongly influenced by electric fields because of its high mobility even at room temperature.[3] Lithium combines readily with acceptors and oxygen to form complexes which are stable at room temperature.[4,5] As a result of this pairing, donor and acceptor levels associated with unpaired impurities are removed from the forbidden gap.[4] Lithium is thus sufficiently mobile and reactive to be interesting in any study of impurity damage interactions in silicon.

Experimental Details

We chose to investigate the diffusion length degradation in lithium doped silicon by means of the electron-voltaic effect;[6] consequently we required rectifying contacts or junctions. Because of the ease of fabrication, including the avoidance of high-temperature processing, we used surface-barrier devices in our early work. At a later time, our study was expanded to include diffused solar cells.

Surface-Barrier Units

The surface barriers were made by evaporating gold onto a polished surface of the material. The material was either low-dislocation and floating-zone (F.Z.) or quartz-crucible (Q.C.) silicon which had already been doped with phosphorus. The main difference in the two classes of material is the oxygen content which is typically 10^{15} - 10^{16}/cc in the F.Z. and 10^{17} - 10^{18}/cc in the Q.C. material.

Prior to fabrication, lithium was diffused into the starting material at 400-550°C; using either a mineral oil dispersion, pure lithium, or a lithium-tin alloy as the source. The addition of lithium led to a drop in resistivity. The lithium doping level was assessed by four-point probe measurements on the diffused material and capacitance measurements on the completed device after accounting for the initial phosphorus doping. The resistivity measurements indicated lithium concentrations up to 10^{17}/cc; while the capacitance measurements, on the other hand, indicated concentrations a factor of 5 to 10 less in the immediate vicinity of the barrier. The smaller values may be due either to precipitation of lithium at the surface[4] or to the influence of the barrier field on the lithium concentration near the surface. In the units made from untreated material, the donor concentrations obtained from capacitance and resistivity measurements agreed closely with each other.

Diffused Solar Cells

The approach used in studying the diffused solar cell is the following. Pre-existing p-on-n cells made by diffusing boron into phosphorus doped silicon were cut into several parts; the coatings and contacts were removed from some of them. After diffusing lithium into these units, the contacts were reapplied. The untreated specimens were used for comparison purposes.

The lithium doping level in the diffused solar cells was assessed by resistivity and capacitance measurements, and the disparity in concentration mentioned above was found here also. In most cases, the capacitance measurements indicated little or no lithium in the vicinity of the junction even though resistivity measurements on the back surface showed that appreciable amounts of lithium were in the material.

All of the units were bombarded with 1 MeV electrons in air. The temperature of the samples did not exceed 30°C during irradiation. The resistivity values of the lithium diffused units quoted in the results are those deduced from the capacitance measurements, unless otherwise specified.

Results of Surface Barrier Study

Data obtained on surface barriers made from Q.C. material are shown in Fig. 1. The diffusion length in an untreated and a lithium diffused sample are plotted against the integrated flux of 1 MeV electrons. The unit containing lithium has a lower resistivity than the parent material and a smaller value of diffusion length at every flux. This behavior, i.e., that the diffusion length in high resistivity material is less affected by radiation than in low resistivity material, is expected on the basis of previous work with solar cells. Indeed, it was found that the dependence of the diffusion length at high fluxes on the initial resistivity of the lithium diffused units coincided with the dependence found in the untreated units. In other words, lithium, in the amounts used, had no apparent effect on the radiation properties of Q.C. material.

The results obtained with F.Z. units are shown in Fig. 2. The presence of lithium now profoundly influences the sample behavior. First of all, the large room-temperature annealing spikes occur only in the barriers containing lithium. This annealing was observed in a time interval as short as one hour. Secondly, the diffusion length in the lithium diffused sample, despite its lower resistivity, is greater than in the untreated sample at all fluxes. In most of the F.Z. samples studied, however, the high-flux values of diffusion length in the lithium diffused units were only comparable to those in the untreated units. Finally, the diffusion length at high fluxes ceases to fall rapidly with flux in the lithium diffused unit.*

Results of Solar Cell Study

No difference in radiation behavior was observed in the p-on-n solar cells made from Q.C. material for the amounts of lithium added to the cells. An effect of lithium was only observed in F.Z. cells, as shown in Figs. 3 and 4. Figure 3 illustrates that room-temperature annealing occurred in the cell containing lithium. The annealing rate now is slower than in the F.Z. surface barriers since the annealing required five days. The diffusion length in the lithium doped cell is smaller at every flux than in the untreated cell. The tabular data in Fig. 3 is the fractional short-circuit current remaining after the stated fluxes and annealing. In current degradation, the cell containing lithium is also somewhat less radiation resistant than the untreated cell.

The data in Fig. 4 was obtained on another group of F.Z. cells. In this case no room-temperature annealing was observed in five days, but the diffusion lengths in the two cells converge to the same value at high fluxes despite the apparent difference in four-point probe resistivities. The difference in behavior of the data in Figs. 3 and 4 may be due to differences in the lithium distribution and/or oxygen concentration in these cells. This variability in the results indicates refinements in the processing procedures are required at this phase of the work.

Some of the F.Z. cells were annealed after a flux of 1×10^{14} e/cm^2 to see if other differences existed in cells with and without lithium. The parameter studied was the room-temperature short-circuit current generated by water filtered tungsten light. The fraction of damage remaining after 10 minute isochronal anneals is shown in Fig. 5 as a function of annealing

*Similar behavior, i.e., the saturation of diffusion length at high fluxes, has been reported by Vavilov et al., except that their data was obtained on surface barriers made from Q.C. material.[7] It is seen that our results with Q.C. material do not reproduce theirs. This lack of agreement may arise from a difference in sample preparation since we are not sure of their fabrication procedures.

temperature. The fraction of damage remaining is defined as the ratio of the drop in current at any temperature from its pre-bombardment value to the drop caused by irradiation. The two cells behave quite differently. A large fraction of the damage is removed from the cell containing lithium in the vicinity of 100°C and the remainder is removed in a second annealing stage which occurs at approximately 235°C. None of the damage is removed from the untreated cell at 100°C; the only change observed in this cell is reverse annealing which occurred around 200°C.

A comparison of the temperatures at which recovery and reverse annealing occur in these cells to published annealing data suggests that the "E" (vacancy-phosphorus) center may be the dominant center involved in the cell containing lithium while the "A" (vacancy-oxygen) center is involved in the untreated cell.[8,9] The second annealing stage in the lithium diffused cell would then indicate some "A" center damage existed in this cell also, but at a much lower level than in the untreated cell.

Figures 6 and 7 demonstrate by means of the spectral response that the annealing process is indeed removing recombination centers from the n-type side of the cell. Both figures show the relative spectral response of the cells per photon vs. photon energy. As annealing proceeds, the red response of the cell containing lithium, i.e., that response arising in the n-type base, increases towards its pre-bombardment value (Fig. 6) while no substantial change occurs in the untreated cell (Fig. 7) in the same temperature range.

Conclusions and Discussion

The following conclusions are drawn from these experiments:

1. Lithium can modify the radiation damage behavior of silicon devices.

2. The oxygen concentration is important in whether or not changes due to lithium can be observed.

3. Despite the promising surface-barrier results, the radiation resistance at room temperature of F.Z. p-on-n solar cells was not improved by the use of lithium.

4. However, when lithium was present in the p-on-n cells, it was possible to anneal approximately 90% of the radiation damage at a temperature near 100°C. No such annealing occurred in the cells which did not contain lithium; these cells exhibited only reverse annealing near 200°C.

It seems reasonable to postulate, on the basis of the known tendency of lithium to form complexes with oxygen and the results of this study, that the effect of lithium on radiation damage resides in its competition with radiation-produced vacancies for the oxygen in the material. If this

is the case, the relative amounts of lithium and oxygen in the material are important in the observed behavior. If the oxygen concentration exceeds the lithium concentration, as it probably does in our Q.C. samples, then the vacancy-oxygen center will be produced to a large extent and no effect of lithium will be seen. If the lithium concentration equals or exceeds the oxygen concentration, however, then the "A" center introduction rate will be greatly reduced, and the vacancy-phosphorus center will be the one which is produced primarily. Since the latter condition on the lithium and oxygen concentrations is satisfied in our F.Z. samples, their behavior was modified by the presence of lithium. These ideas are also supported by the observed annealing behavior of the F.Z. cells.

If we argue that lithium, in effect, can remove the "A" center from the forbidden gap by virtue of its pairing with oxygen, then we are left with the "E" center, assuming it is the new recombination site. A comparison of the introduction rates of the "A" and "E" centers suggests that radiation damage will not be smaller when the "E", and not the "A", center is involved.[10] While our experimental results are in accordance with this conclusion, further study of the lithium-oxygen concentration dependence and annealing behavior are required before these hypotheses are proven.

Acknowledgements

We acknowledge the help of E. Davison, R. Hand, A. Topfer and J. Loferski in this work.

References

1. Watkins, Corbett, and Walker, J. Appl. Phys. 30, 1198 (1959).
2. C.S. Fuller and J. A. Ditzenberger, Phys. Rev. 91, 193 (1953).
3. E. M. Pell, J. Appl. Phys. 31, 291 (1960).
4. Reiss, Fuller, and Morin, Bell Syst. Tech. Jour. 35, 535 (1956).
5. E. M. Pell, "Solid State Physics in Electronics and Telecommunications", Edited by M. Desirant and J.L. Michiels, Vol. 1, part 1, Academic Press, New York, 1960.
6. W. Rosenzweig, Bell Syst. Tech. Jour. 41, 1573 (1962).
7. Vavilov, Kryukova, and Chukichev, Sov. Phys-Solid State 6, 2097 (1965).
8. E. Sonder and L. C. Templeton, J. Appl. Phys. 34, 3295 (1963).
9. T. Tanaka and Y. Inuishi, J. Phys. Soc. Japan 19, 167 (1964).
10. G. K. Wertheim and D. N. E. Buchanan, J. Appl. Phys. 30, 1232 (1959).

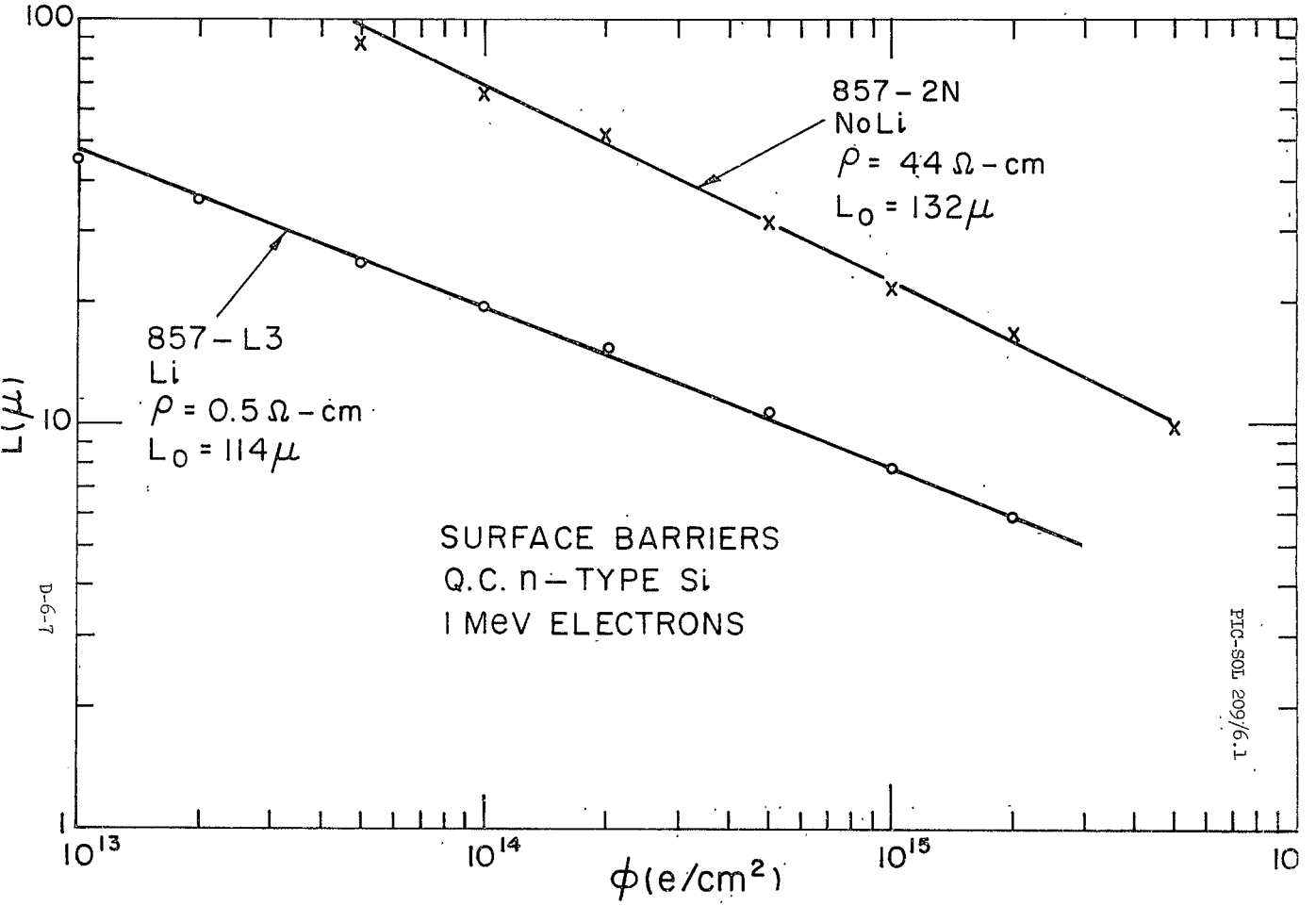
100
10
1
L(μ)
857 – 2N
No Li
ρ = 44 Ω – cm
L0 = 132μ
857 – L3
Li
ρ = 0.5 Ω – cm
L0 = 114μ
SURFACE BARRIERS
Q.C. n – TYPE Si
1 MeV ELECTRONS
D-6-1
FIG-SOU 209/6.1
10^13
10^14
10^15
10
φ(e/cm^2)

Figure 1

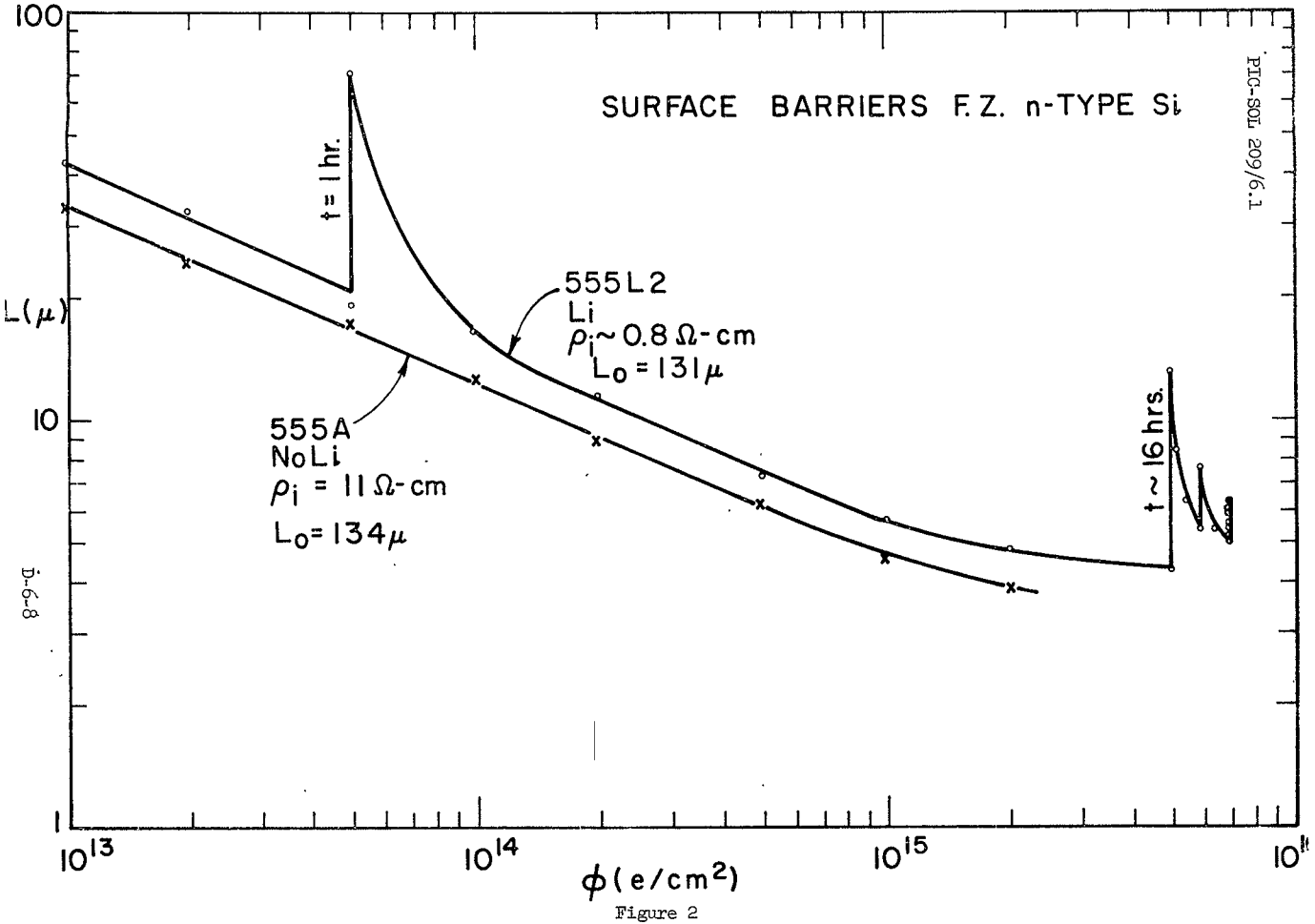
SURFACE BARRIERS F.Z. n-TYPE Si
FIG-SOL 209/6.1
t = 1 hr.
555L2
Li
$\rho_i \sim 0.8\ \Omega$-cm
$L_o = 131\mu$
555A
NoLi
$\rho_i = 11\ \Omega$-cm
$L_o = 134\mu$
t ~ 16 hrs.
L(μ)
100
10
1
10^{13}
10^{14}
10^{15}
ϕ (e/cm²)
D-6-8

Figure 2

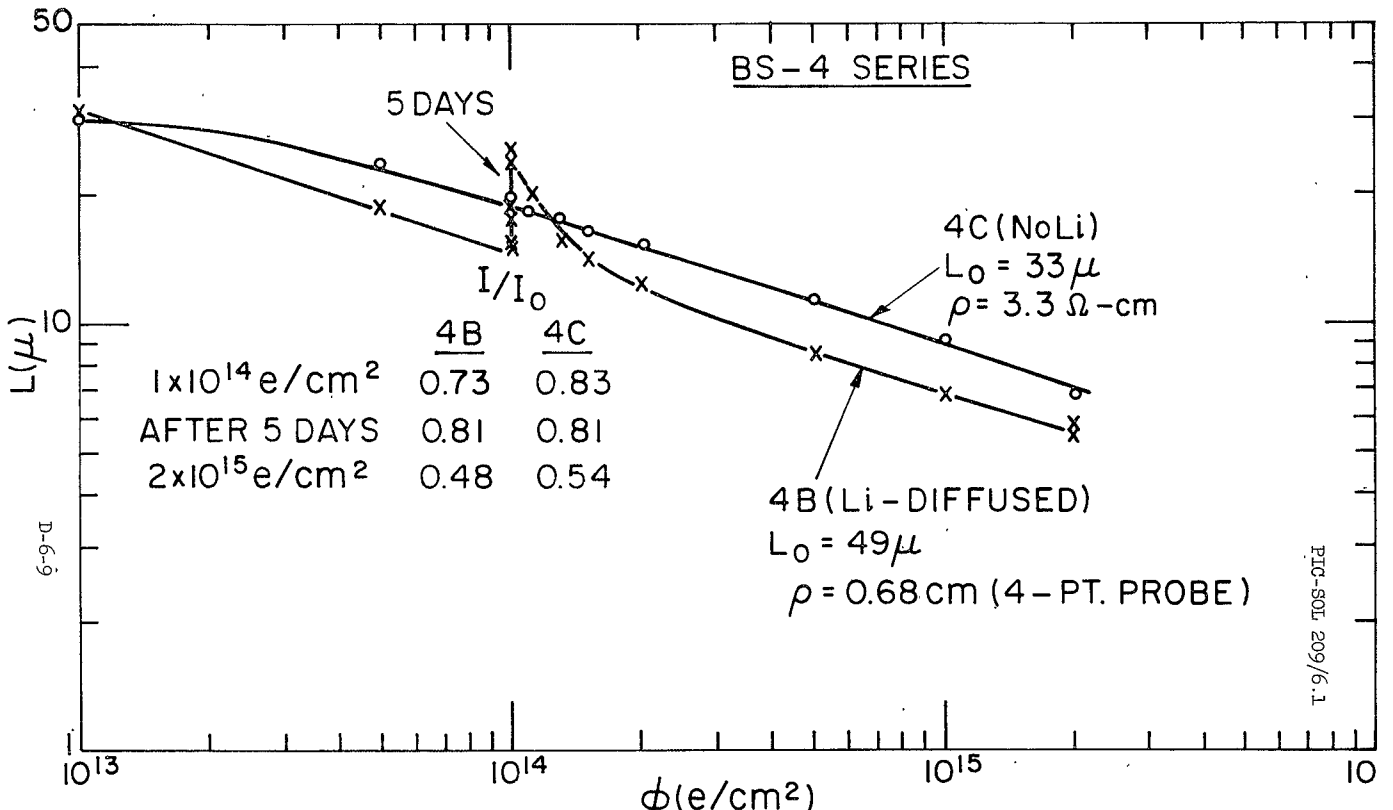
BS-4 SERIES
5 DAYS
I/I0
4B 4C
1x10^14 e/cm^2 0.73 0.83
AFTER 5 DAYS 0.81 0.81
2x10^15 e/cm^2 0.48 0.54
4C (NoLi)
L0 = 33 μ
ρ = 3.3 Ω-cm
4B (Li-DIFFUSED)
L0 = 49 μ
ρ = 0.68 cm (4-PT. PROBE)
L(μ)
φ(e/cm^2)
50
10
1
10^13
10^14
10^15
10
D-6-9
PIC-SOL 209/6.1

Figure 3

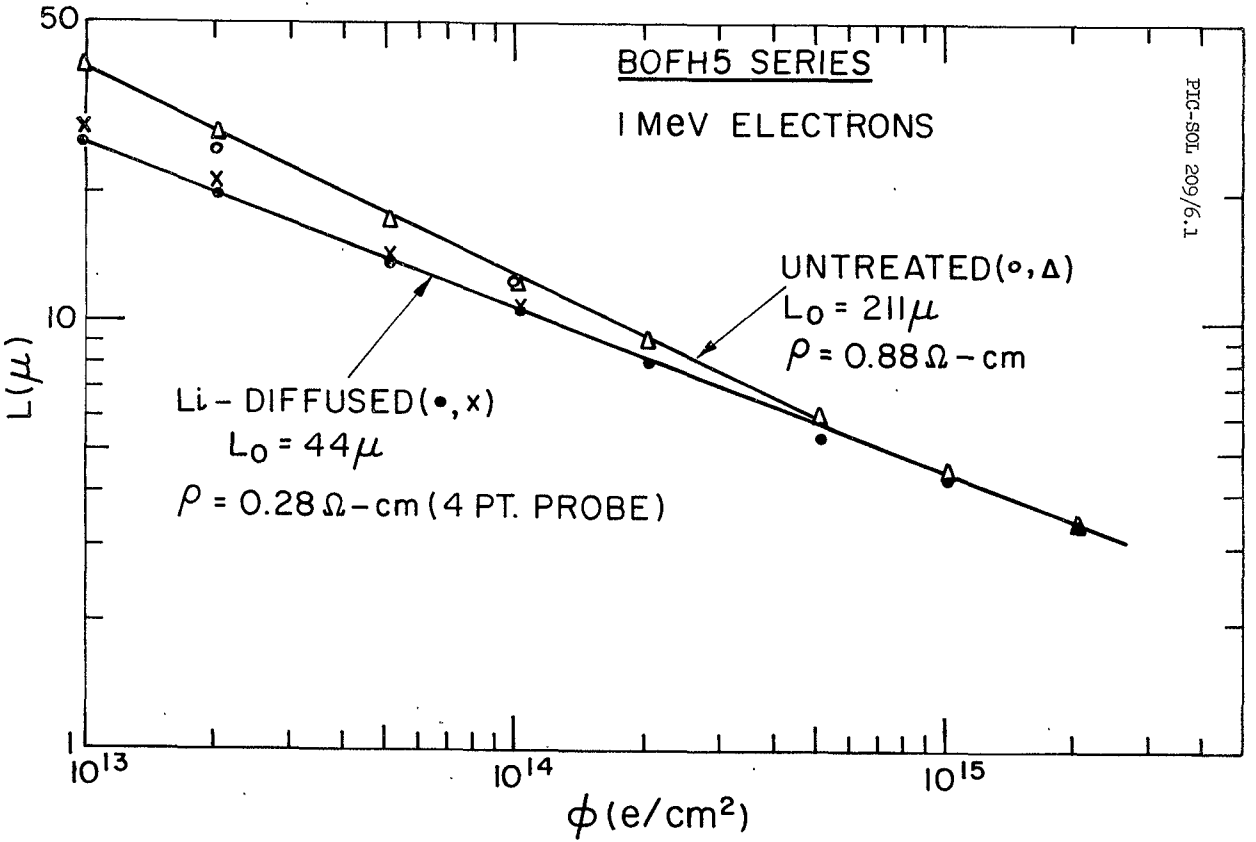

PIC-SOL 209/6.1

Figure 4

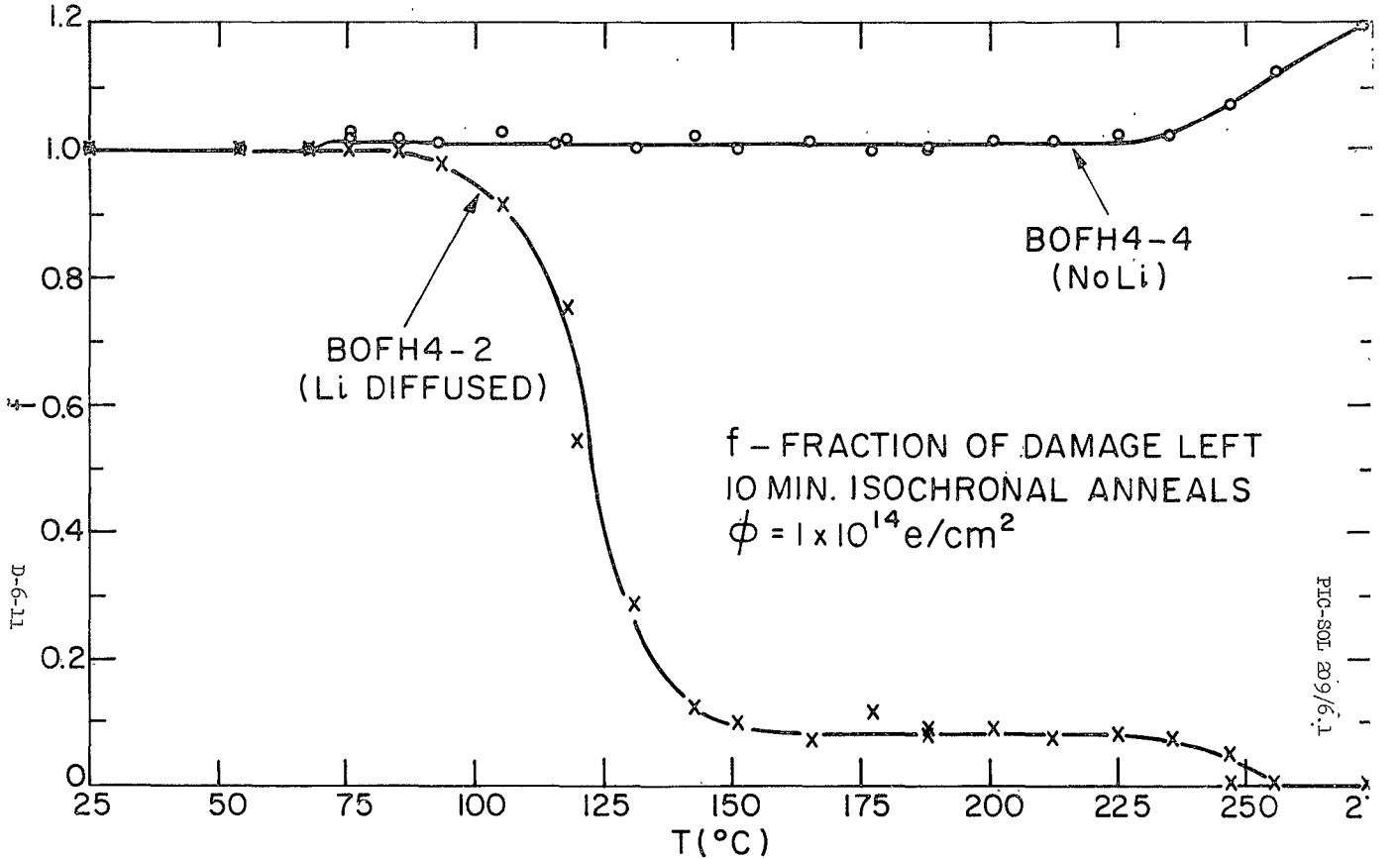
1.2
1.0
0.8
0.6
0.4
0.2
0
f
25
50
75
100
125
150
175
200
225
250
T(°C)
BOFH4-4
(No Li)
BOFH4-2
(Li DIFFUSED)
f – FRACTION OF DAMAGE LEFT
10 MIN. ISOCHRONAL ANNEALS
$\phi = 1 \times 10^{14} e/cm^2$
D-6-11
PIC-SM 2/9/61

Figure 5

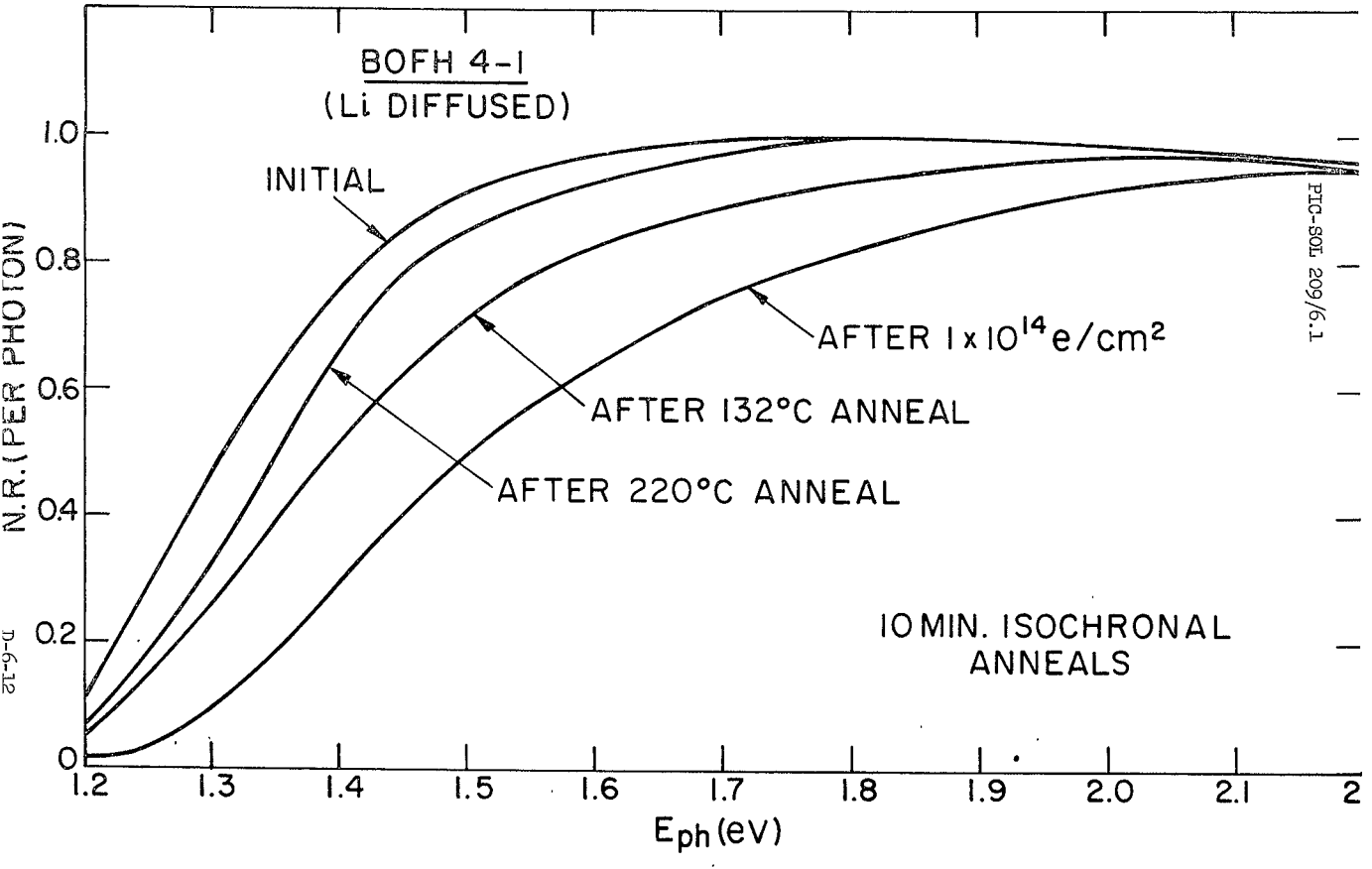
BOFH 4-1
(Li DIFFUSED)
INITIAL
AFTER 1 x 10^14 e/cm^2
AFTER 132°C ANNEAL
AFTER 220°C ANNEAL
10 MIN. ISOCHRONAL
ANNEALS
N.R. (PER PHOTON)
1.0
0.8
0.6
0.4
0.2
0
1.2
1.3
1.4
1.5
1.6
1.7
1.8
1.9
2.0
2.1
2
E_ph (eV)
PIC-SOL 209/6.1
P-6-12

Figure 6

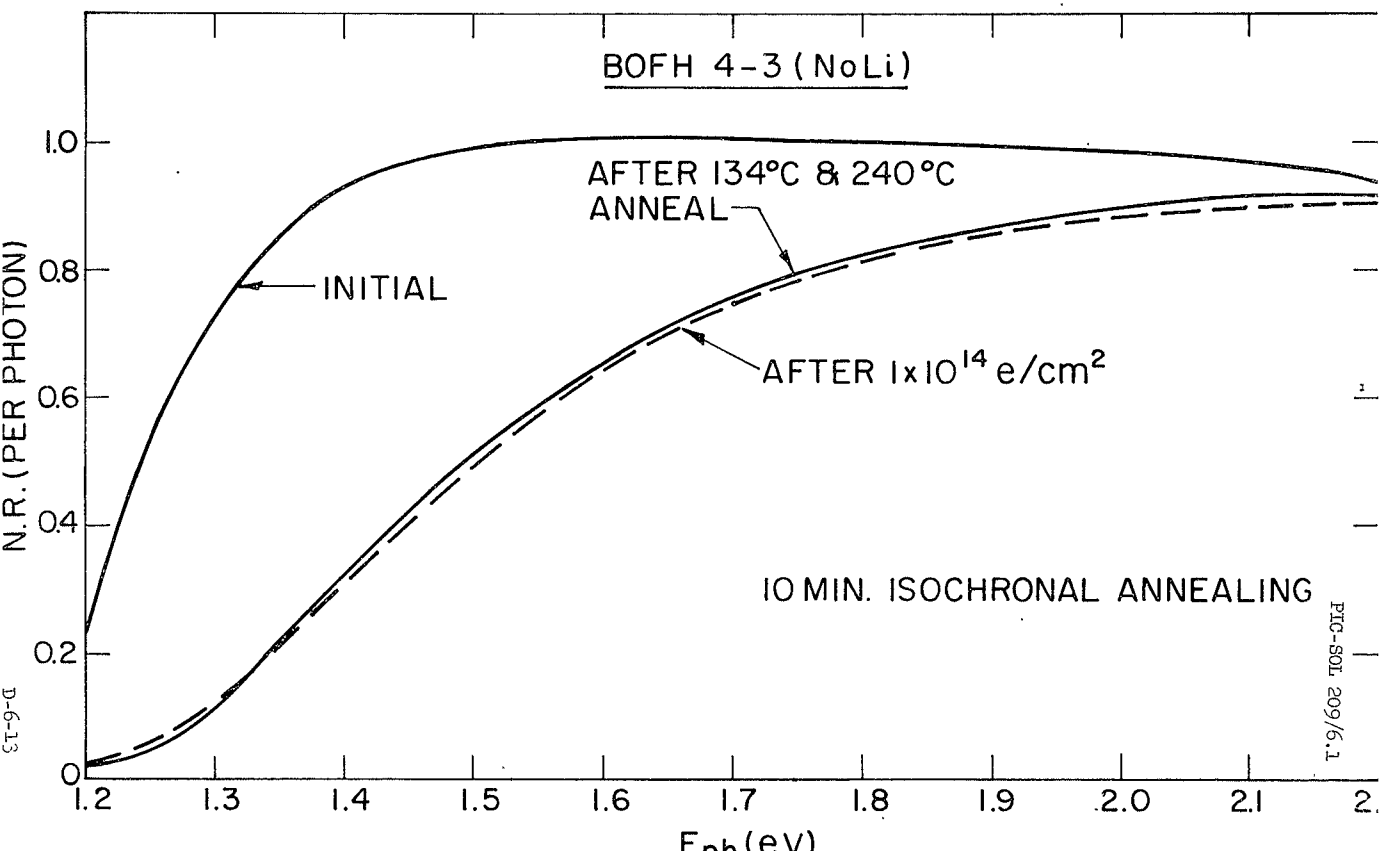
BOFH 4-3 (NoLi)
AFTER 134°C & 240°C ANNEAL
INITIAL
AFTER 1x10^14 e/cm^2
10 MIN. ISOCHRONAL ANNEALING
N.R. (PER PHOTON)
1.0
0.8
0.6
0.4
0.2
0
1.2
1.3
1.4
1.5
1.6
1.7
1.8
1.9
2.0
2.1
Eph (eV)
PIC-80L 209/6.1

Figure 7

Discussion

Session IV, Paper #6

*****

Schach: Are there questions?

Kaye, EOS: I wonder if you'd care to speculate what would happen if you tried to do this with the p-type silicon.

Wysocki: There are a complementary set of centers in p-type silicon to those that I've shown here for n-type silicon. In other words, there's a center in which oxygen is involved and there's a center in which oxygen isn't involved. We are, of course, trying to see some of these effects in p-type silicon, but I have nothing to report at this point. We're looking at it.

Schach: I think any further questions can be carried on at the banquet this evening.

Baicker: I was just going to ask Steve Kaye what exactly he meant by putting lithium in p-type silicon.

Kaye: Putting it in at a lower amount than the dopant, but maybe...

Wysocki: Which may mean much lower concentrations than the oxygen level.

PIC-SOL 209/6.1
Section D-7

LOW ENERGY PROTON DEGRADATION IN SILICON SOLAR CELLS

Presented by

R. G. Downing

TRW Systems

Redondo Beach, California

19 October 1965

LOW ENERGY PROTON DEGRADATION IN SILICON SOLAR CELLS

R. G. Downing
TRW Systems
One Space Park
Redondo Beach, California

Introduction

The energy spectrum of the trapped proton belt around the earth is normally considered to be of the order of E^{-3} to E^{-5}. Because of the steepness of this energy spectrum silicon solar cells, which are necessarily exposed, receive a considerable dosage of low energy protons. Thus it is important to understand the response of solar cells to these low energy protons. Since low energy protons are not considered penetrating radiation, the extrapolation of data obtained with penetrating radiation; i.e., high energy electrons or high energy protons, does not yield meaningful results. The principal reason that extrapolation from penetrating radiation is not valid is that low energy protons produce regions of severe damage near the surface at depths less than a minority carrier diffusion length. Hence, the recombination of carriers in their process of diffusion to the junction becomes a complicated function in the region in which they are diffusing. For these reasons, there is a need for information on the effects of low energy protons on silicon solar cells.

Experimental Techniques

During the course of this contract, two low energy proton experiments have been conducted; the first in December and January, the second in March. The facility utilized for these experiments was the STL 2 Mev proton Van de Graaff. Experiments were conducted at energies ranging from 0.2 Mev to 1.9 Mev. Due to the short range of protons of these energies in air, all of the experiments were conducted in a vacuum chamber. This chamber consisted of remote control apparatus for both mapping the beam and positioning test specimens in the beam. A shielded Faraday cup was used to determine the intensity of the beam as a function of position and to determine the total exposure of the test specimens by simultaneously irradiating the test specimen with the Faraday cup located in an adjacent position of equal intensity. The STL proton Van de Graaff facility does not incorporate a conventional magnetic analyzing assembly. Hence, it was necessary to include in the chamber design a magnetic deflection system to separate the various components of the primary beam and remove all but the primary proton beam for the irradiations. The magnetic deflection system consisted of a 4 inch Varian magnet operated with flat 4 inch pole pieces and a one inch pole gap. Five distinctly separate identifiable beams were observed with this system; m_1, m_2, and m_3 beams at the principal operating energy as

well as m_1 beams at one-half the principal energy and one-third the principal energy. These latter two beams are attributed to break-up of the m_2 and m_3 beams in the drift tube prior to entrance to the magnetic analyzer. The m_1 beam, referred to as the principal beam, consists simply of protons with a charge-to-mass ratio of 1. The m_2 beam with a charge-to-mass ratio of 1/2 is attributed to singly ionized hydrogen molecules which are not completely ionized at the source and are subsequently accelerated to the full potential. The m_3 beam with a charge-to-mass ratio of 1/3 is attributed to tri-atomic, singly ionized hydrogen molecules for which the formation mechanism is not well known. The m_1, m_2, and m_3 beams were present in the primary beam with about equal magnitudes while the 1/2 and 1/3 principal energy m_1 beams were about two orders of magnitude less in intensity. Scatter shields were included in the irradiation chamber to effectively remove the unwanted beam components after magnetic analysis. Experiments were performed at magnetic deflections of the principal beam of 10 and 20 degrees.

In order to investigate the beam, considerable beam analysis with a silicon solid state detector and a 400 channel pulse height analyzer was performed. It was observed that when very small entrance and exit apertures for the magnetic analyzer were used (0.1 inch or less) the analyzed beams were extremely clean with an energy width of the order of a few percent. Also, the principal beam comprised over 95 percent of the total number of particles incident on the detector. In this clean configuration, however, the beam diameter was too small to perform meaningful experiments on solar cells. Since no control over beam spot size could be exercised past the analyzing magnet, much larger apertures were necessarily used to obtain sufficient beam diameters. It was observed, however, that as the analyzing apertures were made larger, the energy width and content of the beam deteriorated. For extremely large apertures the energy width of the beam would approach 30 to 40 percent and the content of the beam attributable to the principal beam was observed to drop to as low as 60 percent. As a result, it was necessary to compromise the irradiating beam content significantly in order to obtain reasonable beam diameters for the conduct of the irradiations.

The test specimens used in these experiments consisted of 1 ohm-cm, 1 cm by 1 cm p/n silicon solar cells and 10 ohm-cm, 1 cm by 1 cm n/p silicon solar cells, both types furnished by Hoffman Electronics Corporation. The bulk of the data was obtained for the 10 ohm-cm n/p cells since they are of principal practical importance; however, sufficient data were obtained for the p/n cells to ensure correlation. Junction depths of both types of cells were 0.5 microns while their initial efficiencies were 8 to 10 percent. Measurements of I-V characteristics were performed using the STL sun simulator (an OCLI unit) and a 2800°K unfiltered tungsten light table. The tungsten light table used in these experiments is the same unit described in previous reports[1] on radiation damage and has been held at a constant intensity for the last four years. The sun equivalent power for this tungsten

source will therefore vary slightly depending on the particular characteristics of the cells under test but usually lies between 130 mw/cm^2 and 140 mw/cm^2 for contemporary silicon solar cells.

Results

The analysis of the data to be presented in this section is based on radiation unduced changes in the I-V characteristics as observed under both tungsten and sun illumination. Changes in short-circuit current, open circuit voltage, and maximum power as a function of integrated proton flux and proton energy are the principal parameters studied and presented here. Changes in other important solar cell parameters such as series resistance, in-beam annealing, and rapid post-irradiation annealing were also observed. Since, however, analysis of the data yielded no significant trends for these parameters, their inclusion in the results is necessarily limited to general mention and discussion.

The degradation of short-circuit current density as a function of proton energy is shown in Figure 1. For each energy shown, 3 to 7 cells were used to obtain the data presented. The data shown in Figure 1 indicate that in the low energy proton region the degradation rates, i.e., the slopes of the degradation curves, seem to vary considerably as a function of energy. The slopes all appear to be steeper than the normal 6.5 to 7 ma/cm^2 - decade observed for penetrating radiation of either electrons or protons. The slopes shown for 1.9 and 1.7 Mev appear to be approximately 10.5 ma/cm^2 - decade increasing to about 12 ma/cm^2 - decade at 1.5 Mev and 15.5 ma/cm^2 - decade at 1 Mev. At this point the slopes appear to start decreasing again indicating about 13 ma/cm^2 - decade at 0.5 Mev and considerably less than that at 0.3 and 0.2 Mev. The degradation rates at these latter two energies were so slow that inadequate beam time was available to obtain sufficient data for slope determination. A group of p on n cells was irradiated at 0.5 Mev for comparison with the n on p cells and, as shown in Figure 1, the degradation rates are identical. Sufficiently low beam intensities for the irradiation of p on n cells were difficult to obtain, and also since principal interest is in the n on p cells, a large amount of information was not obtained for p on n cells other than to verify that their response was similar in nature to the n on p cells. It is also observed in Figure 1 that the knee of the curve, i.e., the point of the intersection of the slope with the initial conditions, seems to reach a minimum value somewhere between 1.9 Mev and 6.7 Mev and then reverses its direction toward higher values of integrated flux with further decrease in proton energy.

A series of post irradiation measurements indicated that considerable room temperature annealing occurs for low energy proton irradiated cells. Recovery of between 20 percent and 90 percent of the short-circuit current was observed in times of the order of days. Annealing of open circuit voltage at room temperatures did not occur. There appeared to be no correlation, however, in the annealing data in that the observed recovery was not a consistent function of either proton energy, time, or amount

of radiation induced damage. In addition to room temperature annealing, in-beam annealing was also observed. Although the beam intensities utilized in the experiment were not sufficiently high to raise the temperature of a solar cell it is quite probable that, due to the short range of the protons, localized heating in the region near the junction where the damage is occurring is responsible for the observed phenonema. In several cases for longer irradiations at the same intensities, I-V curves were actually obtained wherein the open circuit voltage had proceeded with its normal degradation but the short-circuit current had actually been annealed to a higher value than before the irradiation was initiated. For this reason, the short-circuit current data at the higher fluxes were considered invalid and are therefore not shown on the plot of short-circuit current versus integrated flux.

In order to obtain a comparison between observed degradation in short-circuit current under tungsten illumination and equivalent performance under solar illumination in space, a series of measurements was made using the STL sun simulator which is an OCLI unit. The results of this comparison are shown in Figure 2. The typical response for penetrating radiation in the solar simulator versus the standard 2800°K tungsten source, which has been maintained constant over the past four years, is shown in the figure. The expected departure from this typical response is evident in that, for the case of severe damage near the surface of the cell, the degradation under sun illumination is more severe for the same degradation under tungsten illumination due to the higher blue content of solar illumination. However, there is no statistically significant difference observed for proton energies ranging from 0.5 to 1.9 Mev. Some difference would be expected in this range; however, the scatter in the data is apparently greater than the difference in response. On the other hand, a significant departure is observed for proton energies of 0.2 Mev indicating a rapid deterioration of response to the short wavelength component of solar illumination at energies below 0.5 Mev. These curves were used to calculate degradation of output power in space which will be presented in a later section.

Degradation in open circuit voltage versus integrated flux and proton energy is shown in Figure 3. The observed degradation rates, or slopes, are all approximately alike and equal to about 120 mv per decade. There appear to be slight deviations in this slope as a function of proton energy but these deviations are less than the scatter in the data and hence unresolvable. These slopes, however, are considerably greater than the slopes observed in the case of either electron or proton penetrating radiation wherein slopes of the order of 40 to 50 mv/decade are commonly observed for 10 ohm-cm n on p cells. Although examination of I-V characteristics as a function of proton energy seems to imply a greatly increasing sensitivity of open circuit voltage at the lower proton energies, this is not in actuality the case as evidenced by the data in Figure 3. The maximum sensitivity of the open circuit voltage seems to lie somewhere between 1.5 and 2 Mev with decreasing damage sensitivity at energies of 1 Mev and less. The illusion that the open circuit voltage degradation

is increasing at energies of 1 Mev and below is due primarily to the fact that the short-circuit current degradation sensitivity is decreasing very rapidly and in fact at lower energies the open circuit voltage is the principal degradation parameter. The shift from the 40 to 50 mv/decade degradation rate observed for proton energies as low as 6.7 Mev to the steep slopes shown in Figure 3 apparently occurs between 2 Mev and 6.7 Mev.

Due to the peculiar nature of the response of silicon solar cells to low energy protons, extrapolation of data for penetrating radiation to performance in space is not a valid approach. Therefore, the I-V characteristics obtained in these experiments were corrected for actual space conditions through the use of Figure 2 for further analysis. A plot of the degradation of P_{max} versus integrated flux was then obtained as shown in Figure 4. The degradation of P_{max} is observed to be maximum for proton energies of 1.5 and 1.9 Mev while falling off at energies of 1 Mev and below. In comparing these data with data previously obtained at 6.7 Mev it appears evident that the region of maximum overall degradation in the power producing capability of silicon solar cells lies in the region of 2 to 6 Mev and is most probably quite close to 2 Mev. The slopes, as anticipated, are considerably steeper than those observed for penetrating radiation. In the case of penetrating radiation, degradation rates of approximately 15 to 20 percent per decade are commonly observed wherein the slopes observed for proton energies between 1.9 and 0.5 Mev and approximately 45 percent per decade. However, at 0.2 Mev the degradation rate appears to have decreased considerably due to the decreased sensitivity of the short-circuit current degradation. The observed degradation at 0.2 Mev in these experiments is approximately 20 percent per decade in spite of the fact that at these lower proton energies observable degradation in the series resistance of the cell begins to become quite evident and important. Considering the wide variations in degradation rates observed for the short-circuit current, the uniformity of the degradation rates for P_{max} is somewhat surprising and can only be accounted for by unresolvable differences in the degradation rates of other parameters such as open circuit voltage, series resistance, and short term annealing.

Conclusions

The degradation rates for the open circuit voltage, short-circuit current, and P_{max} all increase substantially under low energy proton bombardment relative to degradation rates observed for penetrating radiation. In particular the short-circuit current degradation rate seems to show a very strong dependence on proton energy in the region below 2 Mev. The net result of the degradation in the I-V characteristics is summarized by the degradation in the maximum power producing capability of the cell. Although the power degradation rate is almost twice as high as for penetrating radiation, maximum sensitivity seems to occur in a region between 2 and 6 Mev and most probably very near 2 Mev. For an equal exposure of lower energy protons, the absolute power degration

decreases with further decrease in proton energy below 2 Mev. Hence, the proton radiation sensitivity of silicon solar cells which is increasing with decreasing proton energies seems to reach its maximum sensitivity in a region near 2 Mev and then begins to fall off. Inasmuch as the data shown here are presented as unannealed data, and since measurable annealing at room temperature for short periods of time has been observed, the actual power degradation experienced in space over a period of time will not be as severe as indicated by these data.

Although considerable data were obtained in these experiments, it is difficult to assess a meaningful accuracy to the results due to the compromised proton beam ultimately used. It is estimated that the accuracy of the data is most probably good to within a factor of 2 but it cannot be considered accurate to within 5 or 10 percent. A facility capability of a higher energy and a more complete magnetic analyzing system would be required to improve on the accuracy of the data and cover the range to at least 4 or 5 Mev.

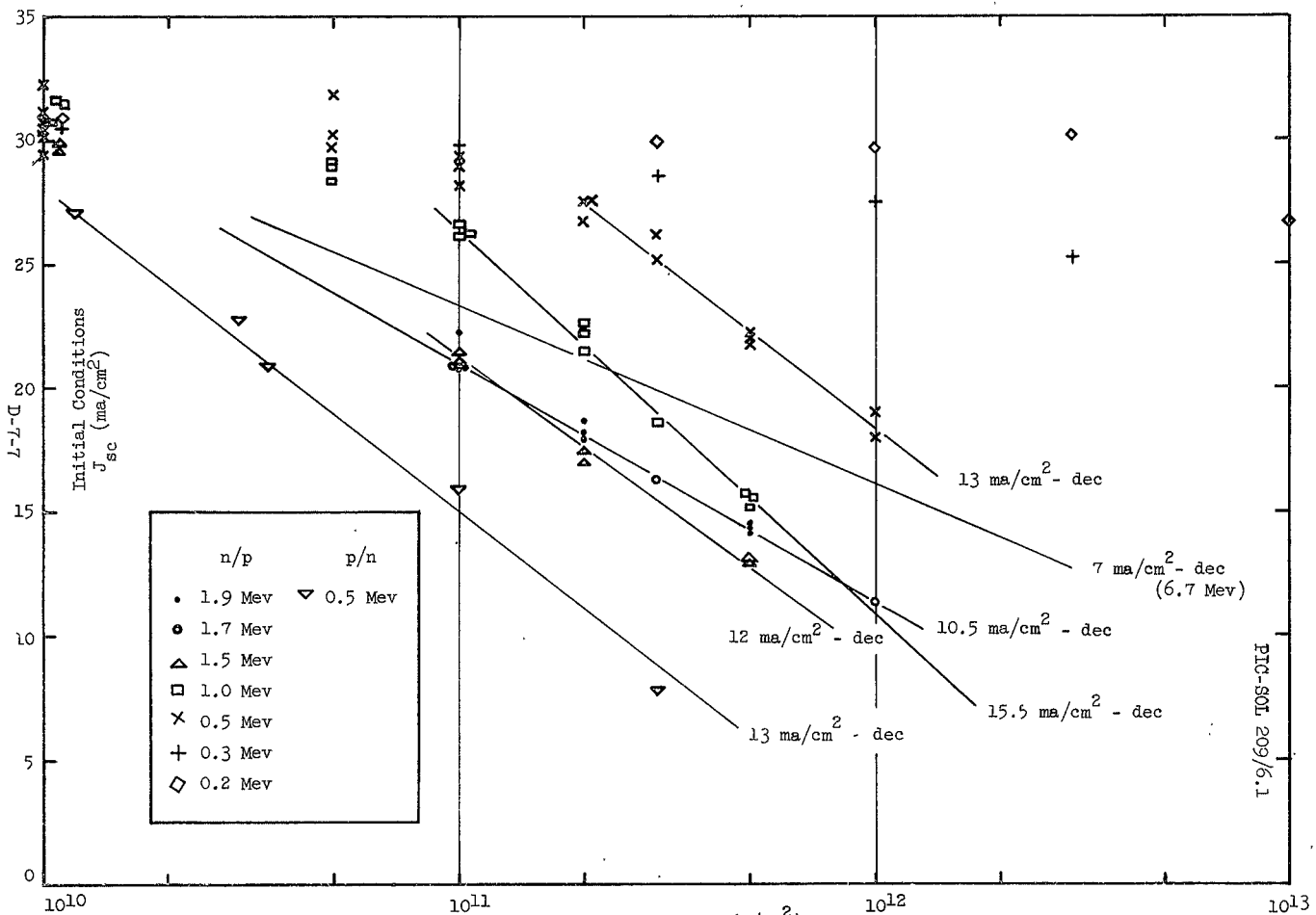

Figure 1 - Silicon Solar Cell Short-Circuit Current Degradation Under Low Energy Proton Irradiation

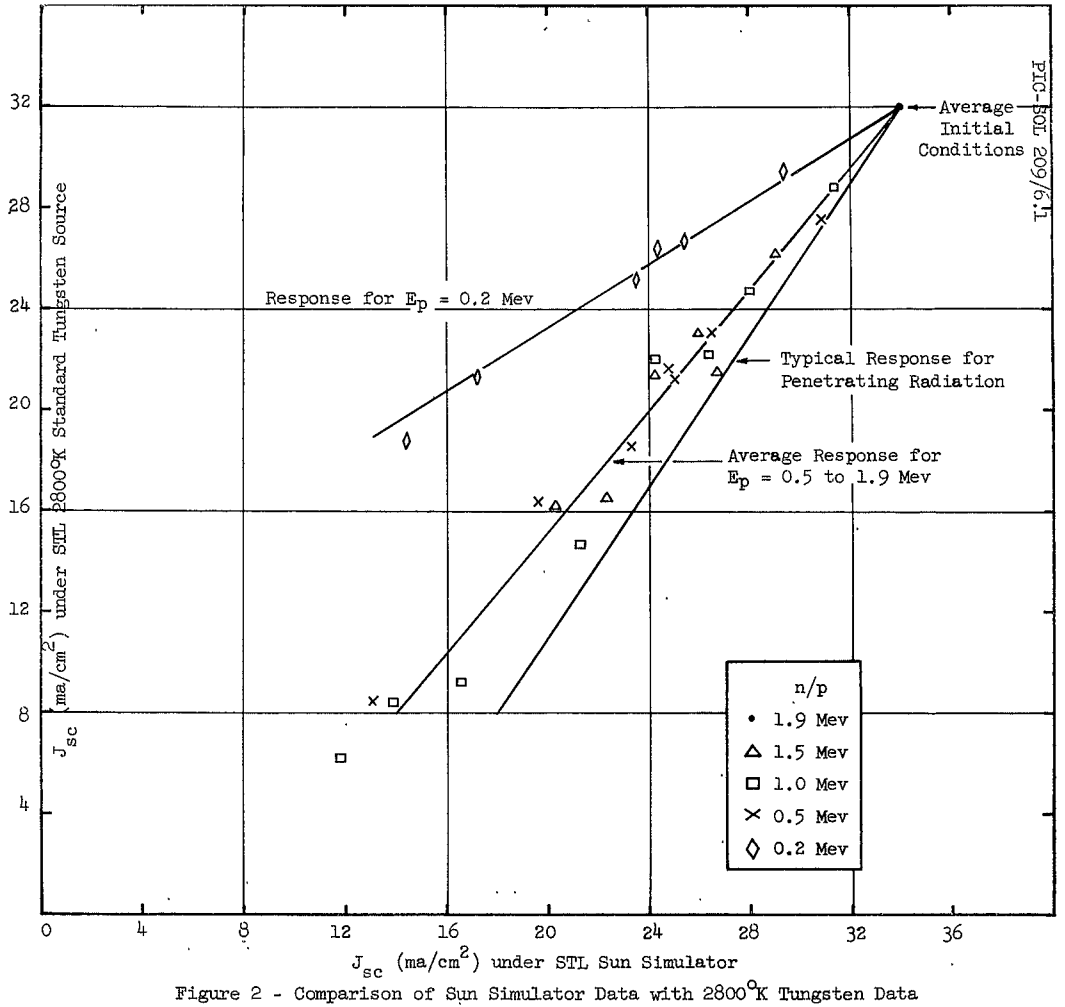

Figure 2 - Comparison of Sun Simulator Data with 2800°K Tungsten Data

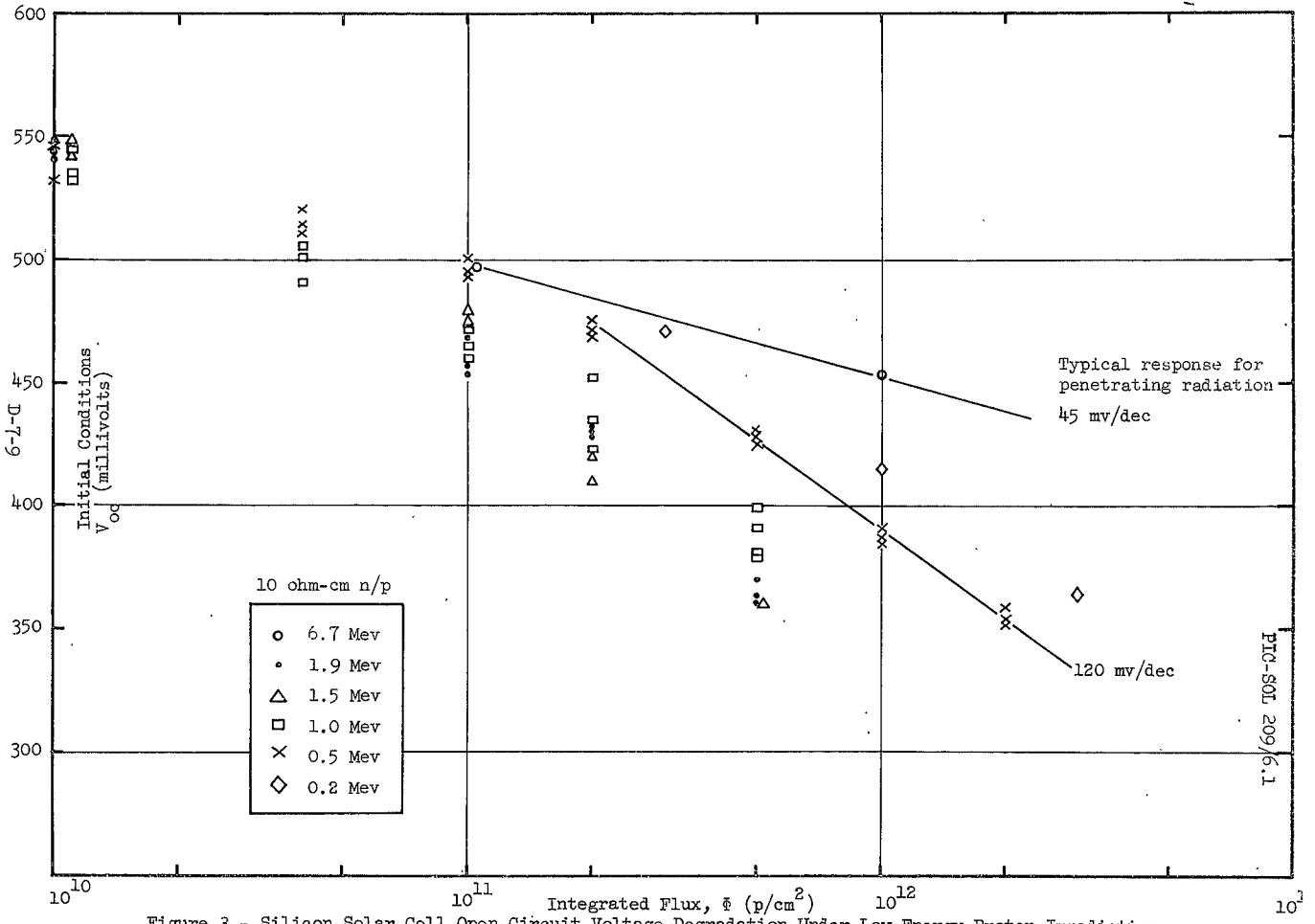

Figure 3 - Silicon Solar Cell Open Circuit Voltage Degradation Under Low Energy Proton Irradiation

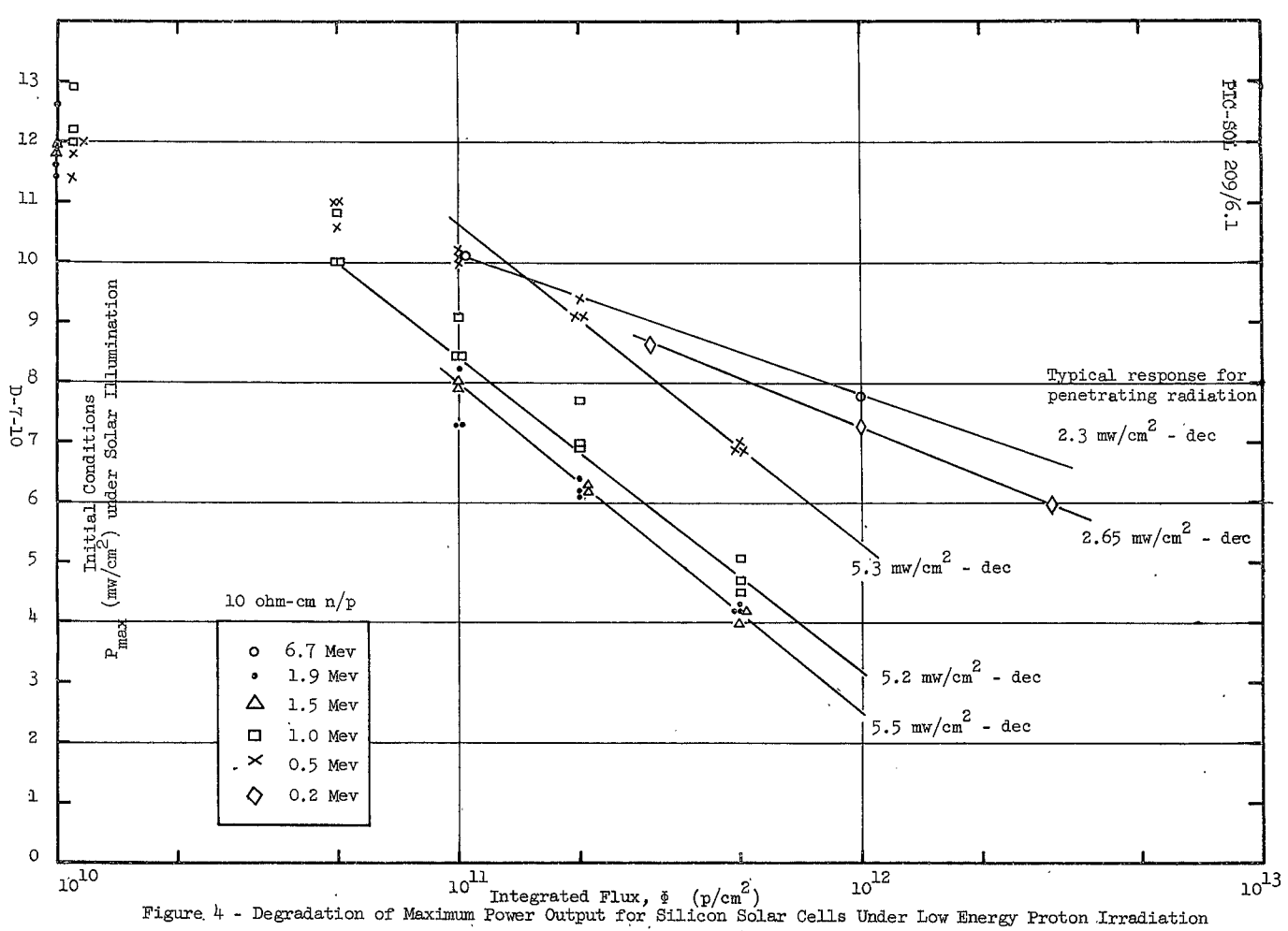

Figure 4 - Degradation of Maximum Power Output for Silicon Solar Cells Under Low Energy Proton Irradiation

Discussion

Schach: Thank you, Gil. Are there questions?

Medved - EOS: Do you have a reasonably good feeling for the range of the protons, say, at 1 Mev as compared to two-tenths of an Mev, and if so, I'd like to make a comment a little later, if there's time in the discussion.

Downing: I think the values of the range of protons in this energy range in silicon and silicon-like material is a fairly well known function. We have been working with a Hans Bischell at USC, who has done some extremely good work on the range of protons in materials, and he feels that this is known to within fractions of a percent. What is the range for 1 Mev? It's in the 10 micron range.

King - Ion Physics: I feel obliged to stand up for our parent corporation in terms of your earlier remarks on the Van de Graaff. (laughter) The sub one mass units that you observed are very frequently observed, and to my knowledge there's no explanation for it. They're observed even when you are on protons, and you can get them on boron, phosphorus, or something else. Second, if you operate that machine properly, you can get down to 50 kilovolts. And third, if you purchase the magnet from High Voltage, you find no difficulty in separating out the various components. (laughter)

Loferski - Brown: I was just wondering about that disagreement between the theory and the experiment at low energies.

Downing: Voltage or current?

Loferski: I'm sorry - low voltages for the proton beam - and on the current on the cell in particular. What I was wondering about - did your model include the front part of the cell?

Downing: Yes.

Loferski: So you were calculating it down to, say, the diffused region, and in spite of this, you didn't get agreement.

Downing: Right.

Loferski: OK.

Medved - EOS: Have you thought of - or have you tried to see what happens with an annealing process after these irradiations. The reason I ask this question is in connection with an earlier question on the paper given yesterday on production of solar cells by ion implantation. Apparently they have seen the advantage of reducing their energy of implantation from the 1 Mev region to roughly 200 kilovolts. And they still require an anneal at 700 degrees C. We are making junctions at an order of magnitude lower in energy and do not require that high a temperature. In

fact, we don't require an anneal - just maintain a reasonably moderate temperature from 3-400 degrees C during bombardment. So this is why I'm asking the question of you - have you looked at the annealing process?

Downing: Not yet for low energy protons, but considerably for electron irradiation.

Dr. King - Ion Physics: I'd like to make a comment on that comment. (laughter) I think it's very important to realize that some people are doing channeling work in ion implantation and they find that it is necessary to go to temperatures of 300 to 500 degrees in order to achieve any kind of lowering of the sheet resistivity. This is obviously annealing of radiation damage, whether they want to appreciate the fact or not. In the work that Dave is describing, the actual energies employed are 80 to 100 kilovolts, and I think if you would continue your curves down, you would have seen that almost no effect due to your bombardment on the short-circuit current. And, as a matter of fact, if you annealed at even very light - very modest temperatures, you would have resulted in cells with no appreciable effects at all.

Medved - EOS: I'd like to make a comment on that comment. I'd only like to invite Dr. King and others who are interested to attend our discussions on ion implantation next week at EOS on Tuesday afternoon. Thank you.

PIC-SOL 209/6.1
Section D-8

A THEORETICAL MODEL FOR LOW-ENERGY PROTON IRRADIATED SILICON SOLAR CELLS*

Presented by

H. Y. Tada

TRW Systems

Redondo Beach, California

19 October 1965

*Not presented at the conference because of time limitations, but included in the proceedings at the request of the sponsors.

Abstract

Nb 617 340

The effect of low-energy protons on silicon solar cells has been theoretically investigated. A model has been generated for low carrier injection levels and the solution is presented in a closed form in terms of physical and geometrical parameters. Both short-circuit current and open circuit voltage calculated from the theory were compared with experimental results. The computed short-circuit current agrees with the experimentally observed decay slope if the magnitude of the degradation is less than 6% for proton energies greater than 0.5 Mev. According to the theory, experimental values of the energy dependent damage constant at moderately high proton energies can be extrapolated back to about 0.5 Mev. on the basis of the energy dependence of the Rutherford scattering cross-section for a reasonable estimate of short-circuit current degradation. A sharp decay of open circuit voltage at low proton energies is also demonstrated by the theory.

Authors

A THEORETICAL MODEL FOR LOW-ENERGY PROTON IRRADIATED SILICON SOLAR CELLS

H. Y. Tada
TRW Systems
One Space Park
Redondo Beach, California

Introduction

Many theoretical analyses have been made in the past concerning the spectral response of a photovoltaic cell.[1-6] These analyses are useful for the radiation damage study of photovoltaic cells when the radiation-induced damage is uniformly distributed throughout the cell. However, if the damage does not extend to the back face, as in the case of low-energy proton irradiation, the reduction of minority carrier lifetime becomes depth dependent, and hence, these analyses are no longer applicable. In fact, the radiation creates an extra boundary at the interface between damaged and undamaged regions.

An extra boundary condition imposed at the radiation-induced interface and the inhomogeneity of physical properties in the two regions alter the solution of steady state continuity equation. Moreover, light illumination induces a photovoltage across the interface of two regions, as reported by Esposito and Loferski.[7] As for low energy proton experimental results, Almelch, et al[8] and Downing[9] have reported that degradation of open circuit voltage takes place at much faster rate than that of short-circuit current. This is in contrast with the earlier observations under penetrating radiation, in which degradation of open circuit voltage is relatively small in comparison with that of short-circuit current.

In order to study and analyze the low-energy proton irradiated photovoltaic cell and to comprehend peculiar phenomena associated with it, a simple model is proposed. The model is for a low carrier injection, which is considered to be adequate for the short-circuit current condition and, to some extent, for the open circuit voltage condition, as long as the number of majority carriers removed by radiation is not substantial. At a high carrier injection, a set of continuity and auxiliary equations, governing minority and majority carrier concentrations, leads to a non-linear differential equation. Therefore, the solution of linear differential equations does not account for conductivity modulation taking place in the base region when high currents flow and when a substantial number of majority carriers are removed by radiation. A change in slope of the I-V characteristic with radiation is therefore not accounted for in the linear analyses.

The proposed model includes a possible field existing in the diffused layer due to the impurity concentration gradient. The radiation damage is expressed in terms of change in diffusion length and minority carrier

concentration. Each region, either damaged or undamaged, is assumed to possess unique physical properties; that is to say, it is assumed that the radiation-induced recombination centers are uniformly distributed in each region. Although conductivity modulation and the subsequent change in the slope of I-V characteristic are not included in the analysis, a possible contribution of photo-induced voltage across a radiation-induced interface to a degradation of open circuit voltage is considered. The solutions for short-circuit current and open circuit voltage are obtained in an analytical form from linear differential equations. The numerical computations are performed with the aid of a computer, and the computed results are compared with experimental data in order to examine the adequacy of the model.

Theoretical Considerations

Basic Equations and Approximations

Before describing the model in detail, let us examine approximate carrier injection level in a typical silicon photovoltaic cell. According to geometrical and physical parameters of a typical cell, listed in Appendix I, the injected carrier concentration in the diffused layer is much smaller than the majority carrier concentration at thermal equilibrium. The minority carrier concentration in the base region, on the other hand, may become comparable to the majority carrier concentration when high currents flow and when the carriers removed by radiation become substantial. Then, the concentration of minority carriers near the junction probably exceeds that of majority carriers due to the diffusion of minority carriers from the diffused layer. In this case the majority carriers have to adjust their concentration with the external supply in order to maintain charge neutrality. This extra supply of majority carriers thus modulates the conductivity in the base region, and consequently, the beta changes with the current level and radiation dose. When a high current flows and an accumulated radiation dose is high, the small carrier injection level model presented here is thus inadequate to describe photovoltaic action even under an ordinary laboratory light source. However, under moderate irradiation and standard laboratory light sources, the low injection level model presented below is adequate.

The continuity and auxiliary equations governing the behavior of minority and majority carrier concentrations are:

$$\frac{\partial p}{\partial t} = g_p - \frac{p - p_o}{\tau_p} - \frac{1}{q} \vec{\nabla} \vec{J}_p \qquad (1)$$

$$\frac{\partial n}{\partial t} = g_n - \frac{n - n_o}{\tau_n} - \frac{1}{q} \vec{\nabla} \vec{J}_n \qquad (2)$$

$$J_p = q \mu_p E - q D_p \vec{\nabla} p \qquad (3)$$

$$\vec{J}_n = q\,\mu_n\,\vec{E} + q\,D_n\,\vec{\nabla} n \tag{4}$$

$$\vec{J} = \vec{J}_n + \vec{J}_p \tag{5}$$

For a completely ionized semiconductor, Poisson's equation becomes:

$$\vec{\nabla}\cdot\vec{E} = \frac{4\pi q}{\epsilon}\left(p - n + N_d - N_a \right) \tag{6}$$

Regardless of n- or p-type, the problem is to solve the above six simultaneous equations with suitable doping concentrations and boundary conditions. The equations can be simplified with the following assumptions:

a. Only steady state is considered ($\frac{\partial p}{\partial t} = \frac{\partial n}{\partial t} = 0$)

b. The photovoltaic cell is a thin large area planar junction device. A contribution of surface states to electrical parameters at other than front and back faces is negligible so that the three dimensional equation can be reduced to one dimension.

c. A constant electric field exists in the diffused layer due to the impurity concentration gradient. This assumption is reasonable, as discussed in Appendix II.

d. The commonly used n on p configuration is considered.

e. The acceptor concentration is constant throughout the cell.

f. A small carrier injection level is considered in the base region.

g. The low-energy proton induced damage is uniform to the depth of the proton range. Unique physical properties, such as minority carrier diffusion length, are associated with each conveniently divided region, either damaged or otherwise, and do not vary with spatial coordinate within the region.

Since the assumptions in each region differ, the derivation of the differential equation is briefly discussed.

In the n-type diffused (surface) region, charge neutrality requires

$$p - n + N_d - N_a = 0 \tag{7}$$

No accumulation of current requires

$$\vec{\nabla}\cdot\vec{J} = 0 \tag{8}$$

If only the first order effect of concentration gradient is considered, then

$$\nabla^2 N_d = 0 \tag{9}$$

By taking a gradient of equation 7 and substituting an assumed condition $\vec{\nabla} N_a = 0$

$$\vec{\nabla} n = \vec{\nabla} p + \vec{\nabla} N_d \tag{10}$$

$$\vec{E} = \frac{\vec{J} - q D_p \left[(\gamma - 1) \vec{\nabla} p + \gamma \vec{\nabla} N_d \right]}{q \mu_p \left[p(\gamma + 1) + \gamma (N_d - N_a) \right]} \tag{11}$$

$$\gamma = \mu_n / \mu_p > 1 \tag{12}$$

Then, by eliminating $\vec{\nabla} \cdot \vec{J}_p$ in equation 1, with the use of equations 3 and 11,

$$\frac{\partial p}{\partial t} - g_p + \frac{p - p_o}{\tau_p} = \frac{-1}{q\gamma(N_d - N_a)\left[1 + p(\gamma+1)/(N_d - N_a)\gamma\right]^2}$$

$$\left\{ \left[\vec{J} - qD_p \gamma \vec{\nabla} N_d \left(1 - \frac{\gamma - 1}{\gamma} \frac{p}{N_d - N_a} \right) \right] \cdot \vec{\nabla} p - qD_p (\gamma - 1) \nabla^2 p - qD_p (2p + N_d - N_a) \left(\frac{p}{N_d - N_a} \frac{\gamma + 1}{\gamma} + 1 \right) \gamma \nabla^2 p \right.$$

$$\left. - \frac{p \vec{J} - qD_p \gamma p \vec{\nabla} N_d}{N_d - N_a} \cdot \vec{\nabla} N_d \right\} \tag{13}$$

As discussed in Appendix I, a small carrier injection model is adequate in this region. The conditions are

$$p/(N_d - N_a) = (p_o + p')/(N_d - N_a) \ll 1 \tag{14}$$

$$N_d \approx n = n_o + n' \tag{15}$$

Then, equation 13 in the steady state becomes

$$D_p \nabla^2 p - \mu_p \vec{E} \cdot \vec{\nabla} p - \frac{p - p_o}{\tau_p} = -g_p \tag{16}$$

The term g_p is the hole generation rate in the diffused layer and takes the following form under illumination with a spectrum $\varphi(\lambda)$.

$$g_p(X) = \int_0^{\lambda g} \left[1 - R(\lambda) \right] \alpha(\lambda) \varphi(\lambda) e^{-\alpha X} \, d\lambda \tag{17}$$

The term $\eta(\lambda)$ is the quantum efficiency and $R(\lambda)$ is the spectral reflection coefficient.

According to the simplified assumption in the p-type base region

$$N_d = 0, \quad \vec{\nabla} N_d = 0, \quad \vec{\nabla} N_a = 0, \tag{18}$$

and equation 7 becomes

$$n = p - N_a \tag{19}$$

$$\vec{\nabla} n = \vec{\nabla} p \tag{20}$$

If the carrier injection level is high so that the minority carrier concentration becomes comparable to the majority carrier concentration ($n \cong N_a$), equations 1 through 6 lead to non-linear differential equation, given by

$$\nabla^2 n + \frac{1-\gamma}{3n(\gamma+2)} (\vec{\nabla} n)^2 + \frac{\gamma \vec{J}}{3qD_n(\gamma+2)n} \cdot \vec{\nabla} n - \frac{\gamma+2}{3D_n \tau_n} (n-n_o) = \frac{\gamma+2}{3D_n} g_n \tag{21}$$

To overcome the difficulties in solving non-linear differential equations, a small carrier injection model is adopted as previously discussed. For small carrier injection, $n/N_a \ll 1$, and equations 1 through 5 reduce to

$$D_n \nabla^2 n - \frac{n - n_o}{\tau_n} = - g_n \tag{22}$$

This is an equation commonly used for spectral analyses of photovoltaic cells. The g_n in equation 22 is the generation rate of electrons in the base region and takes the same form as written in equation 17.

Boundary Conditions

The consideration of an additional boundary at the interface between damaged and undamaged regions will provide the cases for both low- and high-energy proton radiation. Statistical fluctuation of mean free path of primary knock-ons, cascade processes of knock-ons, and diffusion of knock-ons into an undamaged region would presumably contribute to widen the width of interface. However, as long as this width is comparable to or narrower than the estimated width of the depletion region (about 1,000 Å), the location of interface can be defined with the same order of accuracy as that of depletion region, and an additional complication involved in the physical processes associated with the finite width, if any, can be ignored in the same degree as those associated with the depletion region. The location of such an interface is taken as the depth comparable to the range of incident proton.

With the above considerations, a photovoltaic cell may be divided into three regions, the surface diffused layer and the damaged and undamaged base regions where the depth of the damaged region, denoted by b, varies with the incident proton energy. If the proton energy is sufficiently low, it is quite possible that the induced damage lies only in a surface layer, but this case is not considered here. Equation 16 is applicable only to the surface region, whereas equation 22 is applicable to the base region, regardless of damaged or undamaged.

Boundary conditions are expressed in terms of physical parameters some

of which change with radiation. At the front and back faces of the cell, the boundary conditions take the usual form in terms of surface recombination velocity and of a field due to impurity concentration gradient, and are given by

$$\left.\frac{d\,p}{d\,x}\right|_{x=0} = \left(\frac{s(0)}{D_p} - \frac{\mu_p E}{D_p}\right) p(0) \tag{23}$$

$$\left.\frac{dn_2}{dx}\right|_{x=c} = -s(c)\, n_2(c)/D_n \tag{24}$$

Under short-circuit current conditions, the minority carriers are swept out in the depletion region and the junction can be regarded as a sink. Therefore, at the junction

$$p(a) = 0 \tag{25}$$

$$n(a) = 0 \tag{26}$$

At the interface between damaged and undamaged regions, the continuity of electron diffusion current requires,

$$\left.\frac{d\,n_1}{d\,x}\right|_{x=b} = \left.\frac{d\,n_2}{d\,x}\right|_{x=b} \tag{27}$$

Even though the minority carrier concentration in thermal equilibrium changes with radiation, the concentration is much smaller than that of injected carriers by illumination. Therefore, for all practical purposes, minority carrier concentration in both damaged and undamaged regions can be regarded as equal across the interface.

$$n_1(b) = n_2(b) \tag{28}$$

At this point, it is worthwhile to examine a possible shift of Fermi level (relative to intrinsic level) across the interface due to radiation-induced defects. It is true that the use of Fermi level is meaningful only when a cell is in a thermal equilibrium so that it is in the same level throughout the cell, regardless of radiation damage or of n- or p-type. But "the shift of Fermi level" is used in a relative sense so that the shift across the interface could result in the creation of barrier. The exact location of Fermi level can be determined by solving an equation for the conservation of charge, expressed in terms of the concentration of induced defects and residual impurities and their energy levels. Unfortunately, the equation contains higher degree exponents in terms of the differences between Fermi level and either defect or impurity level, and it is rather difficult to solve for the Fermi level. Furthermore, since both induced defect levels and defect introduction rates are unknown at low energies, no attempt has been made to determine the Fermi level.

For a strong p-type semiconductor with one impurity level, the Fermi level relative to intrinsic level may be approximated by

$$\varphi_i - \varphi_f = k\,T \ln \frac{N_a - N_d}{n_i} \qquad (29)$$

The shift due to effective impurity concentration induced by radiation, denoted by prime, is therefore,

$$\Delta\varphi = \varphi_f - \varphi_f' \approx kT \ln \frac{N_a' - N_d'}{N_a - N_d} \qquad (30)$$

Suppose that an appreciable degradation of minority carrier lifetime takes place when the radiation induced defect density is of the order of 10^{13} defects/cc. Since the residual impurity concentration in the base region is of the order of 10^{15} impurities/cc, the shift of the Fermi level is a small fraction of kT.

Under open circuit voltage condition, the Fermi level is disturbed from the thermal equilibrium position to a quasi-Fermi level due to the injected carriers by illumination, some of which recombine either in the bulk or at the surface, until they reach an equilibrium. The amount of disturbed level by carrier injection is thus related to an equilibrium concentration of both minority and majority carriers across the boundary. As discussed in Appendix III and in reference 10, a photo-induced emf is given by

$$V_j = \frac{1}{\beta}\left(\ln \frac{p_n}{p_{no}} - \ln \frac{p_p}{p_{po}} \right) \qquad (31)$$

If the injected carrier density is small compared with the majority carrier concentration, $p_p \cong p_{po}$, and

$$V_j = \frac{1}{\beta} \ln (p_n/p_{no})$$

$$= \frac{1}{\beta} \ln (p_n'/p_{no} + 1) \qquad (32)$$

This is an approximation that Shockley has used in the derivation of the original diode equation[11], in which V_j is an applied voltage across a p-n junction, instead of a photo-induced emf. The boundary condition the junction, according to equation 32, are

$$p'(a) = p_{no} (\exp V_j - 1) \qquad (33)$$

$$n_1'(a) = n_{10} (\exp V_j - 1) \qquad (34)$$

The equations 23 through 28 constitute a set of boundary conditions for a short-circuit current. If the equations 25 and 26 are replaced with the equations 33 and 34, the set of equations are boundary conditions for an open circuit.

It should be noted that V_j appearing in the equation 31 through 34 is a photoinduced open circuit voltage across the junction but does not represent a true measurable quantity across a photovoltaic cell. Since the current does not flow out of a cell, no voltage drop is expected through a series resistance, consisting of surface and bulk resistances and of ohmic resistance at the front and back faces. If an incident proton energy is low, however, the radiation induces damaged and undamaged regions in the base, and an additional photo-induced emf, denoted by V_i, is produced at the interface due to the inhomogeneity of physical properties in the two regions, as discussed in Appendix III. Under the assumptions made in Appendix III, V_i is given by

$$V_i = \frac{1}{\beta} \ln (n_{10}/n_{20})$$

$$= \frac{-1}{\beta} \ln (n_{20}/n_{10}) \quad (n_{10} \geq n_{20}) \tag{35}$$

A measurable open circuit voltage across the cell, V, becomes

$$V = V_j - V_i \tag{36}$$

and the short-circuit current densities for electrons and holes are

$$J^n_{sc} = q D_n \left.\frac{dn_1}{dx}\right|_{x=a} \tag{37}$$

$$J^p_{sc} = -q D_p \left.\frac{dp}{dx}\right|_{x=a} \tag{38}$$

The field term in equation 3 disappears in equation 38, because of the short-circuit condition expressed in the equation 25. The total short-circuit current then becomes,

$$J_{sc} = J^n_{sc} + J^p_{sc} \tag{39}$$

Solutions

A solution of equation 16 for the minority carriers in a diffused layer, takes a form given by

$$p = A_o e^{r_1 x} + B_o e^{r_2 x} - \int_0^{\lambda_g} \frac{\alpha \tau_p (1 - R)}{\alpha^2 L_p^2 + \alpha \mu_p E \tau_p - 1} \eta \varphi e^{-\alpha x} \, d\lambda \tag{40}$$

$$r_1 = \frac{\mu_p E}{2D_p} + \sqrt{\left(\frac{\mu_p E}{2D_p}\right)^2 + 1/L_p^2} \tag{41}$$

$$r_2 = \frac{\mu_p E}{2D_p} - \sqrt{\left(\frac{\mu_p E}{2D_p}\right)^2 + 1/L_p^2} \tag{42}$$

A solution of equation 22, for electrons in the base region, is given by

$$n = A_1 e^{x/L_1} + B_1 e^{-x/L_1} - \int_0^{\lambda_g} \frac{\alpha \tau_1}{\alpha^2 L_1^2 - 1} (1 - R)\, \eta\, \varphi\, e^{-\alpha x}\, d\lambda \qquad (43)$$

Since two regions, damaged and undamaged, are considered in the base, there are two solutions in the base, which are exactly the same form as equation 43, provided that each solution reflects unique physical properties of the region, expressed in terms of minority carrier lifetime or diffusion length. Coefficients, A_o, B_o, and so on, are subject to six boundary conditions and are determined by six simultaneous equations.

The short-circuit current is expressed in equation 39 and the open circuit voltage is given by

$$V_{oc} = \frac{1}{\beta} \ln (J_{sc}/J_o + 1) - V_i \qquad (44)$$

The J_{sc}^n, J_{sc}^p, and J_o are as follows.

$$J_{sc}^p = \frac{q}{m \cosh ma + (s_o - \ell) \sinh ma} \int_0^{\lambda_g} \frac{\alpha(\alpha + s_o)}{\alpha^2 + 2\alpha\ell - 1/L_p^2} \left\{ m e^{\ell a} - \left[(\alpha + \ell) \sinh ma + m \cosh ma \right] e^{-\alpha a} + \alpha \sinh ma\, e^{-\alpha a} \right\} \zeta(\lambda)\, d\lambda \qquad (45)$$

$$J_{sc}^n = q \int_0^{\lambda_g} \frac{\alpha L_1}{\alpha^2 L_1^2 - 1} \left\{ \left[\left(\frac{\Delta_2}{L_2} \sinh y_1 - \frac{\nabla_2}{L_2} \cosh y_1 \right) + \alpha L_1 \left(\frac{\nabla_2}{L_2} \sinh y_1 \frac{\Delta_2}{L_1} \cosh y_1 \right) \right] e^{-\alpha a} + \left(\frac{\nabla_2}{L_2} + \alpha \Delta_2 \right) e^{-\alpha b} \right\} \zeta(\lambda) d\lambda / \left(\frac{\nabla_2}{L_2} \sinh y_1 - \frac{\Delta_2}{L_1} \cosh y_1 \right)$$
$$+ q \frac{L_2}{L_1} \int_0^{\lambda_g} \frac{\alpha L_2}{\alpha^2 L_2^2 - 1} \frac{(\alpha + s_c) e^{-\alpha c}/L_2 - (\nabla_2/L_2 + \alpha\Delta_2) e^{-\alpha b}}{(\nabla_2/L_2) \sinh y_1 - (\Delta_2/L_1) \cosh y_1} \zeta(\lambda) d\lambda \qquad (46)$$

$$J_o = q \left\{ D_p p_{no} \left[s_o + \frac{\left[m^2 - (s_o - \ell)^2 \right] \sinh ma}{(s_o - \ell) \sinh ma + m \cosh ma} \right] - \frac{D_n n_{10}}{L_1} \frac{(\Delta_2/L_1) \sinh y_1 - (\nabla_2/L_2) \cosh y_1}{(\nabla_2/L_2) \sinh y_1 - (\Delta_2/L_1) \cosh y_1} \right\} \qquad (47)$$

$$m = \ell + \sqrt{\ell^2 + 1/L_p^2} \qquad (47')$$

$$\ell = \mu_p E / 2 D_p \qquad (48)$$

$$s_o = s(0)/D_p - 2\ell \qquad (49)$$

$$s_c = - s(c)/D_n \tag{50}$$

$$y_1 = (b - a)/L_1 \tag{51}$$

$$y_2 = (c - b)/L_2 \tag{52}$$

$$\Delta_2 = \frac{1}{L_2} \cosh y_2 + \frac{s(c)}{D_n} \cosh y_2 \tag{53}$$

$$\nabla_2 = \frac{1}{L_2} \sinh y_2 + \frac{s(c)}{D_n} \cosh y_2 \tag{54}$$

$$\zeta(\lambda) = \eta(\lambda) \left[1 - R(\lambda) \right] \varphi(\lambda) \tag{55}$$

The term $\varphi(\lambda)$ is the spectral irradiance of the light source, expressed in terms of the number of photons per cm^2 per second per unit wavelength. Therefore, if $\varphi'(\lambda)$ is a spectral irradiance in the unit of watts/cm^2-micron and if the λ is expressed in the unit of micron

$$\varphi = 5.04 \times 10^{18} \varphi' \lambda \tag{56}$$

Equations 39, 45, and 46 take exactly the same form as those obtained by other investigators[1-4], if the radiation induced interface b approaches the back face c. Then, the solution is applicable to the case of penetrating radiation. Although equation 44 is for an open circuit voltage, this relationship can be immediately be reduced to Shockley's diode equation[11], if (a) V_j is ignored, (b) V_{oc} is regarded as an applied voltage, (c) both surface and field terms are ignored, and (d) the cell geometry is extended to infinity.

Correlation with Experimental Results

The adequacy of the proposed model can be tested by comparing the calculated values with low energy proton experimental results. For this, equations 44 through 47 are programmed in Fortran IV language and computed with the aid of IBM 7094 computer. The means for determining parameter values, the implication and justification of such method, and a method of correlating the calculated values with experimental results are briefly discussed below.

Determination of Parameters

Damage Depth, b - The most important parameter that enters in the solution is the depth of damage, denoted by b. As a first order approximation, the depth may be taken as the range of the low energy proton. However, since the depth of defects created by low energy protons may not be exactly a proton range, this approximation may be inadequate. This is because the proton range is determined almost entirely by ionization in the solid rather than by elastic collisions and the subsequent processes involved in defect production (collision between knock-on atoms and atoms in lattice

sites as well as defect migration) are not accounted for. Unfortunately, it is a difficult task to determine the actual defect depth with a reasonable accuracy because of statistical fluctuations involved in cascade displacement collisions; however, this error is most probably small until ranges as low as a few microns are considered.

Further complications are manifested by an inhomogeneous defect distribution. It is known that an approximate primary displacement cross section is inversely proportional to the incident proton energy when Rutherford scattering dominates. If the total cross section (including higher order displacement collisions) follows such energy dependence to a low cutoff energy, an extremely high defect concentration and concentration gradient is expected near the end of proton path. It is likely that the defects will probably move about and migrate into an undamaged region, increasing the depth somewhat and diffusing a sharply defined boundary as the radiation progresses. Suppose that the defects created near the end of proton path migrate into undamaged region. Since the induced defect concentration and concentration gradient near the end of path is almost identical regardless of incident proton energy, except perhaps those effects by straggling, an increase in the depth by migration will be almost the same regardless of the energy. Therefore, if defect migration is assumed, a fractional increase in the depth is expected to be larger for lower proton energies.

If the experimentally observable quantity is relatively sensitive to b, and if the defect migration actually takes place, obvious inductions are:

a. The deviation of calculated values from experimental results will be larger for lower proton energies.

b. The deviation will also be larger at larger integrated flux.

c. If the experimentally observed quantities change with time after receiving a given dose, the time rate of change will be larger when irradiated with lower proton energies.

Minority Carrier Concentration, P_{no}, n_{10}, and n_{20} - In order to calculate open circuit voltage, the change in minority carrier concentration under irradiation is required. These values of minority carrier concentration are taken from experimentally observed changes in majority carrier removal rate as a function of proton energy and integrated flux.

Since the majority carrier concentration in the shallow diffusion layer is of the order of 10^{18} carriers/cc or greater, the integrated flux required to remove a significant fraction of these carriers is far beyond the limits of interest of the operation of a solar cell as a photovoltaic device. Hence, it is assumed that majority and minority carrier concentration in the diffused layer is constant over the range of integrated fluxes of normal interest in photovoltaic devices. On the other hand, the majority

carrier concentration in the base region is usually of the order of 10^{15} carriers/cc, and hence, the change in carrier concentrations as a function of irradiation cannot be ignored. Generally, however, these changes in carrier concentrations tend to become significant only after considerable change in minority carrier lifetime and corresponding changes in the short-circuit current of the order of 40 to 50% degradation.

The dependence of carrier removal rate on proton energy at low energies is unknown. Hall coefficient measurements, from which the carrier removal rate was deduced, were performed after irradiation with relatively high energy protons (above 10 Mev)(12), in order to introduce more or less homogeneous defects. These experimental points at high energies may be extrapolated back to lower energies, in reference with the energy dependence of either Rutherford scattering cross section or the damage constant for minority diffusion length. Such extrapolation implies that the defects are predominantly introduced by the primary processes of Rutherford scattering, that the nature of defects is identical regardless of proton energy in this range, and that one defect level is dominantly controlling the carrier removal rate, based on the above assumptions and adopted for the subsequent calculation, is shown in Figure 1.

As for the dependence of carrier removal rate on an integrated flux, it is apparent that if the defects are dominantly introduced at one level but the density is small (at a small integrated dose), the number of carriers removed is approximately proportional to the defect density, and hence to the integrated flux. At a sufficiently large integrated flux, however, such a simple relationship may no longer hold, especially when a fractional change in the majority carrier concentration by radiation approaches unity, as demonstrated by Wertheim in his electron experiments(13). The carrier concentration then depends on those parameters that determine the Fermi level, such as nature of the defect, defect density introduced, residual impurity concentration, their energy levels, etc. In the subsequent calculation, it is assumed that one level is controlling the carrier removal, that the material does not change polarity even at a large integrated dose, and that the carrier removal rate is not constant at a high integrated dose and follows the pattern observed by Wertheim in his electron experiments. The values adopted in the computation, according to the above assumptions, are shown in Figure 2.

Other Parameters - It is quite probable that quantum efficiency can be other than unity at high photon energies but sharply drops to zero near the energy corresponding to energy gap. Although some investigations have been done on the quantum efficiency, which is as high as 5 in ultraviolet region, the data probably contain a large error due to the fact that the values were reduced from solar cell experiments with an over-simplified equation. In the subsequent calculation, unit quantum efficiency is taken throughout the spectrum.

Although surface reflection coefficient varies with both incident angle and wavelength, only normal incidence is considered. Thus, the

reflection coefficient is a function of only wavelengths and the values are taken from published data in reference 14.

The dependence of absorption coefficient on wavelength is taken from reference 15.

Both tungsten and sun simulator light sources, which were used in the experiments, are calibrated and used for the calculation.

Correlation with Experiments

The low-energy proton experimental results to which these computations will be compared are those performed at TRW Systems covering the energy ranges of 0.2 Mev to 1.9 Mev[9] and 6.7 Mev to 26 Mev[16]. In these experimental results, the degradation of short-circuit current and open circuit voltage are expressed in terms of integrated proton flux. Thus, the calculated values can be correlated with experiments if the degradation of minority carrier diffusion length in the damaged base region is expressed in terms of integrated flux. This can be easily done with the use of an empirical equation for the minority carrier diffusion length of irradiated silicon given by

$$\frac{1}{L^2} = \frac{1}{L_o^2} + K\,\Phi \qquad (57)$$

where L : Minority carrier diffusion length after radiation
L_o : Minority carrier diffusion length before radiation
K : Damage constant
Φ : Integrated flux

In the above equation, the damage constant (or K value) is a strong function of many material and environmental factors. Therefore the K values used in this comparison are for alike types of silicon under proton irradiation.

The energy dependence of K value has been experimentally studied by many investigators[16,17], using either solar cells or bulk specimens. The conventional method for the measurement of diffusion length employing solar cells, however, does not lead to an explicit value at low proton energies since the damage is not uniform in the active region. In this respect, the published K values are assumed to be acceptable for proton energies down to about 6 or 7 Mev for solar cell type experiments.

Since experimental K values at lower energies are not available, the experimental energy dependence of K values at higher energies[16] are extrapolated to lower energies on the basis that the theoretical Rutherford scattering model is adequate. From the K values at low proton energies determined in this fashion, an integrated flux required to degrade the diffusion length from the initial value L_o to L is determined from equation 57.

Since an electrical parameter is a function of the diffusion length in the damaged region and since the diffusion length and integrated flux are correlated with the use of the extrapolated K value, the computed electrical parameter can be plotted against an integrated flux for comparison with experimental results. The energy dependent K values used for an evaluation of the proposed model are shown in Figure 3.

Since the equation 57 is exclusively used for relating the computed parameters to integrated flux, the method described above is based on the premise that equation 57 holds regardless of proton energies and that only the K value is energy dependent. Further, it is assumed that the diffusion length calculated in this manner is uniform over the damaged region at the value corresponding to that computed for the incident proton energy thus neglecting energy loss in the traverse of the damaged region. Another important aspect for correlation is that the electrical parameter considered be very sensitive to the minority carrier diffusion length in the damaged region. In this respect, short-circuit current is an ideal parameter.

Results and Discussions

Effects of Field and Surface Recombination Velocity on Short-Circuit Current

The contribution of both surface recombination velocity and field in the diffused layer to short-circuit current under a tungsten light is demonstrated in Figure 4.

Surface recombination velocity hardly affects short-circuit current measured under a tungsten light, unless the velocity becomes of the order of 10^{13} cm/sec. This result is somewhat obvious for a tungsten light spectrum for which the number of electron-hole pairs produced in the surface region is very small compared with that in the base region. The effect of surface recombination velocity can also be compared with that of hole transit velocity across the surface region (α/τ); the surface recombination velocity does not affect the hole current appreciably unless it satisfies an approximate condition, $s \gg \alpha D_p/L_p$.

The contribution of field due to impurity concentration gradient is more significant than that of surface recombination. However, the magnitude of total short-circuit current does not change significantly, unless the field approaches 10^3 volts/cm. If the hole diffusion length is comparatively large so that $L_p \gg 2D_p/\mu_p E$, the process is essentially diffusion limited and the field contribution is negligible. But if both hole diffusion length and mobility degrade as the radiation progresses, carrier drift becomes predominant over the diffusion, and the existance of a field will result in some radiation resistance.

Under tungsten light, carrier injection in the surface region is small compared with that in tha base region, and the surface field will make a negligible contribution to short-circuit current, unless hole diffusion length degrades appreciably. If the short-circuit current is plotted against

the degraded base diffusion length under penetrating radiation with consideration of both constant field and degraded hole diffusion length, an agreement between the theoretical curve and experimental points is better without a field term. This implies that an average field in irradiated cells is small enough to be ignored or that the magnitude of field may be large but the field extends to only over a small portion of surface layer. For this reason, the field term is ignored in the subsequent computation.

Short-Circuit Current and Diffusion Length

Computed short-circuit current is plotted against diffusion length in the damaged base region in Figures 5 and 6. The figures are normalized at a diffusion length of 100 microns and a short-circuit current of 25 ma/cm^2 for tungsten spectrum and of 29.5 ma/cm^2 for sun simulator spectrum. As seen in Figure 5, when the radiation introduced damage is uniform throughout the cell, the short-circuit current plotted against a logarithm of diffusion length becomes a straight line under tungsten illumination. This relationship has been experimentally established by Denney et al;[18] however, the computed results agree with experimental results surprisingly well. Under penetrating radiation the short-circuit current can be expressed as

$$J_{sc} \propto \text{Log } L_n \qquad (57)$$

The above straight line relationship is, in a sense, fortuitous and attributed primarily to the tungsten spectrum, the cell configuration and the silicon absorption coefficient. In the computation of short-circuit current under sun spectrum, surface damage by radiation is assumed to be negligible. It is expected that the straight line relationship may fail under a sun spectrum because of the large photon population in the blue region which produces a large number of carriers near the junction, whereas the tungsten spectrum produces carriers mostly in the base region. The degradation of short-circuit current is thus slower under a sun spectrum than under a tungsten spectrum. This trend is clearly evident in Figure 5, in which no damage is assumed for hole diffusion length in the surface layer. Although the experimental data fits the theoretical curve quite closely, the slight bend in the theoretical curve is not evident in the experimental data.

The situation becomes quite different for low-energy protons which produce only partial damage in the sensitive base region (see Figure 6). As the energy becomes lower, the curve deviates from a straight line. At about 0.2 Mev, the computed degradation of short-circuit current is practically negligible, unless the diffusion length in the damaged base region becomes comparable to the depth of damaged base region. When the diffusion length in the damaged region becomes comparable to the depth of damaged base region, only a small fraction of the carriers generated in the undamaged region can pass through the damaged region without suffering recombination.

Short-Circuit Current and Integrated Flux

Computed short-circuit currents as a function of integrated flux under

tungsten light are compared with the experimental results of reference 9, in Figures 7 through 12, for various proton energies. At proton energies of 0.5, 1.0, 2.0, and 10 Mev, not only the magnitude of computed short-circuit current but also the slope of the degradation characteristic agree with the experimental results very well. The largest discrepancy between theoretical and experimental values is less than 6% for the magnitude of short-circuit current and is less than 20% for the integrated flux. Therefore, the proposed model seems to be quite adequate in this proton energy range. However, theoretical values substantially deviate from experimental results for 0.2 and 0.3 Mev protons; the magnitude of short-circuit current deviates as much as 12% and the integrated flux a factor of 8 (see Figure 13).

The large discrepancies observed at 0.2 and 0.3 Mev may be the result of several factors. Considerable room temperature annealing was reported in the experimental data and, further, the annealing was reportedly worst at the lower energies where the degradation rates were so low that higher beam currents were required in the conduct of the experiment. Thus the possibility of localized heating with subsequent annealing of damage is more likely to occur at these lower energies. In this respect, the discrepancy between theoretical and experimental results shown in Figures 11 and 12 is at least in the right direction.

Contrary to the assumptions made in this model, expected inhomogeneous defect distribution and spatially dependent diffusion length in the damaged region may be a primary contributor to the discrepancy. If equation 57, extrapolated K values, and range-energy relationships of protons in silicon are literally and seriously considered for mapping the diffusion length in the damaged region, the spatial dependence under irradiation with 0.3 Mev protons is as shown in Figure 14. Although some averaging processes are expected to take place near the end of proton range due to energy straggling, it is so obvious from the figure that the assumption made for this model, namely, spatially independent diffusion length in the damaged region, becomes increasingly inadequate as the proton energy is decreased.

Although each of the above reasons is plausible, it is not conclusive that either one is a primary contributor to the discrepancies between theoretical and experimental results at 0.2 and 0.3 Mev. At these energies, therefore, a simple conclusion cannot be drawn; however, the model seems to be adequate at 0.5 Mev and higher energies. Moreover, when this model is used to describe the short-circuit current degradation under mono-energetic proton flux, it appears that the energy dependent K value can safely be extrapolated back to about 0.5 Mev.

Open Circuit Voltage and Integrated Flux

The computed open circuit voltage under tungsten light, together with experimental data from reference 9, are plotted for 0.2, 0.5, 1.0, and 2.0 Mev protons in Figures 15 through 18. The integrated flux is determined from the extrapolated K value as discussed before.

Although the theory is able to demonstrate the experimental decay slope of open circuit voltage with respect to proton flux, the difference in the magnitude between them is larger than the cases of short-circuit current. The theory agrees with the experiments very well at the proton energy of 1 Mev, but it overestimates the damage at lower energies and underestimates at higher energies.

The causes of this disagreement may be attributed to those already discussed in connection with the short-circuit current. There are however, additional possible causes for the large discrepancies.

The boundary conditions at the junction used by Shockley[11] (equation 32) are adequate for small carrier injection if the p-n junction is located in an infinite bar. However, when applied to a solar cell, the adequacy may be affected by a finite geometry and an inhomogeneous minority carrier distribution in each region. The spatial dependence of minority carrier concentration might possibly be obtained from a set of boundary conditions which consider a finite geometry, the proton range, and an inhomogeneous induced defect density. Further, since the depth of induced defects is close to the junction at low energies, the carrier distribution is probably highly distorted from the uniform approximation. Thus, it may not be meaningful to define an average n_{10}, and hence V_i, in a small region near the space charge region.

Finally, annealing, as previously discussed, would increase the diffusion length, thereby increasing J_{sc} and decreasing J_o. As a consequence, a larger open circuit voltage would be expected at 0.2 and 0.5 Mev resulting in a closer agreement with experiments.

Conclusions

A simple model is presented to describe the effects of low energy proton bombardment on solar cells. By comparison with experimental results regarding short-circuit current versus degraded base diffusion length after irradiation with 10 Mev protons, the solution expressed in a closed form is adequate for a normal silicon solar cell.

The computed short-circuit current agrees with experimental results very well in the energy range from 0.5 to 10 Mev, provided that the damage constant (or K value) for minority carrier diffusion length in this energy range is obtained from the extrapolation of experimental data at moderately high energies. Unfortunately, the computed short-circuit current deviates from experimental results at 0.2 and 0.3 Mev. Although possible reasons for the discrepancy have been discussed in the test, the predominant cause is not known.

Although a sharp decay of open circuit voltage at low energies is demonstrated by the theory, the agreement with experimental results is not as good as short-circuit current case, except at 1.0 Mev. Since the open circuit voltage is expressed in terms of minority carrier concentration and since the spatial distribution is not uniform because of the finite geometry, the deficiency in the theory for the open circuit voltage may

be simply due to oversimplification in the boundary conditions.

The most significant result from the studies of short-circuit current are that, with the use of this model, experimentally observed damage constants at moderately high proton energies can be extrapolated back to lower energies and that the energy dependence of the K value based on Rutherford scattering and simple displacement theory is valid for proton energies above 0.5 Mev.

Acknowledgement

The author expressed his thanks to Mr. R. G. Downing and Dr. J. M. Denney for suggesting this problem and for technical assistance. He also expresses his sincere appreciation to Dr. R. E. Scott for many helpful discussions during this investigation.

Designation	Front Face	Junction	Defect Depth (Interface)	Back Face
Coordinate, x	0	a	b	c
Type	n-Type, Surface (Diffused) Layer		p-Type, Base Region	
Minority Carrier Concentration	p_n or p		n_1 or n_p	n_2
In Thermal Equilibrium	p_{no} or p_o		n_{10} or n_{po}	n_{20}
Injected	p'_n or p'		n'_1 or n'	n'_2
Majority Carrier Concentration	n_n or n		p_1 or p_p	p_2
In Thermal Equilibrium	n_{no} or n_o		p_{10} or p_{po}	p_{20}
Injected	n'_n or n'		p'_1 or p'_p	p'_2
Surface Recombination Velocity	s(o)			s(c)
Minority Carrier Lifetime	τ_p		τ_{n1} or τ_n	τ_{n2}
Diffusion Length	L_p		L_{n1} or L_n	L_{n2}
Diffusion Constant	D_p		D_n	D_n
Photo-Induced Voltage		V_j	V_i	

Table 1. Boundaries of the Low-Energy Proton Irradiated Solar Cell and the Associated Physical Parameters

APPENDIX I

Approximate Determination of Carrier Injection Level

The determination of carrier injection level is the first necessary step for establishing a proper model for a solar cell and for obtaining suitable boundary conditions. A typical n/p silicon solar cell produces the current density of about 30 ma/cm^2 under normal illumination. Other typical geometrical and physical parameters are:

Base region: $\rho_p = 5$ ohm-cm

$\tau_n = 6.4$ μ-sec

$D_n = 35$ cm^2/sec

$\mu_p = 330$ cm^2/volt-sec

Diffused surface layer:

$\rho_n = 0.01$ ohm-cm

$\tau_p = 0.01$ μ-sec

$D_p = 1$ cm^2/sec

$\mu_n = 200$ cm^2/volt-sec

Junction depth, $a = 0.5$ micron

Cell thickness, $c = 500$ microns

With the aid of the following four equations:

$$L^2 = D\,\tau \qquad \text{(I-1)}$$

$$\sigma = q\,(\mu_n\, n + \mu_p\, p) \qquad \text{(I-2)}$$

$$n_i^2 = n\,p \qquad \text{(I-3)}$$

$$J = q\,g_o \left[L_p \tanh (a/L_p) + L_n \tanh (c-a)/L_n\right] \qquad \text{(I-4)}$$

$L_n = 150$ microns

$L_p = 1$ micron

$p_{po} = 3.8 \times 10^{15}$ holes/cc

$n_{no} = 3.1 \times 10^{18}$ electrons/cc

$n_{po} = 5.9 \times 10^{4}$ electrons/cc

$p_{no} = 72$ holes/cc

In equation I-4, the first term is negligible compared with the second term

$$g_o \approx J/q\,L_n \qquad \text{(I-5)}$$

$$\doteq 1.25 \times 10^{19} \text{ charges/cc-sec}$$

Since the minority carriers injected in the base region predominantly contribute to the current,

$$n' = g_o \tau_n = 7 \times 10^{13} \text{ charges/cc}$$
$$p' = 10^{11} \sim 10^{12} \text{ charges/cc}$$

As a summary of the above rough calculations

(1) The injected minority carrier concentration is much larger than the minority carrier concentration in thermal equilibrium, i.e., $p' \gg p_o$ and $n' \gg n_o$.

(2) The majority carrier concentration, especially that in heavily dopped region, hardly changes with the illumination and is always much larger than the minority carrier concentration, i.e., $n_n \gg p_n$ and $p_p \gg n_p$.

APPENDIX II

Field in the Diffused Layer

The field in the diffused layer may be estimated from the following equation.

$$E = \frac{1}{\beta} \frac{1}{a} \ln \frac{N(x=a)}{N(x=0)} \qquad \text{(II-1)}$$

The $N(x=0)$ and $N(x=a)$ are the impurity concentrations at surface and junction, respectively. The junction will be formed in the neighborhood where the concentration of donor and acceptor is equal. According to the values calculated in Appendix I, the field due to the concentration gradient is of the order of 10^3 volts/cm,* which may be compared with the field necessary to support the injected carriers in this region.

Let us assume that p is of the order of 10^{12} charges/cc. Since the excess holes in the diffused layer are not neutralized by the fixed negative charges on the acceptor ions, the Poisson's equation immediately leads to the field necessary to maintain the injected carrier in the region considered,

$$E = - \frac{4\pi q p' a}{\epsilon} \qquad \text{(II-2)}$$

If the dielectric constant ϵ is 12, the necessary field is approximately 1.2×10^3 volts/cm, which is comparable to the field due to the concentration gradient. Therefore, the calculated built-in field is large enough to maintain the carriers in the diffused layer and hence cannot be ignored.

When the field calculated according to equation II-1 is used, the hole drift velocity is of the order of $10^4 \sim 10^5$ cm/sec, which is much larger than the surface recombination velocity of a normal commercial cell. Therefore, the field term affects short circuit current more than the surface term

---

* This value agrees with the value quoted by P. Iles, Hoffman Electronics Corp.[19] His estimate is about 2,500 3,500 volts/cm in the diffused layer; about one third to one half of the layer is estimated to maintain a fairly uniform impurity concentration so that the field there will make a negligible contribution to short circuit current.

(a typical surface recombination velocity is assumed to be about 200 to 500 cm/sec), which comes in the solution as the result of surface boundary condition.

A field of this magnitude can be of significance in relation to the minority carrier diffusion length. The solution for hole current includes the field term in such a manner that

$$r_1, r_2 = \mu_p E/2D_p \pm \sqrt{(\mu_p E/2D_p)^2 + 1/L_p^2} \qquad \text{(II-3)}$$

When the calculated values are used, the term $\mu_p E/2D_p$ is comparable to $1/L_p$. That is to say, the field term is as equally important as the surface diffusion length.

If $L_p \gg 2D_p/\mu_p E$, the process is diffusion limited. But, as the surface diffusion length degrades, the field term takes over, and the contribution of the surface layer to the short circuit current becomes primarily due to carrier drift rahter than carrier diffusion. In this respect, the field term becomes important for a cell receiving a large radiation exposure.

In conclusion, the field due to the impurity concentration gradient cannot be ignored if it is of the order of 10^3 volts/cm and if any one of the following conditions is satisfied:

(1) The injected carrier concentration in the diffused layer is less than 10^{12}/cc.

(2) The surface recombination velocity is of the order of 10^5 cm/sec or less.

(3) The surface diffusion length is less than 0.1 micron.

For a typical solar cell, the field term can be ignored in some cases but may play a dominant role, all depending on its magnitude in relation to other physical parameters.

APPENDIX III

Derivation of Equation 31 in the Text

The minority carrier concentration in the n-type material is related to the intrinsic electron concentration in such a manner that

$$p_{no} = n_i \exp \beta(\varphi_i - \varphi_f)$$

or $$\varphi_f = \varphi_i - \frac{1}{\beta} \ln (p_{no}/n_i)$$

The term φ_i is the intrinsic level and φ_f is the Fermi level. When carriers are injected by illumination, the Fermi level will shift. If the quasi Fermi level is denoted by φ_p

$$p_n = n_i \exp \beta(\varphi_i - \varphi_p)$$

$$\varphi_p = \varphi_i - \frac{1}{\beta} \ln (p_n/n_i)$$

Since $p_n > p_{no}$, $\varphi_f > \varphi_p$, the change in Fermi level by minority carrier injection in the n-type region is then

$$V_n = \varphi_f - \varphi_p = \frac{1}{\beta} \ln (p_n/p_{no}) \qquad \text{(III-1)}$$

Similary, hole concentration on the other side of junction also changes with carrier injection

$$p_{po} = n_i \exp \beta(\varphi_i - \varphi_f)$$

$$p_p = n_i \exp \beta(\varphi_i - \varphi_p)$$

The shift in the potential in p-type material, V_p is

$$V_p = \varphi_f - \varphi_p = \frac{1}{\beta} \ln (p_p/p_{po}) \qquad \text{(III-2)}$$

The potential difference across the junction, seen by holes, is just $V_n - V_p$,

$$V = V_n - V_p = \frac{1}{\beta} (\ln p_n/p_{no} - \ln p_p/p_{po}) \qquad \text{(III-3)}$$

A similar expression can be derived for electrons by replacing hole concentration with electron concentration. In many practical cases, the majority carrier concentration hardly changes with light illumination ($p_p \approx p_{po}$), and the last term in equation III-3 usually drops out.

The above line of thought can be extended to an inhomogeneous material. Suppose that p-type material consists of two uniform regions which

are distinguishable only by the minority carrier concentration in thermal equilibrium. Let one region be denoted by a subscript 1 and another by 2. Similar to the previous derivation, the shift of Fermi level in region 1 by illumination is

$$\beta V_1 = \ln (n_1/n_{10})$$

Similarly, the injected minority carrier concentration in region 2 induces

$$\beta V_2 = \ln (n_2/n_{20})$$

Then, the photo-induced voltage across the inhomogeneous material is found to be

$$V = V_2 - V_1$$

$$= \frac{1}{\beta} (\ln n_2/n_{20} - \ln n_1/n_{10}) \qquad \text{(III-4)}$$

If the concentration of injected minority carriers by illumination is large compared with that in thermal equilibrium, $n_1 \simeq n_2$ and

$$n_2 = n_{20} + n_2 \gg n_{20}$$

$$n_1 = n_{10} + n_1 \gg n_{10}$$

Then, the photo-induced voltage reduces to

$$V \approx \frac{1}{\beta} \ln (n_{10}/n_{20})$$

References

1 Kleinman, D. A., "Considerations on the Solar Cell," The Bell Sys. Tech. J., 40, 85, 1961

2 Loferski, J. J. and Wysocki, J. J., "Spectral Response of Photovoltaic Cells," RCA Review, 22, 38, 1961

3 Wolf, M., "Drift Fields in Photovoltaic Solar Energy Converter Cells," Proc. IEEE, 51, 674, 1963

4 Dale, B. and Smith, F. P., "Spectral Response of Solar Cells," J. Appl. Phys., 32, 1377, 1961

5 Oliver, J. W., "Charged Particle Radiation Damage in Semiconductors, II: Minority Carrier Diffusion Analysis in Photovoltaic Devices," Rpt. No. 8987-0001-RU-001, STL, Feb 1962

6 Cummerow, R. L., "Photovoltaic Effect in p-n Junctions," Phys. Rev. 95, 16, 1954

7 Esposito, R. M. and Loferski, J. J., "Investigation of the Photovoltaic Effect Associated with a Lifetime Gradient in a Semiconductor," Papers presented at the Conference of American Physical Society, April 1965

8 Almelch, N. et al, "Radiation Damage in Silicon," Rpt prepared under Contract No. NAS5-3788, RCA, May 1964

9 Carter, J. R. and Downing, R. G., "Charged Particle Radiation Damage in Semiconductors, XI: Effects of Low Energy Protons and High Energy Electrons in Silicon," Rpt No 4161-6012-RU-000, STL, May 1965

10 Becker, M. and Fan, H. Y., "Photovoltaic Effect of p-n Junction in Germanium," Phys. Rev. 78, 302, 1950

11 Shockley, W., "The Theory of p-n Junctions in Semiconductors and p-n Junction Transistors," Bell Sys. Tech. J., 28, 435, 1949

12 Carter, J. R. and Downing, R. G., "Charged Particle Radiation Damage in Semiconductors, VII: Energy Levels of Defect Centers in Electron and Proton Bombarded Silicon," Rpt No 8653-6021-KU-000, STL, Feb 1963

13 Wertheim, G. K., "Energy Levels in Electron-Bombarded Silicon," Phys. Rev. 105, 1730, 1957

14 Wolf, M., "Advances in Silicon Solar Cell Development," Energy Conversion for Space Power, Edited by Snyder, N. W., 231, Academic Press, New York, 1961

15 Dash, W. C. and Newman, R., "Intrinsic Optical Absorption in Single-Crystal Germanium and Silicon at 77°K and 300°K," Phys. Rev. 99, 1151, 1955

16 Denney, J. M. and Downing, R. G., "Charged Particle Radiation Damage in Semiconductors, IX: Proton Radiation Damage in Silicon Solar Cells," Rpt No 8653-6026-KU-000, July 1963

17 Rosenzweig, W., et al, "Energy Dependence of Proton Irradiation Damage in Silicon," J. Appl. Phys. 35, 2707, 1964

18 Denney, J. M., et al, "Estimate of Space-Radiation Effects on Satellite Solar-Cell Power Supplies," IRE Trans., MIL-6, No. 1, 14, 1962

19 Private communication with Mr. Iles, P., Hoffmann Electronics Corp.

LIST OF SYMBOLS

(Other than those defined in Table 1)

A_o, A_1	Constant
a (subscript)	Acceptor Level
B_o, B_1	Constant
d (subscript)	Donner level
E	Energy of bombarding particle
$\vec{E}$, E	Electric field
$g_n(x)$	Electron generation rate at a distance of x
g_o	Carrier generation rate
$g_p(x)$	Hole generation rate at a distance of x
i (subscript)	Incident, intrinsic, or interface between damaged and undamaged regions
$\vec{J}_n$	Electron current density
J_o	Saturation current, see equation 47
$\vec{J}_p$	Hole current density
J_{sc}	Total short circuit current density
J_{sc}^n	Electron short circuit current density
J_{sc}^p	Hole short circuit current density
j (subscript)	Junction
K	Damage constant for minority carrier diffusion length
k	Boltzmann's constant, 1.38×10^{-16} ergs/^oK
L	Minority carrier diffusion length after radiation
L_o	Minority carrier diffusion length before radiation
ℓ	See equation 48
m	See equation 47'
N(x=0)	Dopant concentration at the front face
N(x=a)	Dopant concentration at a distance of a

N_a	Acceptor concentration
N_d	Donner concentration
n_i	Intrinsic electron concentration
n (subscript)	Electron or n-type
o (subscript)	Before radiation or thermal equilibrium
p (subscript)	Hole or p-type
q	Electronic charge, 1.6×10^{-19} coul/charge
R, $R(\lambda)$	Spectral reflectivity
r_1	See equation 41
r_2	See equation 42
s(0)	Surface recombination velocity at the front face
s(c)	Surface recombination velocity at the back face
s_o	See equation 49
s_c	See equation 50
T	Temperature
t	Time
V, V_{oc}	Open Circuit voltage
V_n	See equation III-1
V_p	See equation III-2
x	Distance from the front surface
y_1	See equation 51
y_2	See equation 52
α, $\alpha(\lambda)$	Spectral absorption coefficient
β	$= q/kT$
γ	$= \mu_n/\mu_p$
Δ_2	See equation 53
$\nabla 2$	See equation 54

$\Delta\varphi$	Shift in Fermi Level
ϵ	Dielectric constant
ζ , $\zeta(\lambda)$	See equation 55
η, $\eta(\lambda)$	Quantum efficiency
λ	Wavelength
λ_g	Cutoff wavelength
μ	Mobility
μ_n	Electron mobility
μ_p	Hole mobility
ρ	Resistivity
ρ_n	Resistivity in n-type
ρ_p	Resistivity in p-type
σ	Conductivity
φ, $\varphi(\lambda)$, $\varphi'(\lambda)$	Spectral irradiance
Φ	Integrated flux
φ_i	Intrinsic energy level
φ_f	Fermi level
φ_p	Quasi Fermi level due to hole injection

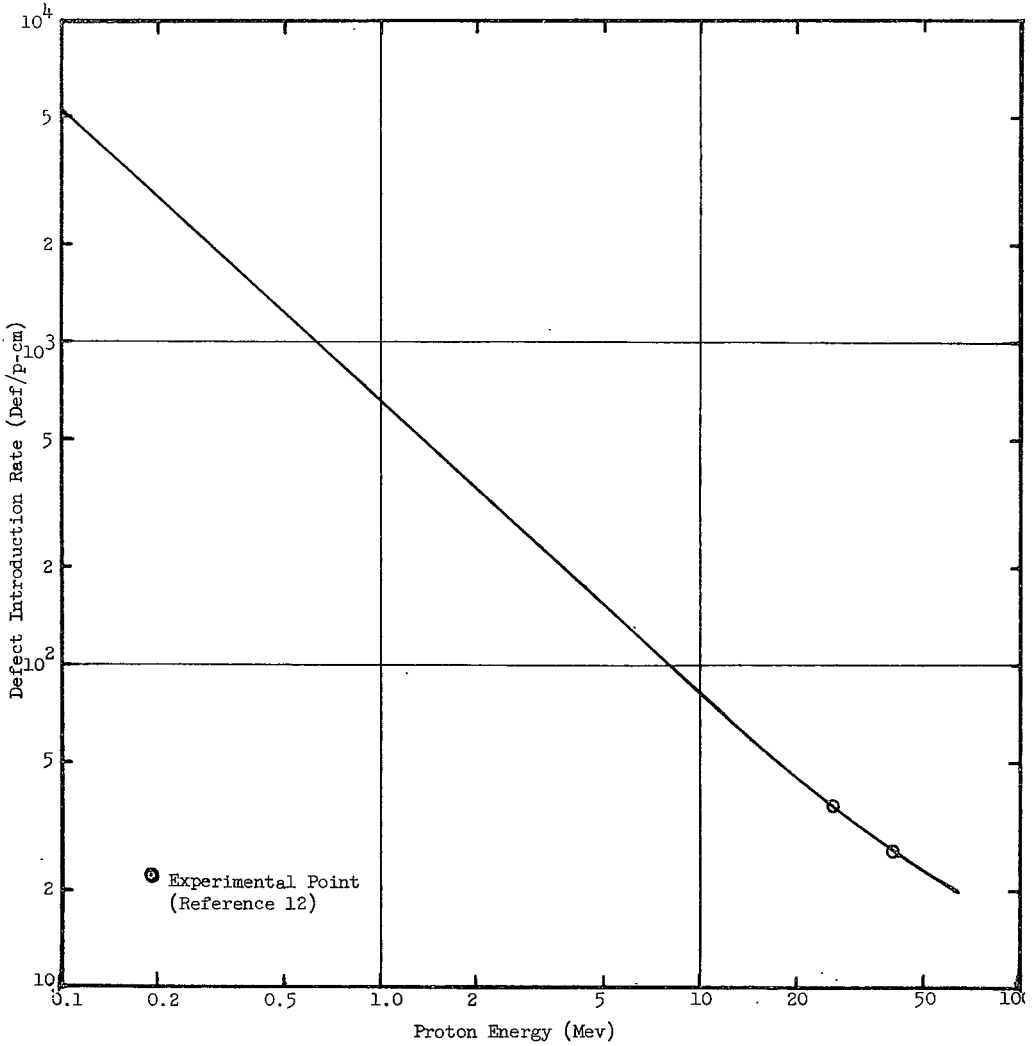
Defect Introduction Rate (Def/p-cm)
10^4
5
2
10^3
5
2
10^2
5
2
10
0.1
0.2
0.5
1.0
2
5
10
20
50
100
Proton Energy (Mev)
Experimental Point
(Reference 12)

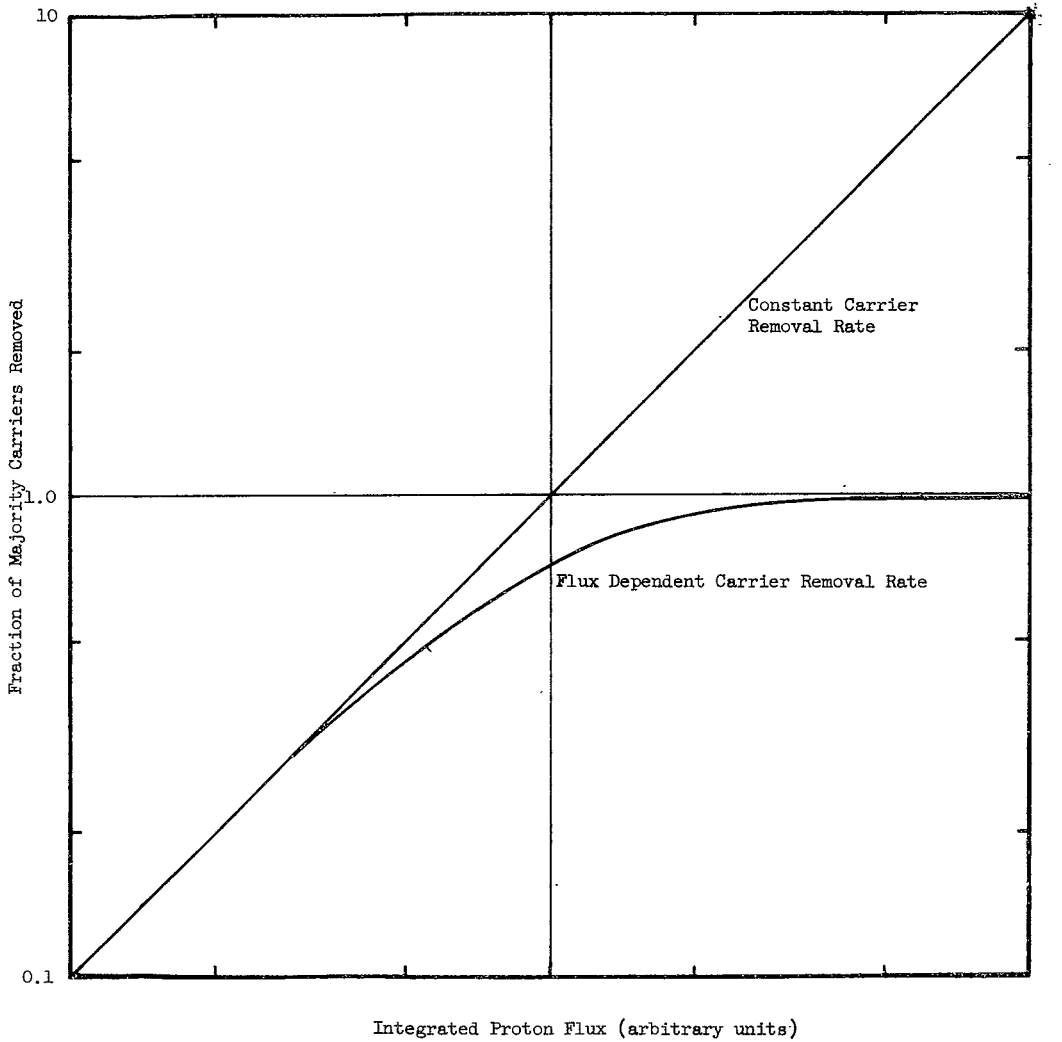
10
1.0
0.1
Fraction of Majority Carriers Removed
Constant Carrier Removal Rate
Flux Dependent Carrier Removal Rate
Integrated Proton Flux (arbitrary units)

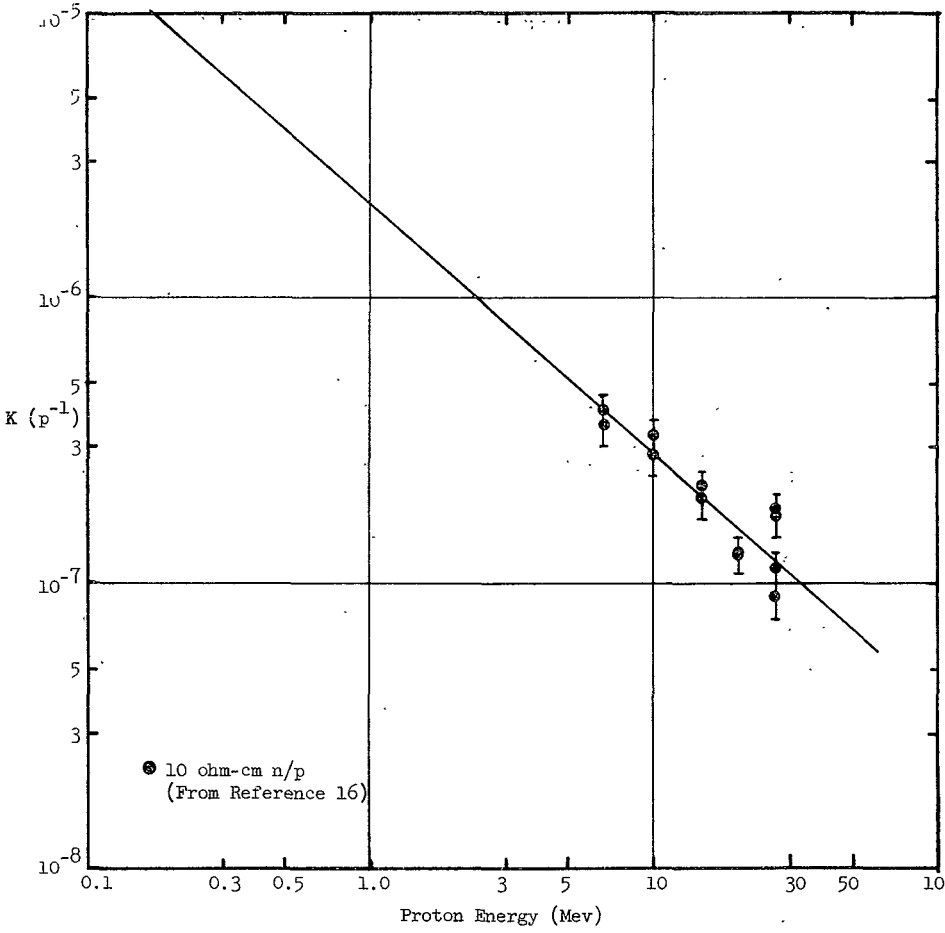
10^{-5}
5
3
10^{-6}
5
3
10^{-7}
5
3
10^{-8}
K (p^{-1})
0.1
0.3
0.5
1.0
3
5
10
30
50
100
Proton Energy (Mev)
10 ohm-cm n/p
(From Reference 16)

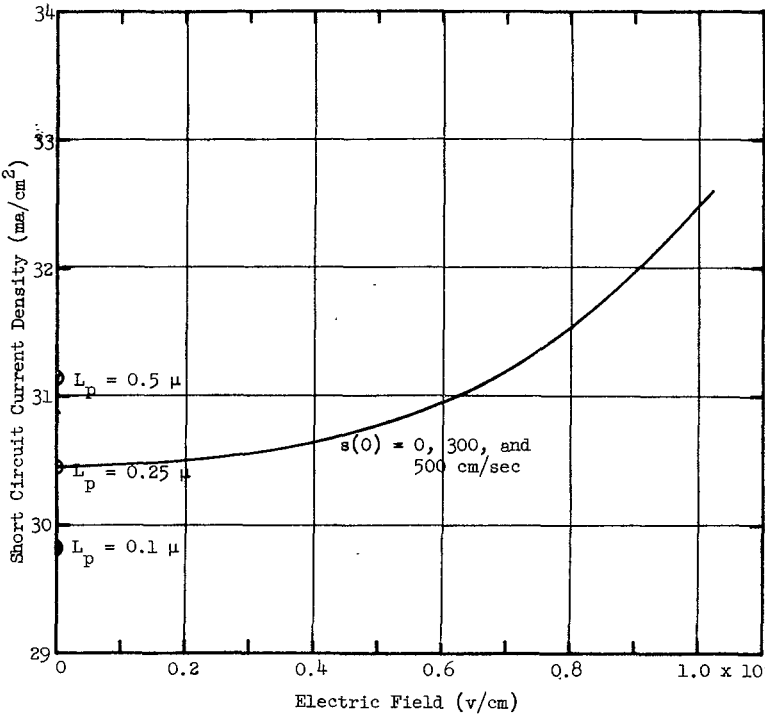
34
33
32
31
30
29
Short Circuit Current Density (ma/cm^2)
L_p = 0.5 μ
L_p = 0.25 μ
L_p = 0.1 μ
s(0) = 0, 300, and 500 cm/sec
0
0.2
0.4
0.6
0.8
1.0 x 10^3
Electric Field (v/cm)

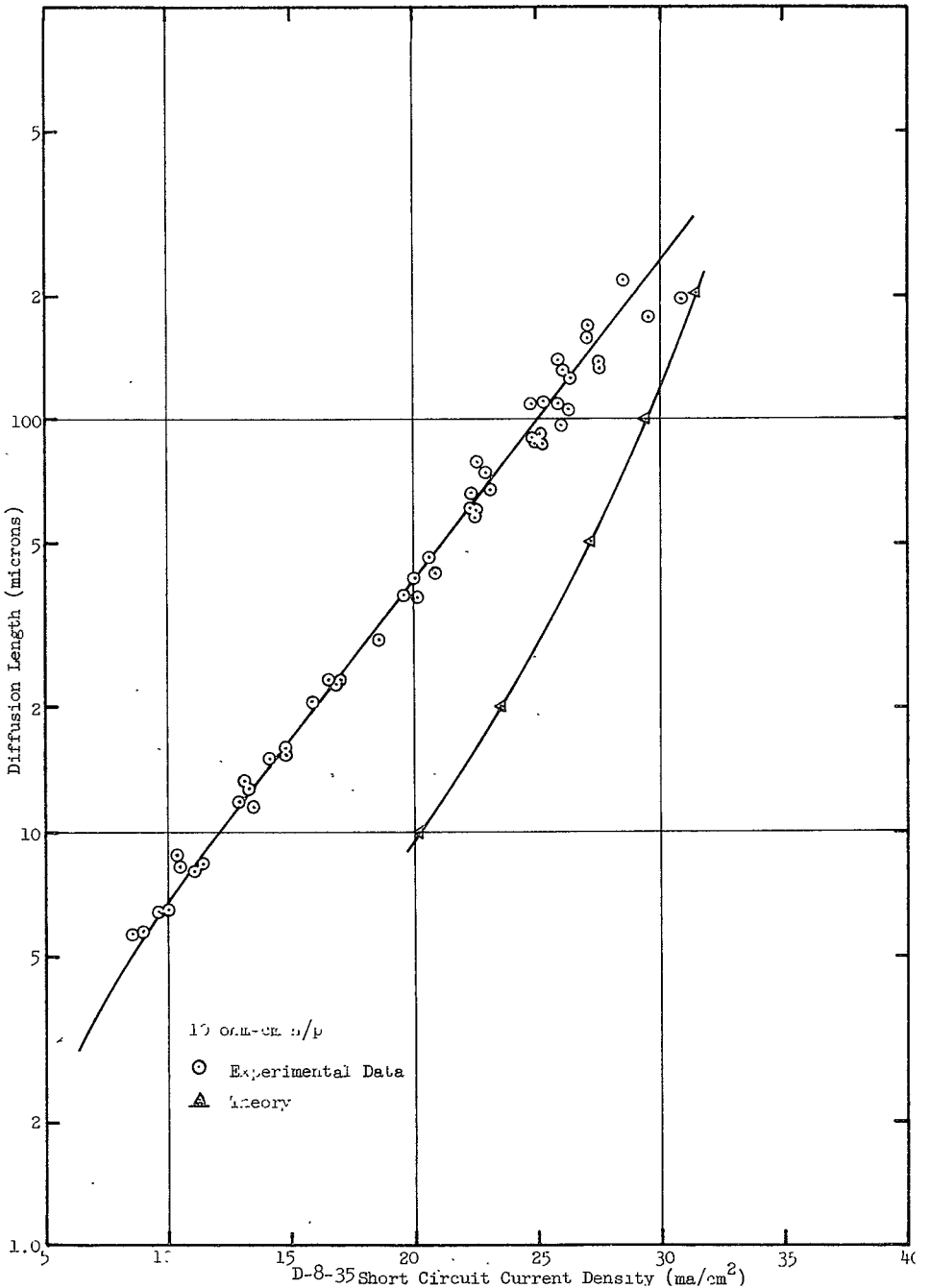
Diffusion Length (microns)
5
2
100
5
2
10
5
2
1.0
15
20
25
30
35
40
D-8-35 Short Circuit Current Density (ma/cm²)
10 ohm-cm n/p
Experimental Data
Theory

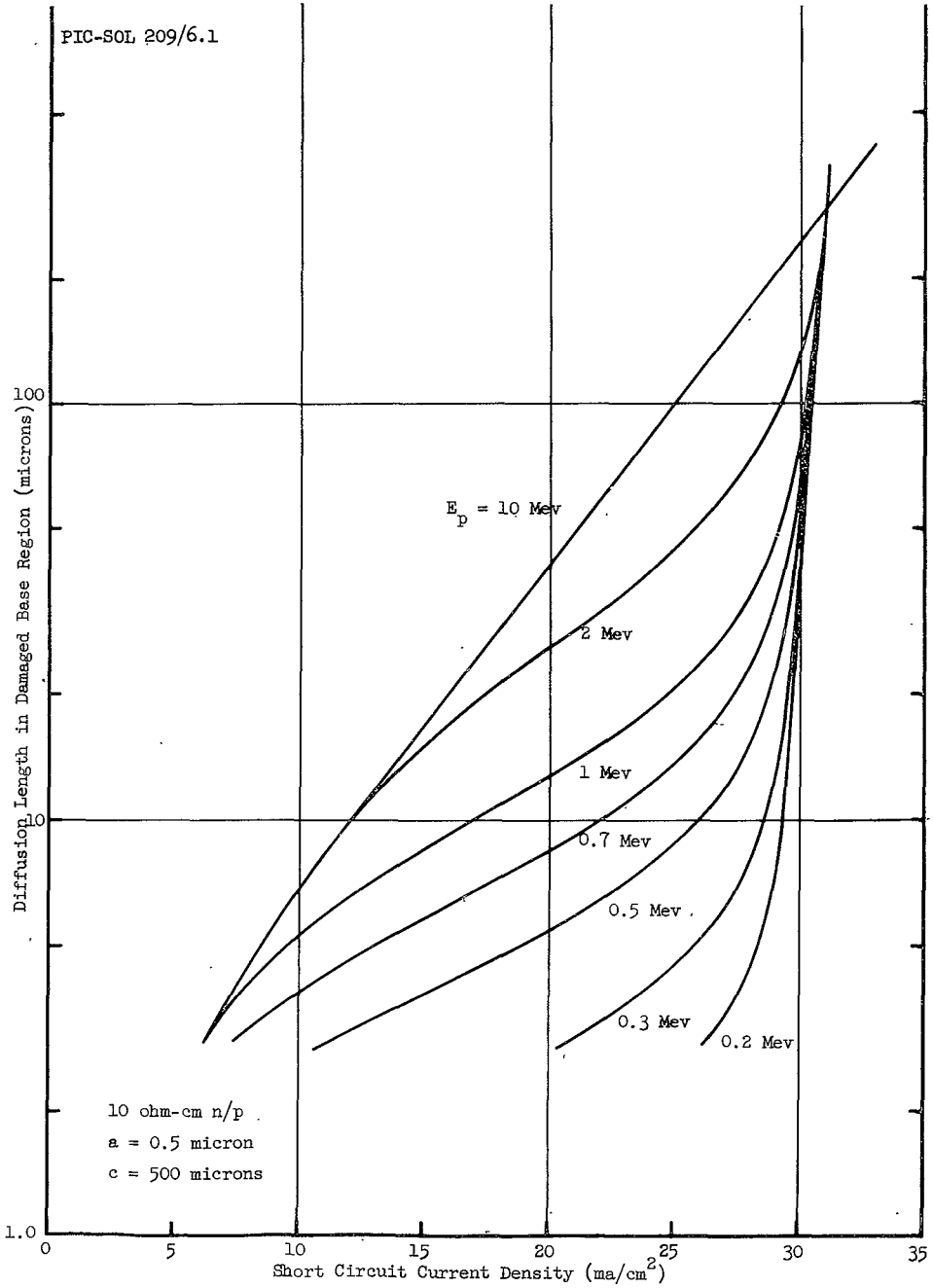
PIC-SOL 209/6.1
100
10
1.0
Diffusion Length in Damaged Base Region (microns)
E_p = 10 Mev
2 Mev
1 Mev
0.7 Mev
0.5 Mev
0.3 Mev
0.2 Mev
10 ohm-cm n/p
a = 0.5 micron
c = 500 microns
0
5
10
15
20
25
30
35
Short Circuit Current Density (ma/cm^2)

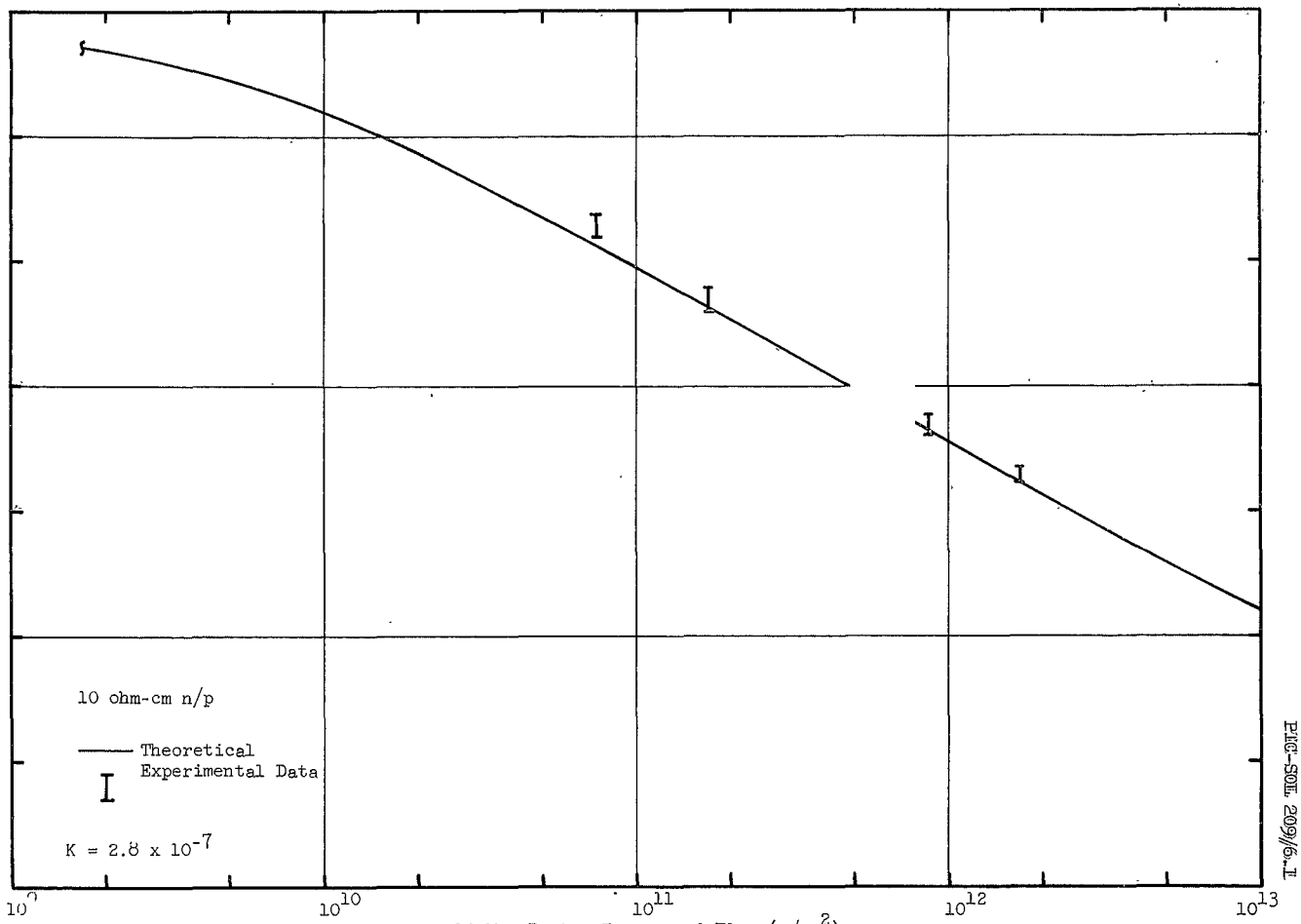

PIC-SOL 2096-1

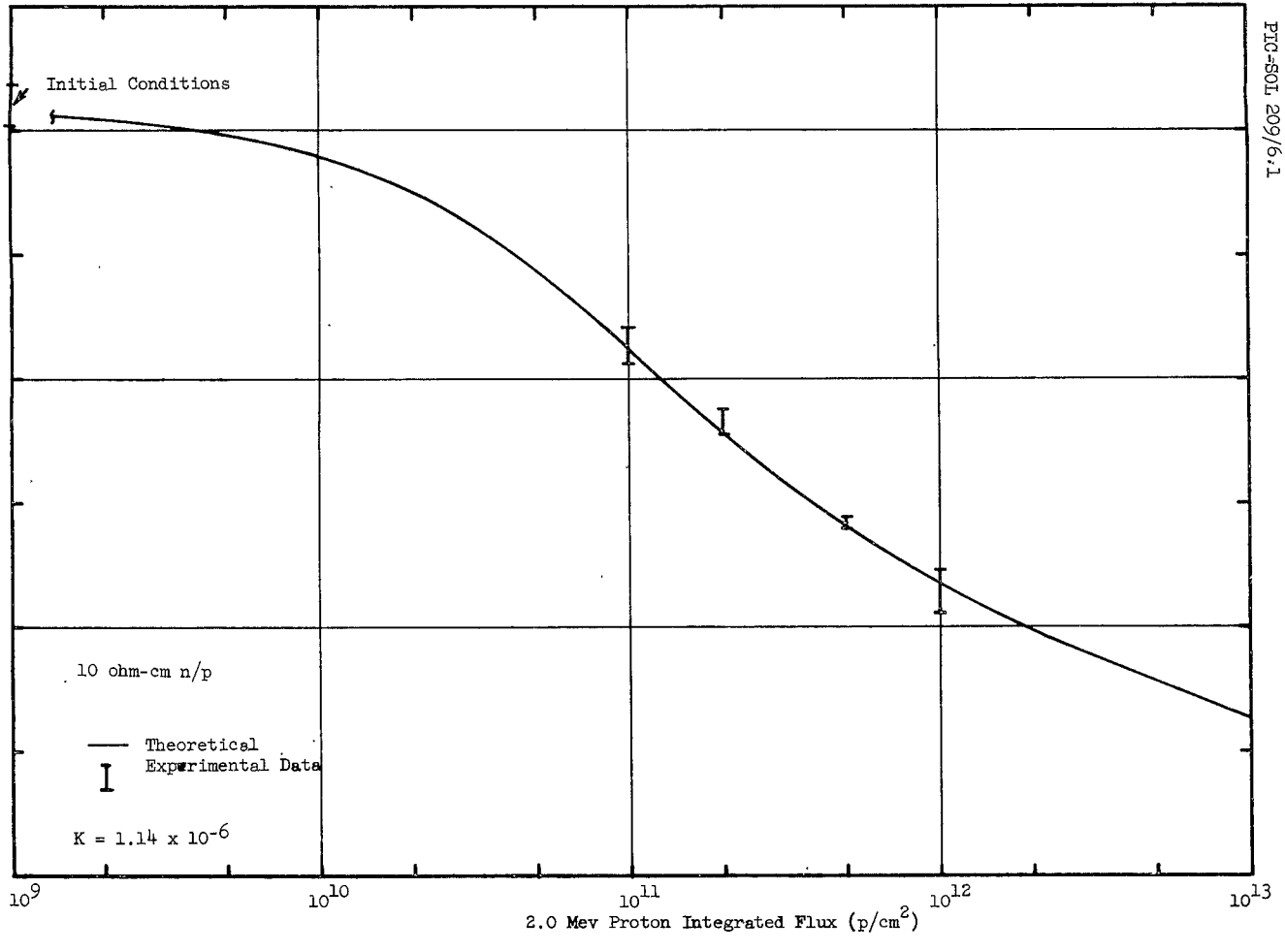
Initial Conditions
30
20
10
0
Short Circuit Current Density (ma/cm²)
10 ohm-cm n/p
Theoretical
Experimental Data
K = 1.14 x 10⁻⁶
10⁹
10¹⁰
10¹¹
10¹²
10¹³
2.0 Mev Proton Integrated Flux (p/cm²)

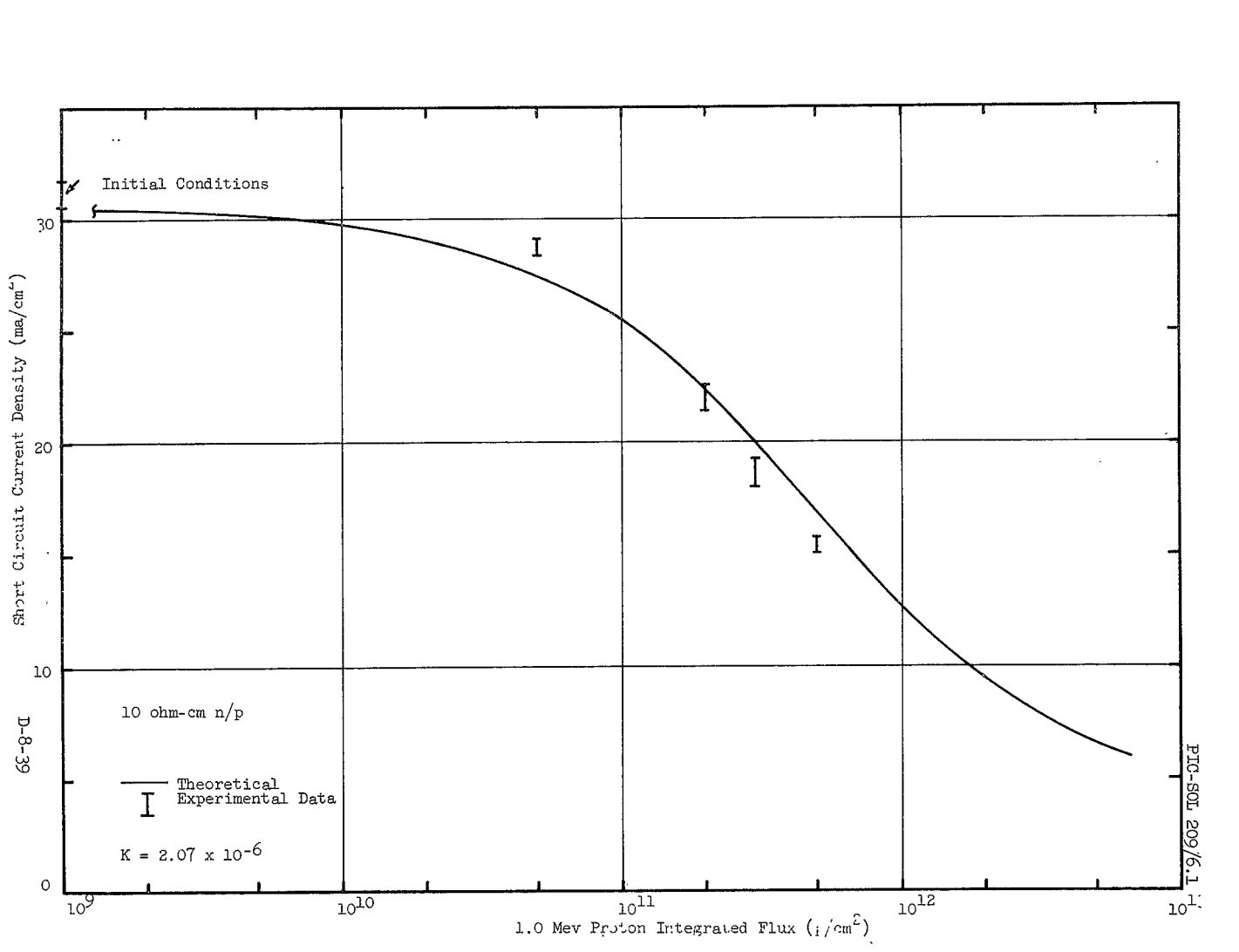
Initial Conditions
30
20
10
0
Short Circuit Current Density (ma/cm²)
10 ohm-cm n/p
Theoretical
Experimental Data
K = 2.07 x 10⁻⁶
10⁹
10¹⁰
10¹¹
10¹²
1.0 Mev Proton Integrated Flux (p/cm²)
D-8-39
PIC-SOL 209/6.1

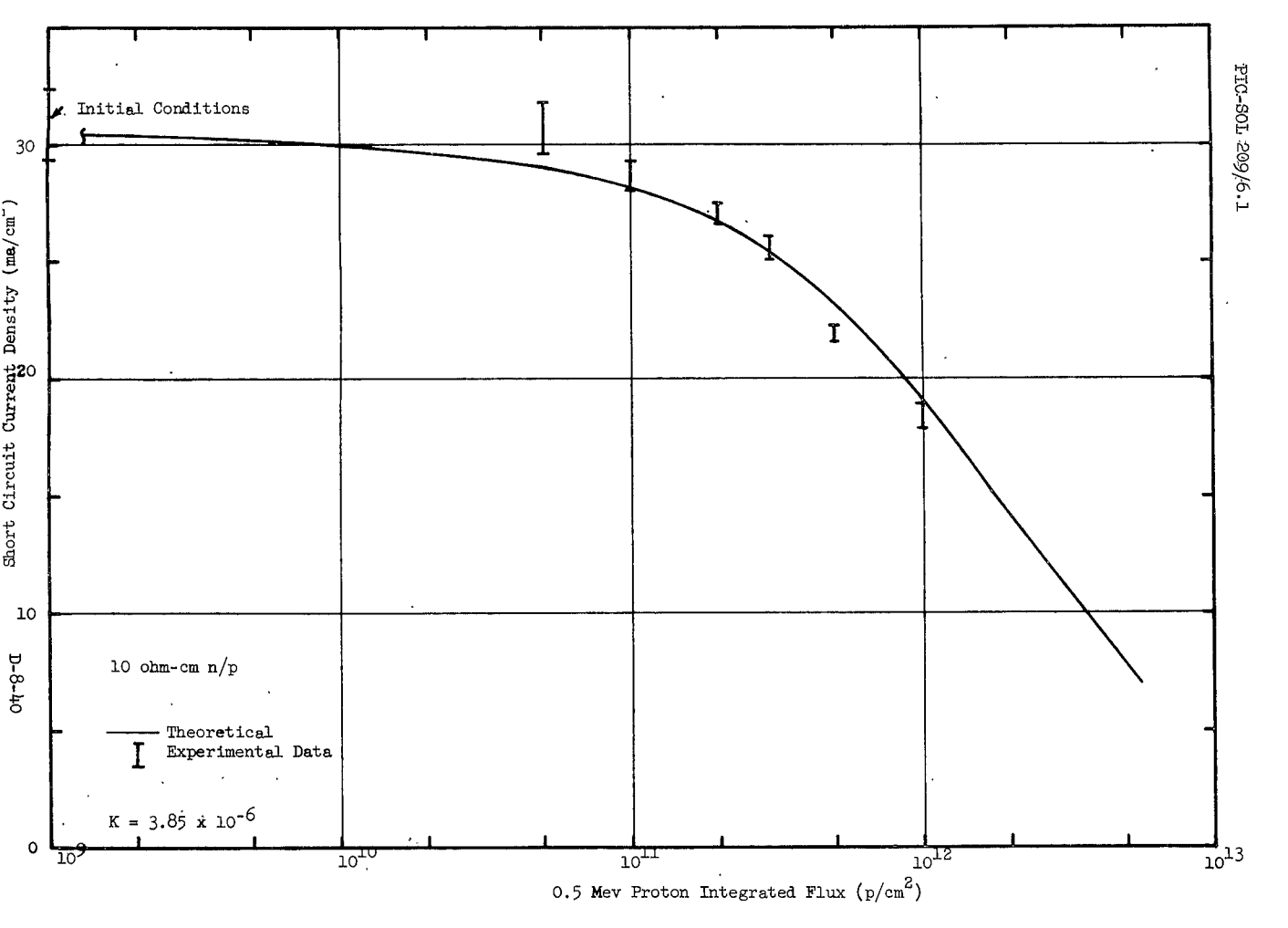
Initial Conditions
30
20
10
0
Short Circuit Current Density (ma/cm²)
10 ohm-cm n/p
Theoretical
Experimental Data
K = 3.85 x 10⁻⁶
10⁹
10¹⁰
10¹¹
10¹²
10¹³
0.5 Mev Proton Integrated Flux (p/cm²)

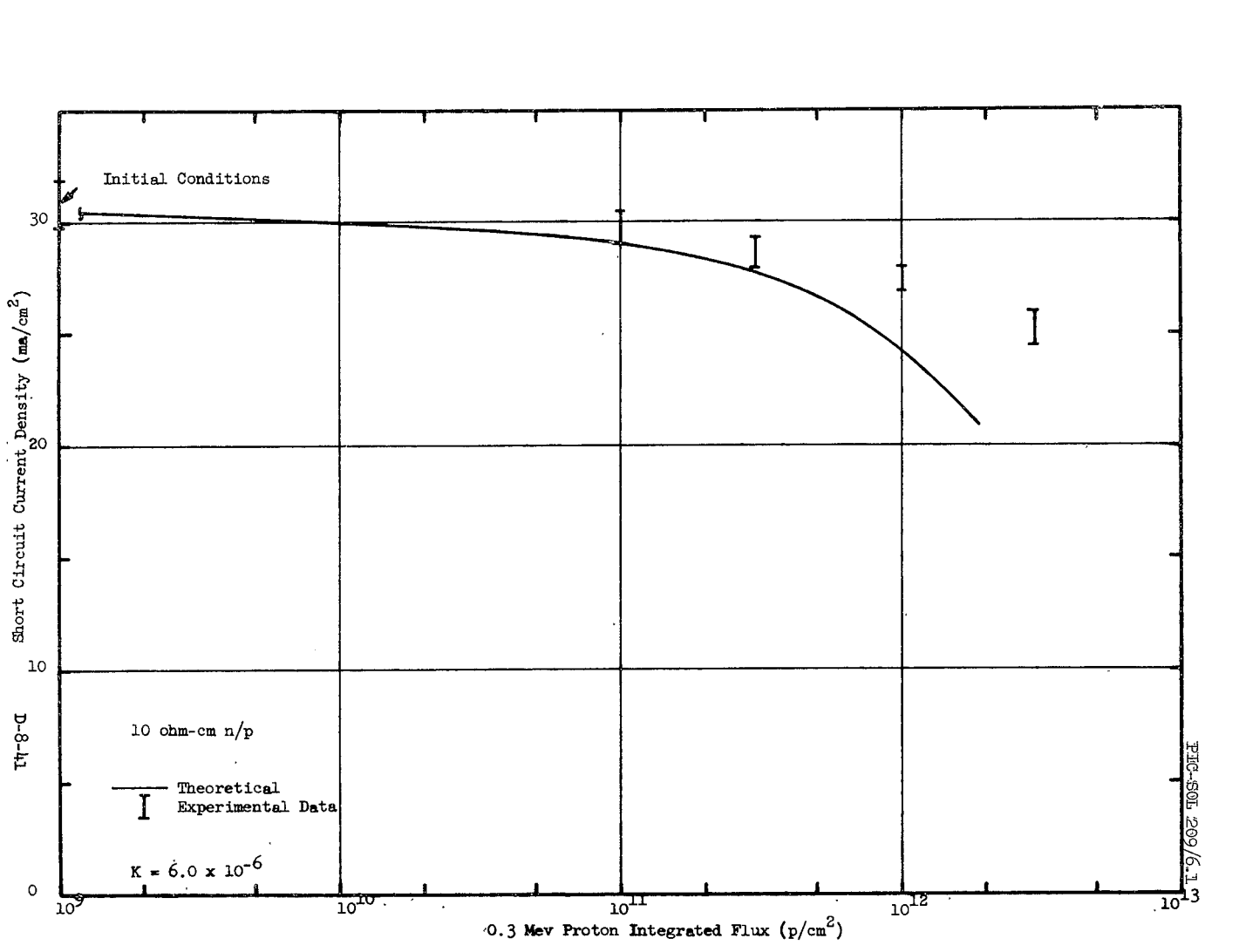
Initial Conditions
30
20
10
0
Short Circuit Current Density (ma/cm^2)
10 ohm-cm n/p
Theoretical
Experimental Data
K = 6.0 x 10^{-6}
10^9
10^{10}
10^{11}
10^{12}
10^{13}
0.3 Mev Proton Integrated Flux (p/cm^2)
D-8-41
PIC-S01 2/6/61

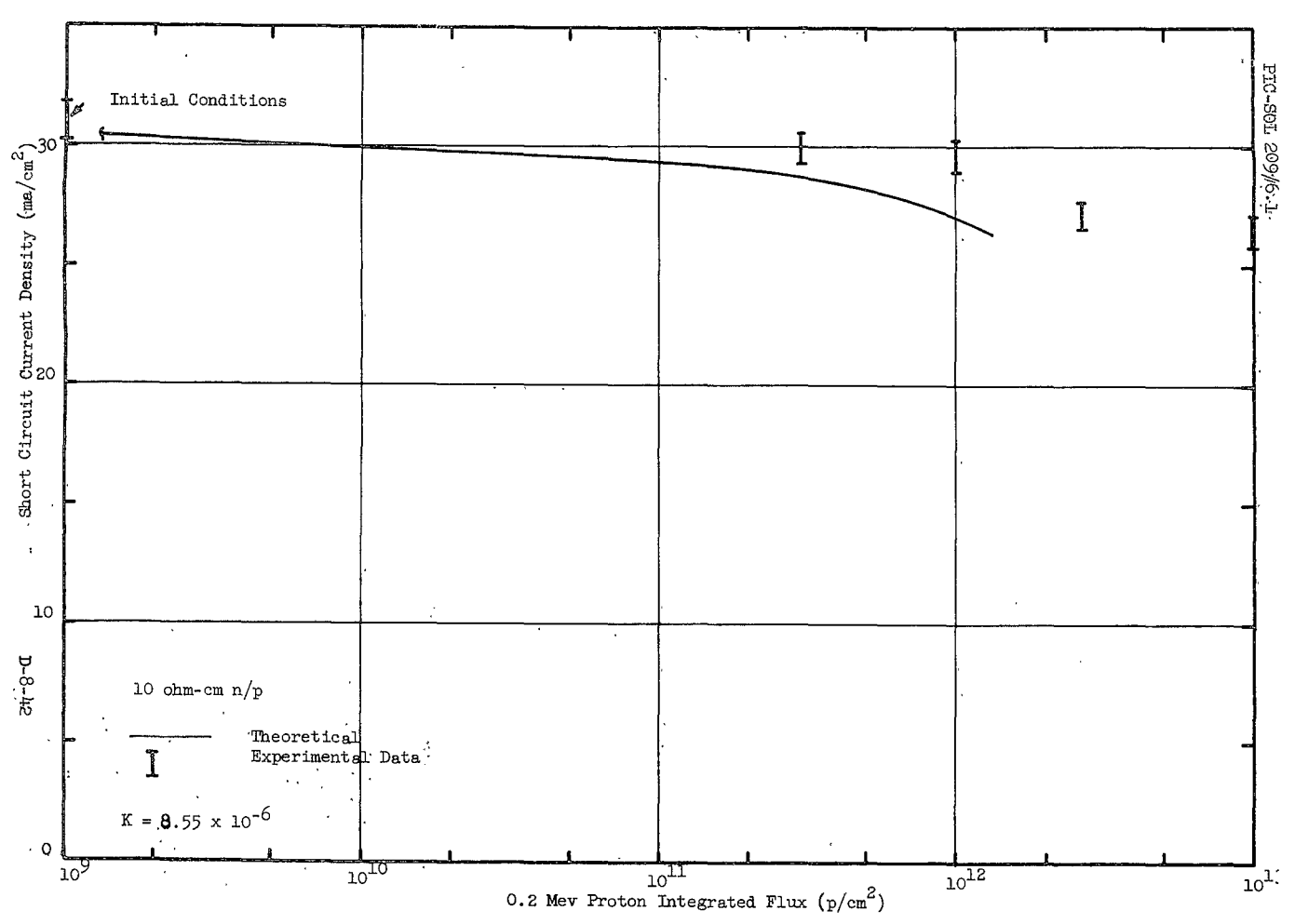
Initial Conditions
Short Circuit Current Density (ma/cm^2)
30
20
10
0
10 ohm-cm n/p
Theoretical
Experimental Data
K = 8.55 x 10^{-6}
10^9
10^{10}
10^{11}
10^{12}
0.2 Mev Proton Integrated Flux (p/cm^2)

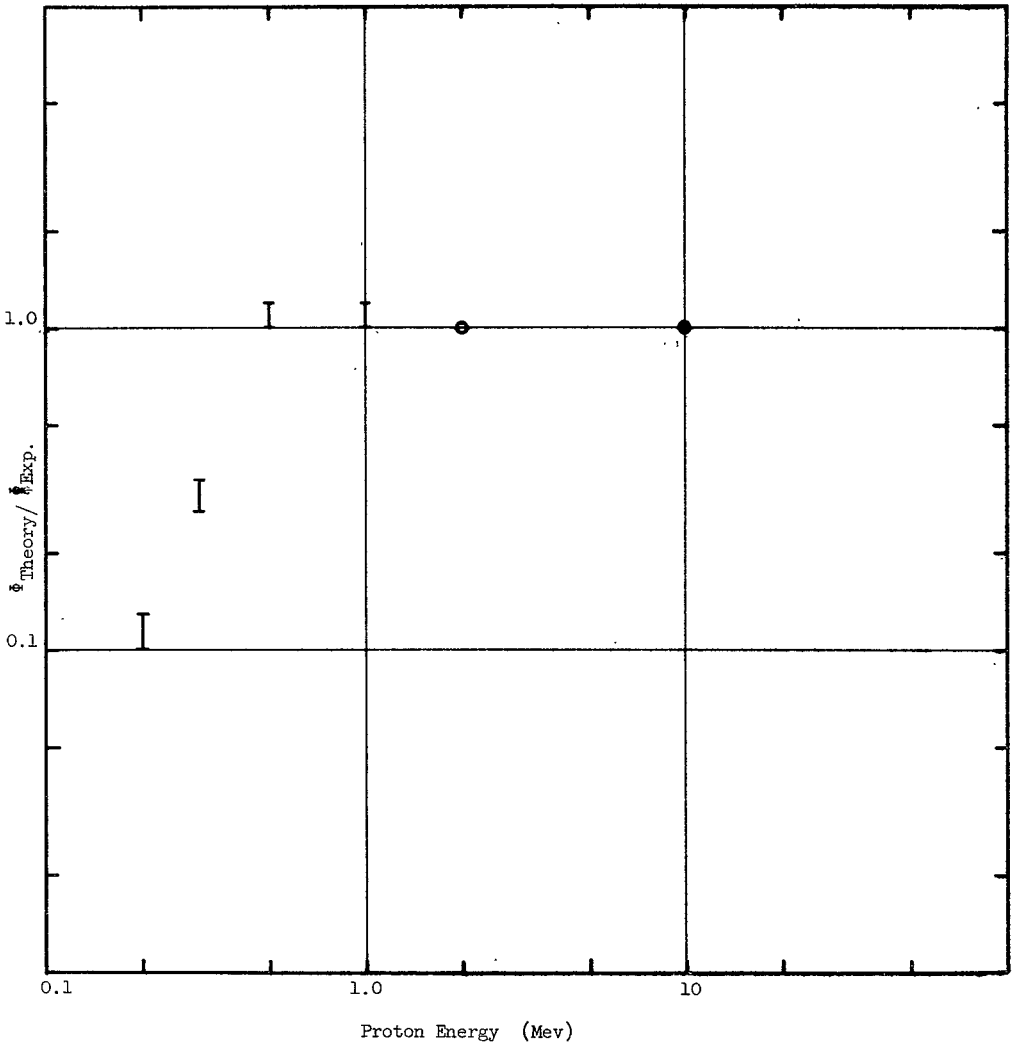
1.0
0.1
$\Phi_{Theory}/\Phi_{Exp.}$
0.1
1.0
10
Proton Energy (Mev)

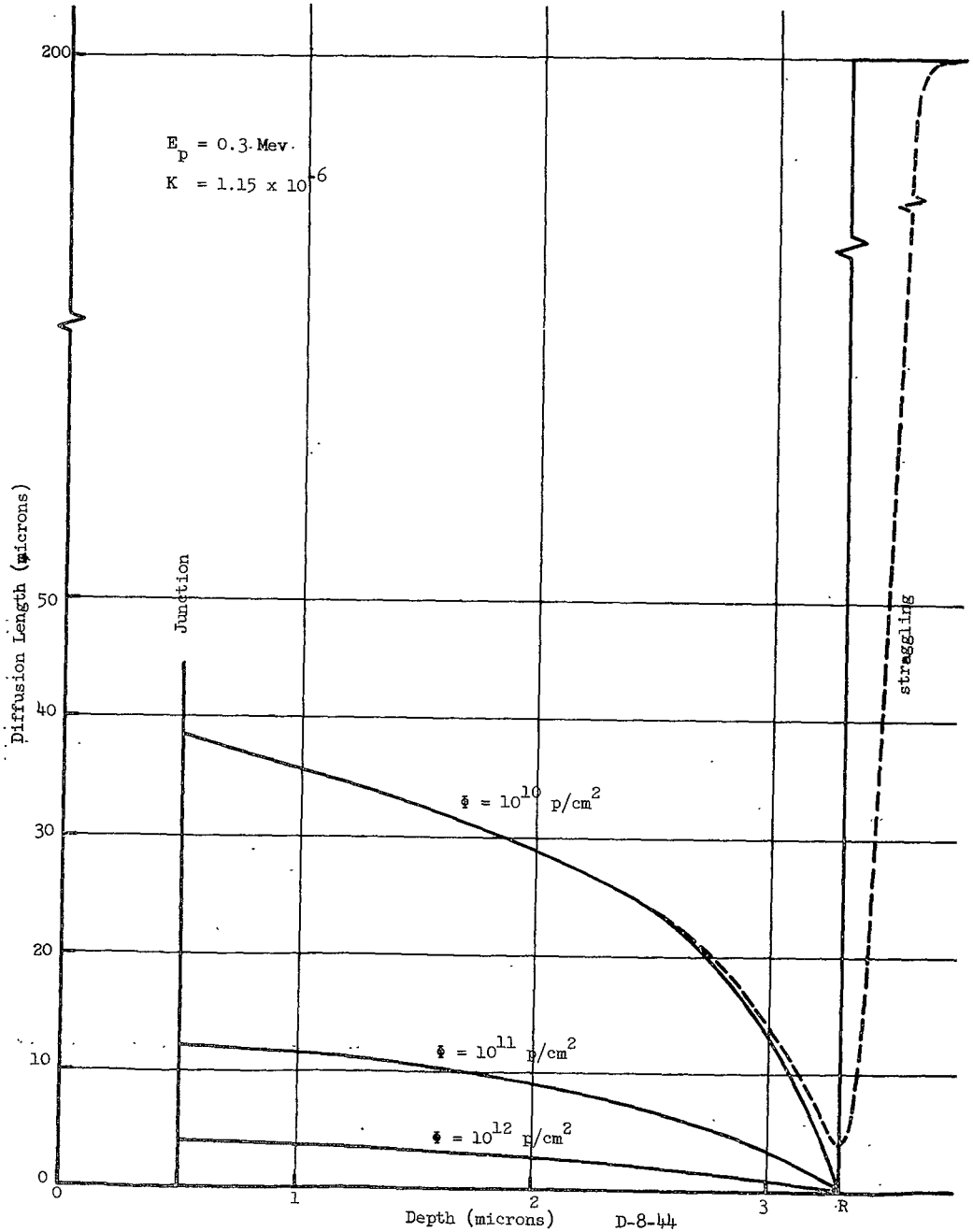
200
50
40
30
20
10
0
E_p = 0.3 Mev.
K = 1.15 x 10^{-6}
Diffusion Length (microns)
Junction
straggling
$\Phi = 10^{10}$ p/cm^2
$\Phi = 10^{11}$ p/cm^2
$\Phi = 10^{12}$ p/cm^2
0
1
2
3
R
Depth (microns)
D-8-44

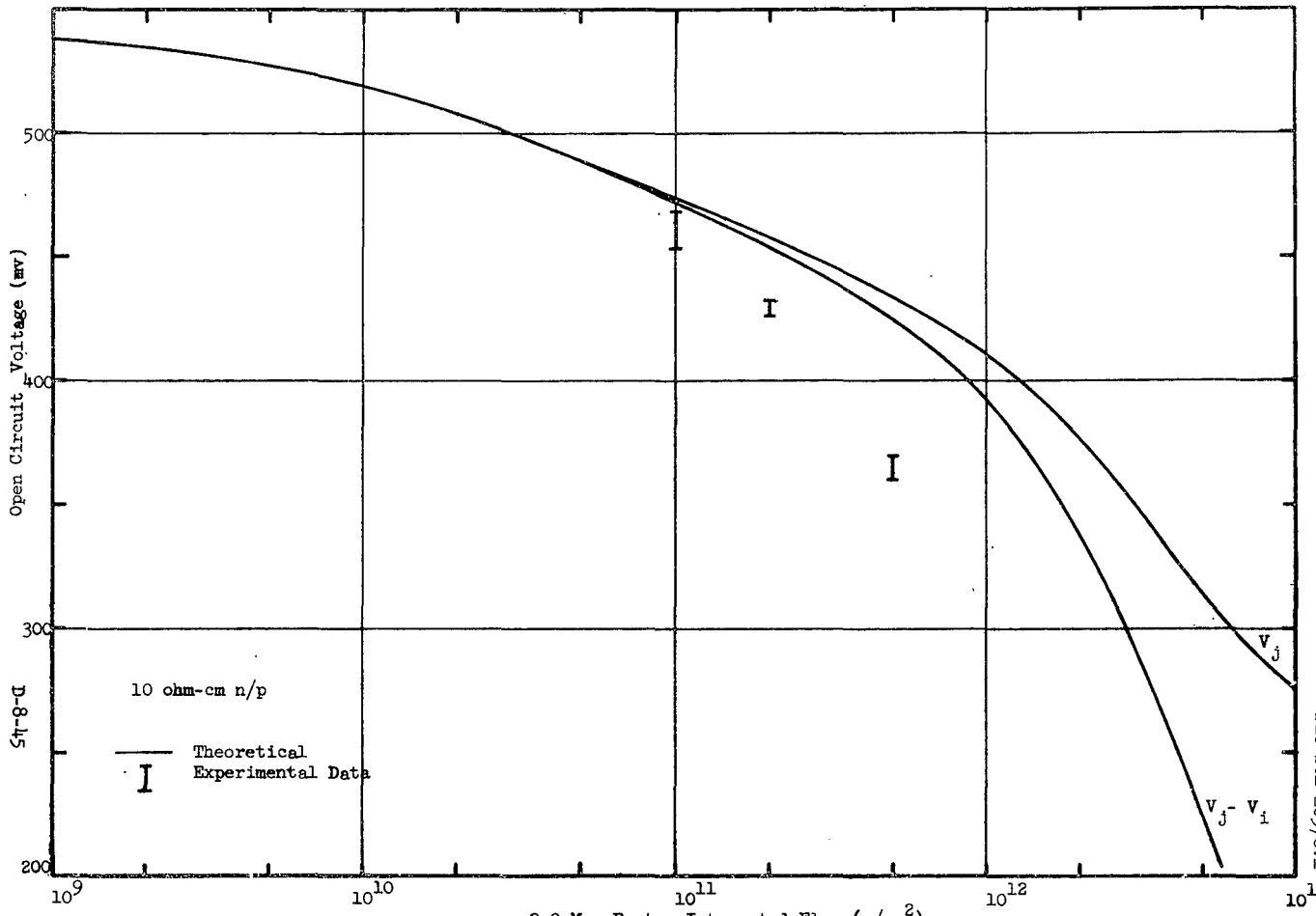
Open Circuit Voltage (mv)
500
400
300
200
10^9
10^{10}
10^{11}
10^{12}
10^{13}
2.0 Mev Proton Integrated Flux (p/cm^2)
I
I
V_j
$V_j - V_i$
10 ohm-cm n/p
Theoretical
Experimental Data
I
D-8-45
PIC-SOL 209/6.1

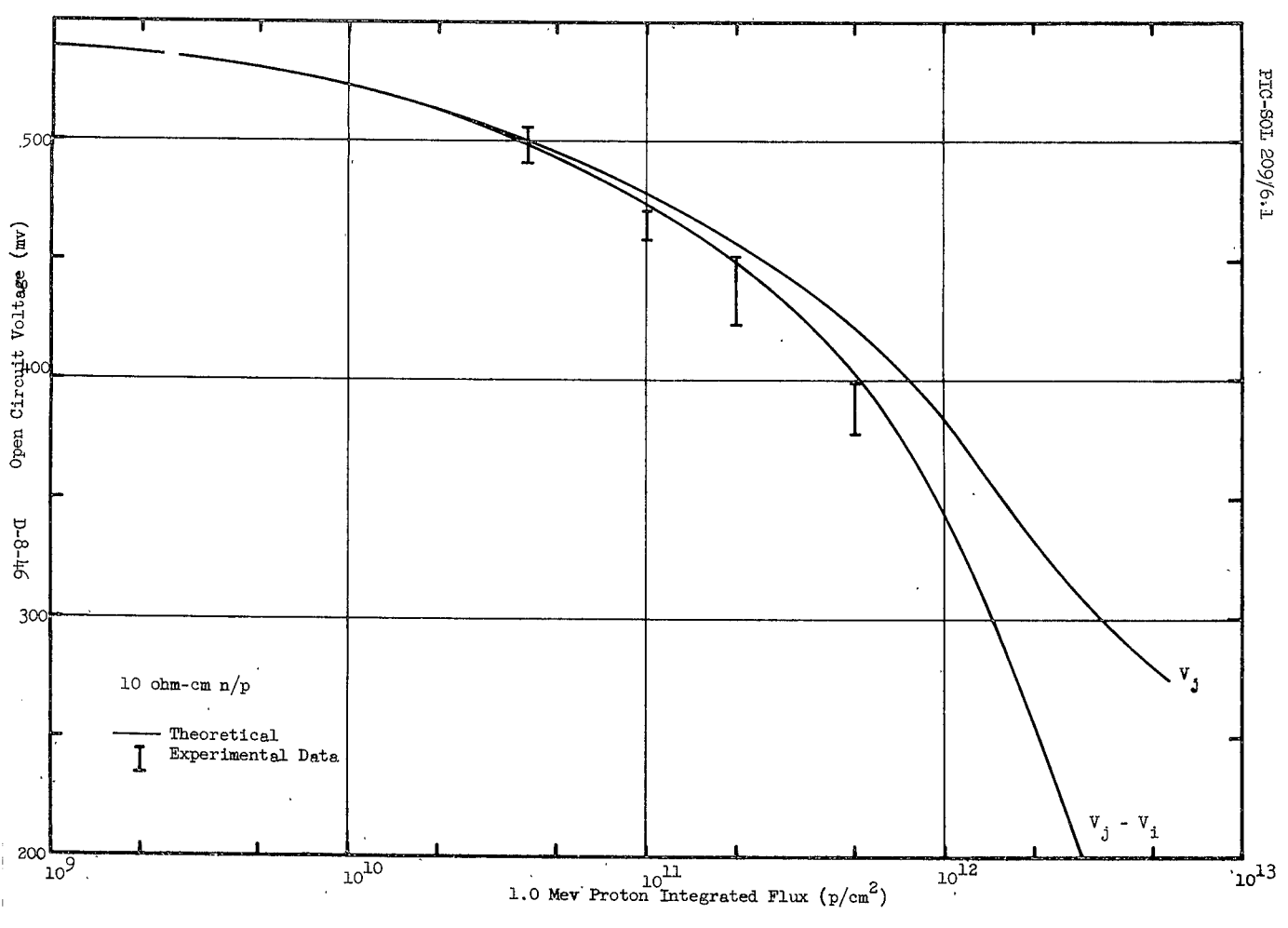
PIC-SOL 209/6.1
D-8-46
Open Circuit Voltage (mv)
500
400
300
200
10 ohm-cm n/p
Theoretical
Experimental Data
V_j
$V_j - V_i$
10^9
10^{10}
10^{11}
10^{12}
10^{13}
1.0 Mev Proton Integrated Flux (p/cm^2)

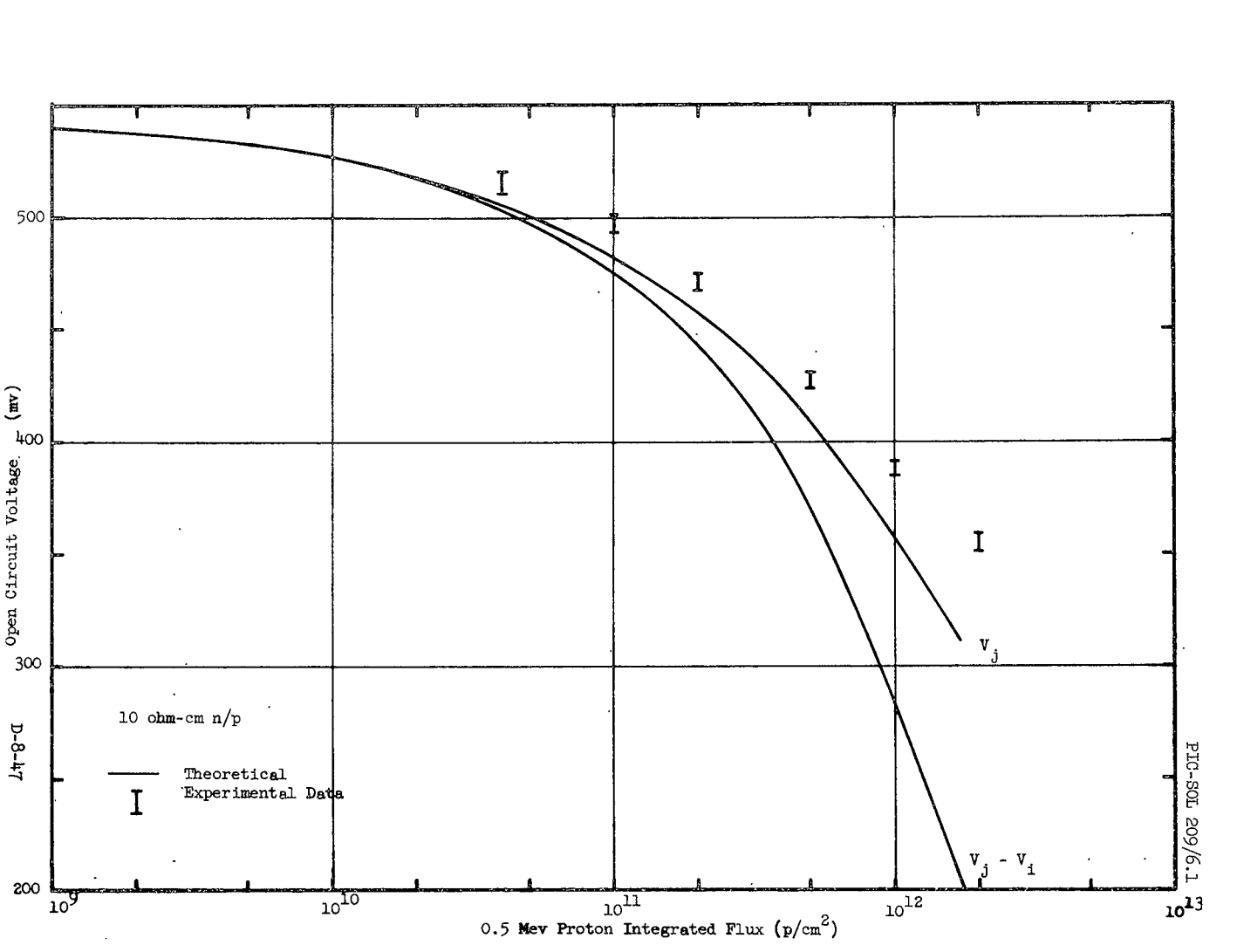
500
400
300
200
Open Circuit Voltage (mv)
10^9
10^{10}
10^{11}
10^{12}
10^{13}
0.5 Mev Proton Integrated Flux (p/cm^2)
V_j
$V_j - V_i$
10 ohm-cm n/p
Theoretical
Experimental Data
D-8-47
PIC-SOM 209/6.1

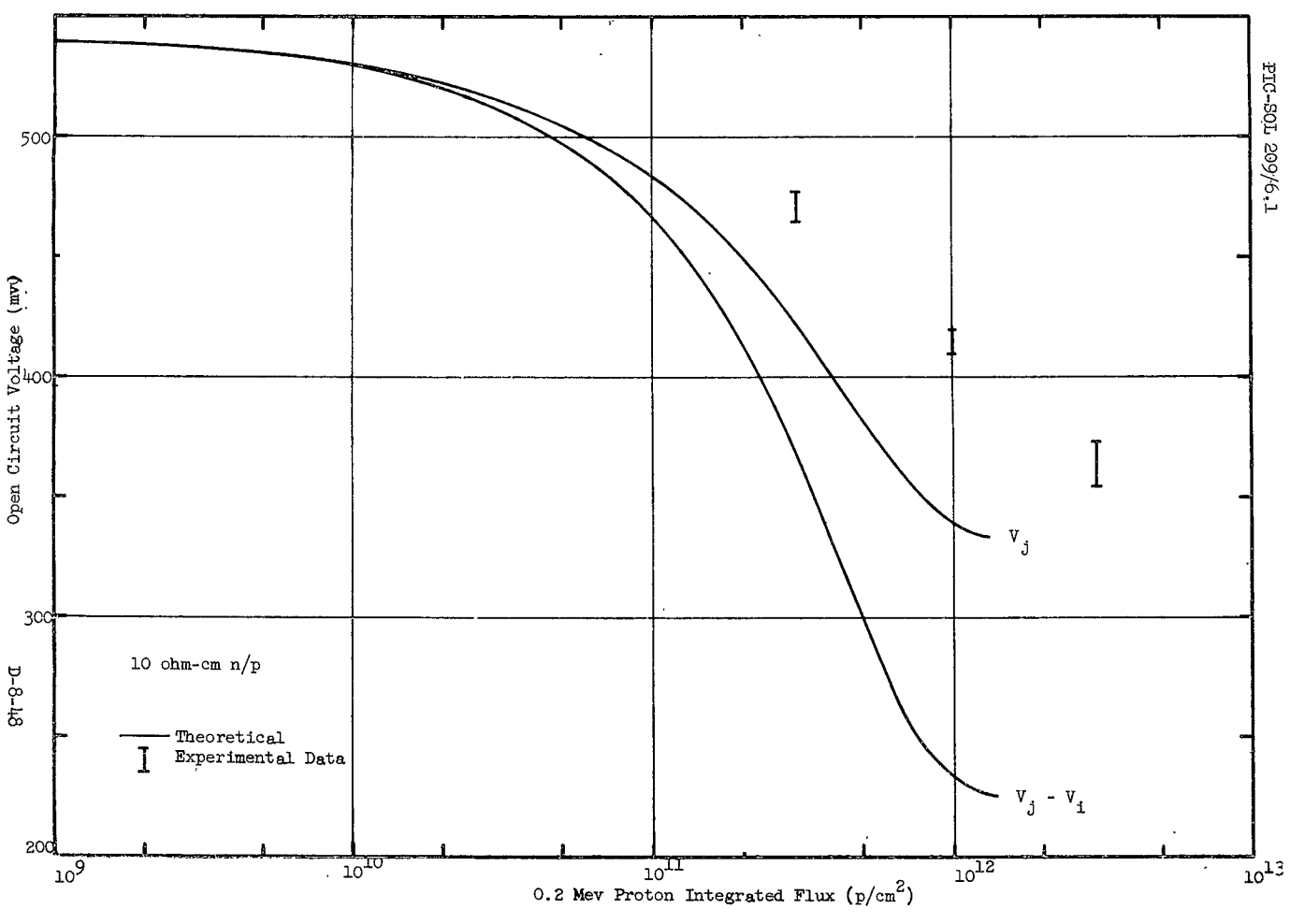
Open Circuit Voltage (mv)
500
400
300
200
10 ohm-cm n/p
Theoretical
Experimental Data
V_j
$V_j - V_i$
10^9
10^{10}
10^{11}
10^{12}
10^{13}
0.2 Mev Proton Integrated Flux (p/cm^2)
D-8-48
PIC-SOL 2696.1

NO.	PRICE	COPIES REQUIRED	DATE REQUESTED	REQUEST NO.
1066-1752				
COVER COLOR	NO. OF PAGES		DATE DUE	DATE RECEIVED
TITLE				

PLATES	QUANTITY	COST	PRESS	QUANTITY	COST
XEROX			BINDERY		
ITEK			IMPRESSIONS		
OTHER			NUMBER OF SHEETS		
TOTALS			TOTALS		
RECEIVED	R & P	WAREHOUSE	INVENTORY		

REMARKS

XX
NMF

1 copy
offset
Kent 240.3
4-29-65

FORM NBS-805
(10-26-64)

CLEARINGHOUSE PRINTING REQUEST

U.S. DEPARTMENT OF COMMERCE
NATIONAL BUREAU OF STANDARDS